EDITE - ED 130

Doctorat ParisTech

T H È S E

pour obtenir le grade de docteur délivré par

TELECOM ParisTech

Spécialité « Électronique et Communications »

présentée et soutenue publiquement par

Gia-Minh HOANG

préparée au CEA-Leti et à EURECOM

le 19 février 2018

Localisation multicapteurs coopérative

pour les véhicules connectés

Directeur de thèse : **Jérôme HÄRRI**, EURECOM
Co-directeur de thèse : **Dirk SLOCK**, EURECOM
Co-encadrement de la thèse : **Benoît DENIS**, CEA-Leti

Jury
M. Giovanni PAU, Professeur, Université Pierre et Marie Curie   Président
M. Henk WYMEERSCH, Professeur, Chalmers University of Technology   Rapporteur
Mme. Valérie RENAUDIN, Directrice de Recherche (HDR), IFSTTAR   Rapporteur
M. Moe Z. WIN, Professeur, Massachusetts Institute of Technology   Examinateur
M. Thomas ENGEL, Professeur, Université du Luxembourg   Examinateur

TELECOM ParisTech
école de l'Institut Mines-Télécom - membre de ParisTech

2018-ENST-0010

T
H
È
S
E

EDITE - ED 130

T H E S I S

**in partial fulfillment of the requirements
for the degree of Doctor of Philosophy**

TELECOM ParisTech

Specialty « Electronics and Communications »

publicly defended by

Gia-Minh HOANG

prepared at CEA-Leti and EURECOM

on February 19, 2018

Cooperative multisensor localization

for connected vehicles

Thesis director : **Jérôme HÄRRI**, EURECOM
Thesis co-director : **Dirk SLOCK**, EURECOM
Thesis advisor : **Benoît DENIS**, CEA-Leti

T
H
È
S
E

Jury members
Mr. Giovanni PAU, Professor, Pierre and Marie Curie University   President
Mr. Henk WYMEERSCH, Professor, Chalmers University of Technology   Reviewer
Mrs. Valérie RENAUDIN, Director of Research (HDR), IFSTTAR   Reviewer
Mr. Moe Z. WIN, Professor, Massachusetts Institute of Technology   Examiner
Mr. Thomas ENGEL, Professor, University of Luxembourg   Examiner
TELECOM ParisTech
a school of Institut Mines-Télécom - member of ParisTech

Abstract

Cooperative Intelligent Transport System (C-ITS) applications assume the availability of a reliable and accurate positioning system. Even if suitable to most Day-1 applications (e.g. route navigation), the Global Navigation Satellite System (GNSS) accuracy, reliability and availability are clearly not sufficient for more demanding Day-2 applications (e.g., highly autonomous driving, advanced safety services including vulnerable road users warning, etc.), which would require a consistent sub-meter localization accuracy regardless of operating conditions. To bridge this gap, Cooperative Localization (CLoc) has been recently identified as a promising strategy. Accordingly, mobile nodes can help each other by exchanging location data (typically, their own position estimates or raw GNSS data), acquiring range-dependent metrics over their respective radio links and finally, fusing the various sources of information. However, conventional CLoc solutions may be partly unsuitable within the context of vehicular ad hoc networks (VANETs), which comes along with unprecedented challenges such as specific mobility patterns, practical operating trade-offs with complexity and vehicle-to-vehicle (V2V) communication capabilities, or even fusion optimality when multiple measurement modalities are available at the vehicles. Thus, one central related research question is as follows: "Can the Day-2 sub-meter localization accuracy be met through CLoc strategies between connected vehicles?"

In this thesis, following a gradually complex approach, we aim at evaluating *how* and *in which* conditions position information from neighboring vehicles and/or associated V2V measurements may improve localization accuracy and resilience. We first develop a generic fusion-based CLoc framework, which can rely on various vehicle-to-everything (V2X) and embedded sensor technologies. We then apply this framework to the standard ITS-G5 Cooperative Awareness Messages (CAMs), and show that it is possible to benefit from neighboring position information and from received signal strength-based range estimates to enhance local accuracy. On this occasion, we also make concrete proposals to handle

messages/data asynchronism (through mobility-based predictions), as well as to reduce both complexity and V2V communication footprint (through links/neighbors selection, messages approximation and transmission control). Next, we extend this framework so as to integrate more accurate V2V measurements based on the impulse radio ultra-wide bandwidth (IR-UWB) technology, while dealing with fusion filter overconfidence and error propagation issues. Finally, under even more challenging conditions with GNSS depraved neighbors or in tunnel conditions, we considered the assistance of extra onboard sensors (inertial unit, wheel speed sensor, camera-based lane detector, etc.), as well as static road-side units (RSUs). The proposed framework and methodology show to typically improve the localization accuracy from 2 m to below 30 cm in 80% of the cases. The proposed framework has been tested analytically and through simplified simulations first, then on realistic mobility data, and finally on real data from a small scale field test.

Contents

List of Figures

List of Tables

Abbreviations

3G	third-generation
3GPP	3rd Generation Partnership Project
4G	fourth-generation
5G	fifth-generation
A-B	aggregate and broadcast
ACC	adaptive cruise control
ACF	autocorrelation function
ADAS	advanced driver-assistance systems
AEBS	advanced emergency braking system
AGNSS	assisted GNSS
AOA	angle of arrival
AP	access point
APIT	approximate PIT
AWGN	additive white Gaussian noise
BCRLB	Bayesian CRLB
BFIM	Bayesian FIM
BSA	Basic Set of Applications
BSS	basic service set
BTP	Basic Transport Protocol
C/A	coarse acquisition
C2C-CC	CAR-2-CAR Communication Consortium
CA	collision avoidance
CAM	Cooperative Awareness Message
CAP	contention access period

CCH	control channel
CDF	cumulative distribution function
CDMA	code division multiple access
CEN	Comité européen de normalisation
CFP	contention free period
CIR	channel impulse response
C-ITS	Cooperative-ITS
CLoc	Cooperative Localization
CRLB	Cramér-Rao Lower Bound
CSMA	carrier sense multiple access
C-V2X	cellular-V2X
CW	continuous waveform
D2D	device-to-device
DARPA	Defense Advanced Research Projects Agency
DCC	decentralized congestion control
DENM	Decentralized Environmental Notification Message
DGNSS	differential GNSS
DGPS	differential GPS
DM	differential measurement
DOP	dilution of precision
DR	dead reckoning
DSRC	dedicated short-range communications
ECEF	Earth-centered Earth-fixed
EDCA	enhanced distributed channel access
EKF	extended Kalman filter
EM	expectation—maximization
eNB	evolved Node B
ESP	electronic stability program
ETSI	European Telecommunications Standards Institute

LTE	Long Term Evolution
MAC	medium access control layer
MANET	mobile ad hoc network
MAP	maximum *a posteriori*
MCM	Monte Carlo method
MDS	multidimensional scaling
MEMS	micro-machined electromechanical systems
MKF	mixture Kalman filter
ML	maximum likelihood
MMSE	minimum mean squared error
mmWave	millimeter wave
MRR	medium-range radar
MS	mobile station
MSE	mean squared error
MTU	maximum transmission unit
NLOS	non line of sight
NTP	Network Time Protocol
OCB	outside the context of a basic service set
OFDM	orthogonal frequency-division multiplexing
OSI	Open Systems Interconnection
O-TDOA	observed TDOA
P2P	point-to-point
PDOA	phase difference of arrival
PDOP	position DOP
PDP	power delay profile
PDU	protocol data unit
PF	particle filter
PHY	physical layer
PIT	point-in-triangulation

PPP	precise point positioning
PS	pre-crash system
PVT	position, velocity, and time
RBPF	Rao-Blackwellized particle filter
RFID	radio frequency identification
RMS	root mean square
RMSE	root mean square error
RSSI	received signal strength indicator
RSU	roadside units
RTK	real-time kinematic
SAE	Society of Automotive Engineers
SBAS	satellite-based augmentation system
SF	superframe
SLAM	simultaneous localization and mapping
SOS	sum of sinusoids
SPS	Standard Precision Service
SRR	short-range radar
SUMO	Simulation of Urban Mobility
SVM	support vector machine
TDMA	time division multiple access
TDOA	Time difference of arrival
TDOP	time DOP
TOA	time of arrival
TOF	time of light
TS	time slot
TTFF	time-to-first-fix
UE	user equipment
UERE	user equivalent range error
UKF	unscented Kalman filter

ULA	uniform linear array
USDOT	US Department of Transportation
UWB	ultra-wide bandwidth
V2I	vehicle-to-infrastructure
V2V	vehicle-to-vehicle
v2X	vehicle-to-everything
VANET	vehicular ad hoc network
VDOP	vertical DOP
VMP	variational message passing
VO	visual odometry
VRU	vulnerable road user
V-SLAM	visual SLAM
WC	worst-case
WGS 84	World Geodetic System 1984
WLAN	wireless local area network
WLS	weighted LS
WSN	wireless sensor network
WSS	wheel speed sensor

Chapter 1

Introduction

1.1 Application Context

Over 1.2 million human losses globally reported each year make road traffic injuries the first cause of death among young people aged 15–29 and the ninth across all age groups[1]. In an attempt to redeem this, the automotive industry has been moving aggressively in the direction of Intelligent Transport Systems (ITS) applications, among which active safety systems[2], advanced driver-assistance systems (ADAS) and autonomous driving are some of the fastest-growing segments. Despite advances in active safety systems (e.g., brake assist and electronic stability program (ESP)) as well as ADAS (e.g., adaptive cruise control (ACC) and pre-crash systems (PSs)), the rate of injuries and fatalities has remained flat due to the increased number of vehicles, the total distance driven in average per driver per year, and system limitations in critical but common driving situations.

To improve the situation, road safety needs to go beyond the current active safety technologies mostly based on ADAS perception systems (e.g., radars, cameras, and lidars) towards proactive safety systems and automated environment monitoring. For this sake, vehicles need to cooperate, that is to say, they need to evolve from *perceptive* and *autonomous* systems into *perceptive*, *connected*, and thus *collectively smarter* systems. Cooperative Intelligent Transport Systems (C-ITS) (a.k.a. *connected vehicle technology* in the U.S.), which rely on vehicle-to-vehicle (V2V) and vehicle-to-infrastructure (V2I) communications (commonly known as vehicle-to-everything (V2X)) [1, 2, 9], are thus a key enabler. When compared to line of sight (LOS) perception sensors, V2X communi-

---

[1] http://www.who.int/mediacentre/factsheets/fs358/en/
[2] On the contrary, passive safety systems include airbags, seat-belts, and vehicle's specific structure.

cation can provide 360-degree awareness up to a kilometer, beyond physical obstructions or adverse weather conditions. More importantly, it can predict the intentions of monitored objects (e.g., neighboring vehicles, motorcycles, pedestrians, etc.) based on received data [1]. Thus, potential road hazards can be anticipated in a much earlier phase. Among the various possible communication technologies for C-ITS, the ITS-G5 (where G5 stands for the 5 GHz frequency band), sometimes abusively depicted as IEEE 802.11p, is currently the main standard in Europe, whereas the U.S. counterpart is called dedicated short-range communications (DSRC)[3].

1.2   Motivation and Objectives

The currently proposed C-ITS Basic Set of Applications (BSA) relies on the availability of Global Navigation Satellite Systems (GNSSs), which provide a positioning accuracy on the order of 3–10 meters in favorable conditions. This is obviously far from being sufficient for advanced C-ITS applications, such as advanced safety services, vulnerable road user detection and accident avoidance, or highly autonomous driving/platooning, which would require a sub-meter accuracy (typically less than 0.5 m -the minimum accuracy level for an autonomous vehicle to be on the right lane) in any operating condition. Such a level of accuracy is not yet available with mass market GNSS technologies (including Galileo), but requires instead expensive advanced dedicated GNSS technologies (e.g., real-time kinematic (RTK), precise point positioning (PPP) or even special differential GNSSs), with still unguaranteed performance in urban environments or under weak/no access to satellite constellations/sided infrastructure.

Instead, we believe we can reach the same level of accuracy through cooperative strategies between vehicles, or more specifically, considering techniques inheriting (or inspired) from a field of wireless localization known as Cooperative Localization (CLoc). While non-cooperative strategies consist in locating mobile nodes uniquely with respect to a set of fixed anchors at known locations, CLoc solutions make use of neighboring nodes (moving or static) as additional "virtual[4] anchors", for instance through distributed message-passing approaches. Such CLoc schemes have been mostly applied to static wireless sensor net-

---

[3]DSRC shall not be confused with CEN DSRC in Europe, which refers to a dedicated communication solution for toll roads.

[4]By "virtual", we mean that the locations of cooperating -possibly mobile- nodes are estimated too, and thus, imperfectly known (contrarily to "true" anchors).

works (WSNs) or even mobile ad hoc networks (MANETs) so far. Similarly in VANETs, vehicles could exchange location data with other vehicles in range (typically, their own position estimates or raw GNSS data), acquire range-dependent metrics over their respective V2V links, and finally fuse these different sources of information. A major advantage of CLoc in comparison with non-cooperative approaches is that it does not necessarily need the presence of fixed elements of infrastructure, nor any prior map containing predefined anchor nodes' locations (even though it could still integrate the latter information). CLoc in VANETs allows vehicles to exploit the (possibly better) positioning capabilities of their neighbors and accordingly, to enhance their own location estimates. Said differently, it benefits from other vehicles' data and measurements, and more generally, from information redundancy and diversity. However, even is CLoc yet remains a very promising approach to enhance localization, in particular in GNSS (partially) denied environments, it is also subject to novel and specific challenges, such as:

- Asynchronous transmission (Tx) events leading to unsynchronized received data from the "virtual anchors";

- High computational complexity and high traffic under exhaustive/systematic cooperation with all the available neighbors;

- Spatial and temporal correlations in sensor measurements;

- Highly dynamic and uncontrolled communication policies of connected vehicles, thus making CLoc in VANETs even more challenging in comparison with conventional CLoc (dedicated to WSNs or MANETs), in particular for a large amount of vehicles.

- Possible propagation of location errors among cooperative vehicles;

- Unfavorable geometry of the cooperative fleet topology, likely degrading localization accuracy along the dimension orthogonal to the road;

- Prolonged GNSS outages and/or unsustainable measurement error accumulation of inertial sensors over time (e.g., gyroscopes), leading occasionally to the fast divergence of position estimates in most pathological cases.

In this work, we ambition to answer the fundamental question "Can sub-meter localization accuracy be met through CLoc strategies between connected vehicles?" For this

sake, we propose to adopt the following research methodology with gradual complexity. After carefully analysis the mismatch between the CLoc needs and the capabilities of current V2V communication standards, we first develop and adapt a cooperative fusion framework based on the currently available ITS-G5 technology. In this phase, we notably assume GNSS availability, even if degraded. One step ahead, deviating from this (simplified) nominal setting, we consider the impact of V2V channel congestion and V2V communication reliability. We then extend our framework to additionally benefit from alternative V2V technologies for high accuracy ranging, and rely on advanced sensors and C-ITS infrastructure to improve performance in most pathological GNSS-denied environments. We finally enhance our proposal to mitigate model mismatch considering realistic mobility traces, and provide preliminary offline experimental validations, considering a small-scale field test.

1.3   Thesis Contributions and Outline

According to the previously described challenges and methodology, the main contributions of this thesis can be summarized as follows:

- The first contribution is a comprehensible review of state of the art contributions in the two fields of vehicular communications and vehicular localization. Focusing on the accuracy requirements from C-ITS applications, a gap analysis is also provided in order to figure out the suitable communication technologies, localization techniques, fusion architecture and algorithms for the CLoc approach, while pointing out related open challenges. This topic is addressed in Chapter 2.

- Based on this gap analysis, the second contribution is a generic CLoc framework adapted to the vehicular context. This contribution is detailed in Chapter 3 and led to conference paper [10] and journal paper [11].

- The third contribution consists in adapting the previous generic CLoc framework specifically to the ITS-G5 technology. We develop V2V CLoc through the standard Cooperative Awareness Messages (CAMs) based on data fusion. Since there could be numerous vehicles involved which are endowed with heterogeneous modalities, capabilities, and operating conditions, one challenge is the trade-off between accuracy,

complexity, and communications. Thus, we first build a link selection algorithm to identify the most informative neighbors. This contribution is also addressed in Chapter 3 and led to conference paper [10].

- Still regarding the same trade-off, the fourth contribution is to propose a new V2V communication strategy and message format to match the CLoc requirements under imposed V2V communication limitations and capabilities. Accordingly, the transmission control policy is then revised to optimize the communication footprint conditioned by the accuracy requirements. Besides, spatial correlations found in V2V measurements are also mitigated to maintain the accuracy level. This aspects is treated in Chapter 4 and led to conference paper [12] and journal paper [11].

- Fifth, one limitation of the first approach lies in the utilization of the signal strength associated with received CAMs. Hence, we propose a hybrid V2V CLoc scheme integrating accurate impulse radio ultra-wide bandwidth (IR-UWB) ranging capabilities. We first highlight that the unbalanced levels of uncertainty between GNSS and IR-UWB may lead to performance gain or loss depending on the data fusion algorithm. We then propose two enhancements to compensate for this drawback. This topic is detailed in Chapter 5 and led to conference papers [13, 14].

- Sixth, imperfect mobility knowledge and constrained mobility patterns causing harmful geometric effects are solved through hybrid V2X multisensor CLoc. Since information from individual sensors (e.g., inertial sensors, wheel odometry, and camera-based lane detector) or V2X communications affects each component of position error differently, we benchmark the performance of various combinations of these modalities in different environments including tunnels. This topic is addressed in Chapter 6 and led to conference papers [15, 16].

- Seventh, we validate this fusion framework under more realistic assumptions/constraints in terms of erratic vehicular mobility by exploiting traces from a dedicated simulator called SUMO (rather than regular steady-state synthetic models), while considering a mixed urban/sub-urban environment. First practical experiments are also carried out to validate the proposed theoretical solutions, based on real integrated platforms. This comparative study shows that a sub-meter accuracy is possible through CLoc

and gives practical guidelines to the system design and operation of reliable and accurate location services for C-ITS. This contribution is addressed in Chapter 7.

Finally, we conclude the thesis together with some remarks in Chapter 8.

Chapter 2

State of the Art in Vehicular Localization

2.1 Introduction

In this chapter, we start by introducing the Cooperative-ITS context including foreseen applications and communication technologies in Section 2.2. Then Section 2.3 provides an overview of vehicular localization systems, pointing out their main limitations and challenges. Finally, Section 2.4 provides a gap analysis to develop the CLoc framework in the next chapters.

Although we focus uniquely on the vehicular context in this chapter for the sake of conciseness, general comparative descriptions of radio-based localization metrics (along with their prefered underlying technologies/standards), localization algorithms and fusion architectures, are also available in Appendices C, B and D respectively. On this occasion, we detail the main advantages and drawbacks of the different solutions.

2.2 Cooperative-ITS

2.2.1 V2X Applications

As vehicles have been equipped with wireless communication capability to directly communicate with each other and with infrastructure, we envision an entirely new paradigm of applications. C-ITS applications will be a unique revolutionary way to detect and avoid accidents through the awareness of vehicles of their surroundings beyond the sensor
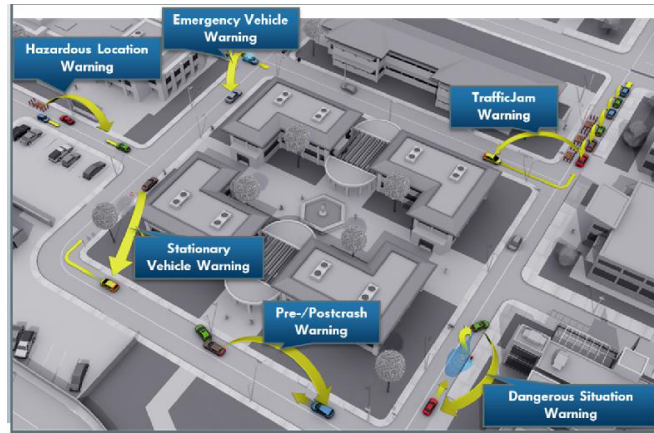
Figure 2.1: Examples of Day-1 applications and the scenarios V2V communications can address (Source: C2C-CC).

capabilities. Extensive list of potential applications/services are compiled and assessed by many projects, industry/government consortia [17]. Typically, C-ITS applications are classified as safety, transport efficiency, and infotainment applications. In the scope of this thesis, we only focus on C-ITS safety applications which require high accuracy localization.

Day-1 Applications

The objective of Day-1 applications is to increase the awareness for the drivers. To achieve this goal, each vehicle broadcasts periodically its status data (e.g. their position, speed, acceleration). Besides, they also broadcast situation-based information when an emergency situation is detected, e.g. an accident or if an emergency vehicle is in action. Figure 2.1 illustrates some typical Day-1 applications relying on V2V communications such as emergency vehicle warning, hazardous location warning, dangerous situation warning, etc. identified by CAR-2-CAR Communication Consortium (C2C-CC).

Day-2 and Beyond

Focusing on information exchange (between traffic participants), the C2C-CC applications roadmap envisions four main phases to deploy direct V2V communications, as illustrated in Figure 2.2. When moving from previous phase to subsequent phase, vehicles exchange more information, thus enabling new applications and classes of use cases [1].

- Phase 1: The initial awareness driving phase allows vehicles to broadcast their status data (i.e., position, speed, events) so that neighboring vehicles are aware of them and of hazardous events detected on the road.
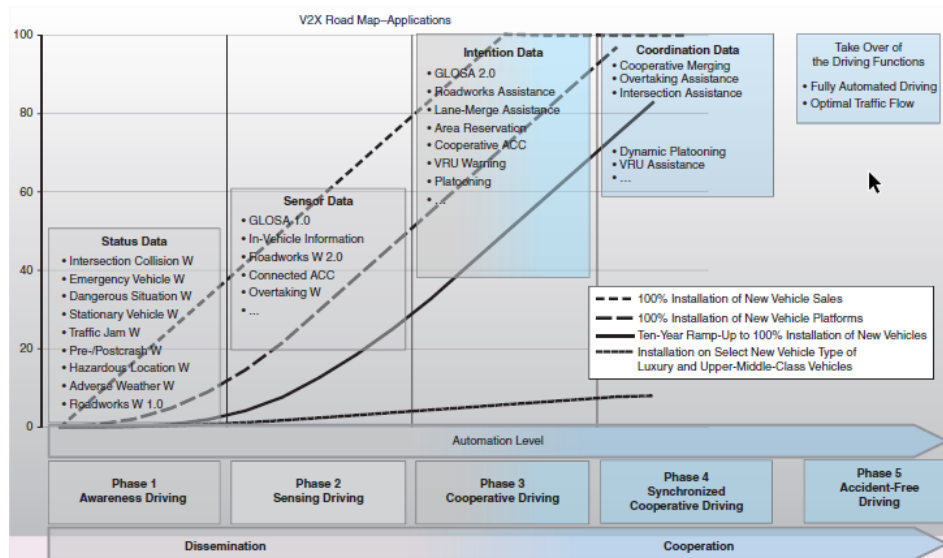
Figure 2.2: The C2C-CC applications road map.

- Phase 2: The sensing driving phase enables vehicles to disseminate their sensor data (i.e., detected objects, field of view obtained from the on-board sensors like cameras and radar). Thus vehicles can see with the eyes of others to detect hidden objects (e.g., around a corner) or enable a more accurate view of the environment (e.g., an intersection with various VRUs) [1].

- Phase 3: The cooperative driving phase allows vehicles to share their intention data (i.e., intention, trajectories). This information is used to predict the behaviors of another vehicle or a pedestrian, and thus optimize the vehicles' decision and maneuvers.

- Phase 4: The last synchronized driving phase (levels 4 and 5 in Figure 2.2) happens when vehicles exchange coordination data (i.e., synchronized trajectories) to achieve fully automated driving and optimal driving patterns.

When reviewing this roadmap, one may question whether there are special requirements on localization accuracy for higher automation levels. Table 2.1 summaries the localization requirements for C-ITS applications. For instance, in the cooperative driving phase (i.e., phase 3), the prediction vehicles' behaviors requires lane-level or even higher where-in-lane-level localization accuracies. Otherwise, a vehicle is not certain of what other vehicles will behave in the next several seconds, especially when they are close to each other. Thus, it is implied that from Day-2, each vehicle is equipped with high accuracy localization service at least at sub-meter level.

Table 2.1: Localization requirements for C-ITS applications (Dempter, 2014).

Type	Level	Accuracy requirement 95%	RMSE	Communication latency
V2V	road-level	5	meter	0.1
	lane-level	1.5	sub-meter	0.1
	where-in-lane-level	1	decimeter	0.01–0.1
V2I	road-level	5	meter	1–5
	lane-level	1.1	sub-meter	1
	where-in-lane-level	0.7	decimeter	0.1
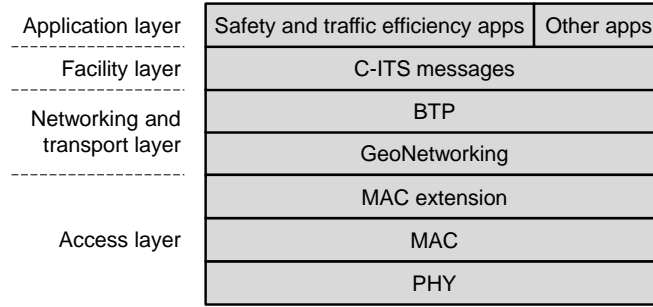
Figure 2.3: The C-ITS protocol stack (partial reproduction of [1,2]).

2.2.2   V2X Messages and Services

C-ITS Protocol Stack

The C-ITS protocol stack for vehicles and RSUs contains four layers as illustrated in Figure 2.3.

- The access layer combines the physical and data link layers in the open systems interconnection model (OSI model).

- The networking and transport layer provides new protocols for routing and addressing in VANETs called GeoNetworking with Basic Transport Protocol (BTP).

- The facility layer contains C-ITS messages to enable application functionality.

- The application layer is not fully standardized [2].

CAM and DENM

The ETSI standard allows nodes to communicate via two major types of messages: Cooperative Awareness Messages (CAMs) and Decentralized Environmental Notification Message (DENMs). CAMs are distributed within the V2V or V2I network by vehicles and RSUs.
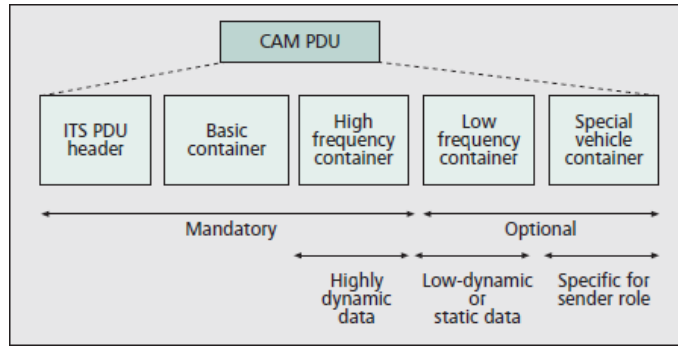
Figure 2.4: CAM structure (ETSI EN 302 637-2).

CAM   CAMs are periodic messages that broadcast status (e.g., position, speed, acceleration/braking information) to neighbors within a single hop distance in order to improve the awareness for the drivers. If CAMs are sent by an RSU, these include the basic attributes of the RSU. Relevant use cases, which benefit from CAM, are collision risk warning, intersection collision warning, emergency vehicle warning, slow vehicle indication, etc.

CAMs are transmitted at frequency ranges between 1–10 Hz, depending on the vehicle dynamics (e.g. change of position by 4 m, speed by 0.5 m/s, and heading by 4°), application, current channel load, and decentralized congestion control (DCC) parameters. Average the CAM size is between 300–800 bytes, depending on the content, including all security trailers. As illustrated in Figure 2.4, a CAM is constructed by an ITS protocol data unit (PDU) header and a set of containers. The position is carried in the basic container while the speed and the heading are stored in the high frequency container. Low frequency container can carry optional and larger data such as path history. Finally, the special vehicle container enables a flexible message format for specific needs, while minimizing the channel load.

DENM   DENMs are event-driven short messages that broadcast to alert road users of changes in vehicle behavior (or infrastructure status) that violate the continuity implied by periodic CAMs. When detecting an event, vehicles immediately geo-broadcast a DENM to all vehicles in a relevant area and possibly over multihop. The DENM transmission is repeated with a certain frequency and certain range depending on the event, and persists as long as the event is present to ensure that vehicles entering the relevant area later can receive the information [2, 18].

Relevant use cases, which benefit from DEMNs, are emergency electronic brake light,

collision risk warning, road adhesion, hazardous location, etc. Besides, DENMs can also be used for traffic efficiency use cases, such as road-work warning, traffic condition warning, etc.

Local Dynamic Map

In the previous section, the CAMs and DEMN provides information about the local environments. This information has to be stored for multiple applications leading to the idea of local dynamic map (LDM). Standardized by ETSI, LDM is a conceptual database in an ITS station (vehicle) and manges topographical, positional and status information related to ITS stations within a geographic area surrounding the host station [7]. It consists of 3 layers from low level to high level as follows:

- Transient static data (e.g., roadside infrastructure);

- Transient dynamic data (e.g. weather situation, traffic information);

- Highly dynamic data (e.g., CAMs).

2.2.3   V2X Technologies

We have identified various potential C-ITS applications enabled by V2X communications. Future connected vehicles will be equipped with various communication technologies and protocols. One key challenge is to select or to develop an appropriate communication technology that can meet the diverse application requirements in different countries following different traffic rules and legal frequency bands. In this section, we provide an overview of the currently available technologies and protocols for the communication subsystem and performs a gap analysis with respect to the system requirements. Several candidates have been considered for vehicular V2V/V2I communications including non-specific personal area networks (e.g., Bluetooth and ZigBee) or even future 5G technologies (e.g., mmWave). However, V2X communications is based on one of two main technologies: IEEE 802.11p/ITS-G5/DSRC and cellular networks.

IEEE 802.11p/ITS-G5 (known as DSRC in the U.S.)

IEEE 802.11p provides the physical (PHY) and medium access control (MAC) layers of the protocol stack for ITS-G5 in Europe [19] and DSRC in the U.S. [20]. This technol-

ogy is derived from the most widely used IEEE 802.11 (WiFi) technology with specific amendments for vehicular communications.

The PHY layer of the ITS-G5 is based on an orthogonal frequency-division multiplexing (OFDM) from IEEE 802.11a standard but operates in 10-MHz channels instead of the original 20-MHz channels [7, 17, 21, 22]. Hence, data rate is limited in the range of 3 Mbps to 27 Mbps. The data rate of the main safety channel, referred to channel 178 (5.9 GHz) called control channel (CCH) in Europe or channel 172 (5.86 GHz) called collision avoidance safety channel in the U.S., is 6 Mbps [17]. The typical line of sight (LOS) range is from 300–1000 m, but the main purpose is to provide 360-degree non line of sight (NLOS) awareness that cannot be achieved by ADAS sensors such as radar, lidar and camera. To increase coverage, multi-hop communication such as GeoNetworking in the European C-ITS protocol stack is available [22].

The MAC layer is based on an enhanced distributed channel access (EDCA) of IEEE 802.11e standard, which uses carrier sense multiple access (CSMA) with collision avoidance (CSMA/CA) and four MAC queues for prioritizing traffic [17]. To cope with highly dynamic and frequently fragmented network, vehicles can transmit messages directly and immediately without delays for exchanging control frames through a new operational mode called outside the context of a basic service set (BSS) or OCB mode. As there is no centralized coordinator to schedule transmissions between vehicles, a decentralized congestion control (DCC) strategy is used to control the channel congestion and the communication quality and fairness. It is done by adjusting Tx power, Tx rate, and Tx modulations. The European version only controls the rate to vary between 10 Hz and 2 Hz according to the channel load where the US version (SAE 2945.1) is more complex, as it adjusts the Tx power and the Tx rate according to the channel load and the number of neighbors.

Though many discussions are undergoing at standardization bodies related to selecting the best communication technologies for V2X communications, the technology of choice has been IEEE 802.11p, which is the only one currently available, fully tested and actually under deployment in the U.S.[1], Japan[2], and in Europe[3]. It is expected that all new vehicles sold on the U.S. market will be equipped with DSRC starting from 2019, and similarly on

---

[1]In 2015, V2X pilot projects for IEEE 802.11p was funded by the USDOT in three cities including over ten thousand vehicles implementing diverse applications and an investment of more than $45 million according to `https://www.its.dot.gov/pilots/`.

[2]Toyota has installed IEEE 802.11p to approximate 100000 cars [23].

[3]Volkswagen publicly announced the selection of IEEE 802.11p to support V2X applications in `https://www.volkswagen-media-services.com` on 28 June 2017.

the European market thereafter [7].

4G LTE V2X

Long Term Evolution (LTE) is the fourth-generation (4G) technology for cellular networks. The 4G systems have theoretical data rates of 100 Mbps for high mobility communications (e.g., trains and cars). Standard cellular systems such as 3G and beyond 3G are promising candidates for V2I communications, but still cannot support V2V communications that are at the heart of the C-ITS applications [21]. To answer this urgent call, in 2017, 3rd Generation Partnership Project (3GPP) group has introduced LTE sidelink or device-to-device (D2D) communications under Release 14 including two new communication modes (mode 3 and mode 4) specifically designed for V2V communications.

- Scheduled resource allocation (mode 3) in which evolved Node B (eNB) schedules the radio resources. This mode is only available when in coverage.

- Autonomous resources selection (mode 4) in which user equipment (UE) randomly selects the radio resources from a (pre)configured resource pool.

Within the context of safety-related communications, mode 4 is currently the only valid strategy for safety-critical V2X communications due to required awareness of any LTE UEs (vehicles) without the availability of cellular coverage.

5G mmWave V2X

Millimeter wave (mmWave) spectrum in the range of 30–300 GHz is occupied by military, radar and backhaul [24]. Given possibly large spectrum availability, mmWave enables access to very large bandwidth communication channels, leading to gigabit data rates and millisecond latency. Historically, the mmWave bands were limited in use due to their inherent high propagation path losses and lack of low-cost commercial hardware, among other reasons [7]. With rapid advances in mmWave circuitry and the foreseen increased network densification (smaller cell sizes), mmWave technology finds myriad applications e.g., fifth-generation (5G) cellular connectivity. In 5G technology, mmWave plays an important role in augmenting the currently saturated radio spectrum bands for wireless communications. Then mmWave V2X communications are enabled through 5G systems i.e., 5G base stations serve as infrastructure for V2I communications, and 5G D2D mode

supports V2V communications [25]. Although mmWave technology is appealing with high data rates, it also still faces numerous open challenges, mostly at the PHY layer level (e.g., beam alignment rapidity under high mobility scenarios, low-cost hardware integration of agile antenna systems, multi-user tracking, short transmission ranges, etc.). For specific mmWave V2X communication systems, three main problems are identified in [25] i.e., accurate mmWave vehicular channel models, market penetration rate of mmWave V2X-capable vehicles, and simple and fast mmWave beam alignment algorithms for vehicular communications.

2.3 Vehicular Localization and Navigation Systems

2.3.1 Satellite-Based Localization

Due to the universal availability of satellites and large penetration into the mass market, Global Navigation Satellite Systems (GNSSs) have become a *de facto* standard solution for outdoor positioning, especially for vehicle navigation. A GNSS refers to a constellation of multiple artificial satellites transmitting signals from space encoding navigation messages to enable the GNSS receivers to determine locations. Currently, the American NAVSTAR Global Positioning System (GPS) and the Russian Globalnaya Navigatsion-naya Sputnikovaya Sistema (GLONASS) are the only available GNSSs[4]. The European Galileo is in the process of launching and is expected to be fully operational by 2020. The three systems will be compatible with each other allowing GNSS receivers to work with Galileo, GPS and GLONASS simultaneously. In this section, we briefly present the most popular GPS system. Other GNSS systems are conceptually similar to the GPS but have several differences. More details about these systems can be found in many textbooks.

The GPS system consists of three major segments [4, 26–28]:

- The space segment consists of a constellation of 24 satellites orbiting at an altitude of about 20200 km and transmitting radio signals to users on shared L1 (1575.42 MHz), L2 (1227.60 MHz), and L5 (1176.45 MHz) frequencies for different applications based on code division multiple access (CDMA). Each satellite transmits different codes such as coarse acquisition (C/A) codes for public use and encrypted precision (P) codes or P(Y) codes for military uses.

---

[4]The Chinese BeiDou, the Indian IRNSS, and the Japanese QZSS are still regional services at the time this thesis is being written.

- The control segment consists of ground-based networked facilities of monitor stations, master control stations, and ground antennas for monitoring the satellites' signals and status, performing analyses, and transmitting orbit and time corrections to the space segment, respectively.

- The user segment consists of a GPS receiver equipment capable of receiving the signals from the GPS satellites and processing the encapsulated information to determine its 3-D position and time information.

GNSS positioning relies on the principle of trilateration, which is a technique of determining the position of a target by measuring its distances from known position marks (i.e., known position satellites herein). The GNSS receiver measures at least four ranges to four satellites, three for calculating the 3-D position and the fourth for correcting receiver clock error. The latter time synchronization is indispensable as the GNSS receiver determines the propagation time by correlating the satellite-generated ranging code with the receiver-generated replica code. This propagation time is transformed into a "pseudorange" after being simply multiplied by the speed of light. Yet the pseudorange does not match the geometric range due to several error sources as follows [26]:

$$\rho_u^i = R_u^i + c\delta_u + c\delta^i + \varepsilon^i + \zeta_u^i, \tag{2.1}$$

where ρ_u^i is the pseudorange between receiver u and satellite i, R_u^i the geometric distance between them, c the speed of light, δ_u the clock error of receiver u, δ^i the clock error of satellite i, ε^i the error due to ionosphere, troposphere, and orbit of satellite i, and ζ_u^i the effect of thermal noise in receiver u and multipath error of satellite i. And $R_u^i = \sqrt{(x_i - x_u)^2 + (y_i - y_u)^2 + (z_i - z_u)^2}$, where (x_u, y_u, z_u) is the position of receiver u and (x_i, y_i, z_i) is the position of satellite i using the ephemeris data encapsulated in the navigation messages. The position of the receiver can be estimated by iterative LS or EKF and is given in an Earth-centered Earth-fixed (ECEF) system, which can be transformed to World Geodetic System 1984 (WGS 84) in the form of latitude, longitude, and height [26].

Generally, the accuracy of the position estimation depends on both the pseudorange error (aka user equivalent range error (UERE)) and the user/satellite geometry (aka dilution of precision (DOP)) [4, 26–28]. On the one hand, the UERE comprises common and

Table 2.2: Standard deviations of range measurement errors in a single-frequency GPS receiver [4].

Contributing source	Standard deviation [m]
Common error	
Satellite clock error	2
Ephemeris error	2.5
Ionospheric delay	5
Tropospheric delay	0.5
Noncommon error	
Receiver noise	0.3
Multipath	1
Total (root sum squares)	6

noncommon errors. Common mode errors are highly correlated among receivers separated by baselines up to 200 km and are caused by satellite clock error, ephemeris error, and atmospheric effects (i.e., ionosphere and troposphere delays). Noncommon errors depend on environment and receiver hardware/software and are caused by multipath and receiver noise, respectively. The typical standard deviation of these errors for a single-frequency GPS receiver in Standard Precision Service (SPS) is given in Table 2.2. From the table, ionosphere error is dominant for single-frequency receivers. Dual-frequency equipment in Precise Positioning Service (PPS) can nearly completely remove this atmospheric error leading to a smaller pseudorange error budget of about 1.5 m [26].

On the other hand, when the satellites are clustered in a smaller region, the area of overlap of the signals (i.e., the area of uncertainty) is larger as illustrated in Figure 2.5. For this reason, error propagation from pseudorange estimates to position estimates is as follows

$$\text{cov}(\widehat{\mathbf{x}}_u) = \mathbf{D}\sigma_{\text{UERE}}^2, \tag{2.2}$$

where $\text{cov}(\widehat{\mathbf{x}}_u)$ is the covariance of estimated state vector $\widehat{\mathbf{x}}_u = [\widehat{x}_u, \widehat{y}_u, \widehat{z}_u, \widehat{\delta}_u]^\dagger$ whose the first three components are the estimated 3-D position and the last is the estimated clock error, σ_{UERE}^2 the standard deviation of the UERE (e.g., in Table 2.2), and $\mathbf{D}$ a 4×4 symmetric matrix translating UERE to each component of $\text{cov}(\widehat{\mathbf{x}}_u)$. From this formula, different DOP variants are defined including Geometry DOP (GDOP), Position DOP (PDOP), Horizontal DOP (HDOP), Vertical DOP (VDOP), and Time DOP (TDOP) [4, 26–28]. By using multiple constellations, the DOP can be improved resulting in better positioning and timing accuracies. It is worth noting that this principle will be reused in Section 3.5 for the selection of vehicular links.
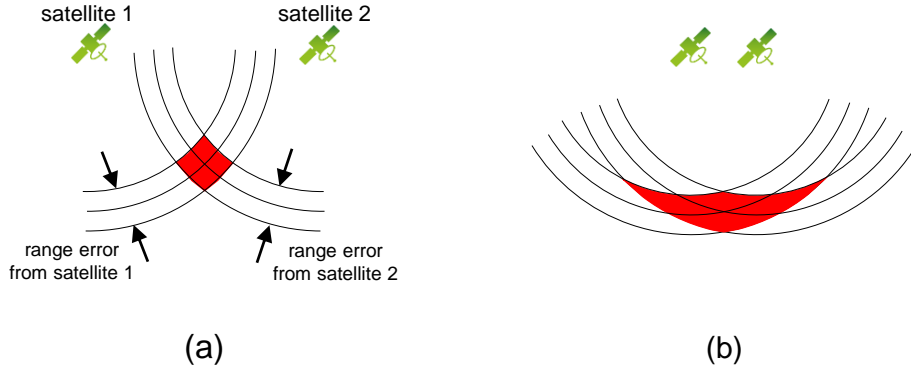
Figure 2.5: Effect of DOP in satellite-based positioning systems.

GNSS Augmentations

GNSS augmentations are techniques that enhance accuracy, robustness, and reliability by integrating external information in the position estimation. A number of techniques are briefly reviewed below.

Differential GNSS Differential GNSS (DGNSS) uses a network of ground-based reference stations to broadcast the differential corrections to the common pseudorange errors such as ionosphere and troposphere errors to the users (rovers) in local region. DGNSS accuracy decreases as the distance from the reference station increases. An accuracy of about 1 m can be achieved for users in the range of few tens of kilometers from the reference station [4]. However, this accuracy is only possible within much shorter baselines in dense multipath environments such as urban areas because multipath error decorrelates very quickly.

Real-time kinematic Real-time kinematic (RTK) in principle is a carrier-phase DGNSS. The carrier-phase of GPS signal is modeled as

$$\varphi_u^i = \frac{1}{\lambda}R_u^i + \frac{c}{\lambda}\delta_u + \frac{c}{\lambda}\delta^i + \frac{1}{\lambda}\varepsilon^i + N_u^i + \varsigma_u^i, \tag{2.3}$$

where φ_u^i is the carrier phase of the signal received from satellite i by receiver u, λ the wavelength of the GPS signal, ς_u^i the carrier phase observation noise, N_u^i the integer ambiguity, which corresponds to the number of cycles between the receiver and satellite when phase tracking starts. The carrier wave for the GPS signal is about 19 cm (for L1) enabling centimeter-level ranging accuracy [4]. The configurations of DGNSS and RTK

in terms of deployment and architecture are similar as both systems require a reference station (base) to broadcast differential corrections to a user (rover) through communication links. The difference is that the noise of carrier-based ranging is much smaller than that of the code-based one in the DGNSS. Yet, integer ambiguity resolution in (2.3) has to be fixed and this processing can take time from seconds to minutes. The RTK can be used for baselines of up to 50 km, yielding positioning errors inferior to 10 cm [4]. In case of frequent GNSS signal blockage, RTK is not appropriate because the rover has to track the GNSS signals continuously to avoid reinitialization.

Precise point positioning   Precise point positioning (PPP) requires a network of reference stations located worldwide to generate the satellites clock and orbit corrections to users via satellites. Together with a dual-frequency GNSS receiver (to remove the first order effect of the ionosphere), PPP provides positioning accuracy of a decimeter or even better [4]. When compared to the RTK, the PPP does not depend on a base station, thus provides full accuracy given satellites availability (i.e., a global positioning approach) at the price of very long and uncontrolled convergence time up to 30 minutes in case of cold start from scratch. Both RTK and PPP use carrier-based techniques.

Satellite-based augmentation systems   The satellite-based augmentation system (SBAS) uses geostationary (GEO) satellites to broadcast corrections to users in wide areas, even at continental scale. The system includes several reference stations that monitor and collect data from GNSS satellites, before relaying to its master stations to compute integrity and differential corrections. This information is then uplinked to the GEO satellites then relayed to the SBAS users. Thus, the SBAS improves the integrity by detecting erroneous measurements very quickly, as well as accuracy and availability by providing the differential corrections and extra GEO range measurements [4, 26]. When compared to DGNSS, the SBAS yields similar accuracy but better integrity. Besides, the SBAS does not need any base stations. When compared to PPP, both receive corrections from satellites. Yet, the PPP is more accurate than the SBAS, because the PPP is a carrier-based method whereas the SBAS system is a code-based one.

Assisted GNSS   Assisted GNSS (AGNSS) uses a cellular network to reduce the time-to-first-fix (TTFF) which is the actual time required by a GNSS receiver to achieve a position

estimation and thus improve the startup performance i.e., saving at least 30 seconds [29]. Nowadays AGNSS is extensively used in GNSS-capable cellular phones. There are two types of AGNSS [29, 30]:

- Mobile station (MS)-based: Assistance information (almanac and ephemeris) is sent to the handset to acquire satellites more quickly.

- MS-assisted: Assistance information (timestamped pseudoranges) is sent to the network server to calculate the position.

2.3.2   Sensor-Based Localization

Dead Reckoning and Integrated Systems

Dead reckoning (DR) computes the current position based on the previous position by either measuring the change in position or measuring the velocity and integrating it [27]. DR can be implemented in various configurations depending on the employed sensors. If only involving inertial sensors aka inertial measurement unit (IMU) (typically combining three orthogonal gyroscopes and three orthogonal accelerometers), DR refers to inertial navigation. We first give an overview of several sensors commonly found in existing automotive navigation systems. It shall be noted that the list is far from being exhaustive. A more complete but still comprehensive survey can be found in [27, 31].

Gyroscope   The gyroscope (aka gyro) measures angular velocity in a particular axis. A change in vehicle's heading is then obtained by integrating the gyroscope's output. Errors that appear in a typical gyro's output include noise, a (time-varying) bias, scale factor error, g-sensitivity, and cross-axis sensitivity [32, 33]. The scale factor and fixed bias are deterministic by nature and can be calibrated at sensor level [33, 34]. The bias instability refers to bias drift, typically modeled as a random walk [33, 35]. The thermal noise and the bias instability result in angle random walk regarding the angle information and second-order random walk in the integrated signal respectively. The error characteristics strongly depend on the type of gyroscopes, which are commonly among mechanical, optical, and micro-machined electromechanical systems (MEMS) gyroscopes.

Accelerometer   The accelerometer measures specific forces along an axis, thus providing information about the acceleration of the host vehicle. The main sources of error for

MEMS accelerometers are similar to those for gyroscopes. The important difference between errors arising from accelerometers is that they are integrated twice in order to track position, whereas rate-gyro signals are only integrated once to track orientation [33]. An accelerometer can be classified as mechanical, solid state, or MEMS devices whose error characteristics are different from one another.

Odometer The odometer measures the rotation of the wheels a vehicle, thus providing the speed and traveled distance. If a couple of odometers are placed on the two rear or front wheels, or on the wheels on either side of a vehicle, heading change of the vehicle can be estimated by differencing the wheel speeds.

Then the process of DR (and inertial navigation) can briefly be described as [33, 36]:

- The 2-D/3-D orientation, or attitude of the vehicle (with a body frame attached to it) relative to a global frame in which we are navigating is tracked by using a gyroscope, a digital compass, or a differential odometer.

- The orientation information is then used to project the body frame acceleration, velocity, or traveled distance into the global frame of reference.

- The traveled distance, velocity, or acceleration are then integrated over time to obtain position and velocity estimates in the global frame of reference.

This integration also accumulates the errors of the sensors resulting in a positioning error that grows unbounded over time and traveled distance. For an INS, uncorrected biases in the accelerometers and gyroscopes cause errors in position, which grows proportionally to the square and cube of time respectively [36]. In addition, an initial alignment (position and orientation) must be provided and could be challenging and expensive especially for orientation (e.g., magnetometer, dual GNSS antenna, gyrocompassing). However, the advantages include high-bandwidth output (50–1000 Hz), self-contained navigation without an external information subject to disturbance or blockage, and high accuracy in terms of relative positioning in the short term.

GNSS/INS Fusion When compared to the INS, GNSS provides position and velocity estimates with bounded errors, has low output rate (typically 4–10 Hz), and depends on external sources. The pros and cons of the INS and the GNSS are complementary, so in
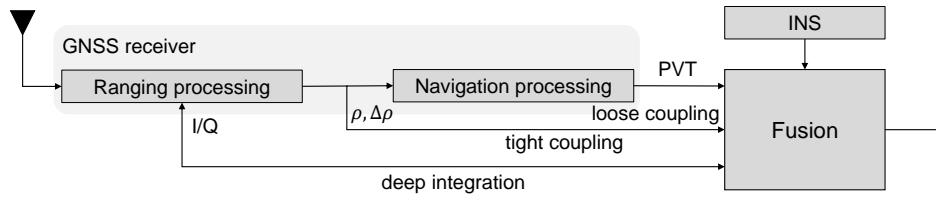
Figure 2.6: Integrated GNSS/INS system architectures.

practice, they are usually integrated into a single solution. In an integrated GNSS/INS, GNSS prevents the INS from drifting, while the INS smooths the GNSS and bridges signal outages [27]. There are three most common architectures for integrating INS and GNSS, and they mainly differ on the type of information shared between individual units as illustrated in Figure 2.6.

- In loosely coupled GNSS/INS, the INS and GNSS function independently. The outcomes of the two systems are then fused to produce a third solution. The fusion is performed at the position, velocity, and time (PVT) level.

- In tightly coupled GNSS/INS, the INS and GNSS are reduced to their basic sensor functions. Specifically, pseudoranges, pseudorange rates, acceleration, and angular velocity are combined into single solution.

- In deep integration (aka ultra-tightly coupled), the architecture of the GNSS is fundamentally different from the conventional architecture in such a way that the INS is now a part of the GNSS architecture but not a separate system. This architecture integrates in-phase (I) and quadrature (Q) components from the correlator of the GNSS with the INS data.

In summary, when moving from the loose to the deep integration architectures, one gain accuracy and robustness at the expense of sacrificing system simplicity, redundancy, and independence of the INS and GNSS [28]. Particularly comprehensive studies about real-time integration of these architectures can be found in Petovello's Ph.D. thesis [37] which uses tactical-grade IMU and in Godha's Ph.D. thesis [38] which uses low cost MEMS-based IMU for land vehicle navigation.

Perception Systems

Radar   Radio detection and ranging (radar) has been massively deployed in the automotive industry for the detection of objects and obstacles, as well as for the estimation

of their positions, speeds, and azimuth-elevation angles relatively to the equipped vehicle. Automotive radars are typically operating at mmWave frequencies, most often at in 24 GHz and 77 GHz to achieve high range and velocity resolutions [5, 39]. Radar simultaneously transmits and receives a special waveform, typically a pulsed continuous waveform (CW) or frequency modulated continuous waveform (FMCW)[5], to extract information about neighboring vehicles or obstacles out of received waves (i.e., back-scattered waveforms) [5, 39]. In principle, the range to a target is determined based on the round-trip time delay whereas the estimation of the target velocity is based on the Doppler effect. Besides, the direction estimation can be made by means of an antenna array enabling electronic or mechanical beam steering. Automotive radar sensors can be classified based on their operating ranges: long-range radar (LRR) (10–250 m range) for ACC and AEBS; medium-range radar (MRR) (1–100 m range) for cross-traffic alerts, lane-change assist, rear-collision warning, and blind spot detection; and short-range radar (SRR) (0.15–30 m range) for parking aid, obstacle detection, and precrash [39]. Table 2.3 provides examples of commercialized automotive radar systems. Radar is robust in almost all environmental conditions. However, data association problems are challenging in certain detection and tracking scenarios.

Hammarsten *et al.* [40] uses SRR for vehicle localization and mapping. First, a 3-D occupancy grid map of the static environment is developed using DGPS and radar. Next, a vehicle driving through the same area can be located by map matching with new radar measurements. Rao-Blackwellized particle filter (RBPF) or maximum likelihood (ML) estimator can then be used as localization method. Localization accuracies within 0.3 m are observed in most estimates on both simulation and real data. However, 3-D occupancy grid map, which requires significant computational expenses, is the main drawback of this work.

Ward *et al.* [41] also use SRR to localize a vehicle based on iterative closest point (ICP) scan matching against saved radar data from a previous pass through the same road. These ICP matches are inputed as vehicle state measurements in an EKF. This approach does not require large amounts of mapping data to be processed offline as in [40].

Recently, MIT's Lincoln Laboratory has developed a novel ground-penetrating radar that maps underground geological features in order to provide autonomous vehicles with

---

[5]Other radar waveforms are compared and summarized in [39].

Table 2.3: Examples of commercialized automotive radar systems [5].

Sensor	Frequency	Bandwidth	Range	Azimuth angle	Accuracy	Cycle
Bosch LRR3	77 GHz	1 GHz	250 m	$\pm 15°$	0.1 m, 0.12 m/s, -	80 ms
Delphi ESR	77 GHz	-	174 m	$\pm 10°$	1.8 m, 0.12 m/s, -	50 ms
Continental ARS30x	77 GHz	1 GHz	250 m	$\pm 8.5°$	1.5%, 0.14 m/s, 0.1°	66 ms
SMS UMRR Type 40	24 GHz	250 MHz	250 m	$\pm 18°$	2.5%, 0.28 m/s, -	79 ms
TRW AC100	24 GHz	100 MHz	150 m	$\pm 8°$	-, -, 0.5°	-

real-time localization in all-weather conditions [42]. The radar data of subterranean objects are recorded along with GPS tags to build the subsurface map. This map is then used for online vehicle localization. Cross-track accuracies of 4.3 cm (rms) at speeds up to 100 km/h during a night-time snow-storm are achieved.

Lidar   Light detection and ranging (lidar) is a laser-based ranging system that measures the time of flight (TOF) of light pulses reflected by objects in a similar fashion as radar. Such lidar equipped with a spinning platform, known as laser scanner, and mounted on top of a vehicle enables a 360-degree field of view. Specifically, the result is a dense point cloud providing a 2-D or 3-D map of the environment. Lidar has been mostly devoted to high-definition mapping and cartography applications so far. Over a decade since the 2005 DARPA Grand Challenge and the 2007 DARPA Urban Challenge, lidar has been preferred enabler of ADAS and semi-autonomous/autonomous driving systems. They have been used for detecting other vehicles, objects, VRUs, road borders, etc. as well as localization and mapping with very high accuracy (1–10 cm for 10–50 m ranges) regardless of day or night operations [6]. Nevertheless, main limitations include weather sensitivity [5], slow scanning repetition rates when compared to its rival camera systems, and limited operating range (typically 10–50 m for centimeter accuracy). The cost of lidar systems is notoriously too high for mass market deployment, though largely depending on application requirements. Although many manufactures are delivering low-cost devices to replace the most recognized 75000$ 64-beam Velodyn HDL-64E on the rooftop of Google's self-driving cars, these devices come with some reduced features (e.g., fewer beams, shorter range, narrower field of view to address less demanding applications) which cannot be used for high-accuracy localization and mapping. The characteristics of some commercialized automotive lidars are summarized in Table 2.4.

As an example, Levinson *el al.* [43] fuse 3-D lidar, GPS, IMU, and wheel odometry data to produce a offline high-resolution map of the environment, including characteris-

Table 2.4: Examples of commercialized automotive lidar systems [5].

Sensor	Dim. resolution	Range	Azimuth angle	Accuracy	Cycle
Quanergy M8-1	3-D	150 m	360°	0.05 m, -, 0.03°	33 ms
Ibeo LUX	2-D	200 m	110°	0.1 m, -, 0.125°	20 ms
Continental SRL1	2-D	10 m	27°	0.1 m, 0.5 m/s, 0.125°	10 ms
Velodyne HDL-64E S2	3-D	120 m	360°	0.02 m, -, 0.09°	50 ms

tic static features. Online vehicle localization is performed by correlating current lidar measurements with this map in a PF framework. The system significantly outperforms conventional GPS-IMU-odometry-based methods in terms of relative accuracy. This work is extended in [44] using probabilistic maps with higher precision, learning to update the map over time, and increased robustness to dynamic environments. A myriad of papers about lidar-based localization for road vehicles are reviewed in [45].

Visual camera Visual camera senses environment through pixel analysis and can capture and interpret high-level information (e.g., color, texture, and contrast) for classification and thus, for scene understanding. Today, cameras are equipped in high-class vehicles for ACC, traffic sign recognition, lane keeping assistance, and object detection (pedestrians, vehicles, etc.) [5, 6]. However, visual camera is an angle sensor without depth information so that range and range rate from an object in the environment cannot be directly derived from a single 2-D image from a single (monocular) camera. The unknown depths can be estimated by comparing frames captured at different times and at different positions (of the vehicle). On the other hand, an additional depth sensor (e.g., laser rangefinder, infrared depth sensor) or a stereo camera can directly infer the distance information to viewed objects, which is of the highest importance to automotive applications. The latter system with two visual cameras operates in the same way as humans with two eyes. Generally, 3-D information can be constructed from 2-D images captured by multiple cameras. However, when compared to radar, lidar, and TOF camera, the ranging error of visual camera is superior [5, 6] and increases with distance [46]. For example, errors of 6.44% at 5–80 m distances are achieved with monocular cameras in [47] whereas smaller errors of around 1% at 10–95 m distances are claimed with a stereo camera in [48]. Therefore, vision systems are usually paired with radar or lidar in various ADAS. For the range rate which is required in visual ACC, it has to be estimated by differentiating the ranges. Again, similarly to human eyes, visual cameras are sensitive to

Table 2.5: Usual characteristics of visual camera systems for automotive applications [5,6].

Resolution	Range	Azimuth angle	Attitude angle	Accuracy	Cycle
640×480	3–50 m	50°	40°	-, -, 0.1°	15–25 fps

adverse weather conditions (e.g., fog, rain) and variations in lighting (e.g., poor lighting or strong head lighting of approaching vehicles). Table 2.5 summarizes the general vision system characteristics.

Visual odometry (VO) and visual SLAM (V-SLAM) techniques are dominant in visual localization. The VO first introduced by Nister *el al.* in [49] estimates the vehicle's motion using a sequence of images of the environment captured by monocular or stereo cameras attached to it. A complete survey of VO systems is provided in [50]. The key difference between the VO and the V-SLAM is that the VO only cares about the local consistency of the trajectory while the V-SLAM is concerned with the global map consistency [50]. MonoSLAM presented by Davison *el al.* in [51] is the first V-SLAM algorithm which uses a monocular camera. Based on a probabilistic feature-based map, the method tracks both the estimates and the uncertainty of the state of the camera/vehicle as well as that of all the detected features by an extended Kalman filter (EKF). A survey of V-SLAM algorithms from 2010 to 2016 is presented in [52].

2.3.3   Infrastructure-Based Localization

Static elements of the road infrastructure, such as WiFi access points (APs), RSUs or LTE eNBs, are considered as anchors, and vehicles independently estimate their locations through classical trilateration, range-free cell connectivity information (possibly combined with DR [53]), or even fingerprinting (e.g., possibly assisted by particle filtering [54]). However these solutions strongly depend on the density, the availability and the relative geometry of the road infrastructure.

With the current used ITS-G5 or IEEE 802.11p standard, it is also possible to examine distance information with proprietary software-based solutions since there is no native localization architecture implemented [55]. In [56], the authors estimate the angle of arrival (AOA) of beacon packets transmitted from a RSUs by using linear antenna array.

In [57], a network-centric localization solution for cars in ultra-dense 5G networks is presented. The state of the car is estimated using an EKF with AOA and time of arrival

(TOA) measurements. Sub-meter accuracy for position estimation and meter accuracy for position prediction in short-time of movement are claimed.

2.3.4 Cooperative Localization

The general principle of vehicular CLoc works in two main phases.

In the first phase, each vehicle piggybacks its position-dependent data (e.g., at least its *absolute* GNSS position) in a "Beacon" sent over V2X communication links[6].

In the second phase, through the reception of these "Beacons", a given "ego" vehicle becomes aware of the *absolute* position estimates of its neighbors. The optional task consists of using the "Beacon" signal statistics to sample *relative* position-dependent information from these "virtual anchors". So as to perform localization or localization enhancement, data fusion thus combines the multiple sources of information including:

- Data from other entities representing their local observations through V2X communications (e.g., GNSS data, sensor data, etc.),

- Data from communication signals (e.g., received signal strength indicator (RSSI), TOA, time difference of arrival (TDOA), AOA, etc.),

- Data from on-board sensors (e.g., GNSS data, sensor data, digital map, etc.).

CLoc with V2X Measurements

Extensive research has been devoted to incorporate V2V measurements with diverse sources of information such as GNSS/GPS data, car's kinematics (speed, acceleration, heading, etc.), and even prior knowledge of the road map using different CLoc architectures. With the advent of ITS-G5/DSRC standards, V2V RSSI (or V2V distance estimates based on RSSI) or Doppler shift is primarily utilized in this vehicular CLoc context.

In [58], the authors present a distributed cooperative solution based on a dissimilarity matrix composed of RSSI-based distance estimates. Position estimation is performed by a least squares (LS) estimator yielding accuracy improvement over stand-alone GPS, while using GPS estimates for initialization purposes only. The authors extend this work by additionally incorporating vehicle's kinematics and road constraints based on a extended

---

[6]To remain technology neutral, a "Beacon" is a message periodically broadcast by each node, while V2X refers to any technology capable of D2D communication in a vehicular context.

Kalman filter (EKF) in [59]. However, collecting V2V distance measurements in mesh topology, which is challenging in a fast-moving VANETs, is not discussed the works. Additionally, the RSSI-based ranging error less than 10 m is not realistic according to [60] (see also Appendix C.1). A similar work is proposed in [61] together with a study on communication overhead, its impacts on CLoc accuracy, and protocol improvements. The authors claim to also improve neighboring vehicles' positions at the same time. A very similar CLoc problem is solved by a fast multidimensional scaling (MDS) in [62] and the MDS coupled with a PF prefiltering V2V distances in [63]. A simplified CLoc architecture fusing V2V distance measurements in star topology (to avoid range vector exchanges) and GPS measurements in an EKF is found in [64]. However, since the trilateration is performed with the GPS-based positioned neighbors, the sub-meter localization accuracy cannot be achieved. Particularly, the best scenario with 14 neighboring vehicles only yields about 3.5 m error.

In [65], the target vehicle's position is trilaterated using the neighboring vehicles' positions and range information (assumed to be perfect) in a LS technique. The algorithm is initialized with Kalman filter (KF)-based GPS with kinematics. This also implies that the neighbors communicate their enhanced positions and associated uncertainties rather than the GPS ones.

Different from the majority of CLoc techniques employing distances between the participating nodes, it is proposed in [66] to fuse on-board GPS position and velocity with those of the neighbors and Dopller shifts of the received signals over V2V ITS-G5 in an EKF. An accuracy improvement of up to 48% over the GPS accuracy is reported but still without achieving the sub-meter level. Very recently, a GNSS/ITS-G5 integrated architecture considering both Doppler and range from DSRC is developed in [67] to improve the CLoc performance. For the data fusion, a modified cubature KF is applied to account for the probable anomalies in state estimation.

With an increased number of sensors on vehicles, [68] fuses information from on-board GPS, on-board ranging sensors, and DSRC messages using an EKF. The association for the data coming from independent DSRC and ranging sensors is based on the minimum Mahalanobis distance and Chi-square test. If a neighboring vehicle is discovered by both DSRC and on-board sensors, the corresponding relative distance is cross-checked and corrected. Another strong point lies in the possibility to synchronize all the position

information in DSRC messages using an open-loop KF.

Furthermore, an integrated localization algorithm that exploits all possible data sources, relying on a WLS estimator and exploiting various data sources (e.g., GPS, RFID, V2X and DR), has been proposed in [69]. Another recent work [70] improves GPS vehicle positioning by the fusion with V2X RSSIs through IEEE 802.11p interfaces and inertial sensors on driver's smartphone, and map information if available. A two-state Bayesian framework is proposed including an UKF for prefilering the heading estimation using smartphone inertial sensors, and a core PF to combine all the aforementioned information. The authors perform a comparative evaluation with different combinations of the location information sources using real-word data in an urban scenario i.e., the city of Porto. However, the localization accuracy gain of the fusion approaches against the stand-alone GPS is limited (location errors of 9.47 m and 9.8 m for GPS+V2V+map and GPS, respectively for full trajectory).

CLoc without V2X Measurements

CLoc can also be performed with the information contained in the messages only, without requiring explicit V2V measurements, contrarily to the methods discussed in the previous section. At least a couple CLoc methods have been extensively investigated including CLoc based on GNSS pseudorange information or map exchanges.

CLoc techniques with GNSS pseudoranges are commonly implemented in one of the two following schemes. On the one hand, in [71], a tightly coupled GPS/INS integration is adopted for relative CLoc. Based on the exchange of GPS pseudoranges and vehicles' motion through V2V communications, the relative distances between vehicles are tracked using a PF. Though simulated data of two vehicles is demonstrated, this work can be extended to estimate the relative position of multiple neighboring vehicles, which is completed later in [72]. The latter even obtains experimental results. In [73], V2V distances are estimated based on the sharing of GPS pseudorange measurements through DSRC and a WLS method. Then, a distributed location estimation algorithm uses these distances and the shared GPS fixes to compute the target vehicle's absolute position.

Instead of sharing the GNSS pseudoranges, other studies such as [74, 75] propose to broadcast GNSS pseudorange correction through V2V communications, thus, the receivers can improve their GNSS positions by compensating the common errors. In other words,

the principal of DGNSS is extended from fixed base stations to dynamic base stations such as vehicles. Specifically, each vehicle estimates its position using all their on-board sensors and then the geometric ranges to satellites. It eventually subtracts the latter from the measured pseudoranges and broadcast this information to other vehicles. The receiving vehicles can include this correction in their measured pseudoranges from the same satellites to compensate the common errors. In [74], through simulation, the authors prove that a large amount of the error on the measured pseudoranges can be compensated (5x) and therefore, a more accurate positioning (3.5–6.5x) can be achieved whereas an experiment with 2 vehicles is presented in [75].

By sharing both GPS absolute positions and pseudoranges only via the V2V communications, in [76], Mattern *el al.* present a cooperative map matching method. Each receiving vehicle can then calculate relative positions between itself and transiting vehicles. Assuming that participating vehicles are within drivable areas, matching of groups of vehicles to a lane-level map is performed. This matching is based on the fact that matching of polygons to a map is less ambiguous than point map matching. A very similar approach appears later on in [77]. However, this approach requires that the geometry of the involved vehicles is good enough to remove ambiguity in 2-D space.

In [25], the authors discuss the possibility to exchange raw sensor data (i.e., radar, lidar, camera) between vehicles using 5G mmWave V2X to enlarge sensing range and improve automated driving functions as the current IEEE 802.11p and 4G LTE D2D do not support the Gbps data rates required for raw sensor data exchange. A simplified prototype so-called implicit cooperative positioning (ICP) is presented in [78] to jointly estimate the positions of sensing vehicles and sensed features. Specifically, vehicles jointly localize features (e.g., pedestrians, traffic lights, parked cars, etc.) in the surrounding areas using radars or lidars, and consider them as common noisy reference marks to refine their position estimates. Information on sensed features are simplified by Gaussian distributions fully described by their means and covariances, and further exchanged between cooperating nodes till convergence. However, the distributed data association issue, which may be very challenging (e.g., considering clouds of lidar-based detected points), still needs to be further investigated in depth in this very context and latency issues may be critical at high speed (i.e., the iterative solution requiring the exchange of a few packets between a pair of sensing nodes before achieving convergence).

Table 2.6: Vehicular communication capabilities by today and prospective technologies [7].

Maturity	Technologies	Throughput	Delay	Range
Today	ITS-G5/IEEE 802.11p	3–12 Mbps	≈ 10 ms	300–1000 m
Prospective	4D LTE V2X	≈ 70 Mbps	≈ 50 ms (Mode 1)/ ≈ 10 ms (Mode 2)	300–900m
Prospective	5G mmWave V2X	> 10 Gbps	1 ms	< 200 m

2.4 Gap Analysis and Challenges

From a communication perspective, the backbone of CLoc is the V2X communication technology. Table 2.6 summaries the core V2X technologies that are or will be on-board of future connected vehicles including ITS-G5/IEEE 802.11p, LTE V2X, and 5G mmWave V2X. From this table, the technology of choice for our CLoc investigations is ITS-G5 since it is by far the most mature, while already fulfilling basic CLoc needs in terms of range (thus, cooperation potential), rate (sufficient for basic location awareness) and latency (compatible with current nominal GNSS refresh rates). Moreover, it is fully tested and available on the market today, what is particularly appealing for short-term algorithms implementation and validations. Besides, it already provides adequate location awareness mechanisms. On the contrary, LTE V2X is still under specification (at a quite early stage) and needs several years to be validated while the promising 5G mmWave V2X has an even longer time horizon ahead. Even if the cooperative fusion algorithms described in this thesis are primarily adapted to ITS-G5 communications (and to some extent jointly optimized, as it will be seen in particular in Chapters 2 and 3), note that the overall optimization methodology is however agnostic to the underlying technology and could be applied to other underlying V2X technologies in the near future.

From a location estimation perspective, according to the detailed taxonomy available in Appendix B, we are interested in CLoc algorithms which fall into the following categories:

- Two-step localization due to its low complexity and modularity;

- Distributed architecture to cope with high mobility patterns, frequent fragmentation and rapid evolution of the network topology, short link life time, etc.;

- Absolute localization to fulfill the requirements of the C-ITS applications;

- Probabilistic approach to exploit available statistical models;

- Multisensor fusion to exploit multiple available information sources from a number

of sensors in vehicles;

- Range-based localization as approaches that do not require explicit V2X measurements but just communicate raw GNSS information operate only under satellite coverage, while those exchanging maps or raw sensor data are still quite challenging for current ITS-G5 and even 4G LTE V2X specifications, besides other limitations such as distributed data association and synchronization.

Table 2.7 summaries the relevant technologies that could provide explicit V2X range-dependent measurements. Some technologies can support the exchange location-dependent data and/or the acquisition of radiolocation metrics over V2V or V2I links. For example, though ITS-G5 has been mostly adopted for communication purposes, it can support limited ranging capability through RSSI measurements. On the contrary, IR-UWB is a technology primarily intended for accurate ranging but it can hardly communicate data at high rates (say above a few tens of Mbps) while achieving simultaneously sufficient transmission ranges (say, beyond about 100 m). Throughout this thesis, we thus build our CLoc framework in a gradually complex way. As a starting point, we fuse on-board GNSS positions with opportunistic RSSI readings based uniquely on ITS-G5 under simplified working assumptions first in Chapter 3, before considering more realistic V2V wireless channel and protocol constraints in Chapter 4. This first combination of technologies is intended as a nominal baseline (making opportunistic use of ITS-G5 only) and as such, it is expected to offer only quite moderate accuracy. As RSSI is neither accurate enough, nor reliable enough (as discussed in details in Appendix C), Chapter 5 presents a hybrid V2V CLoc scheme combining on-board GNSS and IR-UWB V2V TOF measurements while still using the ITS-G5 to communicate position estimates to neighboring vehicles. Our CLoc framework is completed in Chapter 6 to include inertial/DR sensors (and even possibly, camera-based lance detectors) under full V2X cooperation (i.e., including both V2V and V2I links, considering systematically ITS-G5 for data communication, along with IR-UWB TOF or ITS-G5 RSSI for range-dependent measurements).

To combine multiple information sources, we use a hybrid data fusion architecture mainly due to its flexibility for proof of concept, besides the following reasons. On the one hand, low level architectures are highly complex with more parameters to control, difficult to extend with new modalities, and they also require deep access to the devices (e.g.,

Table 2.7: V2X range-dependent measurement capabilities by today and prospective technologies [8].

Maturity	Technologies	Frequency	Metric	Links
Today	ITS-G5/IEEE 802.11p	5.9 GHz	RSSI	V2V/V2I
Today	ZigBee/IEEE 802.15.4	2.4 GHz	RSSI/PDOA	V2V/V2I
Today	IR-UWB/IEEE 802.15.4a or proprietary	4 GHz	TOA (TOF)/TDOA	V2V/V2I
Prospective	4G LTE V2X	2 GHz	Not defined	V2V/V2I
Prospective	5G mmWave V2X	30–100 GHz	AOA, AOD, TOA	V2V/V2I
Prospective	WiFi extension	2GHz	Not defined	V2V/V2I

GNSS pseudoranges). On the other hand, high level architectures requires that all the involved sensors can independently estimate the state vector before fusing their results, which can not always be realized.

To implement the hybrid fusion architecture above, PF is chosen as core filter fusion engine due to its suitability to nonlinear and non-Gaussian dynamics. By using PF, we can make our study generic enough to possibly integrate other location metrics/technologies (considering the increasing number of sensors in today vehicles) which may be characterized by complex models. Besides, the complexity of PF is not an issue in the vehicular context since the relative extra-cost to supply adequate powerful hardware and software capabilities looks still relatively reasonable (i.e., in comparison with the cost of the whole car).

Even if CLoc yet remains a very promising approach to enhance geo-localization, in particular in GNSS (partially) denied environments. The combination of V2V and GNSS information raises unprecedented and specific challenges that require in-depth understanding and careful assessment as follows:

- Asynchronism of CAM transmissions and local estimations among the involved vehicles (thus requiring advanced prediction mechanisms before fusing the received data);

- High computational complexity and high data traffic under exhaustive/systematic cooperation with all the available neighbors (thus requiring low-complexity and context-aware links selection mechanisms);

- Measurements space-time correlation under constrained vehicle mobility and refreshment rates (thus requiring correlation mitigation at both signal processing and protocol levels);

- Limited CAM payloads and V2V channel congestion (thus requiring V2V message simplifications and transmission rate/power adaptation);

- Whenever both GNSS and accurate V2V ranging based on IR-UWB are available, propagation of location errors among vehicles and/or fusion filters overconfidence, depending on local GNSS quality and dispersion (thus requiring mitigation mechanisms at both signal processing and protocol levels);

- Poor GDOP along the dimension orthogonal to the road, due to highly constrained VANET mobility and topology;

- In challenging but common tunnel environments, prolonged GNSS outages and unsustainable error accumulation of inertial sensors over time (e.g., gyroscopes), leading to the fast divergence of position estimates.

The previous key points will be addressed in the following chapters.

Chapter 3

V2V Cooperative Localization

3.1 Introduction and Related Works

As already seen in Chapter 2, vehicular localization is mostly enabled today by GNSS. So as to improve further the localization accuracy, GNSS augmentations or a maps of landmarks/anchors can be used. However, the GNSS augmentations have to face specific issues (e.g., deployed base stations for DGNSS and RTK, unguaranteed convergence time for PPP). On the one hand, perception-based localization using lidars requires high definition maps (of landmarks), which are costly and time-consuming to maintain up-to-date. On the other hand, static elements of the road infrastructure, such as RSUs or LTE eNBs, are considered as anchors, and vehicles independently estimate their locations through classical trilateration, range-free cell connectivity information, or even fingerprinting. However these solutions strongly depend on the density, the availability and the relative geometry of the road infrastructure. For instance, as illustrated on Figure 3.1, one single V2I link with respect to a RSU would be insufficient to get the "ego" vehicle positioned through standard trilateration with no ambiguity.

On the contrary, as illustrated in Figure 3.1, instead of considering only RSUs as static anchors, CLoc refers to strategies that consider neighboring vehicles as additional "virtual anchors". More specifically, their periodically broadcast ITS-G5 CAMs can be used primarily to receive and fuse the encapsulated GNSS-aided data (raw or refined estimates) but, also opportunistically, to measure range-dependent metrics e.g., RSSI. The goal of an "ego" vehicle is thus to infer its position (as part of its so-called "state" in the following) based on its own estimated GNSS position, on V2V RSSI readings with respect
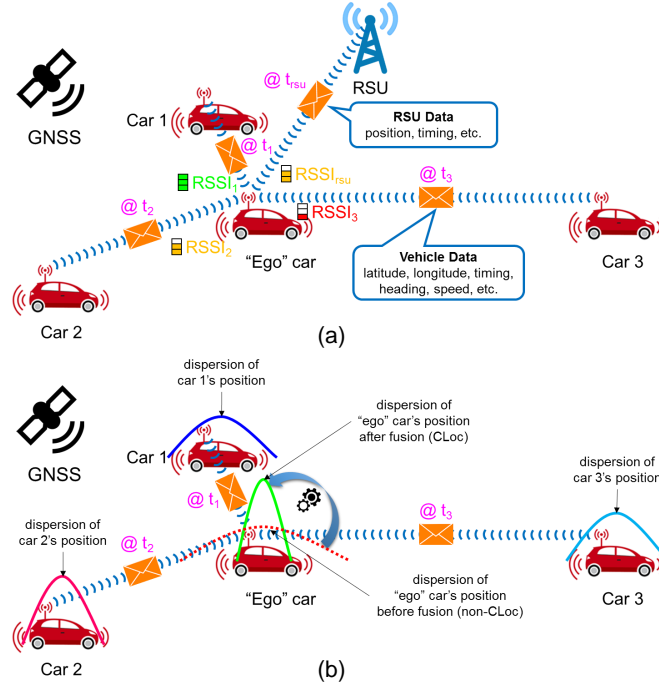
Figure 3.1: (a) Cooperative cars periodically exchange CAMs to maintain awareness of each other and to support distributed CLoc. Both the transmission time $@t_i$ and the received power level $RSSI_i$ depend on the transmission car i (and thus, on the V2V link). (b) "Ego" car receiving asynchronous CAMs from one-hop "virtual anchors" to perform distributed CLoc. The dispersion of CLoc location estimates (through both GNSS and ITS-G5) is expected to be lower than that of non-CLoc estimates (i.e., standalone GNSS).

to one-hop neighbors (measured out of incoming CAMs), and on imperfect state information from these neighbors viewed as "virtual anchors" (i.e., estimated locations and their related uncertainties, encapsulated in the CAMs). The "ego" vehicle then contributes to improve the localization of other vehicles by sharing its own fusion-based position estimates in subsequent CAMs. We do not consider V2I communications for now to assist positioning but more generic V2V configurations, since RSUs shall be mostly deployed in the most critical areas/environments as seen in Chapter 6 within a tunnel scenario. A major benefit of CLoc in comparison with noncooperative approaches is that it does not need any prior map containing predefined anchor nodes' locations. It shall also benefit from other vehicles' data and communications, and more generally, from information redundancy and diversity.

Despite the significant localization improvements expected with CLoc (in particular in GNSS denied environments), the intrinsic mobile nature of both "virtual anchors" and vehicular wireless channels makes that the indicated GNSS positions, as well as the received power over V2V links, are still conditionally subject to strong errors and harmful

fading conditions respectively, as it will be seen in more details in Chapter 4. Beyond, CLoc is also prone to even more specific challenges. On the one hand, the transmission intervals between CAMs are constrained by channel load conditions, leading to non periodic transmissions and accordingly, non synchronous data reception from "virtual anchors" (see Figure 3.1). If not appropriately addressed by advanced filter designs in charge of performing data fusion [79], this can lead to severe localization errors and hence, cooperation is less beneficial or even harmful. On the other hand, there exists a trade-off between localization accuracy and complexity (under limited embedded capabilities, latency, power consumption, etc.), as well as communication impairments (e.g., increased network traffic, channel congestion, packet loss, etc.). As an example, exhaustive cooperation, which aims at integrating all the V2V links with respect to available neighbors (i.e., regardless of the link quality) can generate high computational complexity (in the fusion step) and heavy communication loads (due to uncensored transmissions), while incorporating uninformative (e.g., too redundant) or largely erroneous data.

Thus, in this first technical chapter, we propose to define a nominal flexible cooperative GNSS/ITS-G5 fusion framework that addresses the previous specific challenges. The chapter is organized as follows. In Section 3.2, we present the problem formulation and the system model. The prediction-based data resynchronization is suggested in Section 3.3 while the general GNSS/ITS-G5 data fusion for V2V CLoc based on a nonparametric filter is described in Section 3.4. Then Section 3.5 addresses computationally efficient link selection algorithms employing theoretical performance bounds to integrate only the most informative neighbors and measurements. Numerical results are presented in Section 3.6. Finally, Section 3.7 gives a summary of related personal contributions, as well as intermediary conclusions.

3.2 Problem Formulation and System Model

The state-space model is a mathematical abstraction of any localization and tracking problem, from which many different model-based filtering techniques can be applied. It is generally usual to consider models that are linear for state dynamics and nonlinear for

observations [80, 81]:

$$\mathbf{X}_{i,k} = \mathbf{F}_i \mathbf{X}_{i,k-1} + \mathbf{B}_i \mathbf{u}_{i,k} + \mathbf{G}_i \mathbf{w}_{i,k}, \qquad\qquad (3.1a)$$

$$\mathbf{z}_{i,k} = \mathbf{h}_i(\mathbf{X}_{i,k}, \ldots) + \mathbf{n}_{i,k}, \qquad\qquad (3.1b)$$

where $\mathbf{X}_{i,k}$ is the state vector of vehicle i collecting the components of interest for the system (e.g., position, velocity, heading, etc.) at its local discrete time k or $t_{i,k}{}^1$, $\mathbf{u}_{i,k}$ the control inputs (e.g., steering, throttle settings, braking forces), $\mathbf{F}_i$ the state transition matrix, $\mathbf{B}_i$ the matrix that applies the effect of each control input component in the vector $\mathbf{u}_{i,k}$ on the state vector, $\mathbf{G}_i$ the matrix that applies the effects of each noise component in the process noise vector $\mathbf{w}_{i,k}$, $\mathbf{h}_i(\mathbf{X}_{i,k}, \ldots)$ the transformation matrix that maps the state vector parameters $\mathbf{X}_{i,k}$ (and possibly other vehicles' states) into the measurement/observation $\mathbf{z}_{i,k}$, which is corrupted by a measurement noise term $\mathbf{n}_{i,k}$.

In general, the GNSS positions of different vehicles are collected asynchronously leading to asynchronous enhanced position estimates (i.e., after filtering/fusion), as shown in Figure 3.2. For ease of notations, we consider a global timeline divided into time windows indexed by k so that all the events of position estimates occurring within this time slot granularity share the same index k (see Figure 3.2). Throughout this dissertation, we will use the notations in Table 3.1, some of them being also illustrated in Figure 3.2.

At time instant k, the "ego" vehicle i has the set $\mathcal{N}_{\to i,k}$, $i \notin \mathcal{N}_{\to i,k}$ of vehicles in communication range in the time interval $(k-1, k]$ and the set $\mathcal{S}_{\to i,k} \subseteq \mathcal{N}_{\to i,k}$ of selected "virtual anchors" for CLoc. Also at this vehicle i's instant, a vehicle j, $j \in \mathcal{N}_{\to i,k}$ has the state vector $\mathbf{X}_{j,k_i} \neq \mathbf{X}_{j,k}$ which is sampled according to its own time schedule. We also introduce the following set of notations to gather different vehicles' states: $\mathbf{X}_{\mathcal{N}\to i,k<k_i} = \{\mathbf{X}_{j,k}\}_{j\in\mathcal{N}_{\to i,k}}$, $\mathbf{X}_{\mathcal{N}\to i,0:k<k_i} = \{\mathbf{X}_{\mathcal{N}\to i,0<0_i}, \ldots, \mathbf{X}_{\mathcal{N}\to i,k<k_i}\}$, $\mathbf{X}_{\mathcal{N}\to i,k} = \{\mathbf{X}_{j,k_i}\}_{j\in\mathcal{N}_{\to i,k}}$, and $\mathbf{X}_{\mathcal{N}\to i,0:k} = \{\mathbf{X}_{\mathcal{N}\to i,0}, \ldots, \mathbf{X}_{\mathcal{N}\to i,k}\}$. Given all the available measurements $\mathbf{z}_{i,1:k}$ and the set of neighbors' self-perceived beliefs $bel(\mathbf{X}_{\mathcal{N}\to i,0:k<k_i})$ communicated to vehicle i (cooperative awareness), the goal of vehicle i is to track its own belief $bel(\mathbf{X}_{i,0:k})$, as well as to build and update a LDM of its immediate neighbors' beliefs $bel(\mathbf{X}_{\mathcal{N}\to i,0:k})$. Then we can obtain from the beliefs any 2D position, along with its associated confidence interval. The following

---

[1]Due to asynchronously sampled time instants (i.e., $t_{i,k} \neq t_{j,k}$ if $i \neq j$), the index k is meaningful only locally. For notation brevity, the subscript indicating the "ego" vehicle is deliberately omitted hereafter in some cases (e.g., $\mathbf{X}_{i,k}$ instead of $\mathbf{X}_{i,k_i}$). If, however, it is included, the associated variable is strictly considered with respect to the timeline of the stated vehicle index (see $\mathbf{X}_{j,k_i}$ in Table 3.1).

Table 3.1: Mathematical notations used for state-space modeling in the general filtering/fusion framework.

Notation	Description
$t_{i,k}$	Vehicle i's sampling instant according to its estimation timeline (e.g., GNSS sampling instants).
$\mathbf{x}_{i,k} = (x_{i,k}, y_{i,k})^\dagger$	Vehicle i's 2-D position at time $t_{i,k}$.
$\mathbf{v}_{i,k} = (v_{i,k}^x, v_{i,k}^y)^\dagger$	Vehicle i's 2-D velocity at time $t_{i,k}$.
$\mathbf{X}_{i,k} = (\mathbf{x}_{i,k}^\dagger, \mathbf{v}_{i,k}^\dagger)^\dagger = (x_{i,k}, y_{i,k}, v_{i,k}^x, v_{i,k}^y)^\dagger$	Vehicle i's state vector at time $t_{i,k}$.
$\mathbf{X}_{j,k_i} = (\mathbf{x}_{j,k_i}^\dagger, \mathbf{v}_{j,k_i}^\dagger)^\dagger = (x_{j,k_i}, y_{j,k_i}, v_{j,k_i}^x, v_{j,k_i}^y)^\dagger$	Vehicle j's state vector at vehicle i's sampling instant $t_{i,k}$. If $j \equiv i$, $\mathbf{X}_{j,k_i} \equiv \mathbf{X}_{i,k}$.
$\mathbf{X}_{i,0:k}, \mathbf{X}_{j,0:k_i}$	Sets of all states $\mathbf{X}_{i,k}$, $\mathbf{X}_{j,k_i}$ up to (and including) time $t_{i,k}$ respectively.
$t_{j,k<k_i}$	Vehicle j's latest sampling instant seen by vehicle i at time $t_{i,k}$ (timestamp in latest CAM). If $j \equiv i$, $t_{j,k<k_i} \equiv t_{i,k-1}$.
$\mathbf{X}_{j,k<k_i}$	Vehicle j's state vector at time $t_{j,k<k_i}$. For $i \equiv j$, $\mathbf{X}_{j,k<k_i} \equiv \mathbf{X}_{i,k-1}$ (at $t_{i,k-1}$).
$\mathcal{V}$	Set of connected vehicles of cardinality $|\mathcal{V}|$ in the considered VANET.
$\mathcal{N}_{\rightarrow i,k} \subset \mathcal{V}$	Set of vehicle i's neighbors of cardinality $|\mathcal{N}_{\rightarrow i,k}|$, $i \notin \mathcal{N}_{\rightarrow i,k}$ in its communication range $r_{\max}$ in the time interval $[t_{i,k-1}, t_{i,k})$.
$\mathcal{S}_{\rightarrow i,k} \subseteq \mathcal{N}_{\rightarrow i,k}$	Set of vehicle i's "virtual anchors" of cardinality $|\mathcal{S}_{\rightarrow i,k}|$, $i \notin \mathcal{S}_{\rightarrow i,k}$ whose CAMs are selected to feed its fusion engine.
$\mathbf{X}_{\mathcal{N}\rightarrow i,k} = \{\mathbf{X}_{j,k_i}\}_{j\in\mathcal{N}_{\rightarrow i,k}}$	Aggregate state vector of vehicle i's $|\mathcal{N}_{\rightarrow i,k}|$ neighbors in communication range at time $t_{i,k}$ (synchronized state).
$\mathbf{X}_{\mathcal{N}\rightarrow i,k<k_i} = \{\mathbf{X}_{j,k_i}\}_{j\in\mathcal{N}_{\rightarrow i,k}}$	Aggregate state vector of vehicle i's $|\mathcal{N}_{\rightarrow i,k}|$ neighbors in communication range (asynchronous state).
$\mathbf{X}_{\mathcal{S}\rightarrow i,k} = \{\mathbf{X}_{j,k_i}\}_{j\in\mathcal{S}_{\rightarrow i,k}}$	Aggregate state vector of vehicle i's $|\mathcal{S}_{\rightarrow i,k}|$ "virtual anchors" at time $t_{i,k}$ (synchronized state).
$\mathbf{X}_{\mathcal{S}\rightarrow i,k<k_i} = \{\mathbf{X}_{j,k<k_i}\}_{j\in\mathcal{S}_{\rightarrow i,k}}$	Aggregate state vector of vehicle i's $|\mathcal{S}_{\rightarrow i,k}|$ "virtual anchors" (asynchronous state).
$\mathbf{z}_{i,k}^{\text{GNSS}} = (z_{i,k}^x, z_{i,k}^y)^\dagger$	Vehicle i's 2-D GNSS position at time $t_{i,k}$.
$z_{j\rightarrow i,k}^{\text{RSSI}}$	Approximated/extrapolated RSSI values at exact filtering time $t_{i,k}$ under some circumstances.
$\mathbf{z}_{\mathcal{S}\rightarrow i,k}^{\text{RSSI}} = \{z_{j\rightarrow i,k}^{\text{RSSI}}\}_{j\in\mathcal{S}_{\rightarrow i,k}}$	Set of vehicle i's RSSI measurements to its "virtual anchors" $\mathcal{S}_{\rightarrow i,k}$ at time $t_{i,k}$.
$\mathbf{z}_{i,k}$	Vehicle i's observation vector at time $t_{i,k}$ (i.e., $\mathbf{z}_{i,k}^{\text{GNSS}}$ and/or $\mathbf{z}_{\mathcal{S}\rightarrow i,k}^{\text{RSSI}}$).
$\mathbf{z}_{i,1:k}$	Set of all vehicle i's observations up to (and including) time $t_{i,k}$.
$\mathbf{Z}_i^k$	Set of all observations of vehicle i and its "virtual anchors" that conditions the filtering result at vehicle i at time $t_{i,k}$.
$\mathbf{Z}_j^{k<k_i}$	Set of all observations of vehicle j, $j \in \mathcal{S}_{\rightarrow i,k}$ and its "virtual anchors" that conditions the filtering result at vehicle j at time $t_{j,k<k_i}$.
$\mathbf{Z}_{\mathcal{S}\rightarrow i}^{k<k_i} = \{\mathbf{Z}_j^{k<k_i}\}_{j\in\mathcal{S}_{\rightarrow i,k}}$	Set of all observations that conditions the filtering results at the set $\mathcal{S}_{\rightarrow i,k}$ of "virtual anchors" of vehicle i.
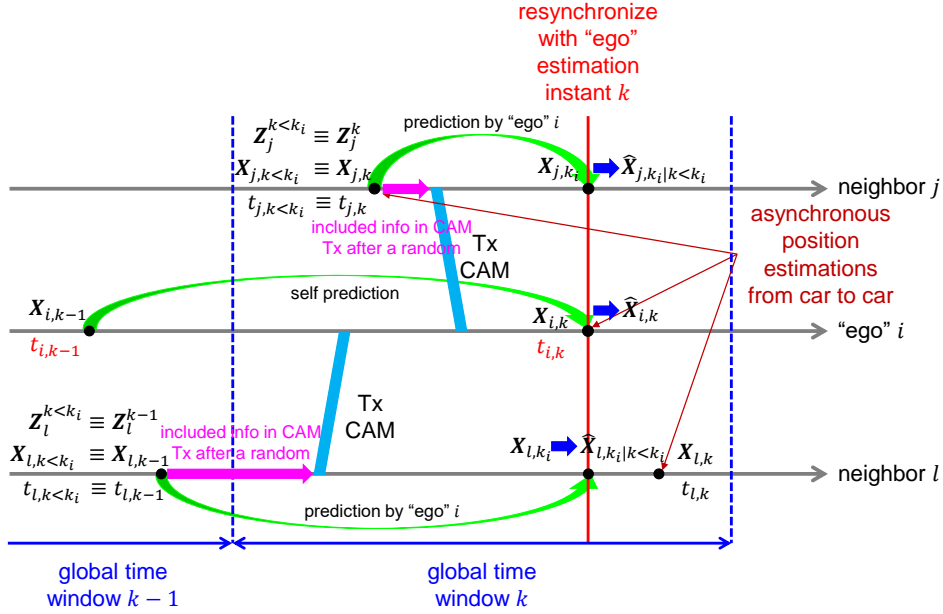
Figure 3.2: Example of space-time schematic managed by the "ego" i whose neighbors are vehicles j and l. Due to asynchronous estimates, the "ego" i needs to perform prediction of received information at its time of interest $t_{i,k}$.

sections describe in detail the two main components for implementing the filter, namely mobility and observation models.

3.2.1   Gauss–Markov Mobility Model

To make use of Bayesian filtering techniques later on, we adopt the so-called Gauss–Markov mobility model (GMM), which is a stochastic mobility model suitable for the vehicular context [81]. It describes well the correlated velocity of the vehicle as a Gauss–Markovian process and enables good predictions of the vehicle's position and velocity [82], while remaining still analytically tractable[2]. In discrete time, the predicted velocity in 2-D is computed based on its previous value and a random Gaussian process [81, 82], as follows:

$$v_{i,k+1}^{(\cdot)} = \alpha_i v_{i,k}^{(\cdot)} + (1 - \alpha_i)\bar{v}_{i,k}^{(\cdot)} + \Delta T \sqrt{1 - \alpha_i^2}\, w_{i,k}^{(\cdot)}, \qquad (3.2)$$

where $(\cdot)$ can be either x- or y-coordinate, α_i is the memory level, ΔT the time step, $\bar{v}_{i,k}^{(\cdot)}$ the asymptotic 1-D cruising velocity which evolves slower than ΔT, and $a_{i,k}^{(\cdot)} = \sqrt{1 - \alpha_i^2}\, w_{i,k}^{(\cdot)}$ the 1-D temporally uncorrelated centered Gaussian (acceleration) noise. However, note that vehicles usually move along the lanes on the roads. Intuitively, the uncertainty along the road direction is much higher than that along the dimension orthog-

---

[2]The evaluation of this work over real or synthetic mobility traces are left to Chapter 7.

onal to the road [59]. If $(\sigma_i^a)^2$ and $(\sigma_i^o)^2$ represent the variances of the uncertainties along and perpendicular to the road respectively, therefore $(\sigma_i^a)^2 \gg (\sigma_i^o)^2$. As a road runs in a direction with an angle Ω counterclockwise from x-axis, a transformation must be applied to account for the high uncertainty in the along-track direction, providing information on road geometry within the prediction model (3.1a) to reduce uncertainty and achieve better predictions. Thus, the process noise covariance matrix expressed in a 2-D Cartesian coordinates is no longer diagonal, as follows:

$$
\begin{aligned}
\mathbb{E}\{\mathbf{w}_{i,k}\mathbf{w}_{i,k}^\dagger\} &= \mathbb{E}\left\{ \begin{pmatrix} w_{i,k}^x w_{i,k}^{x\dagger} & w_{i,k}^x w_{i,k}^{y\dagger} \\ w_{i,k}^y w_{i,k}^{x\dagger} & w_{i,k}^y w_{i,k}^{y\dagger} \end{pmatrix} \right\} \\
&= \begin{pmatrix} \cos\Omega & -\sin\Omega \\ \sin\Omega & \cos\Omega \end{pmatrix} \begin{pmatrix} (\sigma_i^a)^2 & 0 \\ 0 & (\sigma_i^o)^2 \end{pmatrix} \begin{pmatrix} \cos\Omega & -\sin\Omega \\ \sin\Omega & \cos\Omega \end{pmatrix}^\dagger .
\end{aligned}
\tag{3.3}
$$

Therefore, the resulting mobility model (3.1a) has the following form:

$$
\underbrace{\begin{pmatrix} \mathbf{x}_{i,k} \\ \mathbf{v}_{i,k} \end{pmatrix}}_{\mathbf{X}_{i,k}} = \underbrace{\begin{pmatrix} \mathbf{I}_2 & \alpha_i \Delta T \cdot \mathbf{I}_2 \\ \mathbf{0}_2 & \alpha_i \cdot \mathbf{I}_2 \end{pmatrix}}_{\mathbf{F}_i} \underbrace{\begin{pmatrix} \mathbf{x}_{i,k-1} \\ \mathbf{v}_{i,k-1} \end{pmatrix}}_{\mathbf{X}_{i,k-1}} + \underbrace{(1-\alpha_i)\begin{pmatrix} \Delta T \cdot \mathbf{I}_2 \\ \mathbf{I}_2 \end{pmatrix}}_{\mathbf{B}_i} \bar{\mathbf{v}}_{i,k}
$$
$$
+ \underbrace{\sqrt{1-\alpha_i^2}\begin{pmatrix} \Delta T^2 \cdot \mathbf{I}_2 \\ \Delta T \cdot \mathbf{I}_2 \end{pmatrix}}_{\mathbf{G}_i} \mathbf{w}_{i,k},
\tag{3.4}
$$

where $\bar{\mathbf{v}}_{i,k} \equiv \mathbf{u}_{i,k}$ and $\mathbf{I}_2$ is the identity matrix of size 2. Note that the memory level α_i can be tuned to account for various mobility behaviors in many scenarios [83].

From a traffic simulation point of view, we utilize this model to generate vehicular mobility traces. From the tracking point of view, we use this model to perform the prediction of the "ego" position[3]. We first assume that each vehicle has perfect knowledge about its own mobility model i.e., GMM parameters or more generally, a conditional transition probability density function (pdf) $p(\mathbf{X}_{i,k}|\mathbf{X}_{i,k-1})$ (known *a priori* for highly controlled mobility regimes or possibly self-calibrated on the wing based on previous state estimates). However, this perception is usually an approximation of the true mobility statistics. Mismatch models as well as more realistic/synthetic mobility traces are left to

---

[3]In the following section, it will also be employed to predict the neighboring positions to resynchronize related data before fusion.

Chapter 6 and Chapter 7, respectively. Finally, it is reasonable to assume the vehicles'
mobilities and their *a priori* states are mutually independent [84, 85].

3.2.2 Observation Model

GNSS Absolute Position

The 2-D position $\mathbf{x}_{i,k}$ is first determined by a GNSS receiver and the corresponding mea-
surement $\mathbf{z}_{i,k}^{\text{GNSS}} = (z_{i,k}^x, z_{i,k}^y)^\dagger$ is contaminated by additive noise $\mathbf{n}_{i,k}^{\text{GNSS}} = (n_{i,k}^x, n_{i,k}^y)^\dagger$, as
follows:

$$z_{i,k}^x = x_{i,k} + n_{i,k}^x, \tag{3.5a}$$

$$z_{i,k}^y = y_{i,k} + n_{i,k}^y. \tag{3.5b}$$

The latter errors affecting 2-D coordinates, $n_{i,k}^x$ and $n_{i,k}^y$, are firstly supposed to be indepen-
dent and identically distributed (i.i.d.) centered Gaussian and mutually independent with
known variances σ_{GNSS}^x and σ_{GNSS}^y respectively, for the sake of simplicity [59, 61, 64, 65].

V2V Received Power

The RSSI measurements are directly performed out of the received CAMs, originally used
to encapsulate and share geographical awareness information over V2V channels. The
approximated/extrapolated RSSI $z_{j \to i,k}^{\text{RSSI}}$ (on a dB scale) at vehicle i at local time $t_{i,k}$ (i.e.,
while occupying position $\mathbf{x}_{i,k}$) with respect to vehicle j (i.e., occupying position $\mathbf{x}_{j,k_i}$),
is assumed to be measured in LOS and to follow the widely used log-distance path loss
model[4]:

$$z_{j \to i,k}^{\text{RSSI}} = P_0(d_0) - 10 n_p \log_{10}\left(\frac{\|\mathbf{x}_{i,k} - \mathbf{x}_{j,k_i}\|}{d_0}\right) + s_{j \to i,k}, \tag{3.6}$$

where $P_0(d_0)$ [dBm] is the averaged received power at a reference distance $d_0 = 1$ m,
n_p the path loss exponent, $\|\cdot\|$ the Euclidean distance, and finally $s_{j \to i,k}$, a shadowing
component that is assumed i.i.d. centered Gaussian with standard deviation σ_{Sh} in a
specific environment.

    In the following filtering schemes, observation vectors will be composed of GNSS and/or

---

[4]Without loss of generality, we assume a simplified log-distance model in this work, but the proposed
core data fusion engine is not restricted to it. In Chapter 7, we will consider real experimental data
to calibrate the corresponding model parameters. Beyond, we shall mention the necessity/difficulty of
pre-calibrating this kind of path loss model in real systems.

V2V RSSI measurements, depending on the cooperation level and the available measurements.

3.3 Resynchronization of Cooperative Information

To perform data fusion, the related inputs have to be meaningful at the desired fusion/filtering time. Specifically, the related inputs, namely the positional data received from neighboring vehicles, the associated RSSIs, and the positional observation from on-board GNSS, have to be made consistent (i.e., spatially coherent) and meaningful at a common point in time. Nevertheless, as these available sources of information are adversely asynchronous in the high speed vehicular context due to channel load conditions leading to irregular messages brodcast and temporal misalignment between vehicles' positional sample instants. Data resynchronization can be then naturally achieved via an early prediction step applied to the neighboring beliefs (accounted in received CAMs) and similarly to that of the "ego" vehicle. Particularly, an "ego" vehicle i predicts the beliefs of its "virtual anchors" in order to perform fusion at its time k, as follows:

$$bel(\mathbf{X}_{j,k_i}) = \int p(\mathbf{X}_{j,k_i}|\mathbf{X}_{j,k<k_i})bel(\mathbf{X}_{j,k<k_i})d\mathbf{X}_{j,k<k_i}, \quad j \in \mathcal{N}_{\rightarrow i,k}. \tag{3.7}$$

Note that vehicle i must make assumptions about the mobility of its neighbors, i.e., $p(\mathbf{X}_{j,k_i}|\mathbf{X}_{j,k<k_i})$, typically assuming the same model as in (3.4) (under the same notations). Intuitively, it yields:

$$
\begin{aligned}
\mathbf{X}_{j,k_i} = &\underbrace{\begin{pmatrix} \mathbf{I}_2 & \alpha_j(t_{i,k} - t_{j,k<k_i})\mathbf{I}_2 \\ \mathbf{0}_2 & \alpha_j\mathbf{I}_2 \end{pmatrix}}_{\mathbf{F}_j(t_{i,k}-t_{j,k<k_i})} \mathbf{X}_{j,k<k_i} + (1-\alpha_j)\underbrace{\begin{pmatrix} (t_{i,k} - t_{j,k<k_i})\mathbf{I}_2 \\ \mathbf{I}_2 \end{pmatrix}}_{\mathbf{B}_j(t_{i,k}-t_{j,k<k_i})} \bar{\mathbf{v}}_{j,k} \\
&+ \sqrt{1-\alpha_j^2}\underbrace{\begin{pmatrix} (t_{i,k} - t_{j,k<k_i})^2\mathbf{I}_2 \\ (t_{i,k} - t_{j,k<k_i})\mathbf{I}_2 \end{pmatrix}}_{\mathbf{G}_j(t_{i,k}-t_{j,k<k_i})} \mathbf{w}_{j,k}, \quad j \in \mathcal{N}_{\rightarrow i,k}.
\end{aligned}
\tag{3.8}
$$

Note that the parameters α_j, $\bar{\mathbf{v}}_{j,k}$, and $\mathbb{E}\{\mathbf{w}_{j,k}\mathbf{w}_{j,k}^\dagger\}$ can be either communicated to the recipient through a CAM or estimated from the previous trajectory or assumed to be known for a particular mobility pattern.
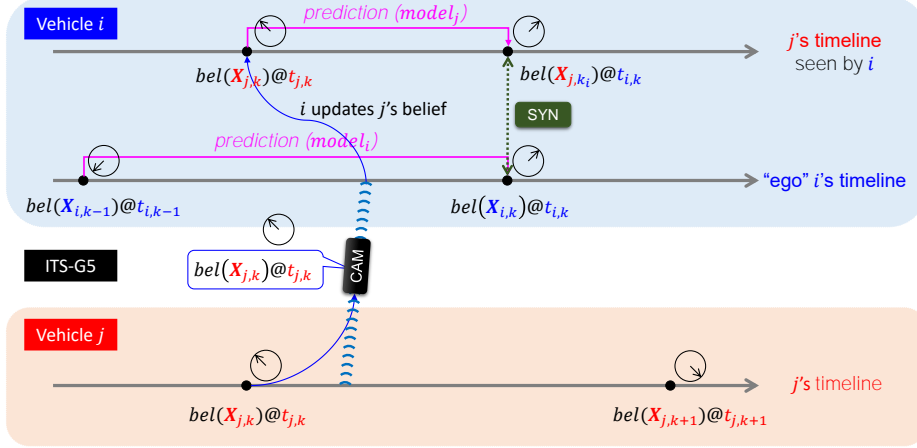
Figure 3.3: Example of CLoc space-time data management at the "ego" vehicle i with respect to its neighboring vehicle j. Due to asynchronous sampled time instants $t_{i,k} \neq t_{j,k}$, vehicle i needs to perform a prediction of the received information i.e., $bel(\mathbf{X}_{j,k})$ at any fusion time of interest $t_{i,k}$ i.e., $bel(\mathbf{X}_{j,k_i})$.

So far, we have just resynchronized both "ego" and neighboring position estimates. But RSSI readings are also not perfectly synchronous (e.g., the CAM broadcasts may occur at different rates and/or they can be event-driven) neither with estimation times, nor with each other. However, we claim that these RSSIs can still be used at the estimation time for some reasons: first, with 100-ms refresh rate, the average elapsed time between the measured RSSI and the estimation time is about 50 ms, leading to a distance error of about 1.5 m in the worst case when a vehicle is static and the other runs at about 110 km/h[5]. This distance is too small to cause a remarkable change in the RSSI (e.g., see Figure 7.7 in our small-scale field measurement campaigns, given a single RSSI value, the distance can vary up to ± 20 m); second, as the shadowing is correlated over space and time, as discussed in Chapter 4, the ideal RSSI value at the desired time is not so different from the ones measured in the last 50 ms; and last, the GNSS data can also be extrapolated at the measured RSSI time, even if it is quite problematic in our case. Since we receive much more CAMs (and thus RSSIs) than GNSS positions, it turns out that the fusion is performed at very high rate (CAM rate × number of neighbors) and there are not enough GNSS measurements for all the fusion iterations although reusing the same GNSS information may cause overconfidence issues. Even more importantly, with inaccurate RSSIs, it is worth collecting several measurements to improve the GDOP.

---

[5]In most common platooning cases or highly correlated mobility (e.g., highways), stable V2V distances between vehicles are usually observable.

3.4 GNSS/ITS-G5 Data Fusion Based on Particle Filter

As the observation model of interest linking the state vector to the measurements is non-linear here (e.g., see (3.6)), nonparametric filters relying on numerical approximations (e.g., the PF) are expected to outperform the KF-based methods in terms of accuracy, at the price of higher computational load [80, 86–88]. However, in the vehicular context, the relative extra-cost to supply adequate powerful hardware and software capabilities looks still reasonable (comparing with the cost of the whole car). The PF approximates the posterior[6] by a set of random samples with associated weights and to compute the MMSE estimates based on these samples and weights. Accordingly, the optimal solution

$$\widehat{\mathbf{X}}_{i,k} = \int \mathbf{X}_{i,k} p\big(\mathbf{X}_{i,k}, \mathbf{X}_{\mathcal{S}\to i,k}\big|\mathbf{Z}_i^k, \mathbf{Z}_{\mathcal{S}\to i}^{k<k_i}\big) d\mathbf{X}_{i,k} d\mathbf{X}_{\mathcal{S}\to i,k} \tag{3.9}$$

is approximated by

$$\widehat{\mathbf{X}}_{i,k} \approx \sum_{p=1}^{P} w_{i,k}^{(p)} \mathbf{X}_{i,k}^{(p)}, \tag{3.10}$$

where $\{\mathbf{X}_{i,k}^{(p)}\}_{p=1}^P$ is a set of particles (samples of the state vector) with associated weights $\{w_{i,k}^{(p)}\}_{p=1}^P$, $w_{i,k}^{(p)} \propto p(\mathbf{X}_{i,k}^{(p)}, \mathbf{X}_{\mathcal{S}\to i,k}^{(p)}|\mathbf{Z}_i^k, \mathbf{Z}_{\mathcal{S}\to i}^{k<k_i})/q(\mathbf{X}_{i,k}^{(p)}, \mathbf{X}_{\mathcal{S}\to i,k}^{(p)}|\mathbf{X}_{i,k-1}^{(p)}, \mathbf{X}_{\mathcal{S}\to i,k<k_i}^{(p)}, \mathbf{z}_{i,k})$ with the importance distribution $q(\cdot)$, which is chosen to easily draw samples. Otherwise, it is challenging and expensive from the computation point of view to samples directly from the posterior due to its complex functional form [86–89].

A classical and intuitive choice for computing these weights involves the measurement likelihood function [80, 87]. Typically, the importance distribution can be chosen as follows:

$$q(\mathbf{X}_{i,k}, \mathbf{X}_{\mathcal{S}\to i,k}|\mathbf{X}_{i,k-1}^{(p)}, \mathbf{X}_{\mathcal{S}\to i,k<k_i}^{(p)}, \mathbf{z}_{i,k}) = p(\mathbf{X}_{i,k}|\mathbf{X}_{i,k-1}^{(p)}) \prod_{j\in\mathcal{S}\to i,k} p(\mathbf{X}_{j,k_i}|\mathbf{X}_{j,k<k_i}^{(p)}). \tag{3.11}$$

This PF is called bootstrap PF. To the best of our knowledge, most PFs are practically implemented in a bootstrap manner due to its simplicity. We then propose to apply the PF described in Algorithm 1 as the nominal filter/fusion engine of our CLoc framework.

---

[6]In this first proof of concept, we assume that CAMs encapsulate the particles cloud to account for local estimates uncertainty, what could result in prohibitive overhead under current standard specifications. However, this issue has been investigated and reported in Chapter 4 without contradicting the first findings exposed herein.

Algorithm 1 Bootstrap PF for GNSS/ITS-G5 data fusion (iteration k, "ego" vehicle i)

1: **Collection of CAMs:** Receive CAMs from the set $\mathcal{N}_{\to i,k}$ of local neighbors, read the RSSI values, extract the particle beliefs $\{\mathbf{X}_{j,k<k_i}^{(p)}, w_{j,k<k_i}^{(p)}\}_{p=1}^P$, $j \in \mathcal{N}_{\to i,k}$.

2: **Data Resynchronization:** Perform prediction of both "ego" and neighboring particle beliefs based on mobility models at the "ego" estimation instant k (i.e., $t_{i,k}$)

$$\mathbf{X}_{i,k}^{(p)} \sim p(\mathbf{X}_{i,k}|\mathbf{X}_{i,k-1}^{(p)}), \qquad w_{i,k|k-1}^{(p)} = 1/P, \qquad p = 1,\ldots,P,$$

$$\mathbf{X}_{j,k_i}^{(p)} \sim p(\mathbf{X}_{j,k_i}|\mathbf{X}_{j,k<k_i}^{(p)}), \qquad w_{j,k_i|k<k_i}^{(p)} = 1/P, \qquad p = 1,\ldots,P, \qquad j \in \mathcal{N}_{\to i,k},$$

and build the LDM of vehicle i's neighbors (as another possible output of the algorithm)

$$\widehat{\mathbf{X}}_{j,k_i|k<k_i} \approx \frac{1}{P}\sum_{p=1}^P \mathbf{X}_{j,k_i}^{(p)}, \quad \mathbf{\Sigma}_{j,k_i|k<k_i} \approx \frac{1}{P}\sum_{p=1}^P (\mathbf{X}_{j,k_i}^{(p)} - \widehat{\mathbf{X}}_{j,k_i|k<k_i})(\mathbf{X}_{j,k_i}^{(p)} - \widehat{\mathbf{X}}_{j,k_i|k<k_i})^\dagger, \quad j \in \mathcal{N}_{\to i,k}.$$

3: **Link Selection:** Select the subset $\mathcal{S}_{\to i,k} \subset \mathcal{N}_{\to i,k}$ of appropriate links.

4: **Observation Update:** Calculate the new weights according to the likelihood[7] (by using the proposal distribution in (3.11))

$$w_{i,k}^{(p)} \propto p(\mathbf{z}_{i,k}|\mathbf{X}_{i,k}^{(p)}, \mathbf{X}_{\mathcal{S}\to i,k}^{(p)})$$
$$= p(z_{i,k}^x|x_{i,k}^{(p)})p(z_{i,k}^y|y_{i,k}^{(p)}) \prod_{j\in S_{\to i,k}} p(z_{j\to i,k}^{\text{RSSI}}|\mathbf{x}_{j,k_i}^{(p)}, \mathbf{x}_{i,k}^{(p)}), \quad p = 1,\ldots,P,$$

normalize them to sum to unity, and compute the approximate MMSE estimator and its empirical covariance as the main filter outputs

$$\widehat{\mathbf{X}}_{i,k} \approx \sum_{p=1}^P w_{i,k}^{(p)}\mathbf{X}_{i,k}^{(p)}, \quad \mathbf{\Sigma}_{i,k} \approx \sum_{p=1}^P w_{i,k}^{(p)}(\mathbf{X}_{i,k}^{(p)} - \widehat{\mathbf{X}}_{i,k})(\mathbf{X}_{i,k}^{(p)} - \widehat{\mathbf{X}}_{i,k})^\dagger.$$

5: **Resampling:** Generate a new set $\{\mathbf{X}_{i,k}^{(p*)}\}_{p=1}^P$ by resampling with replacement P times.

6: **Broadcast:** Encapsulate the posterior belief $\{\mathbf{X}_{i,k}^{(p*)}\}_{p=1}^P$ in a CAM and broadcast.

3.5 Low-Complexity Link Selection

Actually CLoc performance is strongly affected by the number of neighbors and their geometric configuration while processing and fusing all incoming information. On the other hand integrating fusion-oriented data from numerous neighbors generates high computational complexity and requires significant overhead (and possibly, extra channel load) at the network level in comparison with more conventional CAM usage. Thus relevant operating trade-offs (e.g., in terms of required number of packets, CAM payload occupancy, refresh rates) must still be found for a better exploitation of cooperation potential, while complying with practical protocol constraints. Regarding the link selection itself, previous works relying on the approximated Cramér-Rao Lower Bound (CRLB) of cooperative position estimates as criterion (e.g., [90, 91] or more recently, a combination of this bound and a pre-validation step through innovation monitoring in the V2V context [92]). In this case, the selection is simply based on a comparison of the best positioning errors expected for given sub-sets of the available neighbors. The best sub-set leading to the presumed
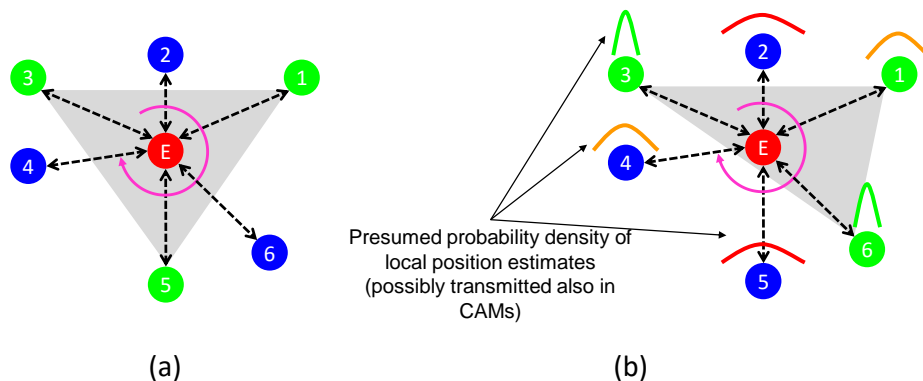
Figure 3.4: Sets of selected cooperative neighbors (green) with respect to the "ego" vehicle (red), following (a) non-Bayesian and (b) Bayesian CRLB criteria. In this example, the wrongly positioned vehicle 5 could trick the non-Bayesian selection scheme (and thus, be included in the selected fusion set), whereas the Bayesian version would account for its location uncertainty (and reject it as unreliable neighbor).

minimum error is selected. It is approximated in the sense that the theoretical bounds calculation, which would require the knowledge of all exact positions, admits erroneous positions as inputs (e.g., estimated or predicted), while considering that the latter would not fundamentally change the aspect of the relative VANET topology (i.e., in comparison with the true topology)[8]. However, they cannot properly account for mobile neighbors uncertainty, whereas more recent Bayesian formulations of such bounds [93], which can account for the prior uncertainty of all estimated positions. Figure 3.4 illustrates the difference between them. And most of them have not yet been applied into the V2V context. Besides, the simpler but complementary filter innovation monitoring approach in [92] is used to detect link-wise inconsistent measurements and thus, reject harmful ones.

We thus propose new link selection algorithms that aim at more efficient CLoc procedures under various GNSS conditions, by enabling lower footprint with respect to communication means and lower computational complexity. More specifically, we propose a couple of low complexity link selection criteria based on non-Bayesian and Bayesian versions of the CRLB characterizing cooperative location estimates given a subset of the available neighbors, in conjunction with a fast sub-optimal closest search instead of performing a computationally greedy exhaustive search (i.e., by restricting heuristically the CRLB-based comparison to a subset of the geographically nearest neighbors).

---

[8]This may be sufficient already in non-CLoc, when considering only a selection of V2I links and measurements with respect to known static anchors (i.e., RSUs).

3.5.1   Link Selection Criteria

Non-Bayesian Cramér-Rao Lower Bound

The non-Bayesian CRLB or CRLB characterizes here the best achievable performance (in the minimum expected mean squared error (MSE) sense) for any non-biased (position) estimator (i.e., conditioned on a given set of reference neighbors). From the positioning point of view, this criterion reflects both the pair-wise radio link quality and the geometry of the reference vehicles relatively to the "ego" one or GDOP. The bound is determined by processing an inverse of the Fisher information matrix (FIM) [94, 95]. Consider at the "ego" estimation instant k, $\mathbf{x}_{i,k}$, the position of the "ego" vehicle i and $\{\mathbf{x}_{j,k_i}\}_{j \in \mathcal{S}_{\rightarrow i,k}}$, the positions of its selected reference vehicles, the FIM is defined as

$$\mathbf{J}_{i,k} = \sum_{j \in \mathcal{S}_{\rightarrow i,k}} \mathbb{E}_{s_{j \rightarrow i,k}} \left\{ -\Delta_{\mathbf{x}_{i,k}}^{\mathbf{x}_{i,k}} \log p(z_{j \rightarrow i,k}^{\mathrm{RSSI}} | \mathbf{x}_{i,k}, \mathbf{x}_{j,k_i}) \right\}, \tag{3.12}$$

where $\Delta_{\mathbf{x}}^{\mathbf{x}} f(\mathbf{x})$ denotes the Laplacian of $f(\mathbf{x})$. Note that as its name suggests, the non-Bayesian CRLB treats both $\mathbf{x}_{i,k}$ and $\{\mathbf{x}_{j,k_i}\}_{j \in \mathcal{S}_{\rightarrow i,k}}$ as deterministic variables even though they are actually random (i.e., affected by estimation noise). Accordingly, the expectation in (3.12) is taken with respect to the measurement noise only (i.e., over the shadowing). Under the assumption of centered Gaussian shadowing in (3.6), the expectation can be computed in closed-form solution [94]:

$$\mathbf{J}_{i,k} = \sum_{j \in \mathcal{S}_{\rightarrow i,k}} \frac{1}{\tilde{\sigma}_{\mathrm{Sh}}^2} \frac{(\mathbf{x}_{i,k} - \mathbf{x}_{j,k_i})(\mathbf{x}_{i,k} - \mathbf{x}_{j,k_i})^{\dagger}}{\|\mathbf{x}_{i,k} - \mathbf{x}_{j,k_i}\|^4}, \tag{3.13}$$

where $\tilde{\sigma}_{\mathrm{Sh}} = \sigma_{\mathrm{Sh}} \log 10/(10 n_p)$. Nevertheless, neither the true position $\mathbf{x}_{i,k}$ of the "ego" vehicle nor that of its neighbors $\{\mathbf{x}_{j,k_i}\}_{j \in \mathcal{S}_{\rightarrow i,k}}$ are known, thus, the approximate FIM $\widehat{\mathbf{J}}_{i,k}$ can be computed with the predicted positions instead i.e., $\widehat{\mathbf{x}}_{i,k|k-1}$, $\{\widehat{\mathbf{x}}_{j,k_i}\}_{j \in \mathcal{S}_{\rightarrow i,k}}$ as follows:

$$\widehat{\mathbf{J}}_{i,k} = \sum_{j \in \mathcal{S}_{\rightarrow i,k}} \frac{1}{\tilde{\sigma}_{\mathrm{Sh}}^2} \frac{(\widehat{\mathbf{x}}_{i,k|k-1} - \widehat{\mathbf{x}}_{j,k_i})(\widehat{\mathbf{x}}_{i,k|k-1} - \widehat{\mathbf{x}}_{j,k_i})^{\dagger}}{\|\widehat{\mathbf{x}}_{i,k|k-1} - \widehat{\mathbf{x}}_{j,k_i}\|^4}. \tag{3.14}$$

Thus, the bound on the location MSE can be expressed in terms of the FIM as follows:

$$\mathrm{MSE}(\widehat{\mathbf{x}}_{i,k}) \geq \mathrm{tr}\left(\widehat{\mathbf{J}}_{i,k}^{-1} \right). \tag{3.15}$$

This expression shows the expected MSE conditioned on a particular subset $\mathcal{S}_{\to i,k} \subseteq \mathcal{N}_{\to i,k}$ of neighbors, as the cost function to be minimized by the link selection algorithm (i.e., with the subset as optimization variable).

Bayesian Cramér-Rao Lower Bound

The Bayesian CRLB (BCRLB) considers the positions as realizations of random variables [90, 95]. Therefore, besides the radio link quality and the geometry of the reference neighbors relatively to the "ego" vehicle, this criterion also captures the uncertainties of the "ego" and neighbors' estimated positions. Assume that at "ego" estimation time epoch k, $\mathbf{x}_{i,k} \sim p(\mathbf{x}_{i,k}|\mathbf{z}_{i,1:k-1})$, the position of the "ego" i and $\{\mathbf{x}_{j,k_i} \sim p(\mathbf{x}_{j,k_i}|\mathbf{z}_{j,1:k})\}_{j \in \mathcal{S}_{\to i,k}}$, the positions of its selected reference vehicles, the Bayesian FIM (BFIM) is now expressed as [93]

$$\mathbf{J}_{i,k}^B = \mathbf{J}_{i,k}^P + \sum_{j \in \mathcal{S}_{\to i,k}} \left[(\mathbf{J}_{j,k_i}^P)^{-1} + (\mathbf{J}_{j \to i,k}^M)^{-1} \right]^{-1}, \tag{3.16}$$

where $\mathbf{J}_{i,k}^P$, $\mathbf{J}_{j,k_i}^P$ are the *a priori* FIMs of the positions of the "ego" i and its reference neighbors $j \in \mathcal{S}_{\to i,k}$ respectively, while $\mathbf{J}_{j \to i,k}^M$ denotes the FIM obtained from the link measurement $(j \to i)$. In particular, the prior FIMs are defined as

$$\mathbf{J}_{i,k}^P = \mathbb{E}_{\mathbf{x}_{i,k}} \left\{ -\Delta_{\mathbf{x}_{i,k}}^{\mathbf{x}_{i,k}} \log p(\mathbf{x}_{i,k}|\mathbf{Z}_i^{k-1}) \right\}, \tag{3.17}$$

and

$$\mathbf{J}_{j,k_i}^P = \mathbb{E}_{\mathbf{x}_{j,k_i}} \left\{ -\Delta_{\mathbf{x}_{j,k_i}}^{\mathbf{x}_{j,k_i}} \log p(\mathbf{x}_{j,k_i}|\mathbf{Z}_j^{k<k_i}) \right\}. \tag{3.18}$$

Assuming $p(\mathbf{x}_{i,k}|\mathbf{Z}_i^{k-1}) \sim \mathcal{N}(\mathbb{E}\{\mathbf{x}_{i,k}\}, \mathbf{\Sigma}_{i,k|k-1}^{-1})$ and $p(\mathbf{x}_{j,k_i}|\mathbf{Z}_j^{k<k_i}) \sim \mathcal{N}(\mathbb{E}\{\mathbf{x}_{j,k_i}\}, \mathbf{\Sigma}_{j,k_i}^{-1})$ in first approximation, thus $\mathbf{J}_{i,k}^P = \mathbf{\Sigma}_{j,k|k-1}^{-1}$ and $\mathbf{J}_{j,k_i}^P = \mathbf{\Sigma}_{j,k_i}^{-1}$. On the other hand, the term related to the measurements is now calculated as follows:

$$\begin{aligned}
\mathbf{J}_{j \to i,k}^M &= \mathbb{E}_{s_{j \to i,k}, \mathbf{x}_{i,k}, \mathbf{x}_{j,k_i}} \left\{ -\Delta_{\mathbf{x}_{i,k}}^{\mathbf{x}_{i,k}} \log p(z_{j \to i,k}^{\text{RSSI}}|\mathbf{x}_{i,k}, \mathbf{x}_{j,k_i}) \right\} \\
&= \frac{1}{\tilde{\sigma}_{\text{Sh}}^2} \mathbb{E}_{\mathbf{x}_{i,k}, \mathbf{x}_{j,k_i}} \left\{ \frac{(\mathbf{x}_{i,k} - \mathbf{x}_{j,k_i})(\mathbf{x}_{i,k} - \mathbf{x}_{j,k_i})^\dagger}{\|\mathbf{x}_{i,k} - \mathbf{x}_{j,k_i}\|^4} \right\}.
\end{aligned} \tag{3.19}$$

Note that the expectation over the measurement noise is performed analytically in (3.19) still considering the Gaussian shadowing (in dB). Besides, as the expectation with respect to $\mathbf{x}_{i,k}$ and $\mathbf{x}_{j,k_i}$ is tedious to derive analytically, we propose to use numerical integration instead, following a Monte Carlo approach. Accordingly, we draw P samples $\{\mathbf{x}_{i,k}^{(p)}\}_{p=1}^P$

and $\{\mathbf{x}_{j,k_i}^{(p)}\}_{p=1}^{P}$ from $p(\mathbf{x}_{i,k}|\mathbf{Z}_i^{k-1})$ and $p(\mathbf{x}_{j,k_i}|\mathbf{Z}_j^{k<k_i})$, $j \in \mathcal{S}_{\to i,k}$ respectively, leading to

$$
\begin{aligned}
\mathbf{J}_{j \to i,k}^{M} &= \frac{1}{\tilde{\sigma}_{\mathrm{Sh}}^2} \int \frac{(\mathbf{x}_{i,k} - \mathbf{x}_{j,k_i})(\mathbf{x}_{i,k} - \mathbf{x}_{j,k_i})^{\dagger}}{\|\mathbf{x}_{i,k} - \mathbf{x}_{j,k_i}\|^4} p(\mathbf{x}_{i,k}|\mathbf{Z}_i^{k-1}) p(\mathbf{x}_{j,k_i}|\mathbf{Z}_j^{k<k_i}) d\mathbf{x}_{i,k} d\mathbf{x}_{j,k_i} \\
&\approx \frac{1}{\tilde{\sigma}_{\mathrm{Sh}}^2} \frac{1}{P} \sum_{p=1}^{P} \frac{(\mathbf{x}_{i,k}^{(p)} - \mathbf{x}_{j,k_i}^{(p)})(\mathbf{x}_{i,k}^{(p)} - \mathbf{x}_{j,k_i}^{(p)})^{\dagger}}{\|\mathbf{x}_{i,k}^{(p)} - \mathbf{x}_{j,k_i}^{(p)}\|^4}.
\end{aligned}
\tag{3.20}
$$

Note that this Monte Carlo integration is still in compliance with the claimed low complexity link selection for two reasons: (i) we only calculate (3.20) for a smaller subset of potential neighbors, which will be presented in the next section and (ii) part of this calculation can be reused later on when updating the weights of the PF (e.g., particle-based V2V distance in the denominator). Finally, similarly to the non-Bayesian CRLB, the final bound on the MSE can be calculated by replacing the FIM $\widehat{\mathbf{J}}_{i,k}$ in (3.15) with the BFIM $\mathbf{J}_{j \to i,k}^{B}$

$$
\mathrm{MSE}(\mathbf{x}_{i,k}) \geq \mathrm{tr}\left\{ (\widehat{\mathbf{J}}_{i,k}^{B})^{-1} \right\}.
\tag{3.21}
$$

The goal is again to identify the best subset $\mathcal{S}_{\to i,k} \subseteq \mathcal{N}_{\to i,k}$ that minimizes the best conditional positioning MSE.

3.5.2   Link Selection Algorithm

Previously, we have derived the cost functions to be minimized (in the MSE sense) for the link selection problem. Particularly, considering the "ego" vehicle i at time k and given the set $\mathcal{N}_{\to i,k}$ of perceived neighboring vehicles, we are now interested in solutions to search for the minimum MSE conditioned on all possible subsets of length S of $\mathcal{N}_{\to i,k}$ denoted by $\mathcal{P}_S(\mathcal{N}_{\to i,k})$ to find $\mathcal{S}_{\to i,k}^*$ yielding the best contribution to the CLoc problem resolution. The optimal link selection would result from an exhaustive search, which is by far too complex in case of high V2V connectivity and thus, not really intended for implementation in a real system. This exhaustive search simply evaluates the cost functions for CRLB or BCRLB, for all the possible combinations listed by $\mathcal{P}_S(\mathcal{N}_{\to i,k})$. For instance, choosing 4 links out of 10 leads to 210 combinations, what seems still reasonable but evaluating 4845 combinations in case of 20 neighbors appears much more challenging. Therefore, in order to reduce the computational burden, one straightforward approach is to develop a search algorithm that hopefully yields the same solution as that of the exhaustive approach (or at least an equivalent solution). A closer look at the (B)FIMs in both criteria (e.g., in (3.13)

Algorithm 2 Sup-optimal closest search of S most informative links among C most potential ones (iteration k, "ego" car i)

1: **if** $|\mathcal{N}_{\rightarrow i,k}| > C$ **then**
2:     estimate $\bar{d}_{j\rightarrow i,k} = \left\| \widehat{\mathbf{x}}_{j,k_i|k<k_i} - \widehat{\mathbf{x}}_{i,k|k-1} \right\|$ with respect to $j \in \mathcal{N}_{\rightarrow i,k}$
3:     sort the set $\{\bar{d}_{j\rightarrow i,k}\}_{j\in\mathcal{N}_{\rightarrow i,k}}$
4:     get C nearest neighbors from $\mathcal{N}_{\rightarrow i,k}$ to build $\mathcal{C}_{\rightarrow i,k}$
5: **else**
6:     $\mathcal{C}_{\rightarrow i,k} = \mathcal{N}_{\rightarrow i,k}$
7: **end if**
8: **if** $|\mathcal{C}_{\rightarrow i,k}| > S$ **then**
9:     create the set $\mathcal{P}_S(\mathcal{C}_{\rightarrow i,k})$ of all subsets of $\mathcal{C}_{\rightarrow i,k}$ of size S
10:     **for** $s = 1$ to $|\mathcal{P}_S(\mathcal{C}_{\rightarrow i,k})|$ **do** $\triangleright$ subset index
11:         let $\mathcal{P}_S(\mathcal{C}_{\rightarrow i,k})[s]$ be the s-th subset in $\mathcal{P}_S(\mathcal{C}_{\rightarrow i,k})$
12:         determine the bound on the MSE

$$\text{MMSE}(\widehat{\mathbf{x}}_{i,k})[s] = \begin{cases} \text{tr}\left\{(\widehat{\mathbf{J}}_{i,k}[s])^{-1}\right\}, & \text{if non-Bayes,} \\ \text{tr}\left\{(\widehat{\mathbf{J}}_{i,k}^{B}[s])^{-1}\right\}, & \text{if Bayes,} \end{cases}$$

        where $\widehat{\mathbf{J}}_{i,k}[s]$, $\widehat{\mathbf{J}}_{i,k}^{B}[s]$ are with the set $\mathcal{P}_S(\mathcal{C}_{\rightarrow i,k})[s]$
13:     **end for**
14:     select the best subset $s^* = \arg\min_s \{\text{MMSE}(\widehat{\mathbf{x}}_{i,k})[s]\}$
15:     $\mathcal{S}_{\rightarrow i,k}^* = \mathcal{P}_S(\mathcal{C}_{\rightarrow i,k})[s^*]$
16: **else**
17:     $\mathcal{S}_{\rightarrow i,k}^* = \mathcal{C}_{\rightarrow i,k}$
18: **end if**

---

and (3.19)) reveals that its link-dependent sub-components are inversely proportional to the squared distances between the nodes. Intuitively, this means that performing CLoc with more distant neighbors leads to suffer from larger MSE or in other heuristic words, the optimal subset of neighbors is expected to be formed among the nearest ones (say, the 8–10 closest neighbors are expected sufficient on most common European highways having 3 lanes). Of course, this intuitive interpretation could be applied with other kinds of V2V metrics but it is all the more noticeable within CLoc based on RSSI measurements due to the considered log-normal path loss model. Thus, we search the best combination among a subset of the physically closest neighbors only, as shown on Algorithm 2 (lines 2–4).

3.6   Numerical Results

3.6.1   Simulation Settings

All the simulations carried out for performance evaluation are based on MATLAB, which are more flexible and suitable in the specific wireless localization context (estimation algorithms) than network simulators, which are more devoted to communication aspects. In particular, as illustrated in Figure 3.5, we model a three-lane road (of most common kind in Europe), where 15 connected cars are driving steadily (in the same north-east

direction) and exchanging CAMs over ITS-G5 technology. The vehicles establish a pure VANET with uniquely V2V links and may benefit from GNSS signals depending on operating environments. We systematically consider a group of 15 vehicles, focusing our analysis on a segment of the entire vehicles flow. CAMs could indeed be received up to practical transmission ranges of 1000 m. However we consider a nominal selective CLoc scheme that incorporates only the messages from its nearest neighbors, which are assumed more reliable and informative due to lower possibility to get NLOS and higher quality of the range-dependent measurement [96, 97]). Accordingly, we consider that simulating 15 vehicles is enough to avoid border effects or artifacts, while preserving the generality of the obtained CLoc results.

As for the CAM transmission policy, we assume that each vehicle periodically broadcasts its position every 100 ms corresponding to the critical CAM rate of 10 Hz (equal to the "core" BSM rate in the U.S. [98]) for several reasons: first, this assumption is valid on high speed mobility scenarios (e.g., highways) where dynamic-related conditions in [19] (e.g., traveling distance to send a message) are used to trigger to get critical rates; second, the positions can be collected up to 10 Hz thanks to the high-rate GNSS receivers; third, we are interested in how the cooperative information can improve the CLoc accuracy[9]. Besides, the random CAM generation time between the instant at which CAM generation is triggered (typically, when the GNSS position is sampled) and the instant at which the message is delivered to the transport layer is uniformly drawn in the interval $[0, 50]$ ms (complying with [19]) to minimize the probability of simultaneous transmissions and temporal correlated packet collisions[10]. Table 3.2 summarizes the other important parameters used for our simulations.

We have claimed that the BCRLB-based link selection criterion is able to capture the uncertainties of the "ego" and the neighboring position estimates, contrarily to the standard CRLB-based criterion. Accordingly, two scenarios are investigated to emphasize the pros and cons of each solution.

In the first evaluation scenario (S1), we consider vehicles traveling through a urban canyon (see Figure 3.5). GNSS estimates at each vehicle are affected by varying stan-

---

[9]Injecting too many packets to the channel with limited capacity causes traffic congestion. As this work is positioning-oriented, communication behavior is not examined to the fullest but left for further studies, for instance in Chapter 4.

[10]Collision may recur for several subsequent transmissions due to the quasi-periodic nature of CAM transmissions [99].

Table 3.2: Other important simulation parameters considered for the evaluation of links selection algorithms.

Parameter	Description
Mobility model	Gauss-Markov mobility model
Memory level α	0.95
Sampling period ΔT	0.1 [s]
GNSS/CAM rate	10 [Hz] (critical) [19]
CAM generation time	$\mathcal{U}(0, 50)$ [ms] (complying with [19])
Path loss exponent n_p	1.9 (V2V in highways) [100]
Standard deviation of shadowing σ_{Sh}	2.5 [dB] (V2V in highways) [100]
Number of particles	500
Number of selected links	4^{a}

[a] For extra diversity from the minimum number required for non-ambiguous 2-D positioning.

dard deviations with large spatial correlation as depicted in Figure 3.5(a) whereas the V2V RSSI-based measurement quality is assumed to remain unchanged. Four different positioning schemes are then compared in terms of accuracy and service continuity i.e., stand-alone filtered GNSS, exhaustive CLoc, CRLB-based selective CLoc, and BCRLB-based selective CLoc.

In the second evaluation scenario (S2), we consider a heterogeneous configuration where vehicles have the same visibility to satellites, but suffer from disperse and independent GNSS precision levels due to different receiver capabilities (e.g., high-class or basic receivers) as illustrated in Figure 3.5(b).

These two scenarios are complementary and cumulative, as S1 describes the degradation from GNSS signals, whereas S2 considers the degradation from GNSS receiver capabilities, both being common in real conditions.

3.6.2 Scenario Evaluation

Homogeneous GNSS (S1)

Figure 3.6 shows the RMSEs of the position estimates of all vehicles as a function of time. Note that the 15 vehicles need approximately 8 s to completely enter/leave the different areas (due to its length of $60 \times 4 = 240$ m and speed of about 30 m/s) causing some transitions in GNSS precision levels, as depicted on the same figure. As expected, the CLoc outperforms the non-CLoc (i.e., stand-alone filtered GNSS) in terms of accuracy and service continuity (i.e., preventing the error from flourishing in harsh/lost conditions). In favorable GNSS conditions, the gains yielded by CLoc over non-CLoc are modest (rela-
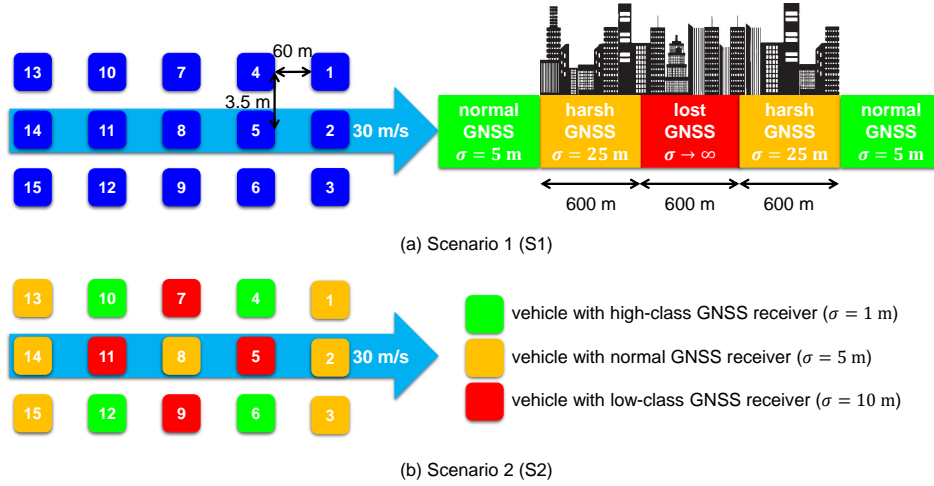
Figure 3.5: Topology of the evaluated VANET and associated configurations for S1 (urban canyon) and S2 (different classes of GNSS receiver) for the evaluation of links selection algorithms.
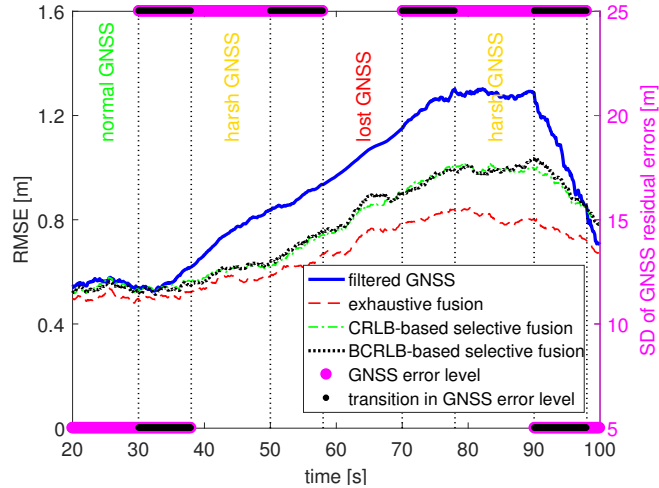
Figure 3.6: Localization RMSEs (over vehicles) as a function of time for non-CLoc, CLoc with exhaustive fusion, and CLoc with selective fusion when GNSS quality varies depending on the geographic area (S1).

tive drop in RMSE of about 9% by exhaustive CLoc and no drop by selective approaches) whereas in harsh or lost GNSS environments, huge improvements in accuracy are observed. In particular, in comparison with non-CLoc, a relative fall in RMSE of 33% is experienced by exhaustive CLoc and of about 21% by both selective schemes in harsh areas whereas in GNSS-denied periods, relative drops of 30% and of 21% are reported respectively. The reason can be understood as follows: in comparison with the GNSS position, RSSI measurements to "virtual anchors" can contribute to the positioning performance but in a modest way due to the non-linear relationship between received power and state (derived from the distance to the known "virtual anchors"), the uncertainties of "virtual anchors"
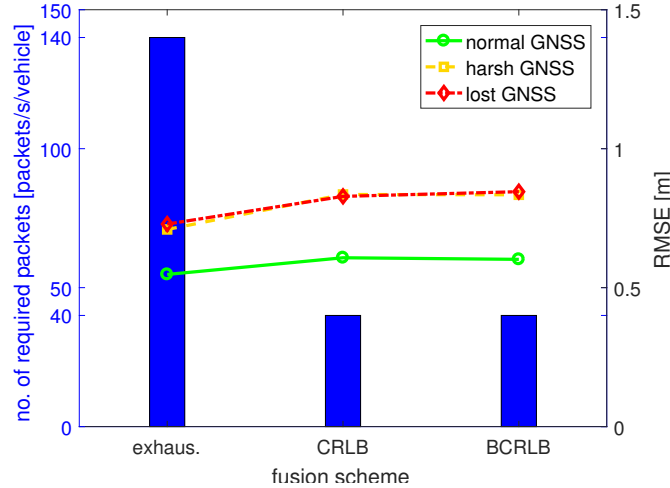
Figure 3.7: Trade-off between the number of required packets for CLoc and the localization RMSE (over vehicles and time) with or without selective cooperation in different GNSS conditions (S1).

and the GDOP, the extrapolated/approximate RSSI values at fusion time, the RSSI shadowing dispersion, etc. In other words, when the accuracy of the filtered GNSS remains high enough, there is little room for improvement by fusing with ITS-G5 as a source of range-dependent information through RSSI and vice versa, when GNSS performance is degraded, the accuracy gain through ITS-G5 is more noticeable.

Quantitatively, both CRLB and BCRLB-based selective fusion schemes are quasi equivalent, and suffer both from a RMSE increase of 10%, 18%, and 14% in normal, harsh, and lost GNSS respectively in comparison with exhaustive CLoc due to the information loss. Note that in our scenario, the positioning error in harsh GNSS conditions is superior than that in lost GNSS. This is not really contradictory since the "harsh" zone is composed of 2 distinct areas (see again Figure 3.5) and the latter (i.e., that after the "lost" period) is more severe due to errors accumulation during the "lost" interval (i.e., reflecting the memory effect pointed out in [65]). From the communication point of view, selective CLoc dramatically reduces the number of required packets (more than 70% shown in Figure 3.7) considering an error increase of 14–18% in worst cases and of 10% in normal cases. Last but not least, from the processing and fusion points of view, the complexity of the particle-based core engine is mainly related to the weights update (see line 4 in Algorithm 1). Particularly, the complexity scales as $\mathcal{O}\left(P\left|\mathcal{S}_{\rightarrow i,k}\right|\right)$ where the number of particles P can be large (typically 500–5000). In our scenario, without link selection, $\left|\mathcal{S}_{\rightarrow i,k}\right| = 14$, whereas with link selection $\left|\mathcal{S}_{\rightarrow i,k}\right| \leq 4$.
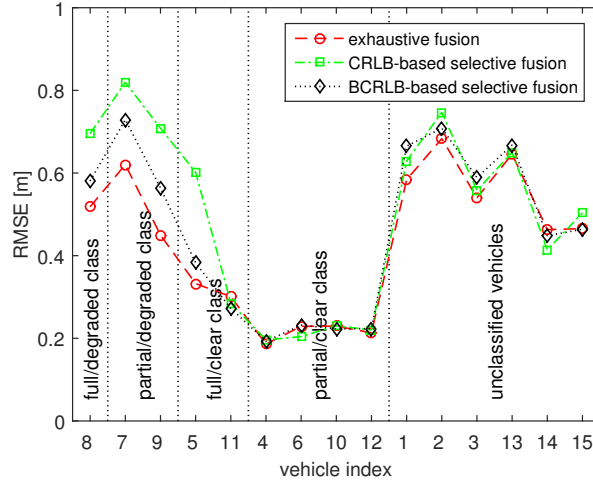
Figure 3.8: Localization RMSEs (over the full trajectory) for different fusion schemes with and without selective cooperation at each vehicle (S2).

In summary, link selection is critical to significantly reduce the computational complexity and also network traffic (if coupled with Tx censorship mechanisms) without losing significant accuracy. In this specific scenario, BCRLB based selection (i.e., by design more adapted to heterogeneous GNSS conditions) can just match the selection scheme based on classical CRLB, as expected. In other words, all the vehicles experience approximately the same GNSS error regime so that the injected prior uncertainty information regarding their estimated positions is quite neutral from a selection perspective.

Heterogeneous GNSS (S2)

While matching the classic CRLB in scenarios considering homogeneous neighboring vehicles uncertainties (as in scenario S1), the BCRLB criterion shows its efficiency when considering more realistic heterogeneous large dispersion of neighboring vehicles uncertainties. Considering our illustrative example, one can classify vehicles into four classes of dispersion: (i) full topology (i.e., cars fully surrounded by neighbors) versus partial topology (i.e., cars on outside lanes); and (ii) clear GNSS (i.e., cars whose nearest neighbors have good GNSS/estimates) versus degraded GNSS (i.e., cars whose closest neighbors have poor GNSS/estimates), as reported in Table 3.3 (the remaining are not classified due to strong border effects).

Figure 3.8 shows the positioning performance in terms of RMSE (over the full trajectory) for each vehicle whereas Figure 3.9 exhibits the empirical CDFs for one representative vehicle of each class. Both confirm that in 2 degraded classes, when the nearest neighbors
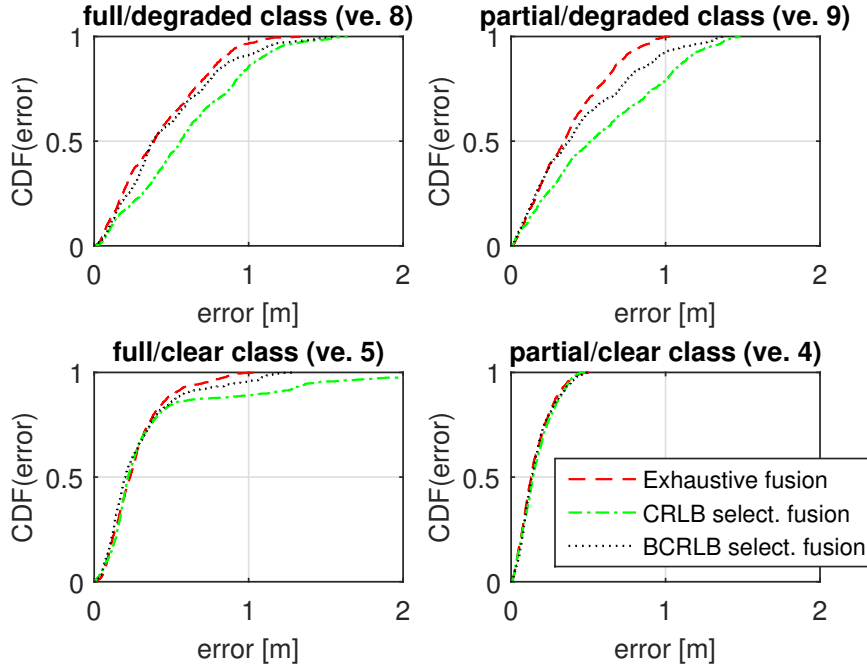
Figure 3.9: Empirical CDFs of localization errors for different fusion schemes with and without selective cooperation at 4 representative vehicles with distinct GNSS quality classes (S2).

Table 3.3: Classification of vehicles in Figure 3.5(b) with respect to the uncertainty dispersion.

Criterion	Full topology	Partial topology
Clear GNSS	5, 11	4, 6, 10, 12
Degraded GNSS	8	7, 9

experience poor GNSS positions or estimates, the classic CRLB criterion neglecting the anchor uncertainties fails to capture the optimal set of neighbors (See the two top sub plots in Figure 3.9). In other words, the strong dependency of RSSI measurements onto distances to the neighbors in the FIM tricks the CRLB to choose among a small subset of the nearest candidates, regardless of their dispersion. As expected, in the 2 clear classes when the nearest neighbors have good GNSS or estimates, the selections are likely to be very similar leading to equivalent performance (See the two bottom sub plots in Fig. 3.9).

In brief, the second scenario accounts for more realistic heterogeneous conditions (at a smaller scale), where the proposed BCRLB solution would be definitely more helpful. Note that we can also assume some vehicles with more advanced sensor package (e.g., lidar, camera, etc.) leading to more accurate estimated positions, thus contributing to achieve even better heterogeneous localization accuracy among vehicles. However, since

we have considered only the fusion of GNSS and V2V information at this stage of the study in this chapter, we simply manipulate the GNSS capabilities.

Preliminary Cooperative Application Impact

Although a larger application evaluation is left to future work, we confront here the link selection performance with tangible application needs. Considering the Highway Capacity Manual (HCM) recommendation of a 2-second time between two successive vehicle in free flow traffic, a typical cooperative traffic safety application would need to have a clear position awareness corresponding to at least the distance between two successive vehicles. This translates to about 30 m and 60 m inter-distance considering a speed of 50 km/h in urban and 100 km/h on highways respectively. In the worst case, exhaustive CLoc yields an error of about 0.85 m (see Figure 3.6). Even while loosing 14–18% of accuracy through selective fusion, one would still get relative longitudinal error of 1.6% (respectively 3%) at 60 m (respectively 30 m)[11], and a fully acceptable increased error of 0.2% between an exhaustive and selective fusion.

3.7   Summary

In this chapter, we have proposed and evaluated elementary functions and building blocks of a data fusion framework for V2V CLoc in the very specific context of GNSS-aided ITS-G5. Our evaluations take account of ad hoc communication and positioning aspects, such as distributed and asynchronous position estimates or random CAM transmissions.

On the one hand, we have pointed out that the transmission intervals between CAMs are constrained by channel load conditions, leading to non-periodic transmissions and as such, asynchronous data reception from "virtual anchors". Accordingly, we have presented a prediction-based data resynchronization mechanism to properly incorporate cooperative information incoming from asynchronous neighboring cars relying on an *a priori* mobility model.

On the other hand, we have stated and solved the link selection problem, as performing exhaustively cooperative schemes is questionable due to heavy required communication traffic and computational processing. Both classic non-Bayesian and Bayesian CRLB crite-

---

[11]Lateral errors might yet remain high regardless of the strategy, as it will be discussed with more details in Chapter 6.

ria have been investigated and incorporated in a computationally efficient search algorithm to reach the subset of the most informative neighbors, while minimizing the performance degradation caused by information loss. We have found that: (i) it is worth employing selective fusion in vehicular CLoc owing to the aforementioned benefits; (ii) the uncertainties of the "virtual anchors" should be monitored to prevent from having wrong cooperative neighbors in some special but common situations.

While considering link selection on the "ego" receiving side, we have also seen that the tolerance regarding the number of packets required in the fusion could induce/inspire more advanced transmission policies (see Chapter 4). Finally, we have illustrated that the use of RSSI over V2V communication link (as direct source of range information) may bring rather limited localization gains whenever the GNSS means already performs reasonably well, thus suggesting the use of more accurate V2V ranging technologies (see Chapter 5).

Chapter 4

Wireless Channel Impacts on V2V Cooperative Localization

4.1 Introduction and Related Works

In Chapter 3, we have shown the promising potential of V2V CLoc to enhance the GNSS solutions in various environments and in different network settings. Nevertheless, in our initial evaluation framework, several simplistic assumptions have been made regarding the V2V wireless channel, which will be relaxed in this chapter.

On the one hand, it has been assumed that the GNSS and the RSSI readings integrated as observations are affected by white error processes (see Section 3.2.2). In practice however, they are strongly correlated over both space and time [26, 30, 79, 101–103], as a result from the combination of locally continuous physical propagation phenomena, highly specific vehicular mobility patterns and constrained refreshment rates. Such spatial correlations are viewed as a drastic limitation of current state of the art CLoc approaches (e.g., degrading fusion filters optimality). Thus, this chapter first concerns the observation noise correlations that may be specifically found under vehicular mobility. Practically speaking, the spatial correlations of observed measurement processes (and thus, their temporal correlations under vehicles mobility) result indeed from the conjunction of different factors triggered by constrained vehicular mobility. First of all, GNSS conditions (good or bad) may not change much over multiple samples and between neighboring vehicles (given a common class of equipment). Similarly, the channel fading conditions (obstructed or not) may not change much between two consecutive CAM transmissions (e.g., every 100 ms) by

60

neighboring vehicles. Jointly or independently, these effects lead to correlated GNSS/RSSI measurements. A major issue when integrating such correlated measures into fusion filters is that they are no longer affected by white Gaussian noise terms (but hence, by dependent contributions) and as such, they break a core assumption of most CLoc fusion approaches [86, 87, 89, 104] leading to inconsistent estimates with large fluctuations. Thus, solutions need to be figured out or adapted to mitigate -or even benefit from- these correlation phenomena in our CLoc context.

On the other hand, CLoc based on PF induces not only high computational complexity but also extra communication cost (e.g., while exchanging particle clouds through message passing [105]) to achieve optimal performance levels. This limitation can be alleviated by adopting parametric message representations (e.g., well-known Gaussian mixture models (GMMs)) instead of propagating explicit particle clouds. In the literature, this has been considered mostly in iterative message passing localization algorithms for generic, static wireless networks so far (typically within WSNs), thus enjoying more stable network connectivity and topology than in VANET scenarios [90, 106, 107]. Alternatively, localization based on variational message passing (VMP) can propagate and multiply circular symmetric Gaussian distributions to produce estimated locations instead of redrawing samples out of explicit distributions received from neighboring nodes, and thus features significantly lower communication overhead [108, 109]. However, the latter solutions also rely on intermediary message approximation steps. All in all, to the best of our knowledge in the vehicular context, no in-depth investigation has been yet carried out in the literature to compare the various parameterization approaches and their performance trade-offs in terms of localization accuracy, communication traffic, channel load, computational complexity, latency, etc., whereas these metrics are expected to strongly impact the practicability and the implementability of PF-based CLoc. Moreover, in case of channel congestion, DCC mechanisms specified by the ETSI recommend to scale the CAM transmission rate from 10 Hz down to 2 Hz (in order not to exceed 60–70% channel load), what is expected to degrade CLoc accuracy accordingly.

This chapter is structured as follows. Section 4.2 formulates the aforementioned problems, namely the space-time correlation of input observation noises and the limited communication channel (in terms of both rate and capacity). In Section 4.3, new methods are proposed at both signal processing and protocol/fusion rate levels so as to mitigate the

harmful impact of observations correlations. On this occasion, the achieved performance is compared with that of initial/nominal CLoc approaches by means of simulations (under both correlated and uncorrelated observation assumptions). Next, Section 4.4 presents and combines message approximation techniques with a new transmission control strategy so as to limit dramatically the channel load. Finally, Section 4.5 provides a summary for the chapter.

4.2   Problem Formulation

4.2.1   Correlations in Observation Noises

In GNSS-aided VANETs, GNSS positions and V2V power measurements (or RSSI readings) used for localization are measured over noisy propagation channels. Generally speaking, these noises are both time-variant and space-variant under typical vehicular mobility (on highways or in urban areas).

On the one hand, time-variant noise can be filtered out by averaging the signal in time or frequency domains (e.g. small-scale fading in RSSI measurements) [30] or using correction models at receivers and information broadcast by transmitters (GNSS satellite clock errors or atmospheric errors) [26].

On the other hand, location-dependent measurements are more challenging as they are significantly impacted by the physical arrangement of surrounding objects in the environment (e.g., buildings, trees, hills, etc.) [97]. More specifically, the spatial correlations of observed measurement processes and thus, their time correlations under car mobility, partly result from the local continuity of electromagnetic interactions in the environment. For GNSS position estimate and V2V range-dependent power respectively, multipath (often dominating the error budgets) [26] and shadowing (i.e., large-scale or slow fading) [30] are major sources of the spatial correlations, especially under constrained mobility patterns and/or constrained acquisition time intervals.

Correlated GNSS Position Errors

A GNSS receiver can experience very large 2-D positioning errors in a narrow street, due to its limited visibility to satellites (i.e., few available satellites causing poor GDOP, biased pseudo-range measurements due to GNSS signal diffraction on building edges, etc.). Intu-

itively, while moving along the street, these GNSS errors will remain of the same order of magnitude for a few tens or even hundreds of meters and as such, will be spatially correlated. The extent of this correlation depends on the environment. In urban canyons, both the number of available satellites and the multipath propagation conditions shall remain unchanged over a distance equivalent to the width of a typical building. In more open-sky environments (e.g., on highways), these conditions remain unchanged over much larger distances. Generally speaking and regardless of the environment, such spatial correlation is always present in VANETs and definitely impacts the use of GNSS data. Motivated by the common idea of modeling the spatial correlation of shadowing with the exponentially decreasing autocorrelation function (ACF) (Gudmundson's model) [102], we adapt it for GNSS residual errors too. This is a fairly reasonable model since its ACF fits well the first order Gauss–Markov process recommended by [110] to model GNSS errors. More particularly, this yields:

$$R_{\text{GNSS}}^{(\cdot)}(\tau) = \left(\sigma_{\text{GNSS}}^{(\cdot)}\right)^2 r_{\text{GNSS}}^{(\cdot)}(\tau) = \left(\sigma_{\text{GNSS}}^{(\cdot)}\right)^2 \exp\left(-\frac{v\,|\tau|\log 2}{d_{\text{cor}}^{(\cdot)}}\right), \qquad (4.1)$$

where $(\cdot)$ can be either x- or y-coordinate, $\sigma_{\text{GNSS}}^{(\cdot)}$ the standard deviation of residual noise in one direction, v the mobile speed, τ the time lag between measurements, and finally $d_{\text{cor}}^{(\cdot)}$ the equivalent correlation distance at which the corresponding normalized ACF is equal to 50%. These correlation distances are of critical importance and can be determined by a prior calibration procedure [30].

Correlated V2V Shadow Process

Spatial correlation also exists for V2V propagation channels (i.e., in terms of slow fading characteristics). They may be intuitively explained by both the relative network topology and the local link obstruction conditions (e.g., generated by the transmitting/receiving cars' bodies themselves, by non-cooperative trucks, by pieces of urban furniture, etc.), which evolve slower under constrained mobility patterns (e.g., platooning on highways, queuing vehicles during rush hours in urban canyons, etc.) than the time intervals between successive transmissions (i.e., 1–10 Hz [19, 98]). Regardless of the environment, spatial correlations in V2V propagation channels thus impact all the vehicles involved in range-dependent information estimation (i.e., based on RSSI readings). An illustration is
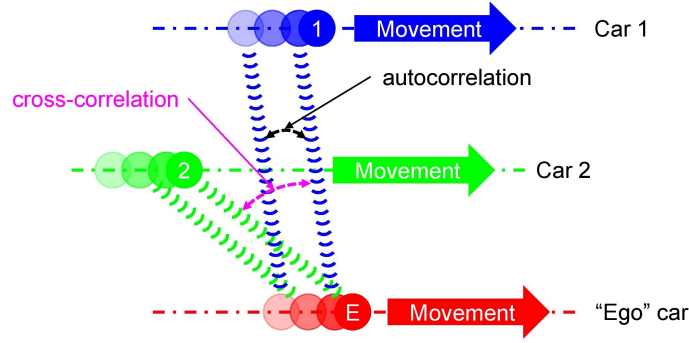
Figure 4.1: Possible shadowing autocorrelations/cross-correlations on/between V2V link(s) having dual mobility in VANETs.

provided on Figure 4.1. Considering the V2V link between the "ego" car and "car 1", successive RSSI readings are auto-correlated if the inter-transmit times between packets are larger than the period change of their mobility patterns and fading conditions. Similarly, considering the two V2V links between "ego" car and "car 1" and "car 2", successive RSSI readings are cross-correlated if the inter-transmit times between packets are larger than the period change between the mobility patterns of "car 1" and "car 2" [1]. The correlated V2V RSSI shadowing properties are again modeled by an exponential ACF [102]

$$R_{\text{Sh}}(\tau) = \sigma_{\text{Sh}}^2 r_{\text{Sh}}(\tau) = \sigma_{\text{Sh}}^2 \exp\left(-\frac{v\,|\tau|\log 2}{d_{\text{cor}}^{\text{Sh}}}\right), \tag{4.2}$$

where, similarly to (4.1), v indicates the speed of the vehicle, τ the time lag, and $d_{\text{cor}}^{\text{Sh}}$ the correlation distance at which the shadowing effect is half of its maximum value.

Gudmundson's model shown above was originally proposed to predict shadowing correlations in cellular networks, that is, for radio links between base stations and mobile stations [102]. Accordingly, in the vehicular context, it could be applied as it is uniquely for links with common end points (e.g., V2I links) but not for links involving two mobile extremities (i.e., V2V links). In other words, a suitable shadowing model dedicated for V2V links has to account for the mobility of both end points and thus, lies beyond the scope of Gudmundson's model. To cope with this problem, an extension of the previous model i.e., the model of Wang *et al.* [111], which generalizes the setting of V2V links with dual mobility, is chosen to model the correlated shadowing map hereafter. Based

---

[1]Cross-correlations and autocorrelation also impact the use of GNSS information at the "ego" car. Successive CAM transmissions of the GNSS information from "car 1" and from "car 2" will indeed integrate also GNSS spatial correlation (as previously described) if their inter-transmit time is higher than the time to move over the GNSS decorrelation distance.

on the assumption that the displacements of the two mobile nodes introduce independent but equivalent contributions onto correlation coefficients, the normalized joint ACF when both the Tx and the Rx are in motion can be approximated by the product of the two normalized ACFs when either the Tx or the Rx moves [111], as follows:

$$
\begin{aligned}
R_{\mathrm{Sh}}(\Delta\mathbf{x}_t, \Delta\mathbf{x}_r) &= \sigma_{\mathrm{Sh}}^2 r_{\mathrm{Sh}}(\Delta\mathbf{x}_t, \Delta\mathbf{x}_r) \\
&= \sigma_{\mathrm{Sh}}^2 r_{\mathrm{Sh}}(\Delta\mathbf{x}_t, 0) r_{\mathrm{Sh}}(0, \Delta\mathbf{x}_r) \\
&= \sigma_{\mathrm{Sh}}^2 \exp\left(-\frac{\|\Delta\mathbf{x}_t\|}{d_{\mathrm{cor}}^{\mathrm{Sh}}} \log 2\right) \exp\left(-\frac{\|\Delta\mathbf{x}_r\|}{d_{\mathrm{cor}}^{\mathrm{Sh}}} \log 2\right) \\
&= \sigma_{\mathrm{Sh}}^2 \exp\left(-\frac{v_t + v_r}{d_{\mathrm{cor}}^{\mathrm{Sh}}} \tau \log 2\right) = \sigma_{\mathrm{Sh}}^2 r_{\mathrm{Sh}}(\tau) = R_{\mathrm{Sh}}(\tau),
\end{aligned}
\tag{4.3}
$$

where $\Delta\mathbf{x}_t = (\Delta x_t, \Delta y_t)^\dagger$ and $\Delta\mathbf{x}_r = (\Delta x_r, \Delta y_r)^\dagger$ represent the 2-D displacements of the Tx and the Rx respectively within a time interval τ. The correlation coefficient R_{Sh} can also be represented as a function of the time lag τ given the knowledge of Tx's and Rx's speeds i.e., v_t and v_r, respectively. From (4.3), one can notice that the joint ACF is now affected by mobility on both extremities of the link, in compliance with generic V2V shadowing needs.

Summarizing, widely observed and reported in GNSS and V2V fading literature [26, 30, 79, 101–103, 112], spatial correlations are yet hardly addressed in previous works dealing with distributed and/or CLoc in the vehicular context. It is however essential to consider a realistic observation model with correlated noises (on both GNSS and V2V RSSI observation ingredients) in order to avoid producing biased and/or unreliable results while assessing CLoc performance.

4.2.2 Limited V2V Message Payload and Channel Capacity

On top of the previous physical aspects related to propagation, the V2X wireless channel is also structurally limited on its own due to standard constraints and limitations. For instance, in the context of a PF-based CLoc, the particle cloud has to be simplified to a few scalars that can be practically conveyed by the CAMs. In addition, the neighboring vehicles receiving these CAMs must be able to simply reconstruct the initial particle cloud out of these scalars, without losing too much information. Each particle cloud can be approximated by a known *a priori* distribution, which is commonly a Gaussian or a mixture of Gaussians. The motivation for choosing a single Gaussian lies in its fine analytical
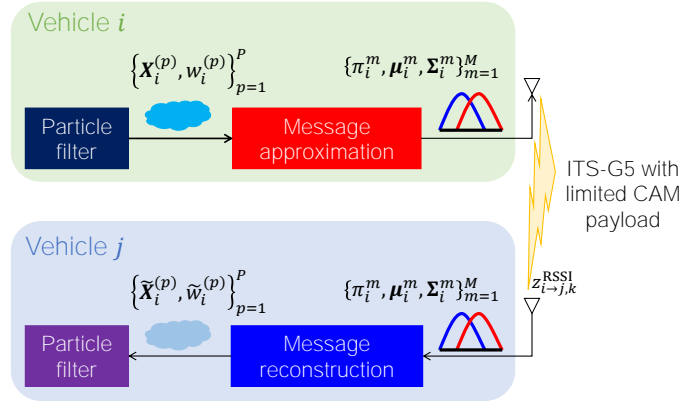
Figure 4.2: Example of awareness data flow in PF-based CLoc framework for two vehicles i and j. Vehicle i first approximates its particle-based state $\{\mathbf{X}_i^{(p)}, w_i^{(p)}\}_{p=1}^P$ by a Gaussian (mixture) distribution, then encapsulates the parameters $\{\pi_i^m, \boldsymbol{\mu}_i^m, \boldsymbol{\Sigma}_i^m\}_{m=1}^M$ in a CAM to broadcast. Receiving vehicle j extracts these parameters to identify the distribution and draw samples from it to reconstruct the approximated $\{\widetilde{\mathbf{X}}_i^{(p)}, \widetilde{w}_i^{(p)}\}_{p=1}^P$.
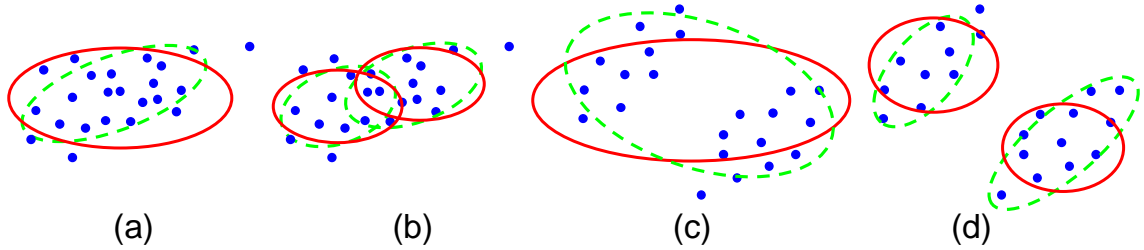
Figure 4.3: Simplified 2-D position representations including nonparametric (i.e., particles as dots) and parametric (i.e., diagonal Gaussian modes as solid ellipses and full Gaussian modes as dashed ellipses) approaches. Unimodal data can be approximated by either unimodal Gaussian in (a) or bimodal Gaussian in (b) and bimodal data can be approximated by either unimodal Gaussian in (c) or bimodal Gaussian in (d). Each explicit particle representation costs two scalars, each diagonal Gaussian mode occupies 4 scalars, and each full Gaussian mode requires 5 scalars. One more scalar is needed for the weight in case of bimodal distribution.

properties (making calculations more tractable) whereas mixtures of Gaussians can usually approximate more complex densities, by tuning the means, covariance matrices, and mixture weights of the Gaussian components involved in the linear combination [113]. Figure 4.2 provides a simplified illustration of the awareness information exchanges enabling CLoc between two vehicles i and j while Figure 4.3 illustrates how 2-D particle-based positions can be approximated by the previous representations in both non-ambiguous and ambiguous geometric cases (see Figure 4.3(a)-(b) and Figure 4.3(a)(c)-(d), respectively).

If location-oriented packets are heavy, only a few could transit over the air per unit of time and thus accuracy would be degraded (i.e., even regardless of ETSI DCC) Moreover, if broadcast rates are deliberately reduced, then accuracy is also expected to be degraded.

To compensate for the information loss, on top of the message approximation, transmission policies enabling adaptive transmit payload, power, and rate need revisions to maintain high accuracy CLoc.

4.3 Mitigation of Observation Noise Correlations

4.3.1 Signal Level Mitigation

Empirical Estimation of Cross-Measurement Correlations

This technique relies on the intuition that the knowledge of cross-correlations between the components of the measurement vector provides relevant information to CLoc [103]. Recalling that, although the x-to-y correlation in GNSS position is commonly assumed to be null, the cross-correlations between links' fading measurements are accounted in the 4-D shadowing map and can be determined. More particularly, an "ego" vehicle can infer from its "ego" position and the constellation of its "virtual anchors" the correlations between links' fading measurements. From the aforementioned 4-D correlated shadowing model, we therefore derive the cross-correlation between two separate links $a = (i \rightarrow j)$ and $b = (l \rightarrow m)$ as follows:

$$R_{\text{Sh}}(a, b) = \sigma_{\text{Sh}}^2 \exp\left(-\frac{\|\mathbf{x}_i - \mathbf{x}_l\| + \|\mathbf{x}_j - \mathbf{x}_m\|}{d_{\text{cor}}^{\text{Sh}}} \log 2\right), \tag{4.4}$$

where $\|\mathbf{x}_i - \mathbf{x}_l\|$ and $\|\mathbf{x}_j - \mathbf{x}_m\|$ are the Euclidean distances between the transmitters i and l and between the receivers j and m, respectively.

For illustration, we consider a simplified example where the "ego" car i moving at speed v_i collects three asynchronous RSSI readings with respect to the three neighbors 1, 2, and 3 during the time interval ΔT (e.g., every 100 ms or equivalently, at the fusion rate of 10 Hz). The covariance matrix for the shadowing experienced over these three links is thus inferred from (4.4) as

$$\mathbf{R}_{\text{Sh}}(1, 2, 3 \rightarrow i) = \begin{pmatrix} \sigma_{\text{Sh}}^2 & R_{\text{Sh}}(1, 2 \rightarrow i) & R_{\text{Sh}}(1, 3 \rightarrow i) \\ R_{\text{Sh}}(2, 1 \rightarrow i) & \sigma_{\text{Sh}}^2 & R_{\text{Sh}}(2, 3 \rightarrow i) \\ R_{\text{Sh}}(3, 1 \rightarrow i) & R_{\text{Sh}}(3, 2 \rightarrow i) & \sigma_{\text{Sh}}^2 \end{pmatrix}, \tag{4.5}$$

with

$$R_{\mathrm{Sh}}(j, l \to i) = \sigma_{\mathrm{Sh}}^2 \exp\left(-\frac{\|\mathbf{x}_j - \mathbf{x}_l\| + v_i |t_j - t_l|}{d_{\mathrm{cor}}^{\mathrm{Sh}}} \log 2\right), \quad j, l \in \{1, 2, 3\}, \qquad (4.6)$$

where t_j and t_l represent the time instants at which vehicle i receives the CAMs from its neighbors j and l, respectively.

Note that (4.6) is deduced after applying (4.4) to a pair of links that has a common end point (i.e., "ego" vehicle i). As vehicle i collects data while moving, cross-link correlation depends on the traveling distance between two corresponding CAMs. Hence, this distance varies from one pair of links to the others. In practice, the true positions (e.g., $\mathbf{x}_j$, $\mathbf{x}_l$ in (4.4)) cannot be perfectly known. Accordingly, a possible and reasonable approximation $\widehat{R}_{\mathrm{Sh}}(j, l \to i), \ j, l \in \{1, 2, 3\}$ leading to $\widehat{\mathbf{R}}_{\mathrm{Sh}}(1, 2, 3 \to i)$ can be estimated as a function of the estimated positions $\widehat{\mathbf{x}}_j, \widehat{\mathbf{x}}_l, \ j, l \in \{1, 2, 3\}$, which are included in/derived from the received CAM payloads. In practice, when the "ego" vehicle has more reference neighbors, the generalization is straightforward.

Differential Measurements

In the literature, there exists a couple of techniques to deal with correlated/colored observation noise. One first approach is to augment the state with the observation noise components [86, 101]. However, this causes a singular measurement noise covariance, which often results in numerical problems [86]. Hence, we concentrate in our work on the second option, referred to as differential measurement (DM). As suggested by its name, the key idea is to whiten the noise by subtracting the correlated part. This problem is solved by building a noise prediction model (from its correlation properties). Being both characterized by the exponential ACF, GNSS residual error and shadowing can be predicted by a Gauss–Markov model. In addition, the most dominant mobility pattern in the vehicular context is platooning-like when vehicles move in groups (coordinated or not). Accordingly, their velocities become highly correlated and thus, the memory levels in the prediction model are almost time-invariant in first approximation[2]. For the GNSS x- and

---

[2]The technique is not limited to highly correlated mobility. In a general case, the memory levels become time-variant i.e., depending on the last known speeds of the participants, leading to prediction noises that are statistically independent but not identically distributed (i.e., varying standard deviation).

y-residual errors $n_{i,k}^x$ and $n_{i,k}^y$ respectively, this yields

$$n_{i,k}^x = \lambda_{\text{GNSS}}^x n_{i,k-1}^x + \widetilde{n}_{i,k}^x, \quad n_{i,k}^y = \lambda_{\text{GNSS}}^y n_{i,k-1}^y + \widetilde{n}_{i,k}^y, \tag{4.7}$$

and for the shadow fading of the link $(j \to i)$, denoted by $s_{j \to i,k}$, this leads to

$$s_{j \to i,k} = \lambda_{\text{Sh}} s_{j \to i,k-1} + \widetilde{s}_{j \to i,k}, \tag{4.8}$$

where $\widetilde{n}_{i,k}^x$, $\widetilde{n}_{i,k}^y$, and $\widetilde{s}_{j \to i,k}$ are zero mean white Gaussian processes with small variances of $(1 - (\lambda_{\text{GNSS}}^x)^2)(\sigma_{\text{GNSS}}^x)^2$, $(1 - (\lambda_{\text{GNSS}}^y)^2)(\sigma_{\text{GNSS}}^y)^2$, and $(1 - \lambda_{\text{Sh}}^2)\sigma_{\text{Sh}}^2$, respectively.

The memory levels are $\lambda_{\text{GNSS}}^x \approx \exp\left(-v_i \Delta T / d_{cor}^x\right)$, $\lambda_{\text{GNSS}}^y \approx \exp\left(-v_i \Delta T / d_{cor}^y\right)$, and $\lambda_{\text{Sh}} \approx \exp\left(-(v_i + v_j)\Delta T / d_{cor}^{\text{Sh}}\right) \approx \exp\left(-2v_i \Delta T / d_{cor}^{\text{Sh}}\right)^3$, where ΔT is the measurement sampling period, v_j and v_i the asymptotic mean speeds of the Tx j and the Rx i, respectively. In the time interval ΔT till the next fusion time k, the "ego" car i communicates with its set $\mathcal{N}_{\to i,k}$ of "virtual anchors" whose cardinality $|\mathcal{N}_{\to i,k}|$ is denoted by $\bar{N}_{i,k}$ for simpler notations. Hence, the prediction model in the vector form is

$$\mathbf{n}_{i,k} = \boldsymbol{\lambda} \mathbf{n}_{i,k-1} + \widetilde{\mathbf{n}}_{i,k}, \tag{4.9}$$

where $\boldsymbol{\lambda} = \text{diag}(\lambda_{\text{GNSS}}^x, \lambda_{\text{GNSS}}^y, \ldots, \lambda_{\text{Sh}}, \ldots)$, $\boldsymbol{\lambda} : \mathbb{R}^{\bar{N}_{i,k}+2} \to \mathbb{R}^{\bar{N}_{i,k}+2}$ represents the diagonal memory matrix, $\mathbf{n}_{i,k} = (n_{i,k}^x, n_{i,k}^y, \ldots, s_{j \to i,k}, \ldots)^\dagger \in \mathbb{R}^{\bar{N}_{i,k}+2}$ represents the observation noise vector, and finally, $\widetilde{\mathbf{n}}_{i,k} = (\widetilde{n}_{i,k}^x, \widetilde{n}_{i,k}^y, \ldots, \widetilde{s}_{j \to i,k}, \ldots)^\dagger \in \mathbb{R}^{\bar{N}_{i,k}+2}$ is the whitened noise vector.

Now, the so-called auxiliary measurement $\widetilde{\mathbf{z}}_{i,k}$ can be expressed as

$$\widetilde{\mathbf{z}}_{i,k} = \mathbf{z}_{i,k} - \boldsymbol{\lambda} \mathbf{z}_{i,k-1} = \widetilde{\mathbf{h}}(\mathbf{X}_{i,k}, \mathbf{X}_{\mathcal{S} \to i,k}) + \widetilde{\mathbf{n}}_{i,k} \tag{4.10}$$

with

$$\widetilde{\mathbf{h}}(\mathbf{X}_{i,k}, \mathbf{X}_{\mathcal{S} \to i,k}) = \mathbf{h}(\mathbf{X}_{i,k}, \mathbf{X}_{\mathcal{S} \to i,k}) - \boldsymbol{\lambda} \mathbf{h}\left(\mathbf{X}_{i,k-1}, \mathbf{X}_{\mathcal{S}_k \to i,k-1}\right)$$

and

$$\widetilde{\mathbf{n}}_{i,k} = \mathbf{n}_{i,k} - \boldsymbol{\lambda} \mathbf{n}_{i,k-1},$$

---

[3]We consider here the fusion/filter rate equal to the GNSS rate i.e., $1/\Delta T$, therefore, only vehicles that send CAMs at this rate (or higher) can become "virtual anchors". If so, the time interval between two consecutive received CAMs/RSSI readings is more or less ΔT due to random CAM generation time and/or congestion control.

where $\mathbf{X}_{i,k} \in \mathbb{R}^{n_x}$, $\mathbf{X}_{\mathcal{S}\to i,k} \in \mathbb{R}^{\bar{\bar{N}}_{i,k}\times n_x}$ are the state vector of "ego" vehicle i and the aggregated state vector of its cooperative neighbors as "virtual anchors" (i.e., the set $\mathcal{N}_{\to i,k}$) respectively, n_x the dimension of the state vector $\mathbf{X}_{i,k}$, $\mathbf{z}_{i,k} = (x_{i,k}, y_{i,k}, \ldots, z_{j\to i,k}^{\mathrm{RSSI}}, \ldots)^{\dagger} \in \mathbb{R}^{\bar{\bar{N}}_{i,k}+2}$ the aggregated measurement vector, $\widetilde{\mathbf{h}} : \mathbb{R}^{n_x} \times \mathbb{R}^{\bar{\bar{N}}_{i,k}\times n_x} \to \mathbb{R}^{\bar{\bar{N}}_{i,k}+2}$ the corresponding model for the new measurement vector $\widetilde{\mathbf{z}}_{i,k} \in \mathbb{R}^{\bar{\bar{N}}_{i,k}+2}$, and $\widetilde{\mathbf{n}}_{i,k} \in \mathbb{R}^{\bar{\bar{N}}_{i,k}+2}$ the prediction noise vector, which is assumed white with a diagonal covariance matrix but cross-correlated with the process noise [86, 101], although this cross-correlation can be neglected at the price of marginal accuracy degradation [101].

Accordingly, our new equivalent observation model can now be written in the same form as (4.10). Note that contrarily to our proposal, the initial differential measurement technique relies on a new measurement $\widetilde{\mathbf{z}}_{i,k} = \mathbf{z}_{i,k+1} - \boldsymbol{\lambda}\mathbf{z}_{i,k}$, which uses the future measurement $\mathbf{z}_{i,k+1}$. This technique is somehow equivalent to 1-lag smoothing [86], thus likely yielding better accuracy gains. Nevertheless, it is inappropriate for real-time tracking in high-mobility contexts such as VANETs.

In addition, in realistic settings, the use of random CAM transmissions introduces specific challenges that should be accounted carefully. Even in case of periodic CAMs, the transmissions are still random due to a so-called CAM generation time between the instant when CAM generation is triggered and the instant when the CAM is delivered to the networking transport layer [19], as illustrated in Figure 4.4. Assume that the CAMs are triggered right after estimating the position, it is possible that the CAM is transmitted and thus received too late with respect to the "ego" estimation time, causing 1) a lack of up-to-date CAMs (e.g., time window $k-1$ in Figure 4.4) and 2) redundant CAMs afterwards (e.g., time window k in Figure 4.4). In the former subcase, the solution is to simply exclude this neighbor j from the list of "virtual anchors" since there is no RSSI measurement with respect to j available at the estimation time (i.e., $t_{i,k-1}$). In the latter subcase, it is reasonable to retain the latest CAM and to drop the oldest CAMs (e.g., the late CAM in Figure 4.4). We observe that this scenario usually occurs as a result of late CAMs. Since there was no observation associated with j at time $t_{i,k-1}$, the DM can not be performed at time $t_{i,k}$. In other words, a late CAM can prevent its transmitter from becoming a "virtual anchor" up to two consecutive "ego" estimates when adopting the DM technique.
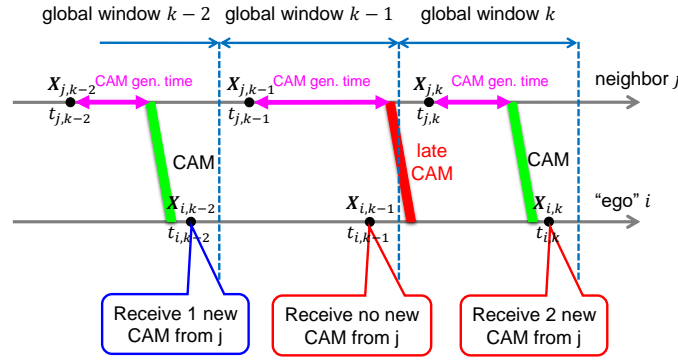
Figure 4.4: Impacts of asynchronous position estimates and CAM transmissions on the information fusion.

4.3.2 Adaptive Fusion Rate

Unlike signal level mitigation approaches, this protocol level solution eliminates correlations by artificially decreasing the cooperative fusion rate (in comparison with the available rate) without manipulating the observations. For each source of information (i.e., GNSS positions and RSSI readings), as the observations are correlated in space with a limited decorrelation distance d_{cor}, a vehicle moving over a distance D along a straight line can temporally collect up to $1 + \lfloor D/(\gamma d_{\text{cor}}) \rfloor$ uncorrelated measurements, where $\gamma \geq 1$ measures the quality of independent instantiations (e.g., $\gamma_1 = 1$ and $\gamma_2 = 2$ correspond to 50% and 75% reduction in the correlation respectively), as shown in Figure 4.5. This simple technique may not be appropriate for GNSS collection because GNSS decorrelation distance can be up to hundreds of meters and GNSS-assisted DR accumulates errors over time and distance. However, it can be more beneficial for RSSIs due to the short shadowing correlation distance in urban environments (e.g. typically 10–20 m [101, 102, 111]). Moreover, recalling that in V2V channels, the decay of the correlation coefficient is affected by both Tx and Rx's displacements (see (4.3)), hence, Rx vehicles can obtain uncorrelated measurements before completing $d_{\text{cor}}^{\text{Sh}}$ or experience more modest correlation effects at the same distance. Thus, an option is to primarily rely on the DM technique for the correlated GNSS sources. The CLoc may be activated to improve the accuracy only if uncorrelated RSSIs are available, leading to reduced fusion rates (in comparison with the standalone GNSS-based filter rate). One advantage of this hybrid scheme is to cut down on computations by avoiding unnecessary fusion steps while maintaining an equivalent tracking performance. Another benefit lies in the ability to adopt the first proposed technique (i.e., empirical estimation of cross-link correlations) to minimize the effects of correlated
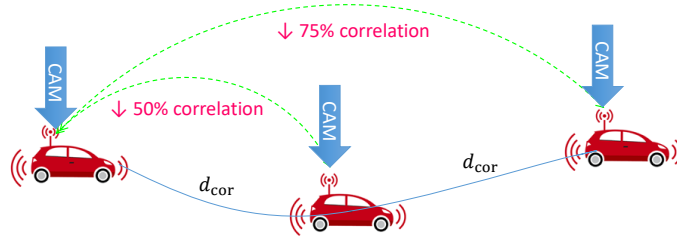
Figure 4.5: Illustration of the adaptive sampling techniques simply deceasing the cooperative fusion rate to collect uncorrelated RSSI measurements.
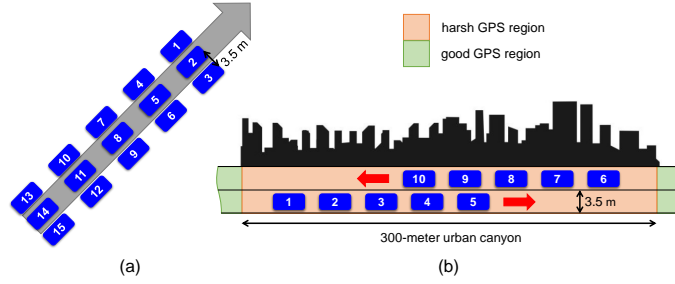
Figure 4.6: Topology of the evaluated VANETs and related attributes in (a) highway/tunnel and (b) urban canyon scenarios.

noises or to approach the standard filtering performance with i.i.d. noises. Additionally, the scenario depicted in Figure 4.4 (i.e., late CAMs) is also interestingly supported with this technique. Remarkably, the strategy (and thus, the impact) is similar to that of DM techniques. In other words, one neighbor sending a late CAM cannot be a reference vehicle.

Finally, in case of channel congestion, the ETSI DCC rules recommend to scale the transmission rate down to 2 Hz, what is still higher than the slowest proposed fusion rate (e.g., 1.43 Hz on Figure 4.9). Accordingly, we do not expect any negative impact from channel congestion cases[4]. We even claim that the system is perfectly resilient to channel congestion situations, besides its clear advantage in terms of overhead.

4.3.3   Numerical Results

Simulation Settings

Our Monte Carlo trials are performed in three representative environments and scenarios, namely the highway, the urban canyon, and the tunnel, which naturally provide contrasted vehicular propagation channels and mobility conditions. In particular, as illustrated in

---

[4]More generally, regardless of correlation mitigation considerations, the actual impact of channel congestion control mechanisms and transmit policies will be investigate in the following (see Section 4.4).

Table 4.1: Mobility model and traffic parameters used for the simulation-based evaluation of techniques mitigating observation noise/dispersion correlations.

Parameter	Highway	Urban Canyon	Tunnel
Memory level α		0.95	
Asymptotic mean speed $\|\bar{\mathbf{v}}_{i,k}\|$	30 [m/s]	15 [m/s]	15 [m/s]
Standard deviation of the noise σ_i^d	1 [m/s^2]	3 [m/s^2]	1 [m/s^2]
Standard deviation of the noise σ_i^o	0.1 [m/s^2]	0.95 [m/s^2]	0.1 [m/s^2]
Sampling period ΔT		0.1 [s]	
Simulation time	100 [s]	12 [s]	100 [s]
Number of lanes	3	2	3
Traffic direction(s)	1 (Common)	2 (Opposite)	1 (Common)
Simulated track length	3,000 [m]	300 [m]	1,500 [m]

Figure 4.6, we first model a three-lane highway (of most common kind in Europe), where 15 ITS-G5 connected cars are driving steadily (in the same north-east direction) at the average speed of 110 km/h (i.e., about 30 m/s) for 3000 m. The latter vehicles establish a pure VANET and can benefit from relatively favorable GNSS signals due to the open sky operating environment. Secondly, we focus on a more critical GNSS-denied scenario. Specifically, the aforementioned VANET goes through a three-lane straight portion of urban tunnel at the average speed of 50 km/h (i.e., about 15 m/s) for 1500 m. Finally, we consider a short urban canyon of 300 m in the form of a two-lane narrow street with opposite traffic directions (i.e., one direction per lane). The related mobility and traffic model parameters are summarized in Table 4.1.

Besides, depending on each scenario configuration and on generated mobility traces, conditional models are applied in terms of both GNSS and V2V RSSI observations based on measurement-based parameters from the recent literature (whenever available), as reported in Table 4.2. To generate spatially correlated GNSS error components $n^x(\mathbf{x})$ and $n^y(\mathbf{x})$, with $\mathbf{x} = (x, y)^\dagger$ indicating 2-D GNSS receiver's position, whose ACF has the same exponential decay as in (4.1), the 2-D correlated GNSS error maps $\hat{n}^x(\mathbf{x})$ and $\hat{n}^y(\mathbf{x})$ can be approximated by generating a finite sum of sinusoids (SOS) (e.g., 100) whose periodicity depends on the GNSS receiver's x- and y-coordinates [114]. It is worth noticing that these two spatially correlated GNSS errors affecting x- and y-coordinates are generated independently hereafter for simplicity. On the other hand, since the spatial joint correlation property of the V2V shadowing is characterized, given both Tx's and Rx's 2-D locations as inputs variables (i.e., $\mathbf{x}_t = (x_t, y_t)^\dagger$ and $\mathbf{x}_r = (x_r, y_r)^\dagger$ respectively), we can simply generate a 4-D spatially correlated shadowing map $\hat{s}(\mathbf{x}_t, \mathbf{x}_r)$ for mobile transceivers by using the SOS-based joint shadowing model in [111]. The details are presented in Appendix F.

Table 4.2: Correlated observation error (GNSS) and/or dispersion (V2V RSSI shadowing) model parameters.

Modality	Parameter	Urban Canyon	Tunnel[a]	Highway
V2V RSSI	n_p σ_{dB} $d_{\mathrm{cor}}^{\mathrm{Sh}}$	low (1.6 [115]) large (3.4 dB [115]) very short (3 m [112])	id. id. id.	low (1.9 [100]) medium (2.5 dB [100]) large (20 m [112])
GNSS position	σ_{GNSS} $d_{\mathrm{cor}}^{\mathrm{GNSS}}$	large (10–30 m [65, 116]) medium/building-dependent (50–100 m)	N/A (no GNSS) N/A (no GNSS)	medium (3-10 m [59, 65, 116]) very large/open sky (100–500 m)

[a] In lack of representative figure/information available for this scenario in the recent literature (to the best of our knowledge), we assume in first approximation 1) rather similar conditions than that of the urban canyon scenario (due to the confined propagation medium, and rather similar conditions in terms of car density and speed) but 2) no GNSS at all and a larger number of lanes having the same traffic direction (see Table 4.1).

Table 4.3 summarizes the remaining common simulation parameters and settings used in the three simulated scenarios, regarding the CAM transmission rate and times, the GNSS refresh rate and the generation of correlated processes.

Table 4.3: Parameters used for the simulation-based evaluation of techniques mitigating observation noise/dispersion correlations.

Parameter	Description
GNSS refresh rate	10 [Hz]
CAM rate	10 [Hz] (critical) [19, 98]
CAM generation time	$\mathcal{U}(0, 50)$ [ms] [19]
Number of cosines for correlation models	100–1000 [111, 114]
Number of particles in PF	1000

In our comparative study, we consider two different positioning contexts, i.e., the filtered standalone GNSS (non-CLoc solution) and the exhaustively fused GNSS+ITS-G5 (CLoc solution), both running at the filter/fusion rate of 10 Hz (i.e., the rate of GNSS refreshment and critical CAM generation). First, we analyze them in unrealistic i.i.d. noise environments, which are widely considered in literature so far, as two benchmark approaches. Second, we test them under realistic correlated conditions. Last, we add two proposed methods to decorrelate the noises, i.e., DM and decreased fusion rate (or adaptive sampling). More specifically, we obtain three solutions including the filtered GNSS with DM (at 10 Hz), the exhaustively fused GNSS+ITS-G5 with DM (at 10 Hz), and the hybrid fused GNSS+ITS-G5 incorporating the filtered GNSS with DM at 10 Hz and ITS-G5 at lower rate.

Regarding the hybrid option, the RSSIs are collected over each traveling distance equivalent to the shadowing correlation length. Thus, the normalized joint ACF (i.e., (4.3)) reduces by $1/2 \times 1/2 = 1/4$ due to dual mobility at both "ego" and neighboring cars. Mathematically, considering 10-Hz refresh rate of the filter/fusion, the decreased fusion

rate can be computed by $r_x = 10 \left\lceil 10^{-\frac{d_{\text{cor}}^{\text{Sh}} \log_2 x}{2v}} \right\rceil^{-1}$, where r_x [Hz] aims at $x\%$ in the normalized joint ACF, and v is the vehicle's average speed. For example, in the highway scenario, 20-m correlation length and 30-m/s speed yield a rate of about 1.43 Hz while in the urban case, 3-m correlation length and 15-m/s speed give a rate of 5 Hz.

Besides, cross-link correlation information is added to the hybrid solution but not with the DM technique, whose differential noise vector is by design white (i.e., having diagonal covariance matrix).

Scenario Evaluation

Highway Scenarios We now analyze the effects of measurement correlation on filtering/fusion performance and evaluate the gains from the proposed techniques by undertaking "step-by-step" investigations. We first consider either GNSS noise or shadowing to be correlated (while assuming the other process to be i.i.d.) and ultimately, we assume both processes to be correlated.

Correlated GNSS noise and i.i.d. shadowing scenario (S1) In this first example, we deal with GNSS noise correlation by applying the DM technique. The results are summarized in Figure 4.7 by means of empirical CDFs. As expected, when the GNSS position noise is decorrelated by DM, huge accuracy improvements are observed in both non-CLoc (i.e., single GNSS) and CLoc (i.e., GNSS+ITS-G5) solutions. More specifically, for the filtered standalone GNSS, the position estimates accounting for the noise correlation experience significant relative drops by 58% in median error and 37% in worst-case (WC) error (defined for a CDF of 90%) from those neglecting the noise correlation. Similarly, massive relative decreases by 75% in median error and 63% in WC error are noticeable after integrating the DM technique in the exhaustively fused GNSS+ITS-G5. On the other hand, Figure 4.7 confirms the advantage of CLoc over non-CLoc regardless of noise decorrelation. A closer look reveals that the filtered GNSS without DM draws less significant accuracy gains from the ITS-G5 than that with DM as correlated noise is a threat to the effectiveness of data fusion. Besides, the positioning performance delivered by the filtered GNSS after whitening the correlated noise remains quite below that achieved in the i.i.d. noise case. Three main reasons can be invoked: first, error transfer from the previous estimate to the current estimate via the new observation model (i.e., $\widetilde{\mathbf{h}}(\cdot)$ in (4.10))
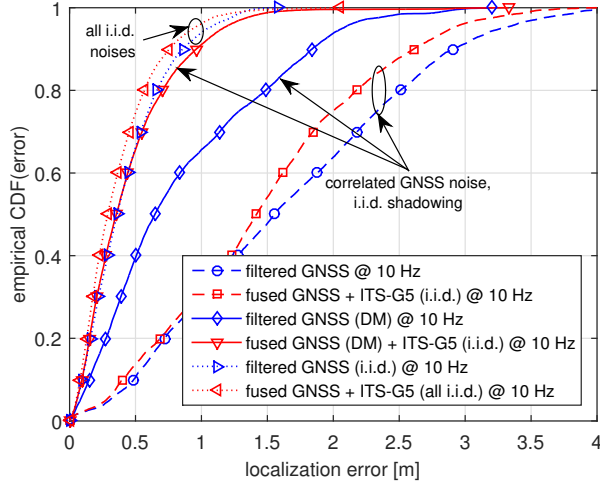
Figure 4.7: Positioning performance comparison of different schemes assuming correlated GNSS noise and i.i.d. shadowing except the two top curves corresponding to both i.i.d. GNSS noise and RSSI shadowing cases in the highway scenario.
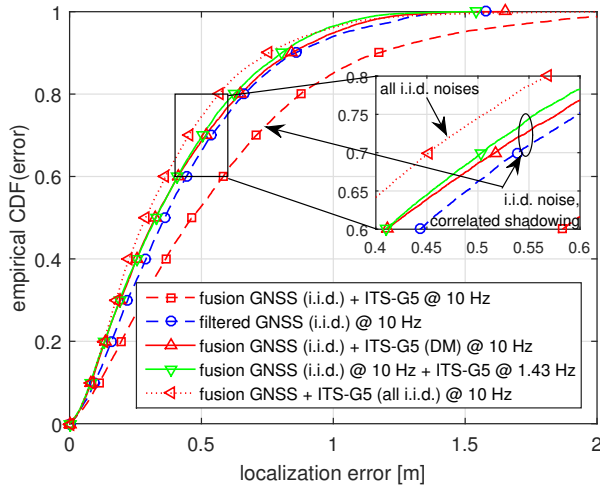
Figure 4.8: Localization performance comparison of different schemes assuming i.i.d. GNSS noise and correlated shadowing except the top curve corresponding to both i.i.d. GNSS noise and RSSI shadowing case in the highway scenario.

after performing DM between the current and the previous measurements; second, model mismatch (i.e., simulating finite SOS based on an exponential ACF versus assuming first order Gauss–Markov noise prediction model); third, possible cross-correlation between the whitened measurement noise and the process noise claimed in [86, 101]. Nevertheless, this problem can be solved by enabling CLoc (i.e., exhaustively fused GNSS (DM) and ITS-G5), which approaches the i.i.d. case, as shown in Figure 4.7.

i.i.d. GNSS noise and correlated shadowing scenario (S2)   In case of correlated shadowing, both DM and decreased fusion rate can be employed for RSSI measure-
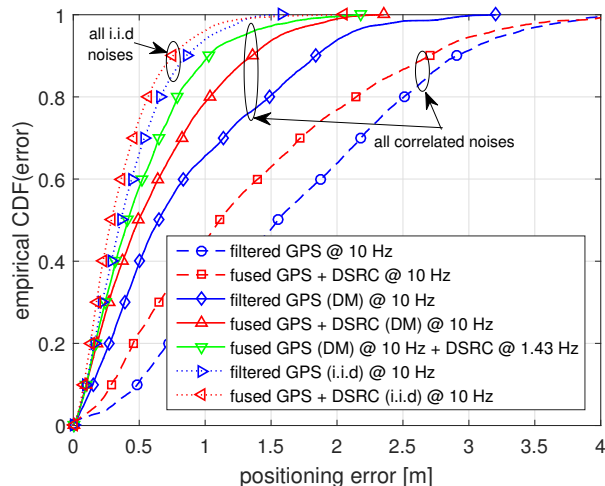
Figure 4.9: Localization performance comparison of different schemes assuming correlated GNSS noise and correlated shadowing, except the two top curves corresponding to both i.i.d. GNSS noise and RSSI shadowing cases in the highway scenario.

ments. Note that when GNSS error is assumed i.i.d., the filtered GNSS achieves very high accuracy (see the second top curve in Figure 4.8). This is challenging to our fusion scheme since RSSI-based positioning is not considered as a high precision solution and as such, may deteriorate the performance of nominal GNSS-based localization [97]. It can be seen clearly from Figure 4.8 that the cooperative GNSS+ITS-G5 solution neglecting shadowing correlation produces erroneous estimates in comparison with the non-cooperative filtered GNSS, confirming that the careless handling of shadowing correlation incurs convergence issues. When the shadowing is decorrelated by either the DM method or by a decreased fusion rate (from 10 Hz to 1.43 Hz), the cooperative GNSS+ITS-G5 option now slightly outperforms the standalone filtered GNSS and closely approaches the GNSS+ITS-G5 fusion option in the i.i.d. case. The reason can be understood as follows. In comparison with GNSS positions, RSSI measurements with respect to "virtual anchors" can contribute to the positioning performance but to a rather modest extent due to the log-distance behavior (in relation to the underlying path loss model). Finally, both extrapolated/approximate RSSI values at the fusion time instant and virtual anchors' uncertainties may alter the positioning performance. In other words, when the accuracy of the filtered GNSS remains high enough (e.g., under i.i.d. assumption and low GNSS noise), there is little room for improvement by fusing with ITS-G5.

Correlated GNSS noise and correlated shadowing scenario (S3)   In this experiment, we let both GNSS position error and shadowing correlated to examine the performance of the proposed algorithms. The results summarized in Figure 4.9 are compliant with that of the previous case (S1) for the filtered standalone GNSS with/without DM. As we have already noted accuracy improvements from noise decorrelation in the filtered standalone GNSS, it is worth verifying how the performance can be further boosted under correlated RSSIs too. The corresponding performance will be seen as a reference. As expected, the cooperative fused GNSS+ITS-G5 with DM yields similar performance improvement (relative drops of 23% in median error and 26% in WC error) over the filtered GNSS with DM. However, this scheme does not approach the corresponding i.i.d. case as in (S1) (see again Figure 4.7) due to the fact that the DM method for RSSIs has the same drawbacks as for GNSS positions (as pointed out in (S1)). Hence, differential RSSIs are less beneficial than i.i.d. RSSIs in (S1). On the other hand, the hybrid fused GNSS+ITS-G5 (i.e., combining the filtered GNSS with DM at 10 Hz and ITS-G5 at 1.43 Hz) enables very favorable positioning results in consideration of collecting temporally uncorrelated RSSI measurements and exploiting the cross-link correlation, thus compensating for the information loss in the fusion model. Quantitatively, the accuracy improvement matches by less than 10% the performance of optimal CLoc when considered under i.i.d. measurements. In comparison with cooperative GNSS+ITS-G5 under the same decreased fusion rate as in (S2) (see Figure 4.8), we observe that the hybrid scheme in (S3) suffers from slightly degraded positioning performance due to GNSS noise correlation.

Finally, Figure 4.10 illustrates the RMSE of the whole VANET's position estimates (i.e., over all vehicles) as a function of time. In addition to confirm again the performance order of the considered algorithms, it shows that the schemes neglecting the noise correlation (see Figure 4.10 (top)) result in inconsistent estimates with large fluctuations whereas the schemes accounting for this correlation bring more stable results (see Figure 4.10 (middle)). Obviously, the most steady position estimates belong to the two i.i.d. cases in Figure 4.10 (bottom). For spatially correlated noise environments, if the correlation information is not taken into account, the filter/fusion will react in the same way to low noise regions as to high noise regions[5]. Furthermore, reminding that Bayesian filter/fusion schemes such as PF produce estimates by incorporating all the measurements

---

[5]In i.i.d. noise environments, the noise terms have the same standard deviation regardless of the regions.
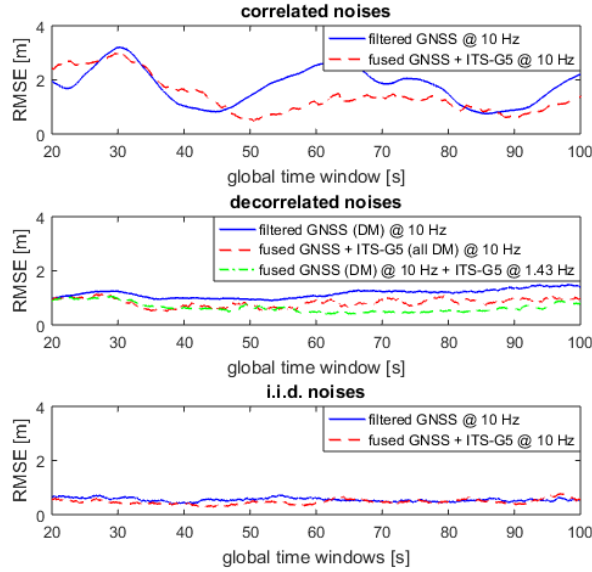
Figure 4.10: RMSE comparison of different filter/fusion strategies divided into three groups: conventional approaches (top), proposed approaches (middle), and optimal (unrealistic) approaches (bottom) in the highway scenario.
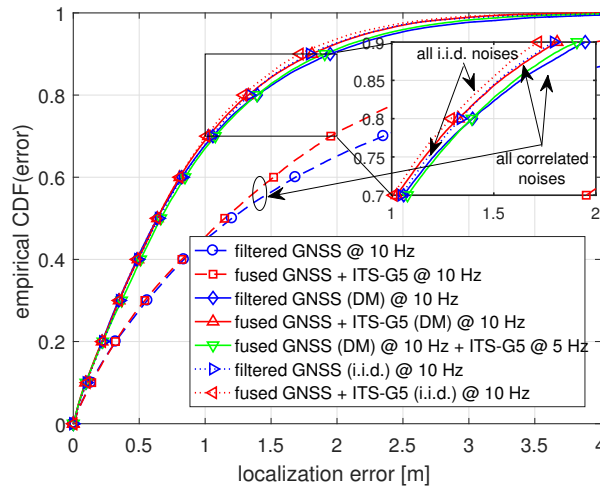
Figure 4.11: Localization performance comparison of different schemes assuming correlated GNSS noise and correlated shadowing, except the two dotted curves corresponding to both i.i.d. GNSS noise and RSSI shadowing cases in the urban canyon scenario.

from the past to (and including) the current instants, increased noise correlation is related to increased noise level as the standard Bayesian filter/fusion cannot average out the error, resulting either in the fast convergence to erroneous values or even in severe divergence.

Urban Canyon Scenario   Just like in the highway environment, we now evaluate the different solutions in the urban canyon scenario. Figure 4.11 shows the performance comparison. We note again the adverse effects of correlated noises on the filtering performance (the two dash curves versus the two dotted curves). From this figure, we also remark that

CLoc provides lower performance gains in comparison with standalone GNSS than in the highway scenario. This can be explained as follows. First, the two platoons traveling in opposite directions along the narrow street (i.e., one single lane per traffic direction) introduce poorer GDOP conditions that tend to spoil the RSSI-based positioning result. That can be even more severe since neighboring vehicles (i.e., considered as "virtual anchors") experience equivalent dispersion of their respective positioning errors. Second, shadowing in urban environments is usually stronger than on highways, leading to higher observation noise in the fusion filter [102]. Interestingly, the three proposed techniques (i.e., the filtered GNSS with DM, the fused GNSS+ITS-G5 with DM, and the hybrid fused GNSS+ITS-G5) now approach closely the ideal i.i.d. cases. This is due to the specificities of the tested urban canyon scenario. It is commonly admitted that urban canyons belong to the most problematic situations with respect to vehicular localization. We reasonably assume that the vehicles entering the urban canyons from other areas would have preliminary produced rather good state estimates, e.g., in open sky areas, along wider avenues or roads with smaller buildings, etc. (see Figure 4.1). Hence, in the short term, the noise prediction model depending on velocity estimation is beneficial to effectively decorrelate the noises. However, in the long term, larger state errors would appear, thus jeopardizing the prediction and further impairing accuracy in comparison with the i.i.d. schemes. This happens in the highway scenario with a simulated track length of 3000 m but not within our short urban canyon scenario of 300 m since the vehicles soon escape from this canyon. A closer look at Figure 4.11 reveals that GNSS+ITS-G5 with DM marginally outperforms the hybrid fused GNSS+ITS-G5 scheme. This is due to the short decorrelation length in urban environments (i.e., 3 m in this case). Accordingly, the correlation between two consecutive RSSI measurements becomes weak. Quantitatively, 10-Hz RSSI measurements, 15 m/s mobility, and a 3-m correlation distance would lead to a normalized joint ACF value of 50%, which can already be considered as a successful decorrelation without decreasing further the fusion rate. However, weakly correlated measurements imply new information contained in each new measurement. As a result, reducing the fusion rate leads to miss such information and hence, to lower accuracy.

Tunnel Scenario   Finally, we are interested in the even more specific GNSS-denied tunnel environment. In this case, we only rely on one single modality, namely RSSI
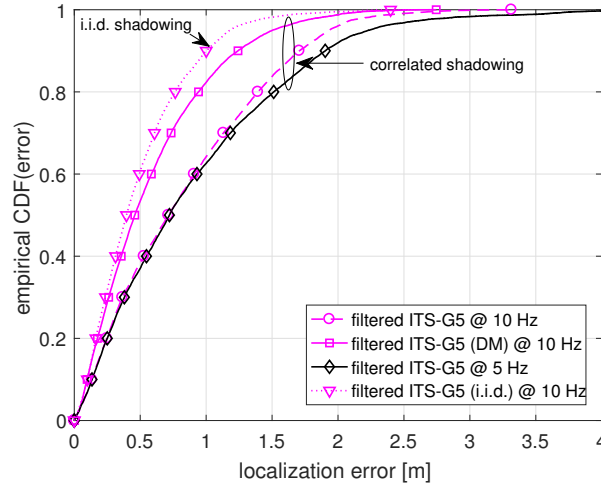
Figure 4.12: Localization performance comparison of different schemes assuming loss of GNSS signal and correlated shadowing, except the top curve corresponding to i.i.d. RSSI shadowing case in the tunnel scenario.

measurements, to perform ad-hoc-based trilateration with respect to neighboring vehicles. Figure 4.12 shows the performance comparison. Once again, we remark that the DM technique decorrelates the shadowing noises to improve accuracy close to that of the ideal i.i.d. case. Considering the filtered ITS-G5 without DM as reference for benchmark purposes, relative accuracy gains of, respectively, 36% on the median error and 27% in the WC error regime are reported. Moreover, it matches by less than 20% the ideal scheme under i.i.d. shadowing. Interestingly, from Figure 4.12, we can see that decreasing the fusion rate provides the poorest performance, which is even worse than that of the original filtered ITS-G5. It can be explained as follows. First, this is again due to very short correlation length, which leads to loose information from naturally decorrelated RSSI measurements while decreasing the fusion rate, as already mentioned in the urban canyon scheme. Second, with a 5-Hz RSSI fusion rate, we need to use prediction (i.e., DR) in order to deliver 10-Hz position estimates because of the GNSS loss. Thus, the positioning error tends to accumulate more easily over time.

Discussion on Practical Context-Aware Correlation Mitigation

We have evaluated our proposed methods in different kinds of environments and scenarios. We have found that the characteristics of the environment, including correlation lengths, mobility patterns, GNSS availability, etc., strongly influence how the CLoc data fusion processes the different input measurements to mitigate the noise correlation. A technique

Table 4.4: Inputs for context-aware correlation mitigation.

Scenario	Modality	
	V2V RSSI	GNSS position
Highway	adaptive fusion rate	DM
Urban canyon	optional	DM
Tunnel	DM	N/A

can be very favorable in one environment but may be less effective in the others. Thus, we suggest a context-aware correlation mitigation strategy that assists the CLoc engine to achieve the best accuracy regardless of the operating conditions. Learning from the previous results, in Table 4.4, we summarize the recommended technique regarding each modality in each environment. When the vehicle enters a specific environment (e.g., based on the *a priori* knowledge of the map), the system could determine the most suitable technique and the associated attributes, before feeding them into the positioning engine to perform correlation mitigation. The aim is to match as close as possible to the accuracy of the optimal schemes under i.i.d. measurements and, accordingly, to provide a constant quality (i.e., highest accuracy) of the navigation service.

4.4 Message Approximation and Transmission Control Strategy

In this new section, we address another major challenge associated with V2X wireless connectivity, namely the reduction of the localization footprint onto data communication channels and vice versa, the compliance of cooperative localization with V2X communication constraints and standardized mechanisms (e.g., in terms of CAM payload and transmission control).

4.4.1 Parametric Message Approximation

Sticking with the PF-based fusion strategy, one first goal is to approximate the heavy particle cloud $\{\mathbf{X}^{(p)}, w^{(p)}\}_{p=1}^{P}$ to facilitate its broadcast to neighboring vehicles using Gaussian or Gaussian mixture distributions, without loosing too much information so as to enable a reliable reconstruction of the related density at the receiving vehicles. The main motivation for using Gaussian representations lies in their tractable analytical properties and mixtures of Gaussians are convenient to approximate very complex densities by using a

sufficient number of Gaussian components, while tuning their means, covariance matrices and weights. Mathematically, a Gaussian mixture distribution is indeed expressed by a linear combination [113] of the form $p(\mathbf{X}) = \sum_{m=1}^{M} \pi^m \mathcal{N}(\mathbf{X}|\boldsymbol{\mu}^m, \boldsymbol{\Sigma}^m)$, where $M \in \mathbb{Z}^+$ denotes the number of Gaussian components, $\{\boldsymbol{\mu}^m, \boldsymbol{\Sigma}^m, \pi^m\}$ are the mean, the covariance matrix and the normalized mixture weight of each multivariate normal density component $m = 1, \ldots, M$, respectively.

Given uniformly weighted particles $\{\mathbf{X}^{(p)}, 1/P\}_{p=1}^{P}$ (thanks to resampling) as input data, one wishes to model these data using a mixture of Gaussians. This data set can be represented as a $P \times n_x$ matrix $\mathbb{X}$ in which the pth row is given by $\mathbf{X}^{(p)\dagger}$. The Gaussian mixture distribution is fully determined by the parameters $\boldsymbol{\pi} = \{\pi^m\}_{m=1}^{M}$, $\boldsymbol{\mu} = \{\boldsymbol{\mu}^m\}_{m=1}^{M}$, and $\boldsymbol{\Sigma} = \{\boldsymbol{\Sigma}^m\}_{m=1}^{M}$. To determine the latter, we employ a ML estimator, assuming that the particles are drawn independently from the true distribution. The log-likelihood function is then determined as $\log p(\mathbb{X}|\boldsymbol{\pi}, \boldsymbol{\mu}, \boldsymbol{\Sigma}) = \sum_{p=1}^{P} \log \left\{ \sum_{m=1}^{M} \pi^m \mathcal{N}(\mathbf{X}^{(p)}|\boldsymbol{\mu}^m, \boldsymbol{\Sigma}^m) \right\}$. Denoting the set of unknown parameters as $\boldsymbol{\alpha} = \{\boldsymbol{\mu}, \boldsymbol{\Sigma}, \boldsymbol{\pi}\}$, the ML estimate is defined by $\hat{\boldsymbol{\alpha}}_{\text{ML}} = \arg\max_{\boldsymbol{\alpha}} p(\mathbb{X}|\boldsymbol{\alpha})$. This solution cannot be analytically determined in closed form for $M > 1$ [113]. However, numerical iterative techniques such as the gradient descent or the expectation maximization (EM) [113] algorithms, can be used to optimize the previous likelihood function.

This message approximation procedure must be computationally efficient from the latency point of view so as to cope with high CAM rates up to 10 Hz. Accordingly, unimodal and bimodal Gaussians are assumed sufficient to capture the salient properties of the true message, whereas multimodal Gaussians (i.e., involving more than 2 modes) are deliberately not considered to avoid solving out too complex optimization problems. Actually, when one cannot rely on enough neighbors (e.g., in sparsely connected networks), the RSSI likelihood function may be multimodal and so is the *posterior* location distribution. However, this information shall be discarded by simply censoring the CAM transmission. Indeed, a too poorly localized vehicle shall not provide unreliable information to its neighbors for CLoc purposes. In contrast, as we expect to benefit from numerous cooperative neighbors in reasonably dense VANETs, the RSSI likelihood function is more prone to be unimodal, as suggested by previous studies like in [117]. Besides, GNSS observation can also help to resolve geometrical ambiguities occurring in such multimodal circumstances.

Note that since the absolute position and the velocity are weakly correlated (e.g., x-

to-v^x and y-to-v^y cross-correlations) in comparison with the internal correlations between their components (i.e., x-to-y and v^x-to-v^y cross-correlations), they can be separated and approximated independently in order to ease the optimization problem (e.g., specifying a 4-D Gaussian distribution for 2-D coordinate and 2-D velocity requires determining 14 parameters). Furthermore, the velocity is naturally unimodal so a Gaussian is sufficient.

4.4.2   Jointly Payload, Rate, and Power Control

Basically, ITS-G5 standard supports critical 10-Hz CAM to provide and maintain a superior quality of position awareness (see Figure 4.13(a)). However, the ITS-G5 channels are vulnerable to such critical broadcast, especially in dense traffic conditions. In this case, the ETSI DCC scales the CAM rate to 2 Hz to avoid congestion, thus loosing four fifth amount of the cooperative information for CLoc[6] (i.e., neighbors' positions and RSSIs). Thus the idea is to design a transmission protocol coping with the ETSI DCC to compensate for such information loss.

Again, CLoc performance strongly relies on neighboring position awareness, as well as on associated range-dependent measurements. Using a single kind of messages for both purposes does not appear fully efficient because the former position can be predicted quite reliably in the short term (e.g., within the sub-second horizon). Hence, we can contextually select what we need to transmit at any instant. More particularly, we propose to mix "tiny" CAMs with reduced payload (i.e., containing only vehicle's ID without estimated state and associated uncertainty parameters) at the critical rate of 10 Hz to provide range-dependent information (i.e., RSSI) and normal CAMs at the lower rate of 2 Hz (in compliance with ETSI DCC). Figure 4.13(b) represents this joint transmission payload and rate adaptation. Accordingly, we let the "ego" vehicle predict the neighbors' states and we reduce the burden of broadcasting critical CAMs. Although additional "tiny" CAMs are required, Table 4.8 shows that they do not increase traffic.

Finally, the objective of "tiny" CAMs is to provide RSSI measurements for CLoc, which is usually restricted to the closest ring of neighboring vehicles (in compliance with the link selection strategies described in Section 3.5.2) due to several reasons (e.g., significantly larger relative RSSI dispersion at large distances, high probability of non-visibility configurations, etc.). Accordingly, it is wasteful to broadcast the "tiny" CAMs at critical

---

[6]This is a general statement, regardless of the observation noise correlation aspects developed in the previous section.
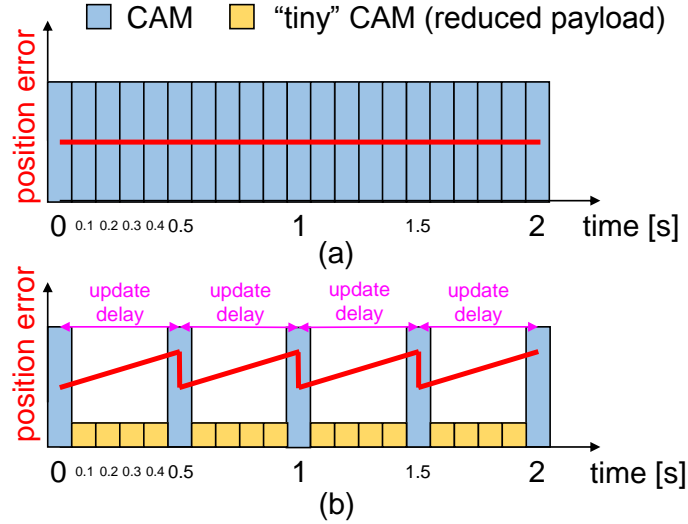
Figure 4.13: Standard CAM transmission policy (10 Hz) in (a) vs. adjusted mixed CAM traffic (including tiny/frequent CAMs at 10 Hz and nominal/infrequent CAMs at 2 Hz) in (b).

transmission power (i.e., 33 dBm to reach the maximum range). In addition to CAM payload and transmission rate control, we thus also propose power control to adaptively manage different ranges (say, 50–100-m for "tiny" CAMs, 800–1,000-m for normal CAMs) to save even more communication traffic. Once a desired transmission range is set *a priori* for each type of CAM, one can roughly determine the corresponding transmission power, assuming the knowledge of the log-distance path loss model in (3.6) and receiver sensitivity (e.g., known by calibration).

4.4.3   Numerical Results

Simulation Settings

We reuse the highway scenario in Section 4.3 for this evaluation, though under an i.i.d. observation noise assumption, as we first need a proof of concept to determine the main trends/results without being interfered by other phenomena, The main simulation parameters are summarized in Table 4.5.

While evaluating the performance of the proposed approaches, we aim at assessing practical operating trade-offs between localization accuracy, communication impairments, and complexity, by undertaking "factor-by-factor" investigations. More particularly, we firstly analyze the effects of parametric message approximation on localization accuracy while assuming a default critical 10-Hz CAM rate. Then we evaluate the effects of ETSI

Table 4.5: Main simulation parameters used to evaluate CAMs transmission control policies.

Parameter	Value
CAM rate	10 [Hz] (critical), 2 [Hz] (congestion)
CAM size	300 [bytes]
"Tiny" CAM size	30 [bytes] (hypothesis)
Transmit power	33 [dBm] (critical, 1,000-m range)
	-5 [dBm] (adaptive, 50–100-m range)
Receiver sensitivity	-87 [dBm] [118]
Number of particles	1000

Table 4.6: Performance comparison of different message representations with respect to communication requirement and localization accuracy.

2-D position	2-D velocity	50th [m]	90th [m]	No. scalars[a]	Payload [bytes]	Broadcast
Particles	Particles	0.3222	0.7573	4000	32000	No
Uni. Gauss. (diag.)	Uni. Gauss. (diag.)	0.3268	0.7628	8	64	Yes
Uni. Gauss. (full)	Uni. Gauss. (full)	0.3253	0.7652	10	80	Yes
Bi. Gauss. (diag.)	Uni. Gauss. (diag.)	0.3255	0.7628	13	104	Yes

[a] Number of scalars that need to be encapsulated in a CAM. Each scalar costs 8 bytes (binary64).

DCC and the proposed transmission control strategy on CLoc performance without any message approximation. Finally, we consider combining both signal-level (i.e., message approximation) and protocol-level (i.e., transmission control) techniques into a single solution.

Performance Evaluation

Signal-Level Message Approximation   Table 4.6 shows the achieved positioning accuracy over 100 Monte Carlo runs in terms of both median and WC (CDF of 90%) localization errors. Table 4.6 also summarizes the CAM overhead associated with each message approximation strategy. While identifying the density modes, the bimodal Gaussian approximation with full covariance matrix does not converge within a few Monte Carlo runs due to the higher-dimensional optimization problem. We thus deliberately ignore them in the performance evaluation. One can remark the modest accuracy degradation caused by parametric message approximations in comparison with the nonparametric approach. This means that, in our localization problem, the posterior distribution is rather simple under practical deployment/connectivity conditions. It can thus be approximated with either unimodal or bimodal Gaussian. More importantly, Table 4.6 shows the minimum awareness payload that needs to be carried by the 300–800-byte CAMs and then transmitted over 6-Mbps ITS-G5 channels with 2312-byte maximum transmission unit (MTU).

Table 4.7: x-Dimensional optimization versus number of iterations.

Representation	x-D optimization	Number of iterations
Bimodal Gaussian (diagonal)	9	45
Bimodal Gaussian (full)	11	187
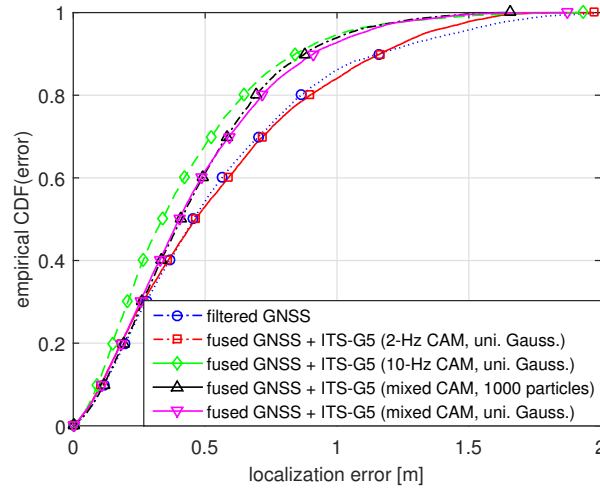
Figure 4.14: Empirical CDFs of localization errors for different schemes with respect to fused modalities, message approximation and transmission control.

Thus, without message approximations, it is almost impossible to perform PF-based CLoc in VANETs using explicit cloud disclosure and passing, as expected.

Since message approximation is solved by iterative methods such as EM in case the closed form solution does not exist, computational complexity and latency are also important factors besides the accuracy performance indicator. Table 4.7 shows an example regarding the number of iterations required to achieve convergence over 1 trial run, given a number of estimated variables (i.e., a problem dimension). As expected, we observe that this number increases dramatically within high-dimensional optimization problems. Based on the previous results, considering a Gaussian mixture distribution provides too marginal accuracy gain but leads to high computation/latency. Thus, unimodal Gaussian with full covariance matrix is advantageous.

Protocol-Level Transmission Control   We now study the impact on both localization accuracy and local channel congestion of different transmission and fusion rate policies, possibly in conjunction with unimodal message approximations. The corresponding empirical CDFs of localization errors are first summarized in Figure 4.14. Note that the red-straight-rectangular curve here on Figure 4.14 is equivalent to the green-straight-triangle

curve Figure 4.9 and the green-dash-diamond curve here on Figure 4.14 is equivalent to the red-dotted-triangle curve on Figure 4.9. Slight differences are mostly due to unimodal Gaussian message approximations. As already illustrated in Chapter 3 and recently in Section 4.3.3, we still observe here that the fusion of several modalities (i.e., GNSS and V2V RSSIs) outperforms the standalone filtered GNSS solution. Interestingly, in case of either triggered ETSI DCC or reduced CAM rate, the fused GNSS and 2-Hz RSSI scheme only yields modest gain in case of high errors (i.e., larger than 1.2 m). This can be explained by the fact that CLoc suffers from a loss of cooperative information (neighboring positions and associated RSSIs). This information loss can be either a temporal loss (from a specific neighbor) or a spatial loss (from the number of cooperative neighbors due to their asynchronous 2-Hz CAM transmissions[7]). Then we observe that the proposed method relying on "tiny" CAMs (still without message approximation i.e., 1000 particles) improves accuracy at a level equivalent to that of fused GNSS with 10-Hz CAM. The observed slight accuracy degradation is due to accumulated prediction errors (see again Figure 4.13(b)) and local cooperation with nearby neighbors only (in a 100-m radius coverage), as constrained by power control with "tiny" CAMs transmissions. In brief, our transmission control strategy intentionally avoids critical CAM exchange but ensures comparable localization accuracy.

Cross-Signal-Protocol-Level Transmission Control   We now combine both signal level and protocol level techniques to achieve simultaneously high precision and communication-efficient CLoc. Specifically, in addition to transmission control, we integrate message approximation with a unimodal Gaussian (shown to be sufficient from previous simulations) when broadcasting CAMs at 2 Hz. Note that the 10-Hz "tiny" CAMs do not include any state awareness. Thus, they do not require message approximation and contribute to save further computations. The result is also shown in Figure 4.14. As expected, we observe marginal accuracy degradation caused by message approximation when considering also transmission control.

Finally, we assess the impact of our proposed transmission control on the channel load. Approximately, with our simulation settings and scenario (i.e., 3-lane highway, 30-m/s speed, 2-s safety rule, steady vehicle movement, etc.), the number of 1-hop neighbors

---

[7]With 10-Hz fusion and asynchronous 2-Hz CAM reception, the sufficient number of cooperative neighbors is not always guaranteed.

Table 4.8: Channel load comparison between different strategies.

Scheme	Channel load
10-Hz CAM	40%
2-Hz CAM	8%
Mixed 2-Hz CAM and 10-Hz "tiny" CAM	8.4%

in normal CAM's range (i.e., 1,000 m) and in "tiny" CAM's range can be up to 100 vehicles (worst case) and 10 vehicles respectively[8]. The channel load is roughly given in Table 4.8[9]. We remark that transmitting critical 10-Hz "tiny" CAMs does not congest the channel (only cost 0.4% channel load) but improves the accuracy gain (relative drop of 13%, 22% respectively and in median and WC errors in comparison with the fused GNSS and 2-Hz CAM). Last but not least, our proposed approach is not limited to the case of triggered ETSI DCC but also applicable to the case of no congestion in order to enable communication-efficient CLoc. In other words, it may be a waste to broadcast full CAMs at 10 Hz while prediction can contribute to save a significant amount of resources.

4.5 Summary

This chapter contributes to the evaluation of CLoc in GNSS-aided VANETs including more realistic V2X constraints, namely correlation effects inherent to the vehicular mobility on the one hand and stringent limitations related to the wireless communication channel and related standardized specifications (e.g., in terms of authorized messages payload, congestion control, etc.) on the other hand. First, simulation models for the GNSS residual errors (i.e., 2-D error maps) and the shadowing process over V2V links (i.e., 4-D shadowing map) have been considered to capture the real-world spatial correlation of practical operating environments. On this occasion, we have first shown that this measurement noise correlation, if not handled carefully, is a threat to Bayesian filters/fusions. Then, two signal level and a protocol level approaches have been proposed and can be combined to almost completely mitigate the deleterious correlation effects, including estimation of cross-link correlations (compensating for information loss), differential measurements (subtracting autocorrelations), and decreased fusion rate (collecting

---

[8]It does not contradict the 15-vehicle scenario (i.e., 250-m road segment) because CLoc only uses nearby neighbors in the range of 200–300 m (where the path loss model is still reliable) though vehicles can receive CAMs from isolated neighbors (up to 800–1,000 m) for maximizing awareness.

[9]The channel load $L[\%]$ may be roughly computed as $L = N \times R \times P/C$, where N is the number of vehicles in range, R the Tx rate, P the packet size, and C the maximum channel capacity (i.e., 6 Mbps).

uncorrelated measurements) respectively. Simulation experiments in canonical vehicular scenarios (urban canyon, tunnel, highway) have shown that the previous noise decorrelation techniques exhibit convincing performance gains over standard approaches that would neglect correlation. Apart from the specific tunnel environment, where decreasing the fusion rate does not seem appropriate, all the other cases lead to very high position accuracy. Beyond, the obtained results also highlight that there exists an optimal combination of correlation mitigation techniques depending on the operating environment and conditions, thus paving the way to context-aware solutions.

This chapter has also addressed the problem of V2V overhead and channel congestion inherent to PF-based CLoc in GNSS-aided VANETs. On the one hand, results show that a significant amount of the CAM payloads could already be saved under standard protocol constraints (i.e., under normal transmission rates and packet sizes) through parametric messages approximation. This comes with almost no accuracy degradation in comparison with impractical solutions that would explicitly send each particles cloud to neighboring cars. Simulations also show that unimodal Gaussian approximations of the local estimates' probability densities are fairly sufficient to achieve the required localization accuracy with much lower computational complexity, while being still robust to occasional geometric ambiguities caused by sparse VANET connectivity. On the other hand, on top of message approximation, the proposed jointly adaptive transmission payload, rate, and power control contributes to maintain the continuity of high-precision location service in channel congestion while reducing significantly communication traffic as well as computation load in congestion-free conditions without trading much accuracy.

In the following chapters, as long as the GNSS measurements take part in the fusion-based CLoc, the decorrelation techniques can always be applied. While the ITS-G5 is the main communication technology throughout this thesis, the message approximation has to be included in the PF-based CLoc. Finally, recalling that we keep on investigating CLoc with gradual complexity, the limitations of ITS-G5 RSSI (as direct V2V observation) suggest to consider evaluating equivalent fusion frameworks with more accurate ranging technologies, which will be investigated in Chapter 5.

Chapter 5

Hybrid V2V Cooperative Localization

5.1 Introduction and Related Works

In the two previous chapters, CLoc has been applied to VANETs to fuse on-board GNSS positions with opportunistic V2V RSSIs out of CAM messages, relying on the V2X ITS-G5 technology. A major advantage of using V2V RSSI lies in the full compliance with future ITS-G5 connected vehicles. Yet, V2V RSSI measurement is a highly parametric technique that requires precise model calibration. Even if performance gains have been conditionally illustrated in comparison with standard GNSS baseline, RSSI-based CLoc still offers rather limited accuracy (with median and worst case errors respectively on the order of 0.3–0.5 m and 0.75–1 m, at most, depending on the operating environment and processing). It can also suffer mostly from limited reliability, especially in non-static multipath environments whose channel parameters (i.e., path loss exponent, shadowing standard deviation, etc.) may fluctuate significantly [30, 59, 96, 97, 100, 112, 115]. Thus, in this chapter, we propose to replace ITS-G5 RSSI readings by new V2V measurements obtained by a more accurate ranging-oriented radio technology, namely TOF measurements based on the impulse radio ultra-wide bandwidth (IR-UWB) technology[1]. Compared to ITS-G5, the latter technology is indeed known to provide centimeter-level distance resolutions at the price of one additional radio transceiver at each vehicle (i.e., in parallel to the ITS-G5 transceiver) and specific cooperative protocols, as seen before (see Section C.2).

---

[1]Other short-range V2V ranging technologies could have been considered too without changing much the outcomes of the study (e.g., ZigBee relying on PDOA measurements [18]).

A comparison is summarized in Table 5.1.

The IR-UWB technology has already been considered extensively for tag, robot, asset, or person localization in indoor environments [21, 84, 96, 119, 120], but only rarely for vehicle localization. For instance, Ko *el al.* [121] use V2V UWB ranging in their GNSS-based CLoc system. However, the main contributions consist in integrating a NLOS GNSS signal detection algorithm to develop multipath-resistant CLoc solutions based on belief propagation and EKF. In VANETs, communication aspects (e.g., specific scheduling to reduce collisions, ranging acquisition latency or overhead and extra-traffic due to beliefs propagation) are absolutely critical and may represent major limitations in the CLoc context, although they remain still unaddressed. In addition, lane-level localization accuracy is not achieved in this work. Petovello *el al.* [122] conduct a field demonstration of V2V IR-UWB ranging to enhance differential GPS (DGPS) relative positioning with three moving vehicles in a test in Calgary, Canada. Specifically, they combine GPS pseudoranges, IR-UWB ranges, and bearing measurements using an EKF to improve the horizontal positioning accuracy in various scenarios. The authors have shown that the combination of DGPS and IR-UWB could be worse than stand-alone DGPS, incriminating timing errors corrupting the IR-UWB data. Besides, the DGPS technology (providing natively accuracy levels on the order of 0.1-0.2 m in optimal operating conditions) challenges IR-UWB to further improve performance, whereas the fusion between standard GPS and IR-UWB is not investigated at all (although the benefits from fusion would be likely more obvious in this case). Another limitation of this study lies in the considered scenario, which simply involves 3 vehicles, thus leading to bad geometry and relative positioning capability. This may not be suitable to key C-ITS applications that shall require absolute positioning information.

In contrast, our approach updates predicted position by combining on-board GNSS absolute position, neighboring fusion-based absolute positions (still broadcast over V2V communications based on ITS-G5), and relative distance measurements via IR-UWB TOF estimation (see Figure 5.1) within a PF. We illustrate that such hybrid CLoc yet cannot fully benefit from IR-UWB ranging accuracy due to the disparity between observation noises affecting GNSS positions and IR-UWB ranges, leading to filter overconfidence (i.e., in badly estimated positions), as well as to bias propagation problems (adversely induced by cooperation). We first investigate the sources of such counter-intuitive effects. Then
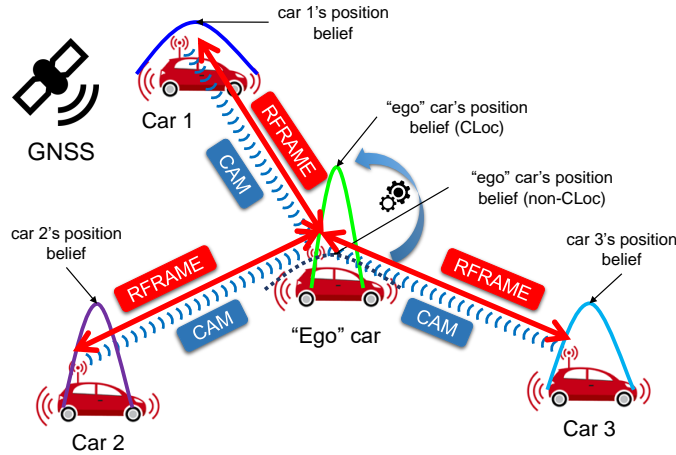
Figure 5.1: "Ego" car receiving CAMs and exchanging ranging frames RFRAME from/with single-hop "virtual anchors" to perform distributed CLoc. The CLoc position belief (i.e., after fusing GNSS positions with ITS-G5 RSSIs or IR-UWB ranges) are expected to be more concentrated than that of non-CLoc (i.e., with standalone GNSS only). The GNSS/ITS-G5 CLoc scheme in Chapter 3 uses ITS-G5 for both communication and localization (distance-dependent RSSI) whereas the GNSS/ITS-G5/IR-UWB scheme in this chapter uses ITS-G5 for communication only and IR-UWB for ranging.

Table 5.1: Comparison of two V2V measurement kinds incorporated in the CLoc problem.

Metric	ITG-G5 RSSI	IR-UWB TOF
Pros	• Full compliance with ITS-G5 V2X • Cheap and simple hardware • No extra specific synchronization (or clock) requirement except that for V2X data communications	• Theoretical cm-to-tens cm level accuracy
Cons	• Limited distance-dependent information accuracy and reliability depending on channel parameters and transmission range • Required calibrated behavioral channel model (power path loss) and parameters • Sensitivity to large fluctuations (shadowing and/or small-scale fading), radio irregularities (uncalibrated Tx power, varying radiating diagram as a function of device attitude, etc.)	• Required perfect synchronization and clock precision (one-way ranging) • Complex ranging protocols, requiring local coordination and possibly inducing extra acquisition latency • Extra hardware in addition to ITS-G5 communication device

we describe a unified GNSS/ITS-G5/IR-UWB data fusion scheme coupling different techniques at both protocol and signal processing levels so as to mitigate error propagation and thus, to improve the effectiveness of fusion-based CLoc under typical GNSS and IR-UWB observation noises.

This chapter is organized as follows. In Section 5.2, we briefly present the IR-UWB ranging protocol and model, the PF-based GNSS/ITS-G5/IR-UWB hybrid data fusion problem, as well as inherent filter overconfidence and error propagation issues. In Section 5.3, we solve out these problems by means of a specific fusion scheduling protocol,

while assuming heterogeneous GNSS capabilities among the cooperating vehicles, where more advanced GNSS receivers must be available at a few vehicles. Then we investigate less restrictive scenarios that would not require accurately pre-positioned vehicles (i.e., without making any assumption about GNSS/GPS on-board quality), by developing an adaptive Bayesian dithering technique in Section 5.4. Numerical results are provided in Section 5.5, and a summary of related contributions and outcomes is given in the last section.

5.2   Problem Formulation

Throughout this chapter, we still assume perfect knowledge of the mobility model (Gauss–Markov mobility model), similarly to Chapter 3 and Chapter 4. In addition, a white noise model assumption is retained for both GNSS absolute position and measured V2V received power (for benchmark only), for several reasons: first, correlated measurements can be transformed into independent data using the proposed techniques in Chapter 4 with some accuracy degradation; second, the goal is to evaluate how much gain the IR-UWB technology can bring in comparison with the best performance achieved through nominal GNSS/ITS-G5 data fusion (so obviously, in white noise environments or under very short decorrelation distances). In the following, we briefly present the V2V IR-UWB range measurement model, as well as the corresponding acquisition protocol.

5.2.1   IR-UWB Ranging Protocol and Model

To obtain IR-UWB ranges, vehicles need to perform a ranging protocol which may be challenging in VANETs. We have identified the following problems:

- One-way ranging protocol is not suitable as vehicles might not be perfectly synchronized due to many reasons (e.g., GNSS-denied environments, insufficient millisecond accuracy provided by Network Time Protocol (NTP)).

- Multiple-way ranging protocols must mitigate clock frequency offset-induced range errors and minimize the number of exchanged ranging frames. Numerous variants are detailed and benchmarked in [123] including: two-way ranging [124], symmetrical double-sided two-way ranging [125], asymmetrical doubled-sided two-way ranging [126], double two-way ranging [127], and burst-mode symmetrical double-sided
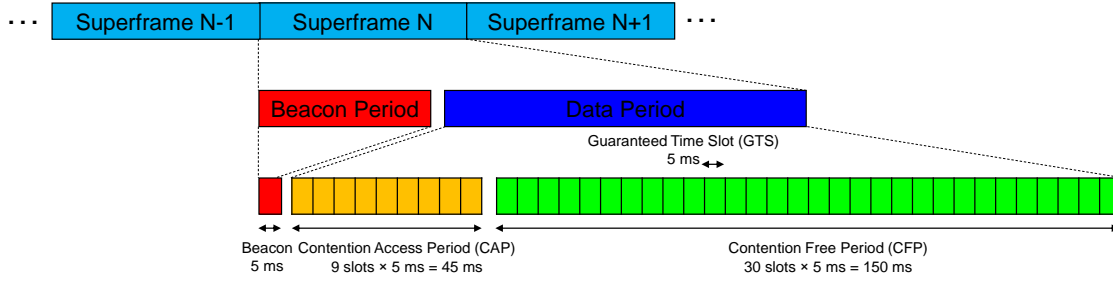
Figure 5.2: Beacon-aided TDMA MAC SF format supporting the localization functionality (SF duration of 200 ms).

two-way ranging [128]. Besides clock drift and clock offset issues, it is indeed important to shorten ranging transactions (and thus reduce acquisition latency, for instance through ranging data aggregation and broadcast), which may cause measurement biases in high mobility contexts (resulting from a lack of spatial coherence as vehicles are moving, between the moments when the first transaction is initiated and the moment when it ends).

- Each vehicle performs ranging with multiple neighbors requiring careful and efficient scheduling to avoid packet collision.

So as to support the previous ranging transactions (initially, not in the vehicular domain), the standard IEEE 802.15.4 beacon-enabled time division multiple access (TDMA) MAC superframe (SF) has been initially modified, as depicted in Figure 5.2. Note that several variants, directly inheriting from the latter MAC structure, have been proposed, leading to different trade-offs in terms of ranging accuracy versus acquisition latency (e.g., [129–132]). In our specific vehicular context, we assume that a vehicle (e.g., temporarily self-elected as local coordinator, if no other coordinator is already detected as active in the area) periodically transmits beacons to synchronize the vehicles in the vicinity in order to indicate the beginning of the SF and allocate time slot (TSs) for ranging. Paired vehicles demand the coordinator for ranging TSs in the contention access period (CAP) and are allocated guarantee time slots (GTSs) in the contention free period (CFP).

Besides, we use a three-way ranging procedure to compensate for the asynchronous vehicles' clocks (i.e., clock drifts and offsets), thus requiring at least 3 adjacent GTS to complete a ranging transaction between two given nodes in the most basic allocation schemes (i.e, with no data aggregation and broadcast). Generally speaking, for a N-node VANET, each vehicle needs $3(N-1)$ GTSs (star configuration) for one estimates

with respect to its one-hop neighbors and the full VANET would require accordingly $3N(N-1)$ GTSs (mesh configuration). This situation may lead to an extremely long SF (or alternatively to multiple SFs) to complete the ranging procedures, which is harmful to CLoc under high mobility, as already highlighted (i.e., resulting in biased and/or severely asynchronous range measurements, low-rate CLoc, etc.). Thus, we assume that a classical aggregate and broadcast (A-B) scheme is applied to minimize the amount of overhead or the number of required GTSs to perform all the possible pairwise measurements in a mesh configuration, similarly to [129–131]. Specifically, such A-B scheme enables to share time resource in such a way that each node initiates specific ranging transactions with all the other nodes, and each transmitted packets can play multiple roles e.g., either a request or a response or even a drift correction packet, depending on the receiving neighbor status and on the current step in the three-way ranging protocol [129,130]. Quantitatively, under full connectivity $3N$ GTSs are needed to guarantee ranging transactions between any pair of nodes, instead of $3N(N-1)$ GTSs. Figure 5.3 illustrates an example of A-B scheme in a SF for 3 vehicles. The extension to more numerous vehicles is straightforward. Although the IR-UWB penetration is out the scope of this study, we hint in Figure 5.3 the fact that several TSs after the first and the second transmission rounds of all vehicles should be reserved for new vehicles to join. Finally, when the ranging/SF is completed, each vehicle is aware of the full distance matrix where $\widehat{d}_{j \to i}$ and $\widehat{d}_{i \to j}$ are different estimates produced by vehicles i and j, respectively of the relative distance between them. So different schemes can be applied to obtain the refined range $\bar{d}_{j \to i}$ (by vehicle i) by either averaging $1/2(\widehat{d}_{j \to i} + \widehat{d}_{i \to j})$ or considering only the latest estimate between them or the nearest estimate based on innovation monitoring to reject outliers[2]. These measurement redundancies may also be beneficial in case some transactions are incomplete (due to the loss of at least one packet over the three required ones), and thus, related range estimates are missing.

Thus far, through a cooperative ranging protocol (e.g., based on the TOF estimation of transmitted packets involved in multiple-way handshake transactions), vehicle i at time

---

[2]Performing marginal innovation monitoring in a tracking filter at the system level (i.e., while integrating multiple links and thus, multiple range measurements with respect to neighbors) can indeed be used to detect link-wise inconsistent measurements and hence, discard outliers.
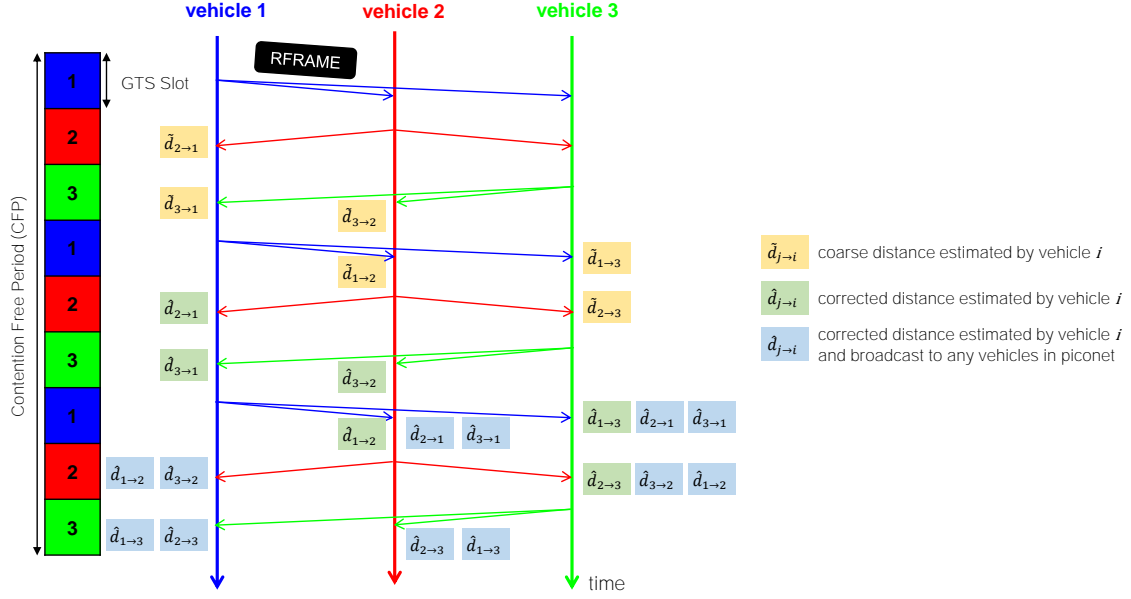
Figure 5.3: Example of the A-B protocol scheme in a SF for ranging within a VANET of 3 vehicles.

$t_{i,k}$ estimates the V2V distance $\widehat{d}_{j \to i,k}$ to node j, $j \in \mathcal{S}_{\to i,k}$ in position $\mathbf{x}_{j,k_i}$:

$$\widehat{d}_{j \to i,k} = \|\mathbf{x}_{i,k} - \mathbf{x}_{j,k_i}\| + n_{j \to i,k}, \tag{5.1}$$

where ranging noise $n_{j \to i,k} \sim \mathcal{N}(0, \sigma_{\mathrm{UWB}}^2)$ with σ_{UWB} the ranging standard deviation. At the protocol level at least since the clock drift compensation mechanisms are expected to remove measurement biases so that noise is assumed to be zero-mean in first approximation (at least in LOS). Accordingly, the standard deviation accounts for both the arrival time uncertainty of each unitary packet involved in a ranging transaction and the residual noise resulting from clock drift compensation mechanisms (i.e., after combining several of these times of arrival).

5.2.2 Fusion Filter Overconfidence and Error Propagation

After presenting the IR-UWB TOF-based range observation model, we rely on a similar PF framework to that used in Chapter 3 for GNSS/ITS-G5 data fusion (see Algorithm 1), while benefiting from more accurate V2V range-dependent measurements and keeping on using ITS-G5 to broadcast fusion results. The new V2V measurements are also nonlinear with respect to the vehicles' positions, thus somehow justifying the choice of a PF as core fusion engine. Our GNSS/ITS-G5/IR-UWB data fusion scheme is based on a (bootstrap)

Algorithm 3 Bootstrap PF for GNSS/ITS-G5/IR-UWB data fusion (iteration k, "ego" vehicle i)

1: **CAM Collection:** Receive CAMs from the set $\mathcal{N}_{\rightarrow i,k}$ of perceived neighbors, extract the parametric beliefs, and draw samples to reconstruct the particle approximate beliefs $\{\widetilde{\mathbf{X}}_{j,k}^{(p)}, 1/P\}_{p=1}^{P}$, $j \in \mathcal{N}_{\rightarrow i,k}$.

2: **Data Resynchronization:** Perform prediction of both "ego" and neighboring particle beliefs based on mobility models at the "ego" estimation instant k (i.e., $t_{i,k}$):

$$\mathbf{X}_{i,k}^{(p)} \sim p(\mathbf{X}_{i,k}|\mathbf{X}_{i,k-1}^{(p)}), \qquad w_{i,k}^{(p)} = 1/P, \qquad p = 1,\ldots,P,$$
$$\mathbf{X}_{j,k_i}^{(p)} \sim p(\mathbf{X}_{j,k_i}|\widetilde{\mathbf{X}}_{j,k}^{(p)}), \qquad w_{j,k_i}^{-(p)} = 1/P, \qquad p = 1,\ldots,P, \qquad j \in \mathcal{N}_{\rightarrow i,k},$$

and build the LDM of vehicle i's neighbors (as another possible output of the algorithm):

$$\widehat{\mathbf{X}}_{j,k_i}^{-} \approx \frac{1}{P}\sum_{p=1}^{P}\mathbf{X}_{j,k_i}^{(p)}, \quad \mathbf{\Sigma}_{j,k_i}^{-} \approx \frac{1}{P}\sum_{p=1}^{P}(\mathbf{X}_{j,k_i}^{(p)} - \widehat{\mathbf{X}}_{j,k_i}^{-})(\mathbf{X}_{j,k_i}^{(p)} - \widehat{\mathbf{X}}_{j,k_i}^{-})^{\dagger}, \quad j \in \mathcal{N}_{\rightarrow i,k}.$$

3: **Observation Query and Aggregation:** Check whether the TDMA MAC superframe or the ranging handshakes with the subset $\mathcal{S}_{\rightarrow i,k} \subset \mathcal{N}_{\rightarrow i,k}$ of IR-UWB paired "virtual anchors" are completed to perform fusion-based CLoc:

$$\mathbf{z}_{i,k} = \begin{cases} (z_{i,k}^{x}, z_{i,k}^{y})^{\dagger}, & \text{if non-fusion instant } k, \\ (z_{i,k}^{x}, z_{i,k}^{y}, \ldots, \widehat{d}_{j\rightarrow i,k}, \ldots)^{\dagger}, \quad j \in \mathcal{S}_{\rightarrow i,k}, & \text{if fusion instant } k. \end{cases}$$

4: **Observation Update:** Calculate the new weights according to the likelihood:

$$w_{i,k}^{(p)} \propto \begin{cases} p(\mathbf{z}_{i,k}|\mathbf{X}_{i,k}^{(p)}), & \text{if non-fusion instant } k, \\ p(\mathbf{z}_{i,k}|\mathbf{X}_{i,k}^{(p)}, \mathbf{X}_{\mathcal{S}\rightarrow i,k}^{(p)}), & \text{if fusion instant } k \end{cases}$$
$$= \begin{cases} p(z_{i,k}^{x}|x_{i,k}^{(p)})p(z_{i,k}^{y}|y_{i,k}^{(p)}), & \text{if non-fusion instant } k, \\ p(z_{i,k}^{x}|x_{i,k}^{(p)})p(z_{i,k}^{y}|y_{i,k}^{(p)}) \displaystyle\prod_{j \in S_{\rightarrow i,k}} p(\widehat{d}_{j\rightarrow i,k}|\mathbf{x}_{j,k_i}^{(p)}, \mathbf{x}_{i,k}^{(p)}), & \text{if fusion instant } k. \end{cases}$$

normalize them to sum to unity, and compute the approximate MMSE estimator and its empirical covariance as the second filter outputs:

$$\widehat{\mathbf{X}}_{i,k} \approx \sum_{p=1}^{P} w_{i,k}^{(p)}\mathbf{X}_{i,k}^{(p)}, \quad \mathbf{\Sigma}_{i,k} \approx \sum_{p=1}^{P} w_{i,k}^{(p)}(\mathbf{X}_{i,k}^{(p)} - \widehat{\mathbf{X}}_{i,k})(\mathbf{X}_{i,k}^{(p)} - \widehat{\mathbf{X}}_{i,k})^{\dagger}.$$

5: **Resampling**

6: **Message Approximation and Broadcast:** Use parametric unimodal Gaussian to approximate the particle "ego" belief and thus broadcast $\{\widehat{\mathbf{X}}_{i,k}, \mathbf{\Sigma}_{i,k}\}$.

PF, as described in Algorithm 3.

This algorithm uses the (joint) mobility model as sequential importance distribution, which does not account for the most recent observation. Hence, particles are generated from the mobility models (Algorithm 3, Step 2), whereas the corresponding weights are updated by simply computing the measurement likelihood given the current observation and the states of these predicted particles (Algorithm 3, Step 4). This suboptimal choice, unfortunately, can lead to specific problems as described below.

First, the efficiency of the bootstrap PF relies critically on the "match" between the prior distribution and the observation likelihood [87, 88]. Since the mobility model is not binded to the observation (and thus, to the likelihood), there might exist a "mismatch" between them. For instance, if the ranging technology is highly accurate leading to concen-
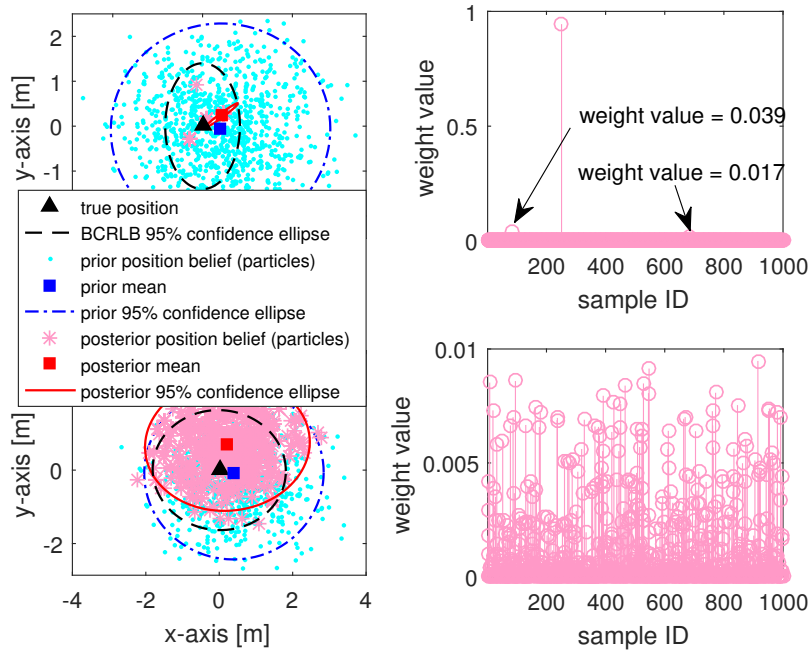
Figure 5.4: Illustration of particles depletion when fusing accurate IR-UWB ranges with GNSS (top subfigures) and no depletion when using inaccurate RSSIs and GNSS (bottom subfigures) in a bootstrap PF. In this scenario, the "ego" vehicle in the center cooperates with its eight nearest neighbors, as shown in Figure 5.7 in one snapshot. Left top/bottom subfigures illustrate the position estimate and the corresponding confidence ellipse at the "ego" car, when fusing 8 IR-UWB ranges/RSSIs with respect to other cars with "ego" and neighboring prior beliefs in comparison with theoretical BCRLB. Right top/bottom subfigures show the updated weights accounting for the collapsed/distributed particle cloud approximating the "ego" posterior density. Main simulation parameters include: prior bias $\sim \mathcal{U}(0, 0.5)$ [m] to account for poor initialization, prior 1-σ uncertainty of 1 [m] on both x- and y-axes independently, $\sigma_{\mathrm{UWB}} = 0.2$ [m], $\sigma_{\mathrm{Sh}} = 2.5$ [dB], and 1000 particles.

trated (joint) likelihood but the mobility is not (due to either imperfect prediction model or poor initialization[3]), then only a few particles close to the true state are assigned significant weights, resulting in particle depletion. As a result, the posterior density support is concentrated to a submanifold of the state space, leading possibly to be overconfident in biased location estimates. Figure 5.4 illustrates this phenomenon with a single snapshot simulation. If, on the one hand, the neighbors' positions are perfectly known, which may not be reasonable in a pure VANET case, the "ego" posterior density is concentrated but located close to the true position. However such estimation is unstable since it does not fix the particle depletion. If, on the other hand, the neighbors' positions are biased (either strongly or weakly), the corresponding error terms are propagated to the "ego"

---

[3]In general, it is reasonable to assume rather poor initial guess. For example, in order to perform V2V IR-UWB ranges, vehicles need to be paired. During this period, they can only rely on GNSS, which does not always provide accurate location beliefs.
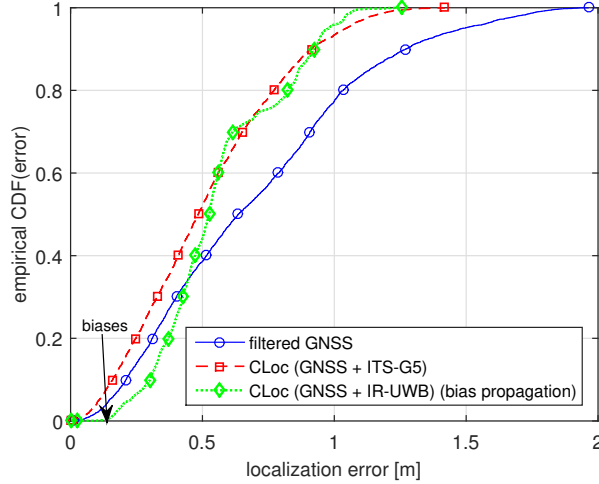
Figure 5.5: Illustration of bias propagation while fusing accurate IR-UWB ranges with GNSS in a bootstrap PF. In spite of the accurate ranges, the GNSS+IR-UWB only gives similar accuracy performance as that of the GNSS+ITS-G5. In addition, its accuracy is the worst in low error regime due to marked biases. The simulation parameters are taken from the heterogeneous GNSS scenario detailed in Section 5.5.

position estimate, which thus quickly converges to an inaccurate value, whereas extremely high confidence is still given to the result (see Figure 5.4 (left top)). Such a situation can be fatal: this malicious information is then broadcast over the network and degrades the position accuracy of all neighbors. Note that the particle depletion does not occur when fusing inaccurate RSSIs because their (joint) likelihood is a broad distribution, indicating that most particles retain a meaningful weight (Figure 5.4 (bottom)).

Second, though the bootstrap PF is implemented in a distributed manner, in the VANET context, the state must be augmented to account for uncertain "virtual anchors" positions i.e., neighboring beliefs (see Algorithm 3, Step 2 and 4). Said differently, the position estimation is performed in high-dimensional space. In this case, there might be no particle in the vicinity to the correct augmented state because the number of particles cannot be sufficiently high to cover all relevant regions concerned by the concentrated (joint) likelihood density [88].

Hence, jointly or separately, the compact distribution of the measurements (e.g., using accurate IR-UWB ranges) and the high dimensionality of the state space both lead to the inefficiency of the bootstrap PF in the very fusion context. Figure 5.5 illustrates this counter-intuitive observation.

To avoid particle depletion, we aim at having more particles with significant weights in order to maintain particle diversity and therefore, to avoid overconfidence issues. One

immediate and intuitive approach is to increase the number of particles. Such a solution can solve the problem at the expense of extremely high computation load, as shown in Figure 5.6 (top). However, it is unsuitable to real-time vehicular tracking under high mobility. Thus, we solve the problem without increasing the number of particles in the following sections.

5.3 Selective and Refined Cooperative Localization

In this section, we present an intuitive data fusion scheduling scheme mostly applicable in restrictive heterogeneous scenarios where several high-quality GNSS devices must be available in the VANETs. In particular, this technique (2-phase CLoc) relies on two main steps, as follows.

5.3.1 Bias Mitigation Phase

In the first phase, each vehicle only cooperates only with the neighbors that have presumably the best position estimates. The reasons behind the selective cooperation are not only to alleviate error/bias propagation but also to keep the joint state (i.e., states of both "ego" vehicle and its "virtual anchors") concentrated[4] and not too high dimensional to be well represented by a finite number of particles without severe particle depletion. Interestingly, it is achieved by extracting the GNSS confidence level (e.g., covariance matrix of GNSS position, besides the uncertainty of the posterior estimate) in the CAMs[5]. Instead of relying uniquely on the posterior belief (which may be overconfident in the context), the underlying GNSS uncertainty -i.e., before fusion/filtering- is expected to be more representative of the possibility to be (still) biased after fusion. In particular, high accuracy GNSS position as absolute information can correct possible bias caused by relative accurate IR-UWB ranges to imperfect anchors by dominating the weights in the observation update (see Step 4 in Algorithm 3) and producing good prior belief (in the next iteration) to improve the "match" with the high (joint) likelihood of IR-UWB ranges. In the approach followed here, vehicles equipped with high-class GNSS receivers (e.g., SBAS, RTK, PPP, etc.) inform their neighbors about their high reliability through

---

[4]For instance, uniform densities require many more particles than that focused on a small region of the state space.

[5]GNSS position and its confidence level are included in the CAMs according to the standard.

CAMs so that the others can avoid integrating so-called malicious "virtual anchors" in their own CLoc calculations.

One may think about the BCRLB-based link selection in Section 3.5 as a relevant solution. Nevertheless, we do not consider this approach for two reasons: first, the aforementioned concentrated beliefs (with presumably unbiased estimate) is essential to alleviate particle depletion problems whereas vehicles with low uncertainties are not always selected by such theoretical bound (see Section 3.6); second, it cannot handle most pathological cases, where neighbors' positional beliefs can be concentrated but biased. A link selection based on a theoretical bound accounting only for the variance would thus fail in removing wrong cooperative neighbors. Note that the selective CLoc eases the particle depletion but does not completely resolve this problem as the (joint) state still remains high dimensional in V2V CLoc. With minimized biases, more survived samples can cover the regions in the vicinity to the correct state thus yielding good estimates while a reasonable loss of diversity in particle population can be recovered after regularization.

Then after a few iterations, by integrating only contributions from the best neighbors (with concentrated beliefs and presumably bias-free position estimates) and thus by avoiding filter overconfidence and bias propagation, poorly positioned vehicles are expected to improve their estimates.

5.3.2   Accuracy Refinement Phase

Once the biases and overconfidence affecting the position estimates of all vehicles have been minimized, each vehicle then benefits from its neighbors as accurately localized "virtual anchors", thus enabling to draw maximum benefits from IR-UWB ranging accuracy. Said differently, exhaustive cooperation can now be performed to boost the localization accuracy to its best achievable level.

5.4   Adaptive Bayesian Dithering

In this section, we continue investigating the same problems under homogeneous GNSS operating conditions (e.g., a group of vehicles entering the same highway) and/or capabilities (e.g., a group of vehicles using GNSS devices from the same class). In comparison with the heterogeneous GNSS scenario, these new cases are more challenging, without
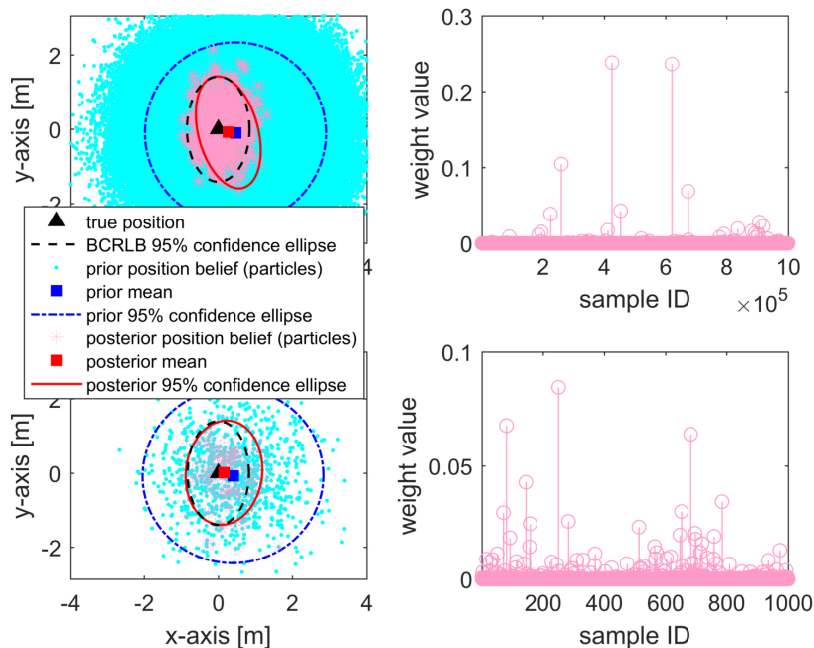
Figure 5.6: Illustration of 2 solutions for particles depletion when fusing accurate IR-UWB ranges with GNSS positions in a bootstrap PF. The two left subfigures illustrate the position estimates and the corresponding confidence ellipses in comparison with theoretical bounds when using a conventional approach with 10^6 particles (top) or the proposed adaptive dithering technique with 1000 particles only (bottom). Right top and bottom subfigures show the updated weights yielding meaningful particle clouds. Except the number of particles and the adaptive dithering technique, the considered scenario and simulation parameters are the same as that in Figure 5.4.

making any assumption about the availability of highly reliable vehicles' positions in the VANETs.

We now rely on a simple but efficient solution called dithering which uses a smoothed (joint) likelihood i.e., assuming deliberately more noise in the observation model than the actual noise affecting real measurements [87, 88]. As a result, more particles are given meaningful weights to maintain particle diversity in order to avoid overconfidence and bias propagation issues. Nevertheless, if performed systematically, accurate measurement information is partly lost and the extent to which noise must be increased in the observation model is questionable. Moreover, as the (joint) likelihood depends on the number of cooperative "virtual anchors", the more numerous the cooperative neighbors, the sharper the (joint) likelihood. Said differently, an excessively smoothed (joint) likelihood in case of a few neighbors tends to loose information whereas a too slightly smoothed likelihood with a high number of neighbors does not solve the depletion problem. Thus, we propose a novel adaptive dithering technique. The idea is to predict the actual performance of the

IR-UWB range-based fusion based on BCRLB, which in first approximation can capture both "ego" and anchors' uncertainties (see Section 3.5) for a given snapshot, without integrating information from previous estimates[6]. Thus far, we can rely on this performance bound to adjust the minimum required amount of added noise in the perception model by manipulating the assumed ranging standard deviation. In this paper, adaptive dithering is implemented in an iterative way, where we start with an *a priori* nominal ranging standard deviation (i.e., corresponding to the best expected technology potential). In every iteration, we gradually increase this standard deviation until the posterior density becomes meaningful and reliable i.e., its empirical covariance is no more smaller than the predicted BCRLB, avoiding overconfidence without spoiling too much the benefits from high accuracy IR-UWB range measurements. The BCRLB for IR-UWB range-based CLoc is calculated similarly to RSSI-based CLoc in Section 3.5.1, except the term related to the new measurements as follows:

$$
\begin{aligned}
\mathbf{J}_{j \to i,k}^M &= \mathbb{E}_{\widehat{d}_{j \to i,k}, \mathbf{x}_{i,k}, \mathbf{x}_{j,k_i}} \left\{ -\Delta_{\mathbf{x}_{i,k}}^{\mathbf{x}_{i,k}} \log p(\widehat{d}_{j \to i,k} | \mathbf{x}_{i,k}, \mathbf{x}_{j,k_i}) \right\} \\
&= \frac{1}{\sigma_{\mathrm{UWB}}^2} \mathbb{E}_{\mathbf{x}_{i,k}, \mathbf{x}_{j,k_i}} \left\{ \frac{(\mathbf{x}_{i,k} - \mathbf{x}_{j,k_i})(\mathbf{x}_{i,k} - \mathbf{x}_{j,k_i})^\dagger}{\|\mathbf{x}_{i,k} - \mathbf{x}_{j,k_i}\|^2} \right\} \\
&\approx \frac{1}{\sigma_{\mathrm{UWB}}^2} \frac{1}{P} \sum_{p=1}^P \frac{(\mathbf{x}_{i,k}^{(p)} - \mathbf{x}_{j,k_i}^{(p)})(\mathbf{x}_{i,k}^{(p)} - \mathbf{x}_{j,k_i}^{(p)})^\dagger}{\|\mathbf{x}_{i,k}^{(p)} - \mathbf{x}_{j,k_i}^{(p)}\|^2}.
\end{aligned}
$$

The overall adaptive dithering technique is summarized in Algorithm 4 and should be triggered before Step 4 in Algorithm 3. Note that $\{d_1, d_2\}$ in line 10 of Algorithm 4 are tuning parameters indicating how close the estimation approaches the theoretical performance bound and can be set to small arbitrary values between $[0, 0.5]$.

5.5   Numerical Results

5.5.1   Simulation Settings

We now evaluate the localization performance of the previous solutions proposed to mitigate filter overconfidence and error propagation, considering the same scenario as in Chapters 3 and 4 i.e., a common 3-lane highway, where a fleet of ITS-G5-connected vehicles (a segment of a larger flow of vehicles) are driving steadily in a common direction at the

---

[6]Note that this static bound is thus deliberately pessimistic in comparison with the best expected tracking performance.

Algorithm 4 BCRLB-based Adaptive Dithering (iteration k, "ego" vehicle i)

1: Compute the Bayesian FIM $\mathbf{J}_{i,k}^B$ for IR-UWB-based CLoc
2: Compute the principal components $\{\lambda_{(1)}, \lambda_{(2)}\}$ by finding the eigenvalues of $[\mathbf{J}_{i,k}^B]^{-1}$, $\lambda_{(1)} \leq \lambda_{(2)}$
3: Begin with the actual ranging standard deviation $\widetilde{\sigma}_{\mathrm{UWB}} = \sigma_{\mathrm{UWB}}$
4: **do**
5: $\quad$ Update the weights $\widetilde{w}_{i,k}^{(p)} \propto p(\mathbf{z}_{\mathcal{S} \to i,k} | \mathbf{x}_{i,k}^{(p)}, \mathbf{x}_{\mathcal{S} \to i,k}^{(p)}, \widetilde{\sigma}_{\mathrm{UWB}})$
6: $\quad$ Normalize the weights to sum to unity
7: $\quad$ Compute the mean $\mathbb{E}\{\mathbf{x}_{i,k} | \mathbf{z}_{\mathcal{S} \to i,k}, \widetilde{\sigma}_{\mathrm{UWB}}\} = \sum_{p=1}^{P} \widetilde{w}_{i,k}^{(p)} \mathbf{x}_{i,k}^{(p)}$
8: $\quad$ Compute the empirical covariance $\mathrm{cov}(\mathbf{x}_{i,k} | \mathbf{z}_{\mathcal{S} \to i,k}, \widetilde{\sigma}_{\mathrm{UWB}}) = \sum_{p=1}^{P} \widetilde{w}_{i,k}^{(p)} (\mathbf{x}_{i,k}^{(p)} - \mathbb{E}\{\mathbf{x}_{i,k} | \cdot\})(\mathbf{x}_{i,k}^{(p)} - \mathbb{E}\{\mathbf{x}_{i,k} | \cdot\})^{\dagger}$
9: $\quad$ Compute the principal components $\{\lambda'_{(1)}, \lambda'_{(2)}\}$ by the eigenvalues of $\mathrm{cov}(\mathbf{x}_{i,k} | \mathbf{z}_{\mathcal{S} \to i,k}, \widetilde{\sigma}_{\mathrm{UWB}})$, $\lambda'_{(1)} \leq \lambda'_{(2)}$
10: $\quad$ Add dither noise Δ to perception model $\widetilde{\sigma}_{\mathrm{UWB}} = \widetilde{\sigma}_{\mathrm{UWB}} + \Delta$
11: **while** $\sqrt{\lambda'_{(1)}} \leq (1 + d_1)\sqrt{\lambda_{(1)}}$ **or** $\sqrt{\lambda'_{(2)}} \leq (1 + d_2)\sqrt{\lambda_{(2)}}$
12: **return** $\widetilde{\sigma}_{\mathrm{UWB}}$
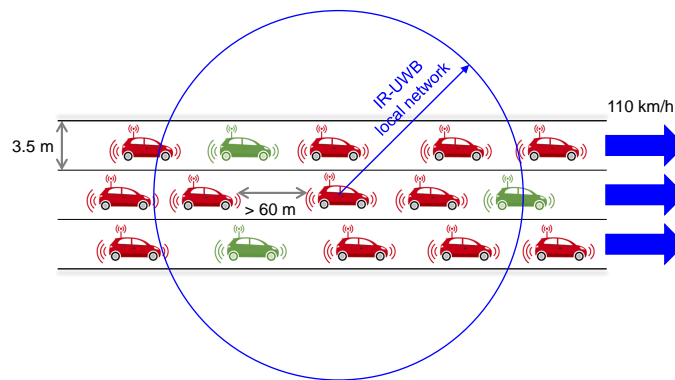
Figure 5.7: VANET scenario evaluated in highway scenario for the mitigation of filter overconfidence and error propagation. For CLoc based on V2V IR-UWB ranging, a vehicle (self-elected as coordinator) periodically transmits beacons to synchronize IR-UWB vehicles in the vicinity (i.e., indicating the beginning of the SF and allocating TSs for ranging). The IR-UWB local network consists of less than 10 vehicles to achieve 5 SF/s.

average speed of 110 km/h (i.e., about 30 m/s), as depicted in Figure 5.7. Furthermore, each vehicle is endowed with IR-UWB ranging capabilities. Table 5.2 summaries main parameters for the simulation framework.

To perform V2V IR-UWB ranging, vehicles are locally synchronized to exchange ranging frames in allocated TSs [7]. For 10-Hz position estimation, we utilize 200-ms SFs (i.e., 5-Hz SFs) leading to 5-Hz fusion rate. Note that vehicles use the stand-alone GNSS positions to input the filter engine when the ranging procedure is ongoing. Due to the 5-ms TSs considered for UWB packets, 100-ms SFs aiming at a critical 10-Hz fusion rate can only synchronize a maximum of 5 vehicles including the coordinator. Thus, with only 4 neighbors, it may be first challenging to have enough accurately positioned neighbors for scheduling and second, it limits the change to boost the CLoc accuracy [8]. We investigate

---

[7] We leave the study of a partial penetration of IR-UWB to future work.
[8] It is not contradictory with our claim about link selection to reduce complexity in Chapter 3. It

Table 5.2: Main simulation parameters for the mitigation of filter overconfidence and error propagation.

Parameter	Value
Memory level α	0.95
Tangential acceleration uncertainty	1 [m/s^2]
Perpendicular acceleration uncertainty	0.1 [m/s^2] (to satisfy road constraints)
Sampling period ΔT	0.1 [s]
Standard deviation of GNSS errors in x- and y-axes	1.5 [m] (SBAS)
GNSS refresh rate	10 [Hz]
CAM rate	10 [Hz] (critical)
SF length	200 ms
TS duration	5 ms
Number of TSs	40 (1 beacon, 9 TSs for CAP, 30 GTSs for CFP)
Ranging protocol	three-way ranging, A-B
Standard deviation of IR-UWB ranging noise	0.2 [m]
Path loss exponent n_p	1.9 (V2V in highways) [100]
Standard deviation of shadowing σ_{Sh}	2.5 [dB] (V2V in highways) [100]
Number of particles	1000
Initial positional error in x- and y-axes	1 [m] (rms) (plausible hypothesis)
Initial velocity errors in x- and y-axes	0.1 [m] (rms) (plausible hypothesis)

two complementary and cumulative scenarios as follows.

In the first heterogeneous scenario, we consider a realistic heterogeneous case where all vehicles are supposed to have the same visibility to the satellite constellation, but suffer from disperse and independent GNSS levels due to different receiver capabilities (e.g., 1.5-m error of SBAS versus 9-m error of degraded basic receivers). The latter GNSS accuracy is intentionally chosen to illustrate the effect of large state prior uncertainty under unbalanced observation noises. Table 5.3 recalls the different tested algorithms including a semi-CLoc variant, as a lighter alternative to the full-CLoc scheme already described in Section 5.3.

In the second homogeneous scenario, we study the case of heterogeneous visibility conditions with respect to satellites. In our comparative study, we consider the filtered standalone GNSS (non-CLoc scheme), the fused GNSS+RSSI, and the GNSS+IR-UWB. In the GNSS+IR-UWB scheme, we compare the localization performance of bootstrap PF with and without adaptive dithering. We also benchmark our proposal with the well-known EKF to verify that the solved problem is not uniquely PF-dependent.

Table 5.3: Description of different CLoc schemes for the mitigation of filter overconfidence and error propagation.

Scheme	Degraded GNSS node	Non-degraded GNSS node
Conventional CLoc	Exhaustive CLoc	Exhaustive CLoc
2-step semi-CLoc	Selective CLoc (first) Exhaustive CLoc (second)	Non-CLoc (all)
2-step full-CLoc	Selective CLoc (first) Exhaustive CLoc (second)	Non-CLoc (first) Exhaustive CLoc (second)
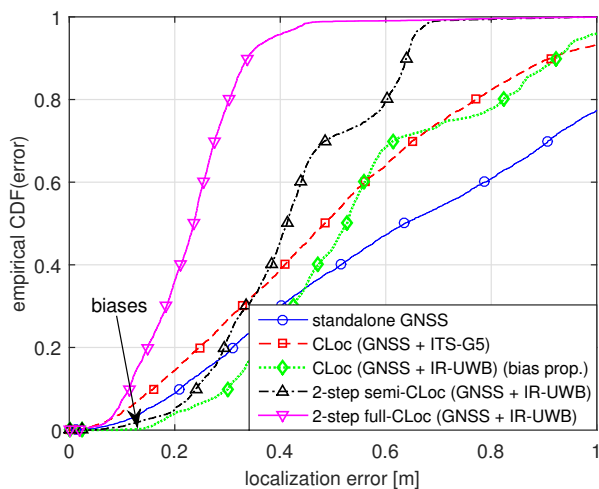
Figure 5.8: Empirical CDFs of localization errors considering degraded GNSS vehicles for different PF fusion schemes and different measurements/technologies for the mitigation of filter overconfidence and error propagation.
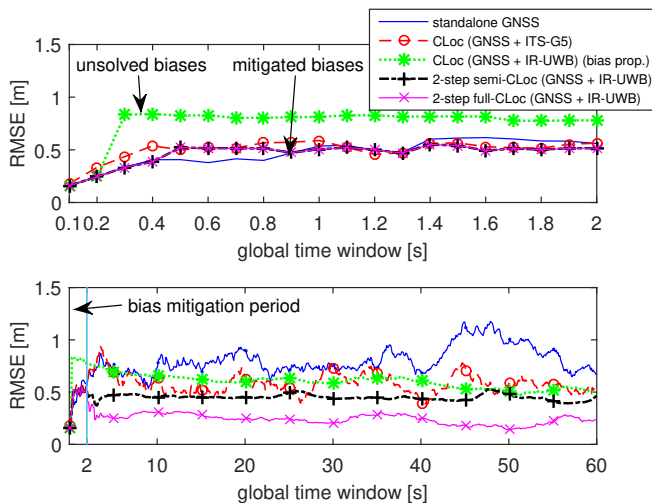
Figure 5.9: Localization RMSEs considering degraded GNSS vehicles as a function of time for different PF fusion schemes and different measurements/technologies for the mitigation of filter overconfidence and error propagation.
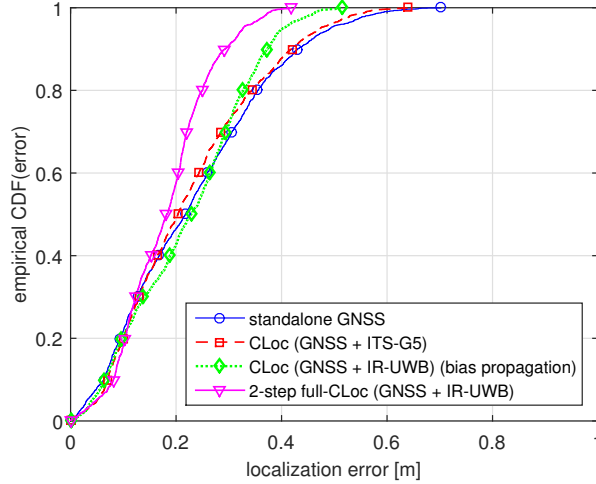
Figure 5.10: Empirical CDFs of localization errors considering non-degraded GNSS vehicles for different PF fusion schemes and different measurements/technologies for the mitigation of filter overconfidence and error propagation.

Table 5.4: Overall performance comparison of different localization schemes for the mitigation of filter overconfidence and error propagation.

Scheme	Degraded GNSS vehicles				
	50th [m]	90th [m]	Pr(0.2 m)	Pr(0.4 m)	Gain[b]
Filtered GNSS	0.63	1.27	8.9%	29.9%	-
CLoc (GNSS+RSSI)	0.48	0.91	14.4%	38.8%	23.8%
CLoc (GNSS+IR-UWB) (bias propagation)	0.53	0.92	4.0%	24.8%	15.9%
2-phase semi-CLoc (GNSS+IR-UWB)	0.41	0.64	5.1%	45.7%	34.9%
2-phase full-CLoc (GNSS+IR-UWB)	0.24	0.34	36.17%	95.7%	61.9%

Scheme	Non-degraded GNSS vehicles[a]				
	50th [m]	90th [m]	Pr(0.2 m)	Pr(0.4 m)	Gain[b]
Filtered GNSS	0.22	0.43	46.6%	86.0%	-
CLoc (GNSS+RSSI)	0.20	0.42	49.1%	87.7%	9.1%
CLoc (GNSS+IR-UWB) (bias propagation)	0.23	0.37	42.6%	94.8%	-4.5%
2-phase semi-CLoc (GNSS+IR-UWB)	0.22	0.43	46.6%	86.0%	0.0%
2-phase full-CLoc (GNSS+IR-UWB)	0.18	0.29	57.7%	99.7%	18.2%

[a] Non-degraded GNSS vehicles do not cooperate in the 2-phase semi-CLoc, hence, the accuracy performance is the same as that of the standalone filtered GNSS approach.
[b] Gain in terms of localization accuracy (negative value in case of degradation) with respect to filtered standalone GNSS solution in median error (i.e., CDF = 50%).

5.5.2   Performances of Fusion Scheduling with Heterogeneous GNSS Capabilities

Figure 5.8 and Figure 5.9 compare the localization performances at vehicles with degraded GNSS capabilities in terms of empirical CDFs of location errors and dynamic RMSEs as a function of time, respectively. Figure 5.10 shows similar comparisons at vehicles with non-degraded GNSS capabilities, by means of empirical CDFs only. As expected and in

depends on the target applications with their specific requirements.

line with previous results in Chapter 3 and 4, the fusion of several modalities (e.g., on-board GNSS position and ITS-G5 RSSIs/IR-UWB TOF-based ranges) yields localization accuracy gains in comparison with standalone solutions (e.g., filtered GNSS only). At first sight, one could expect that accurate IR-UWB TOF-based range measurements would considerably boost the localization accuracy, far beyond what unreliable ITS-G5 RSSIs could initially offer. However, as shown in the three figures (e.g., Figure 5.8, Figure 5.9, and Figure 5.10), when considering conventional PF-based CLoc, fusing GNSS and IR-UWB only provides comparable accuracy with that resulting from fusing GNSS and ITS-G5. Actually, biased location estimates at "virtual anchors" strongly alter the correction potential of IR-UWB ranges. Under degraded GNSS conditions, no gain is observed in comparison with a GNSS+ITS-G5 fusion scheme whereas, at vehicles with non-degraded GNSS, only modest improvements are noted. This can be explained as follows. Our PF fuses three source of information i.e., predicted positions (both "ego" and neighboring vehicles), GNSS positions, and measured distances to the imperfect "virtual anchors". The PF is thus tricked to put exaggerated confidence on IR-UWB-based trilateration due to the small ranging noise variance assumed in the observation model. Accordingly, after integrating biased neighbors estimates, the fusion-based position estimate also becomes biased, but still associated with a high confidence. This effect would be even worse under strong spatial correlation of the GNSS errors when all neighbors might be affected by approximately the same 2-D bias, thus leading in the shift of the overall estimated VANET. In case of non-degraded GNSS (see Figure 5.10), the bias effect does not seem to be severe. The GNSS uncertainty is concentrated so that the filter gives higher weight to the GNSS estimate. Accordingly, it is able to correct the bias caused by the trilateration procedure. However, the performance gain is limited due to the same reason as previously.

Now, when employing the proposed 2-phase CLoc, we observe that when the biases are mitigated in the first step (see Figure 5.9 (top)), the fused GNSS+IR-UWB then yields to remarkable performance in the "accuracy refinement" phase. In particular, we observe in Figure 5.9 (top) that, due to wrong initialization, a conventional GNSS+IR-UWB scheme performing exhaustive fusion gets biased after only 3 iterations, then converges to inaccurate values but keeps on associating large confidence with these values. The proposed CLoc, however, waits until all vehicles' position estimates are improved by the bias refinement phase, before boosting the performance through exhaustive fusion. Comparing

Table 5.5: Overall performance comparison and consistency analysis for the mitigation of filter overconfidence and error propagation.

Scheme	50th [m]	68th[a] [m]	95th [m]	0.2 m	Est. 1-σ [m]	Overconfidence
PF (GNSS)	0.22	0.29	0.53	43%	0.34	No
PF (GNSS+ITS-G5)	0.23	0.28	0.51	42%	0.30	No
PF (GNSS+IR-UWB) (depletion)	0.20	0.32	0.49	48%	0.079	Yes
PF (GNSS+IR-UWB) (dithering)	0.10	0.13	0.24	90%	0.15	No
EKF (GNSS+IR-UWB)	0.17	0.33	0.41	60%	0.062	Yes

[a] It corresponds to standard deviation or 1-σ or rms.

semi-CLoc with full-CLoc, we also show that the latter solution provides much better accuracy. In full-CLoc, degraded GNSS nodes benefit from even more accurate virtual anchors (especially non-degraded GNSS nodes, which perform fusion too). Finally, Table 5.4 summarizes the overall performance comparison. We show the probability to reach a 20 cm and 40 cm position accuracy in case of degraded and non degraded GNSS. Next to it, we provide the accuracy gain, with respect to the baseline standalone GNSS. We draw the attention that the proposed CLoc approach provides a 40 cm position accuracy (almost reaching 100% probability) in both degraded and non-degraded GNSS. It even manages to provide a 20 cm position accuracy with 36% and 57% probability for degraded and non-degraded GNSS respectively. This is a straight 61% and 18% accuracy gain in degraded and non-degraded GNSS respectively.

5.5.3 Performances of Adaptive Bayesian Dithering with Homogeneous GNSS Capabilities

Figure 5.11 depicts the empirical CDFs of localization errors while Figure 5.12 presents the perceived 1-σ estimation errors in the filters, accounting for the (over-)confidence in estimated values. The overall performance comparison and the filter consistency[9] analysis are summarized in Table 5.5. The fused GNSS+ITS-G5 and the standalone GNSS schemes produce comparable accuracy. Then, despite accurate IR-UWB ranges, the fused GNSS+IR-UWB scheme relying on nominal bootstrap PF (without dithering) only yields "local" gains in comparison with the GNSS (set as a reference), as shown in Figure 5.11. For example, the performance is superior in terms of both the median and WC error regimes, but degraded in the lowest error regime below 0.35 m. This multimodal CDF shape indicates that some vehicles (i.e., a sub-group of the whole fleet) are rather poorly

---

[9]The consistency failure happens when the real error (measured by 68th percentile) is beyond the perceived 1-σ estimation error.
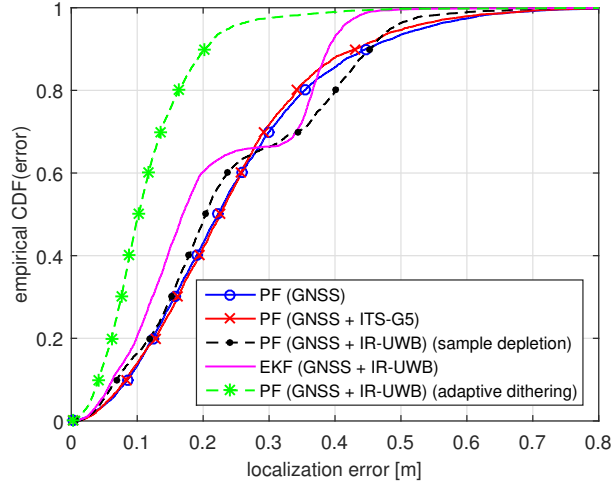
Figure 5.11: Empirical CDF of localization errors for different fusion techniques, schemes, and measurements/technologies for the mitigation of filter overconfidence and error propagation (including accurate V2V range measurements).
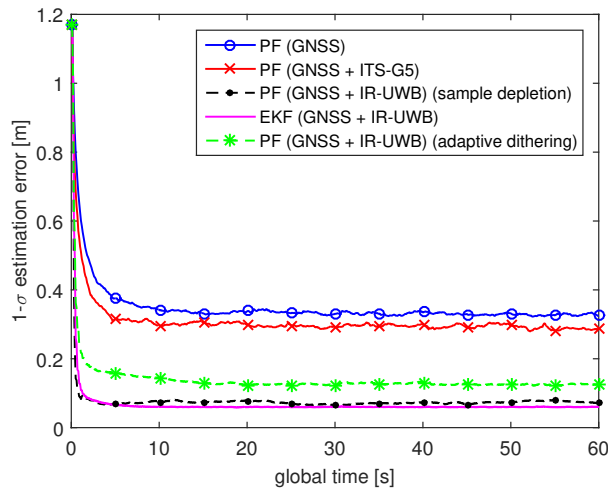
Figure 5.12: Average 1-σ estimation errors perceived by fusion filters for different fusion techniques, schemes, and measurements/technologies for the mitigation of filter overconfidence and error propagation (including accurate V2V range measurements).

positioned. Such counter-intuitive effect mostly results from particles depletion again, leading to overconfidence issues. Accordingly, estimates rapidly converge to inaccurate values, while extremely high confidence is still granted to these estimates. Table 5.5 compares the results from Figure 5.11 and Figure 5.12 to confirm this observation.

The bootstrap PF with adaptive dithering for GNSS+IR-UWB fusion provides the best accuracy, as shown in Figure 5.11. Specifically, we observe significant relative drops of 50% in median error and 51% in WC error (e.g., CDF of 95%) in comparison with a similar fusion scheme without adaptive dithering. In addition, since the particles depletion
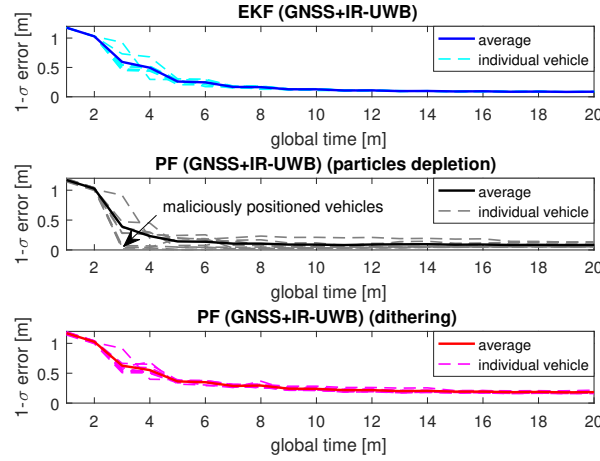
Figure 5.13: 1-σ estimation errors perceived by fusion filters for each vehicle during the first 2 seconds for the fused GNSS+IR-UWB ranges using EKF (top), conventional PF (middle), and PF with adaptive dithering (bottom).

is completely solved by our technique, so is the overconfidence problem (See Table 5.5 and the unimodal CDF shape in Figure 5.11). One can thus draw maximum benefits from accurate IR-UWB range measurements. The corrected GNSS+IR-UWB fusion achieves relative accuracy gains of 57% in median error and 53% in WC error over the GNSS+ITS-G5 scheme.

Finally, Figure 5.11 depicts the failure of conventional EKF to efficiently fuse GNSS and IR-UWB ranges. It also reveals the multimodal shape of the CDF of EKF estimation errors, similarly to that of PF in case of particles depletion. This is due to the poor but realistic initialization conditions (see Table 5.2), thus altering the goodness of the EKF linearization, which depends on the degree of state uncertainty besides the degree of nonlinearity of the models [27, 88]. Note that when the EKF converges to inaccurate values, it also becomes somehow overconfident, as confirmed in Table 5.5. Figure 5.11 also shows that the EKF surprisingly outperforms the conventional bootstrap PF under the chosen settings. Although Figure 5.12 shows that the fused GNSS+IR-UWB schemes using bootstrap PF and EKF have equivalent average perceived 1-σ estimation errors once convergence is achieved, Figure 5.13 (middle) depicts that extremely severe particles depletion occurs at several vehicles leading to unintentionally malicious "virtual anchors", which become harmful to CLoc at other vehicles (i.e., perceived 1-σ estimation error is almost null so that the vehicles are perceived as true reliable anchors whereas their estimated positions are actually biased).

5.6   Summary

In this chapter, we have presented a framework for CLoc based on accurate V2V IR-UWB ranging which is considered as powerful strategy to improve the absolute localization accuracy of future connected vehicles down to the centimeter level. However, that CLoc ends up being inefficient to fuse information sources with significantly different levels of uncertainty (e.g., standard GNSS and IR-UWB TOF) in a conventional PF. This prevents from drawing maximum benefits from the IR-UWB technology, despite its high potential. We have illustrated the harmful effects of overconfidence and bias propagation in such PF-based fusion contexts, which mostly result from particle depletion phenomena. These effects become even more severe in "virtual anchors"-based CLoc when high dimensional belief states must be accounted so that conventionally, a huge number of particles would be required.

On the one hand, we have proposed a fusion scheduling strategy that first selectively incorporates the best "virtual anchors" with the lowest GNSS uncertainties to break the bias propagation, before performing exhaustively cooperative fusion position with all neighbors once the biases have been presumably mitigated. We have compared our strategy with various settings and illustrated the achievable gains under locally heterogeneous GNSS conditions.

On the other hand, we proposed an adaptive Bayesian dithering technique relying on the expected localization performance under nominal IR-UWB ranging accuracy by means of theoretical bound calculations. Relying on these bounds, dither noise is iteratively/gradually added to the perception model assumed in the filter till the empirical estimation covariance is relatively compatible with theoretical expectations. This enables to maintain the particle diversity, avoid overconfidence in wrong estimates, and stop the propagation of possible residual biases over the network.

Admittedly, two main limitations of the results lie in their working assumptions as follows. First, simulations are performed in canonical vehicular scenarios where mobility knowledge is assumed to be known. Second, biases in range estimate induced by the delay of the three-way ranging in case of different vehicles' speeds can be neglected due to highly correlated mobility of highway traffic though they can be opportunistically accounted by dithering noise. The former assumption will be relaxed in the next chapter considering

model-mismatching and further in Chapter 7 exploiting erratic mobility traces from a dataset calibrated in a real city, while using a specific vehicular mobility simulation tool (rather than steady-state synthetic models). The latter will also be taken into account in the extended CLoc including biases estimation for testing the simulated urban scenario, where vehicular mobility changes more frequently due to traffic lights, congestion, etc.

Chapter 6

Hybrid V2X Multisensor Cooperative Localization

6.1 Introduction and Related Works

We begin this chapter by reminding that in the VANET context, the performance of range-based CLoc depends critically on three factors: (i) the uncertainties associated with the estimated positions of both ego vehicle and virtual anchors, (ii) the quality of the V2V range measurements (or more generally, of range-dependent radio measurements), and (iii) the local geometric configuration of the latter anchors relatively to the "ego" vehicle or GDOP. Addressing the two first factors in Chapter 5, we have replaced ITS-G5 RSSI readings by IR-UWB TOF measurements, showing that the related hybrid V2V CLoc scheme can improve greatly the stand-alone GNSS solutions when cooperates with up to ten neighbors. Nevertheless, the last factor has not been investigated to the fullest extent with more challenging network settings and environments.

On the one hand, in vehicular contexts, relative nodes positions are indeed strictly constrained by the topology of occupied roads/lanes and accordingly, they are unequally distributed along the road direction (along-track) and along the direction orthogonal to the road (cross-track). Hence, the along-track location error can usually be significantly reduced, whereas the cross-track error cannot leverage ranging accuracy but mostly reveals poor GDOP.

On the other hand, in large-scale GNSS-denied environments like long tunnels, performing CLoc over large time periods with respect to "virtual anchors" only is subject to

divergence issues. This is due to errors propagation through cooperation in lack of absolute re-calibration means (e.g., re-injecting unbounded biased neighbors' positions from vehicles to vehicles) and/or poor GDOP constrained by both vehicular mobility and road width. Alternatively, in such pathological environments, conventional (non-cooperative) GNSS-based solutions based on a high density of repeaters in the tunnel (e.g., typically, one every 30–50 meters) are notoriously costly and necessitate huge deployment efforts to retrieve just the nominal clear-sky GNSS accuracy conditions (at most, in optimistic cases).

This chapter is structured as follows. In Section 6.2, we present the poor GDOP and error propagation issues. We then solve out the first problem in Section 6.3 by integrating additional sensor measurements into the CLoc framework, while the second point is addressed in Section 6.4 by mixing V2V and V2I measurements or using GNSS repeaters. Simulation results and benchmarks are provided in Section 6.5. Finally, Section 6.6 provides a summary for the chapter.

6.2   Problem Formulation

6.2.1   Poor Relative Geometry Conditions along the Cross-Track Direction

Since mobility is strongly constrained by the roads/lanes and driving rules, the relative vehicles' geometry is rather poorly conditioned in this very context. Specifically, the VANET topology is usually somehow distorted along the direction colinear to the road due to the huge disparity between the longitudinal safety distances (e.g., 20–150 m[1]) and the lateral lane width (e.g., 2.25–3.5 m). Accordingly, the GDOP is likely poor in the direction orthogonal to the road; therefore, the cross-track location error remains high. The CLoc performance is illustrated for a given VANET on Figure 6.1, where the expected positioning error level *before* (prior) and *after* cooperation is theoretically predicted using the BCRLB and represented by means of 95%-confidence ellipses. Figure 6.1 (right bottom) also shows that vehicles maintaining safety distances to the "ego" (regardless of their lane occupancy) mainly improve "ego" along-track positioning whereas vehicles at closer range (obviously on different lanes) generally improve "ego" cross-track positioning. The latter

---

[1]The two-second (or three-second) rule is applied to maintain a safe following distance.
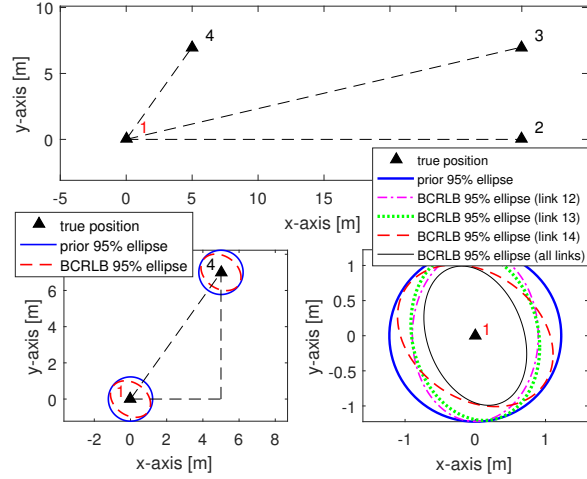
Figure 6.1: Example of expected CLoc localization performance in a 4-node VANET. The top subfigure shows the true vehicles positions. The left bottom subfigure illustrates how a single range-based cooperative transaction mostly increases information (i.e., decreases confidence ellipse) in the direction formed by the two involved nodes' positions. The right bottom subfigure shows the impact of each link separately and of all links on the final "ego" localization performance. Other main parameters (for illustration only) include a prior 1-σ uncertainty of 1 [m] on both x- and y-coordinates independently and a ranging standard deviation $\sigma_{\mathrm{UWB}} = 0.2$ [m].

are tightly constrained due to the limited number of lanes (2 or 3 in each direction for most common European roadways), regardless of V2V communication range. Hence, additional information having beneficial impact on the cross-track error should be incorporated into the initial GNSS+UWB CLoc fusion framework.

6.2.2 Localization Error Accumulation and Propagation

In tunnels, all vehicles' position estimates are subject to significant unbounded biases. Regardless of V2V ranging accuracy, as the position estimated through CLoc at each "ego" vehicle depends on the previous estimate (via the IMU/wheel speed sensor (WSS)-based position prediction) and on the neighbors' estimates (via cooperation), errors tend to accumulate over both time and space. Estimation is then subject to significant unbounded biases unless absolute re-calibration is performed and/or much better GDOP conditions can be achieved. Unfortunately, none of these conditions is usually met in standard tunnels. Since mobility is strongly constrained by the roads/lanes and driving rules, the vehicles' relative geometry is rather poorly conditioned in this context. Accordingly, the GDOP is likely poor in the direction orthogonal to the road; therefore, the cross-track location error remains high. Such situations can be fatal, since such malicious information
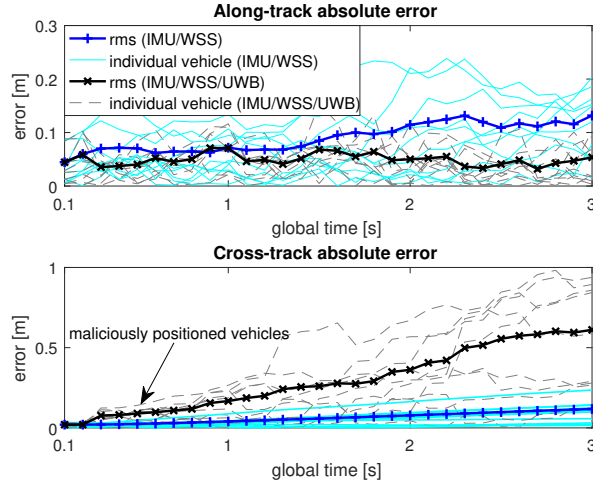
Figure 6.2: 1-σ along-track (top) and cross-track (bottom) errors perceived by fusion filters for each vehicle during the first 3 seconds for non-CLoc (IMU/WSS) and pure CLoc (IMU/WSS/UWB) in a tunnel scenario. Simulation settings and scenarios are given in Section 6.5.

cannot be re-calibrated by absolute means and then is propagated over the network and degrades the position accuracy of all neighbors accordingly. Figure 6.2, which shows the evolution of location error as a function of time in a typical tunnel scenario, illustrates this phenomenon where CLoc uniquely based on V2V IR-UWB measurements yields worse accuracy than IMU/WSS non-CLoc. Figure 6.2(a) confirms the advantage of CLoc to decrease the along-track error whereas Figure 6.2(b) shows that jointly or separately, poor GDOP effects and neighbors' unbounded biased position estimates lead to the faster divergence of CLoc along the cross-track direction (which dominates the total localization error) in comparison with non-CLoc.

6.3   Multisensor Fusion for Improved Cross-Track Localization

6.3.1   Integration of Additional IMU and Wheel Odometry Sensors

Although one can assume that each vehicle knows its own mobility model (i.e., Gauss–Markov mobility model in Section 3.2.1) or more generally, a conditional transition probability density function (pdf) $p(\mathbf{X}_{i,k+1}|\mathbf{X}_{i,k})$ (known *a priori* for highly controlled mobility regimes or possibly self-calibrated on the fly based on previous state estimates), this perception is usually an approximation of the true mobility statistics. To remain mobility-

independent, the well-known kinematic bicycle model is employed as mobility prediction model [88], as follows:

$$x_{i,k+1} \approx x_{i,k} + \Delta T s_{i,k} \cos(\theta_{i,k} + 1/2\Delta T \omega_{i,k}), \tag{6.1a}$$

$$y_{i,k+1} \approx y_{i,k} + \Delta T s_{i,k} \sin(\theta_{i,k} + 1/2\Delta T \omega_{i,k}), \tag{6.1b}$$

$$\theta_{i,k+1} = \theta_{i,k} + \Delta T \omega_{i,k}, \tag{6.1c}$$

where $\mathbf{x}_{i,k} = (x_{i,k}, y_{i,k})^\dagger$ is the 2-D position, $\theta_{i,k}$ the heading, $\omega_{i,k}$ the yaw rate, and $s_{i,k}$ the speed. The signals $s_{i,k}$ and $\omega_{i,k}$ are considered as driving inputs to the mobility prediction model. They can be provided by the gyroscope in the IMU and the WSS respectively. Defining the new state as $\mathbf{X}_{i,k} = (x_{i,k}, y_{i,k}, \theta_{i,k})^\dagger$ and the motion measurement as $\mathbf{u}_{i,k} = (s_{i,k}, \omega_{i,k})^\dagger$, the model in (6.1) can now be represented in a more compact form by a function $\mathbf{f}(\cdot)$, as follows:

$$\mathbf{X}_{i,k+1} = \mathbf{f}(\mathbf{X}_{i,k}, \mathbf{u}_{i,k}). \tag{6.2}$$

Assuming the measurements $s_{i,k}$ and $\omega_{i,k}$ are independent of each other and Gaussian with variances $(\sigma_i^s)^2$ and $(\sigma_i^\omega)^2$ respectively, $\mathbf{u}_{i,k}$ is a 2-D Gaussian vector with covariance matrix

$$\boldsymbol{\Sigma}_{i,k}^{\mathbf{u}} = \begin{pmatrix} (\sigma_i^s)^2 & 0 \\ 0 & (\sigma_i^\omega)^2 \end{pmatrix}. \tag{6.3}$$

In case of there is neither sensors nor mobility knowledge, one simple approach consists in employing a very generic tracking model, e.g. a 2-D version of Newton's force law [81], as mobility prediction model. The corresponding discrete time model is

$$\mathbf{X}_{i,k+1} = \begin{pmatrix} \mathbf{I}_2 & \Delta T \mathbf{I}_2 \\ \mathbf{0}_2 & \mathbf{I}_2 \end{pmatrix} \mathbf{X}_{i,k} + \begin{pmatrix} 1/2\Delta T^2 \mathbf{I}_2 \\ \Delta T \mathbf{I}_2 \end{pmatrix} \widetilde{\mathbf{w}}_{i,k}, \tag{6.4}$$

where $\widetilde{\mathbf{w}}_{i,k} \sim \mathcal{N}((0,0)^\dagger, \widetilde{\mathbf{Q}}_{i,k})$ is the 2-D process noise. It is important to keep the process noise covariance $\widetilde{\mathbf{Q}}_{i,k}$ large enough so as to take into account the model's prediction error (or model mismatch) and preserve filtering stability accordingly [27]. In practice, vehicle's acceleration/deceleration capacity is used to fine-tune this process noise. This model is considered as a baseline to evaluate the IMU/WSS integration while keeping the model-mismatching with the Gauss–Markov model that is used to generate the mobility traffic.

6.3.2　Integration of Additional Camera-based Lane Detection

As already mentioned, the mobility of land vehicles is tightly constrained by the road and lane boundaries. Thus, such contextual information is constructive and can be contributed into the localization problem [27]. We assume herein that lane detection can be performed at each vehicle using for instance a vision-based system (e.g., monocular camera) and a digital map [133]. The latest filtered/fused estimate is cross-checked with the side digital map to identify the current road occupancy and its associated attributes (e.g., lanes number and width). In addition, the camera system scans the road, detects the lanes and the land markers [133]. As a result, the absolute positions of the lane boundaries can be determined and used to constrain the filtered/fused outputs. Contrarily to most common map matching approaches, which simply project the vehicle's position on the center of the road or lane [86], we consider a more realistic approach called *density truncation*. In this method, the posterior density of location estimate is numerically truncated beyond the lane boundaries, which are considered as constraints to restrict the valid state domain. More precisely, particles lying outside a drivable area are removed. Finally, the constrained density is constructed based on the remaining valid samples on the occupied lane. This truncated density is subsequently used to calculate the filter MMSE output. Note that this technique is not entirely appropriate when vehicle changes lanes and the new lane has not been updated yet shortly after the transition. In other words, the error may increase for a short period.

6.4　V2X Cooperative Localization in GNSS-Denied Environments

6.4.1　V2I/V2V Cooperative Localization

We propose to apply the previous filter as the core fusion engine in our CLoc framework, as described in Algorithm 5 (including also side CAM reception, message approximation and CAM broadcast steps). Note that our PF-based data fusion combines V2X measurements (i.e., V2V measurements with respect to mobile "virtual anchors" and V2I measurements with respect to true anchors/RSUs) to give robust and accurate position estimates in Step 3 and 4.

Algorithm 5 Bootstrap PF for hybrid V2X multisensor data fusion (iteration k, "ego" vehicle i)

1: **CAM Collection:** Receive CAMs from the set $\mathcal{N}_{\rightarrow i,k}$ of perceived neighbors, exact the parametric beliefs, and draw samples to reconstruct the approximated particle clouds $\{\widetilde{\mathbf{X}}_{j,k}^{(p)}, 1/P\}_{p=1}^P$, $j \in \mathcal{N}_{\rightarrow i,k}$.

2: **Data Resynchronization:** Perform prediction of both "ego" and neighboring particle clouds based on mobility models in (6.2) at the "ego" estimation instant $t_{i,k}$

$$\mathbf{X}_{i,k}^{(p)} \sim p(\mathbf{X}_{i,k}|\mathbf{X}_{i,k-1}^{(p)}, \mathbf{u}_{i,k-1}), \qquad w_{i,k}^{(p)} = 1/P, \qquad p = 1,\ldots,P,$$

$$\mathbf{X}_{j,k_i}^{(p)} \sim p(\mathbf{X}_{j,k_i}|\widetilde{\mathbf{X}}_{j,k}^{(p)}, \mathbf{u}_{j,k}), \qquad w_{j,k_i}^{-(p)} = 1/P, \qquad p = 1,\ldots,P, \qquad j \in \mathcal{N}_{\rightarrow i,k},$$

and build the LDM of vehicle i's neighbors (as another possible output of the algorithm):

$$\widehat{\mathbf{X}}_{j,k_i}^- \approx \frac{1}{P}\sum_{p=1}^P \mathbf{X}_{j,k_i}^{(p)}, \quad \mathbf{\Sigma}_{j,k_i}^- \approx \frac{1}{P}\sum_{p=1}^P (\mathbf{X}_{j,k_i}^{(p)} - \widehat{\mathbf{X}}_{j,k_i}^-)(\mathbf{X}_{j,k_i}^{(p)} - \widehat{\mathbf{X}}_{j,k_i}^-)^\dagger, \quad j \in \mathcal{N}_{\rightarrow i,k}.$$

3: **Observation Query and Aggregation:** Select the subset $\mathcal{S}_{\rightarrow i,k} \subset \mathcal{N}_{\rightarrow i,k}$ of paired "virtual anchors" and the set $\mathcal{T}_{\rightarrow i,k}$ of paired true anchors. Aggregate the measurements (and the corresponding observation model) $\mathbf{z}_{i,k} = (\mathbf{z}_{\mathcal{S}\rightarrow i,k}^\dagger, \mathbf{z}_{\mathcal{T}\rightarrow i,k}^\dagger)^\dagger$.

4: **Correction:** Calculate the new weights according to the likelihood

$$w_{i,k}^{(p)} \propto p(\mathbf{z}_{i,k}|\mathbf{X}_{i\cup\mathcal{S}\cup\mathcal{T},k}^{(p)}) = \prod_{j\in\mathcal{S}_{\rightarrow i,k}} p(z_{j\rightarrow i,k}|\mathbf{X}_{j,k_i}^{(p)}, \mathbf{X}_{i,k}^{(p)}) \prod_{l\in\mathcal{T}_{\rightarrow i,k}} p(z_{l\rightarrow i,k}|\mathbf{x}_l, \mathbf{X}_{i,k}^{(p)}), \quad p = 1,\ldots,P,$$

normalize them to sum to unity, and compute the approximate MMSE estimator as the second filter/fusion output $\widehat{\mathbf{X}}_{i,k} \approx \sum_{p=1}^P w_{i,k}^{(p)}\mathbf{X}_{i,k}^{(p)}$.

5: **Resampling, Message Approximation, Broadcast**

In this algorithm, we remind that at local discrete time k, the "ego" vehicle i has the set $\mathcal{S}_{\rightarrow i,k}$, $i \notin \mathcal{S}_{\rightarrow i,k}$ of "virtual anchors", the set $\mathcal{T}_{\rightarrow i,k}$ of fixed anchors (i.e., RSUs), and acquires an observation vector $\mathbf{z}_{i,k}$, which is related to its own state $\mathbf{X}_{i,k}$, its neighboring states $\mathbf{X}_{j,k_i}$, $j \in \mathcal{S}_{\rightarrow i,k}$, and its connected RSUs' positions $\mathbf{X}_{l,k_i} = \mathbf{x}_l$, $l \in \mathcal{T}_{\rightarrow i,k}$ via a measurement model.

6.4.2   GNSS Repeater-Aided V2V Cooperative Localization

Another infrastructure-based solution to assist CLoc with absolute positioning capabilities consists in deploying GNSS repeaters in tunnels instead of RSUs. From the localization point of view, the Algorithm 5 is thus modified in Step 3 and Step 4 so as to integrate GNSS observations $\mathbf{p}_{i,k} = (p_{i,k}^x, p_{i,k}^y)^\dagger$, which is assumed to be affected by an i.i.d. Gaussian noise vector $\mathbf{n}_{i,k} = (n_{i,k}^x, n_{i,k}^y)^\dagger \sim \mathcal{N}((0,0)^\dagger, \sigma_{\text{GNSS}}^2 \mathbf{I}_2)$. Accordingly, the measurement vector in Step 3 becomes

$$\mathbf{z}_{i,k} = (\mathbf{p}_{i,k}^\dagger, \mathbf{z}_{\mathcal{S}\rightarrow i,k}^\dagger)^\dagger \tag{6.5}$$
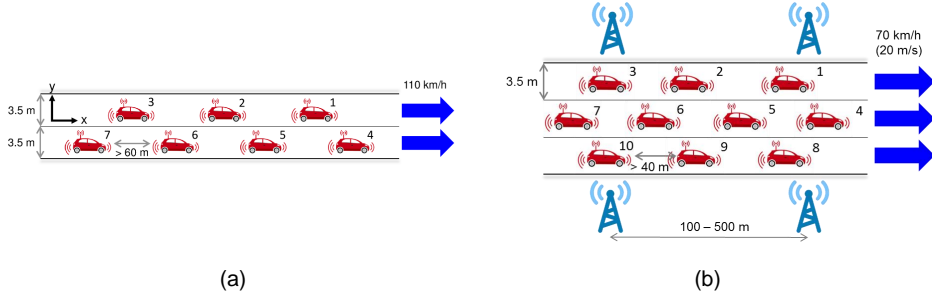
Figure 6.3: Evaluated VANET and related attributes in (a) two-lane highway scenario and (b) 1000-m straight tunnel scenario.

and the particle weights are now updated as follows:

$$
\begin{aligned}
w_{i,k}^{(p)} &\propto p(\mathbf{z}_{i,k}|\mathbf{X}_{i,k}^{(p)}, \mathbf{X}_{\mathcal{S}\to i,k}^{(p)}) \\
&= p(\mathbf{p}_{i,k}|\mathbf{X}_{i,k}^{(p)}) \prod_{j\in S_{\to i,k}} p(z_{j\to i,k}|\mathbf{X}_{j,k_i}^{(p)}, \mathbf{X}_{i,k}^{(p)}), \quad p = 1, \ldots, P.
\end{aligned}
\tag{6.6}
$$

6.5 Numerical Results

6.5.1 Simulation Settings

We now evaluate the performance of the proposed solutions to mitigate the effects of poor GDOP along the dimension orthogonal to the road as well as the divergence of position estimates and error propagation in case of prolonged GNSS outages. We also consider a fleet of ITS-G5-connected vehicles endowed with IR-UWB ranging capabilities. Then two scenarios are investigated as follows.

In the first scenario, we model a horizontal two-lane highway, where 7 vehicles are driving steadily in a common direction at the average speed of 110 km/h (i.e., about 30 m/s) for 60 seconds, as shown in Figure 6.3(a). In this scenario, along-track and cross-track directions arbitrarily coincide with x- and y-axes respectively.

In the second scenario, we consider a 1000-m three-lane straight tunnel, where 10 vehicles are driving steadily in a common direction at the average speed of 70 km/h. In addition, RSUs are deployed along the tunnel, with different inter-site intervals of 500, 200, and 100 meters either on one single side of the road or on both sides as shown in Figure 6.3(b). These units support both ITS-G5 and IR-UWB technologies for both V2I communication and V2I ranging with respect to mobile vehicles. The main simulation parameters are summarized in Table 6.1.

Table 6.1: Main simulation parameters used for the simulation-based evaluation of hybrid V2X multisensor cooperative localization.

Parameter	Value
Sampling period ΔT	0.1 [s]
Gyroscope signal noise	0.1 [deg/s] (rms) [133]
WSS noise	1% actual speed [133]
V2X IR-UWB ranging rate	5 [Hz] (V2V), 10 [Hz] (V2I)
V2X IR-UWB ranging noise	0.2 [m] (rms)
V2X IR-UWB communication range	600 [m]
V2X CAM rate	10 [Hz] (critical)
V2X CAM range	1000 [m] [19]
Path loss exponent n_p	1.6 (V2V in tunnels) [115]
Standard deviation of shadowing σ_{Sh}	3.4 [dB] (V2V in tunnels) [115]
Inter-site RSU interval	500, 200, and 100 [m]
GNSS rate	10 [Hz]
GNSS noise	1.5 [m] (SBAS), 3.6 [m] (SPS) (rms) [134]
GNSS repeater noise	5–10 [m] (rms)
Number of particles	1000
Initial pos. errors in x- and y-axes	1 [m] (rms) (plausible hypothesis)
Initial heading error	4 [deg] (rms) (plausible hypothesis)

6.5.2   Two-Lane Highway Scenario

Figure 6.4 compares the errors along x- and y-axes for different fusion strategies by means of empirical CDFs. Regarding x-axis location errors on Figure 6.4(a), as expected, using the LCs has no impact on the along-track positioning error. Specifically, GNSS and GNSS+LC schemes yield comparable error levels. The GNSS+IMU+WSS option gains significant accuracy over the standalone GNSS solution mostly thanks to the WSS (but not to the IMU). As GDOP is usually good in the along-track direction, the co-operative GNSS+IR-UWB scheme improves accuracy when compared to GNSS and to GNSS+IMU+WSS. Note that the GNSS+IR-UWB solution outperforms GNSS+IMU+WSS considering our simulation settings because the result depends on many parameters such as CLoc conditions, the quality of the gyroscope, etc. To further enhance accuracy, the IMU/WSS and the LC information are included on top of GNSS+IR-UWB. However, only the GNSS+IR-UWB+IMU+WSS scheme exhibits performance gains. The GNSS+IR-UWB+LC scheme surprisingly suffers from accuracy degradation in comparison with GNSS+IR-UWB. This observation can be explained by considering the effect of y-axis errors on Figure 6.4(b). More particularly, due to large y-axis errors within the GNSS+IR-UWB scheme, i.e., 0.53 m and 1.42 m of median and WC (defined for a CDF of 90%) errors respectively, an "ego" vehicle may suffer from singular GDOP. In this case, there exist several neighbors whose relative vectors from an "ego" vehicle are

(a) x-axis (along-track).   (b) y-axis (cross-track).
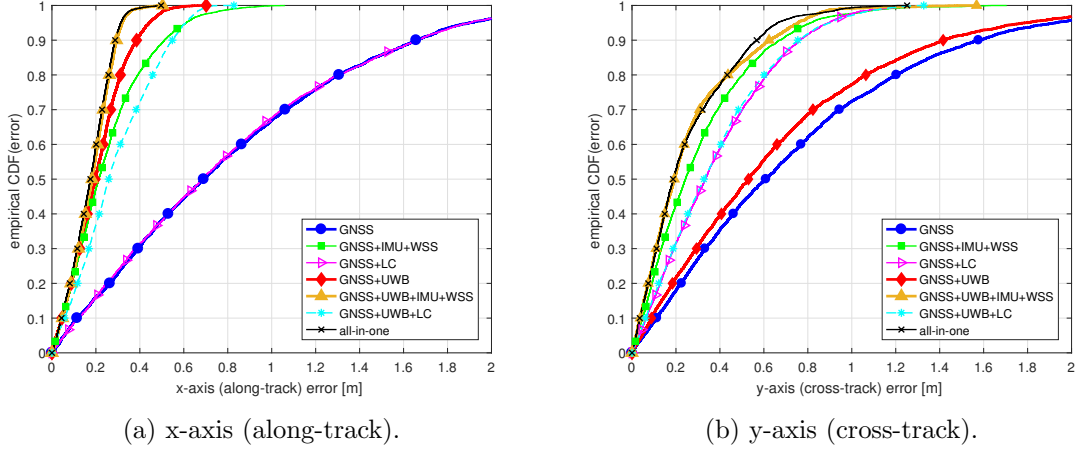
Figure 6.4: Empirical CDFs of x-axis (along-track/left) and y-axis (cross-track/right) localization errors for different fusion schemes in the two-lane highway scenario.

nearly aligned with the road. Accordingly, these misplaced anchors contribute to improve performance on the along-track axis, whereas they tend to increase the error along the cross-track direction (see again Section 6.2.1 or Figure 6.1). The all-in-one solution does not outperform the GNSS+IR-UWB+IMU one simply because the LC information cannot improve the along-track performance.

The performance along the critical y-axis is summarized in Figure 6.4(b). As expected, IMU-based heading measurement and LC integration both contribute to dramatically decrease the error. It also confirms the limited impact of range-based CLoc on the cross-track error in poor GDOP VANETs i.e., with a relative drop by only 13% in terms of median error (compared to GNSS) versus 61% and 46% with non-CLoc schemes such as GNSS+IMU+WSS and GNSS+LC respectively. The integration of IMU yields higher accuracy level than the LC-based solution when considered in non-CLoc schemes (with relative drops by 69% and 46% in terms of median error respectively) and similarly within CLoc schemes (with relative drops by 61% and 46% respectively). This observation is mainly due to the settings e.g., the gyroscope signal noise, the initialization, and the lane width... We can also see that the GNSS+IR-UWB+LC scheme and the GNSS+LC scheme yield comparable y-axis accuracy. Besides, the all-in-one option remains still slightly more accurate than GNSS+IR-UWB+IMU+WSS in terms of y-axis error thanks to the additional LC information.

Finally, Figure 6.5 compares the performance of different schemes in terms of 2-D localization (distance) error and confirms the significant accuracy gains offered by the
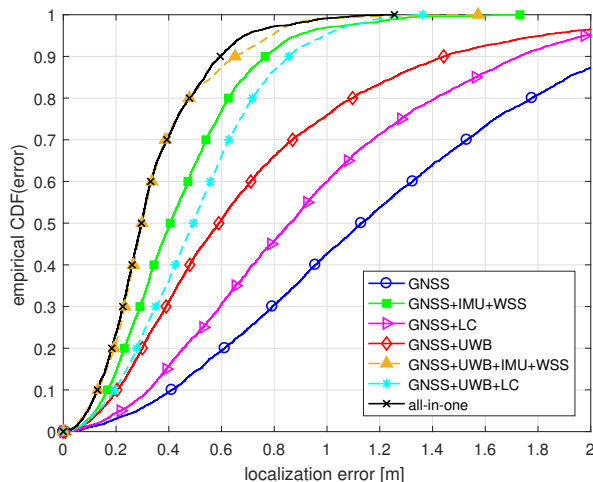
Figure 6.5: Empirical CDFs of overall localization errors for different fusion schemes in two-lane highway scenario.

IMU/WSS and the LC information. The overall performance comparison is also summarized in Table 6.2 for critical error regimes.

6.5.3 Tunnel Scenario

Localization Performance Comparison

The localization performance achieved for different algorithmic and technological options is summarized in Figures 6.6, 6.7, and 6.8 by means of empirical CDFs. DR based on IMU and WSS is by default assumed available at each vehicle and thus considered in all the tested scenarios (either as stand-alone solution or in combination with other technologies).

Figure 6.6 shows spectacular performance gains when using RSUs with accurate IR-UWB ranging capabilities even under reasonably loose deployments i.e., with inter-site RSUs intervals of 500 m on both sides of the tunnel. As aforementioned, conventional DR provides relatively poor performance in the long-term due to error accumulation and resulting drift effects, whereas pure ad hoc V2V cooperation based on both IR-UWB V2V measurements and DR (thus, relying on ill-positioned "virtual anchors") leads to mutual contamination among vehicles and even worse localization performance in the end. The capability to provide CLoc with reliable *absolute* information however strongly depends on the V2I ranging technology available at RSUs. In particular, the addition of V2I range measurements based on IR-UWB yields significant performance gain over DR (relative drops of 88% in median error and 85% in WC error (defined for a CDF of 90%)) and

Table 6.2: Overall performance comparison of different fusion schemes.

Fusion scheme	x-axis (along-track) error				y-axis (cross-track) error				localization error		
	50th [m]	90th [m]	CDF(0.2 m)	Gain[b]	50th [m]	90th [m]	CDF(0.2 m)	Gain[a]	50th [m]	90th [m]	Gain[a]
GNSS	0.69	1.66	16%	-	0.61	1.58	18%	-	1.13	2.10	-
GNSS+IMU+WSS	0.21	0.51	47%	70%	0.24	0.67	43%	61%	0.41	0.77	64%
GNSS+LC	0.69	1.66	16%	0%	0.33	0.76	32%	46%	0.86	1.73	24%
GNSS+UWB	0.20	0.39	51%	71%	0.53	1.42	22%	13%	0.59	1.44	48%
GNSS+UWB+IMU+WSS	0.18	0.29	57%	74%	0.19	0.62	52%	69%	0.30	0.65	73%
GNSS+UWB+LC	0.26	0.55	37%	62%	0.33	0.75	32%	46%	0.49	0.86	57%
All-in-one	0.18	0.29	60%	74%	0.19	0.57	53%	69%	0.30	0.60	73%

[a] Relative gain with respect to standalone GNSS solution in median error (i.e., CDF = 50%).
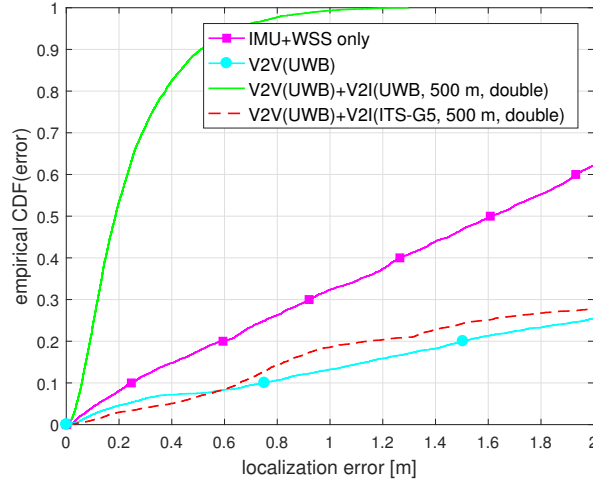
Figure 6.6: Empirical CDFs of localization errors for DR (IMU+WSS), IR-UWB V2V CLoc, and V2X CLoc (with IR-UWB V2V and ITS-G5 or IR-UWB V2I) in the tunnel scenario.

pure ad hoc CLoc (relative drops of 94% and 90% in median and WC errors respectively), while V2I RSSI measurements based on ITS-G5 are not sufficiently informative so that the localization performance is equivalent to that of a pure ad hoc case relying on IR-UWB V2V ranging and DR. RSSI-based positioning is indeed usually not considered as a high precision solution. Thus its contribution to the position estimate correction (by updating the weights in Step 4 of Algorithm 5) is relatively marginal in comparison with that of accurate IR-UWB V2V ranges.

In Figure 6.7, we compare the proposed RSU-based solution with the use of LC (with DR) or GNSS repeaters (with DR), assuming in the latter case systematic GNSS signal availability in the entire tunnel[2] but various quality levels. It is indeed reasonable to assume degraded accuracy in comparison with open-sky conditions due to multipath propagation (e.g., SPS and SBAS accuracy of 1.5 m and 3.6 m respectively [134]). It is thus observed that the *absolute* positional information provided by GNSS repeaters must be accurate enough to be able to re-calibrate position estimates. However, this information is always beneficial for fusion since it is assumed to be bounded and unbiased. Besides, the non-CLoc scheme including LC and DR outperforms the solution based on GNSS repeaters but still cannot reach the performance level of full V2X CLoc including IR-UWB range measurements with respect to both mobile neighbors and RSUs, even if the performance gap is not so significant (increased median and WC errors of 12 cm and

---

[2]This is usually achieved with typical inter-side intervals in the range of $30 - 50$ m.
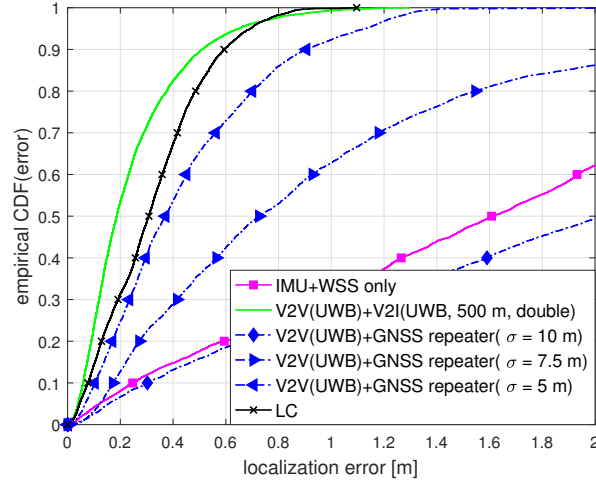
Figure 6.7: Empirical CDFs of localization errors for IR-UWB V2X CLoc, GNSS-repeater-aided IR-UWB V2V CLoc, and lane constraints (with DR only) in the tunnel scenario.

8 cm respectively). Two main reasons can be invoked to explain this phenomenon. First, we have considered a very accurate WSS sensor in our validations [133]. Thus LC naturally tends to correct the only remaining accumulated errors affecting the input heading measurements used in state predictions. Second, the tested RSU deployment (i.e., 500-m inter-site interval) is rather sparse, leading to an average number of 4 connected anchors (as shown in Figure 6.9), what contributes to sustain poor GDOP conditions.

In Figure 6.8, we are interested in more *aggressive* scenarios to boost localization accuracy. In particular, we assume a denser RSU deployment (e.g., down to 100-meter inter-site intervals) and more accurate GNSS repeaters reaching optimistically the open-sky accuracy of SPS or even SBAS. Let us now consider the non-CLoc scheme with LC and DR as a reference baseline. By using massive RSUs, the V2I RSSI now yields better performance and at least outperforms the standalone DR solution (relative decreases of 67% and 24% in median and WC errors respectively) but still cannot be compared with the proposed full CLoc scheme relying on both IR-UWB V2V and V2I range measurements.

Then, we verify *if* and *to which extent* it is possible to improve also the solution based on ITS-G5 V2I RSSI measurements by integrating LC. However, it only gives comparable performance levels with the solution combining DR and LC, due to inaccurate ITS-G5 V2I RSSIs again.

When assuming even more optimistic GNSS repeater accuracy to the level of open-sky at the price of increased cost of deployment, only the solution combining SBAS and DR yields performance gains over the solution combining LC and DR, even though yet the
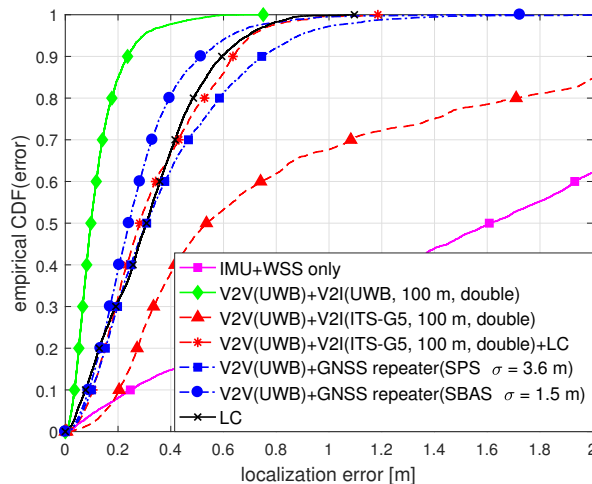
Figure 6.8: Empirical CDFs of localization errors for V2X CLoc (with IR-UWB V2I or ITS-G5 V2I (massive infrastructure) with and without lane constraints) and ideal GNSS-repeater-aided IR-UWB V2V CLoc in the tunnel scenario.

gap is not so remarkable. Under denser IR-UWB RSUs deployment, much better accuracy is achievable through full V2X CLoc (relative drops of 68% and 60% in median and WC errors respectively with respect to the DR and LC).

Deployment Cost Analysis and Discussion

We confront here the trade-off between the accuracy gain and the associated deployment cost. Particularly, we compare the use of IR-UWB RSUs and GNSS repeaters for tunnels. We claim that the IR-UWB RSU approach is more favorable than the GNSS repeater scheme in terms of both accuracy performance and deployment cost. As an illustration, in the considered 1000-meter tunnel scenario, we would need to place about 20–35 repeaters (i.e., one every 30–50 meters) to achieve the accuracy of 0.4–2 m whereas 6–20 IR-UWB RSUs yield 0.2–0.1 m[3]. Motivated by the clear benefits from RSUs, we further compare different RSU configurations, as depicted in Figure 6.9. A closer look at the figure reveals that with a similar number of connected RSUs (as well as a total number of deployed RSUs) (e.g., single-sided 200-meter inter-site RSUs interval vs. double-sided 500-meter and double-sided 200-meter vs. single-sided 100-meter), the shorter inter-site RSUs interval, the better accuracy. It is due to the fact that cross-track error is significantly reduced when vehicles pass by the anchors. Thus, short inter-site RSUs interval shall be preferred to looser double-sided deployment.

---

[3]We assume in first approximation that the deployment efforts -and thus costs/unit- of GNSS repeaters and IR-UWB RSUs are comparable.
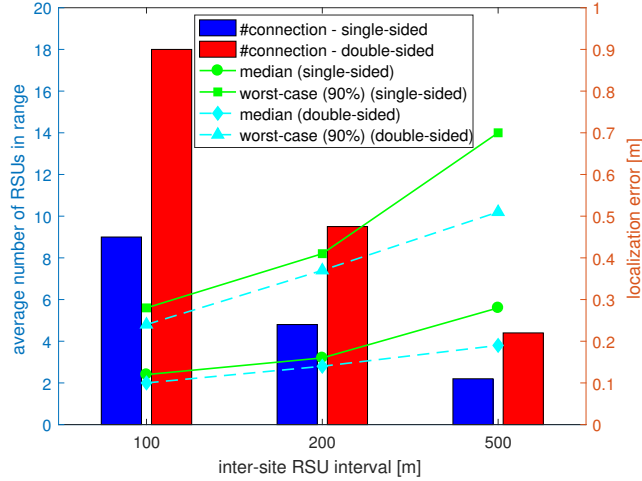
Figure 6.9: Impact of the RSU deployment on IR-UWB V2X CLoc's localization accuracy in the tunnel scenario.

6.6   Summary

In this chapter, we have studied the problem of range-based CLoc in VANETs in the presence of poor cross-track GDOP caused by constrained vehicular mobility. Simulation results clearly indicate that cross-track positioning errors cannot be fully mitigated through conventional range-based cooperation. We solve this problem by additionally integrating the vehicle's heading information issued at IMUs or contextual information such as lane occupancy and boundaries.

We have also investigated the problem of range-based CLoc for VANETs specifically in tunnel environments. Simulation results clearly indicate that in long tunnels, CLoc only with respect to neighboring vehicles is prone to fast divergence and inaccurate position estimates. We solve this problem by additionally integrating V2I measurements with respect to RSUs, which are deployed along the tunnel, relying on an adapted PF-based data fusion framework. By applying the proposed hybrid CLoc with generalized V2X measurements (i.e., V2I on top of V2V), we have found that: (i) V2I IR-UWB range measurements boost the CLoc accuracy even under sparse RSUs deployment; (ii) V2I RSSI only slightly improves the CLoc accuracy in case of massive RSUs deployment; (iii) V2X IR-UWB CLoc is more attractive than the CLoc assisted by GNSS repeaters in terms of both accuracy performance and cost of deployment.

Up to this point, we have "theoretically" addressed and solved a variety of key challenges inherent to CLoc (mostly through canonical simulation scenarios), treating them

somehow gradually or even sometimes independently. For this sake, we have considered the integration of numerous additional modalities on top of the nominal scheme introduced in Chapter 3, depending on the number of available sensors at the vehicles. We are now prepared for further practical validations in Chapter 7.

Chapter 7

Validations through More Realistic Simulations and Experimental Data

7.1   Introduction

In this chapter, the ultimate goal is to validate some of the CLoc algorithms presented in the previous chapters using even more realistic input data. Still following a gradually complex approach, this objective is achieved in two steps, as follows.

First, evaluations are conducted using a specific traffic simulator called Simulation of Urban Mobility (SUMO) [135]. The latter can account for long-term and/or erratic vehicles mobility in complex scenarios (i.e., rather than considering only highly regular mobility models in canonical scenarios, like in the previous chapters). As these mobility traces are generated under varying traffic conditions in a representative urban environment, one can validate the benefits of context-dependent cooperative fusion approaches over larger periods of time, in terms of service continuity and robustness. This first step is also essential to anticipate optimal algorithmic settings and behavior for final field trials. Second, the performance of the proposed algorithms is evaluated by means of experimental data, which is collected at three real vehicles on a portion of road specifically equipped for large-scale test purposes.

The chapter is organized as follows. In Section 7.2, simulation results are presented using SUMO mobility traces in an urban scenario that offers mixed environmental char-

acteristics in view of GNSS performance (i.e., spanning from open environments to urban canyon). Then validations based on experimental data are provided in Section 7.3. Finally, Section 7.4 summarizes and discusses the achieved results, while suggesting a few adjustments regarding future physical proof of concept evaluations and demonstrations.

7.2 Offline Validation Based on Mobility Traces

7.2.1 Simulation Settings

Using the SUMO traffic simulator, 10 vehicles' trajectories have been extracted from a wide-scale urban simulation scenario calibrated for the city of Bologna, Italy. A restricted geographic area has been considered, including several pathological cases (including 1 portion of urban canyon), simulating for 200 seconds (see Figure 7.1). This test environment enables to show:

- The sensitivity to GNSS quality variations as a function of local environmental conditions (e.g., road width and buildings height) (see Table 7.1);

- The sensitivity to erratic mobility while crossing several intersections (e.g., possibly causing harmful mismatch between the mobility models assumed for prediction and actual mobility patterns).

- The sensitivity to the relative topology (and number) of cooperating vehicles.

In the cooperating fleet, each vehicle is alternatively viewed as the "ego" vehicle under testing, whereas the other(s) are viewed as assisting neighbors (or "virtual anchors").

At each vehicle, the fusion engine relies on a PF with 1000 particles. Prediction is based on the bicycle model, using inputs from WSS (i.e., speed) and IMU (i.e., heading). As for data synchronization, "ego" prediction and neighboring prediction are slightly different. Since we cannot instantly access the neighbors' WSS and IMU measurements to perform the corresponding prediction at the "ego", we artificially add extra uncertainties (say, 10% of maximum speed of 15 m/s and 10% of typical heading change of 20°) to the speed and heading values contained in the latest CAMs received from these neighbors. In the correction step, GNSS positions and IR-UWB ranges with respect to the neighbors with informed positions (i.e., for which a CAM has been received) are used to update the
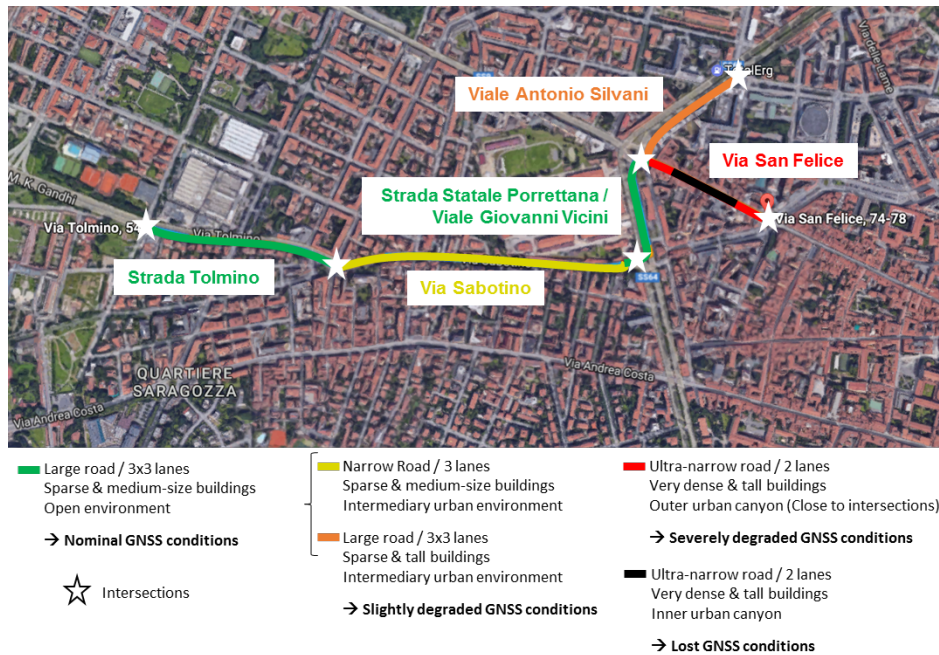
Figure 7.1: Focused geographic area of Bologna city used in calibrated SUMO simulations, with mixed urban environments.

predicted values in our CLoc solution. On the contrary, non-CLoc refers to the data fusion of GNSS position, WSS speed, and IMU heading (i.e., using only local information).

The GNSS model and accuracy depend on both the portion of trajectory and the arbitrarily assigned GNSS kind/class (see tables 7.1 and 7.2), while the WSS and IMU models are similar to that used in Chapter 6 (see Table 6.1). Besides, based on statistics reported in [8, 136] in a urban environment and in systematic LOS, as well as experimental illustrations based on integrated IR-UWB modules taken from [133], the standard deviation of V2V range measurements is assumed to be 0.122 m, whereas the bias has a mean of 0.21 m. Finally, we assume no packet loss for simplicity but still account for non-visibility configurations caused by static building obstructions at intersections. In this case, some ranging measurements become harmful for the fusion and are rejected.

7.2.2 Results

Figure 7.2 and Figure 7.3 show the localization performance of each individual vehicle and over 10 vehicles in terms of empirical CDFs. Figure 7.2(a) shows that non-CLoc yields rather good performance even when the vehicles are equipped with only GNSS SPS receivers (i.e., about 0.8 m in median errors at vehicles 1, 5 and 9). Obviously, with better GNSS receivers like SBAS, DGNSS, and RTK, the performance gets better as

Table 7.1: GNSS quality associated to each portion of road of the Bologna scenario in Figure 7.1.

Street	Environment	GNSS quality
Via Tolmino	open urban environment, large road with 3 by 3 lanes, sparse and medium-size buildings	nominal $\to 1\sigma$
Via Sabotino	intermediary urban environment, narrow road, 3 lanes, sparse and medium-size buildings	slightly degraded $\to 2\sigma$
Strada Statale Porrettana, Viale Giovanni Vicini	open urban environment, large road with 3 by 3 lanes, sparse and medium-size buildings	nominal $\to 1\sigma$
Viale Antonio Silvani	Intermediary urban environment, large road with 3 by 3 lanes, tall buildings	slightly degraded $\to 2\sigma$
Via S. Felice (outer)	urban canyon (close to intersections), ultra-narrow road with 2 lanes, very dense and tall buildings	severely degraded $\to 5\sigma$
Via S. Felice (inner)	urban canyon (inner part), ultra-narrow road with 2 lanes, very dense and tall buildings	lost $\to$ N/A

Table 7.2: GNSS device kinds assigned to simulated vehicles in the city of Bologna.

GNSS device kind	IDs of simulated vehicles
SPS	1, 5, 9
SBAS	2, 6, 10
DGNSS	3, 7
RTK	4, 8

depicted in Figures 7.2 (b), (c), and (d) respectively. Then, CLoc boosts further accuracy. Particularly, for SPS vehicles (i.e., vehicles 1, 5, and 9), the gains are very impressive (about 50% in median errors). For SBAS vehicles (i.e., vehicles 2, 6, and 10) and DGNSS vehicle (i.e., vehicle 3), the gains are less significant but still high in the range 30–40% in terms of median errors. For RTK vehicles (i.e., vehicles 4 and 8), the gains are more modest because RTK is already extremely accurate. Note that we still observe an improvement at vehicle 4 in its high error regime (CDF at 95%) because it goes through the urban canyon with no GNSS signal at all during several seconds at the end of the simulation (see Figure 7.1), so that accuracy is improved through cooperation in this pathological case.

A closer look at Figure 7.2 reveals that except RTK vehicles like 4 and 8, other vehicles have rather different performance levels. It may due to the GNSS quality but via cooperative message exchanges, it is expected that they achieve approximately homogeneous accuracy. One reason lies in the actual connectivity of the vehicles. Although we assume perfect packet reception rate, as already mentioned, we still account for non-visibility configurations. One tangible example is illustrated in Figure 7.4. When the vehicles change their direction and turn from Via Sabotino to Viale Giovanni Vicini (see again Figure 7.1), vehicle 2 is stopped and left behind due to traffic lights so it temporally loses connections
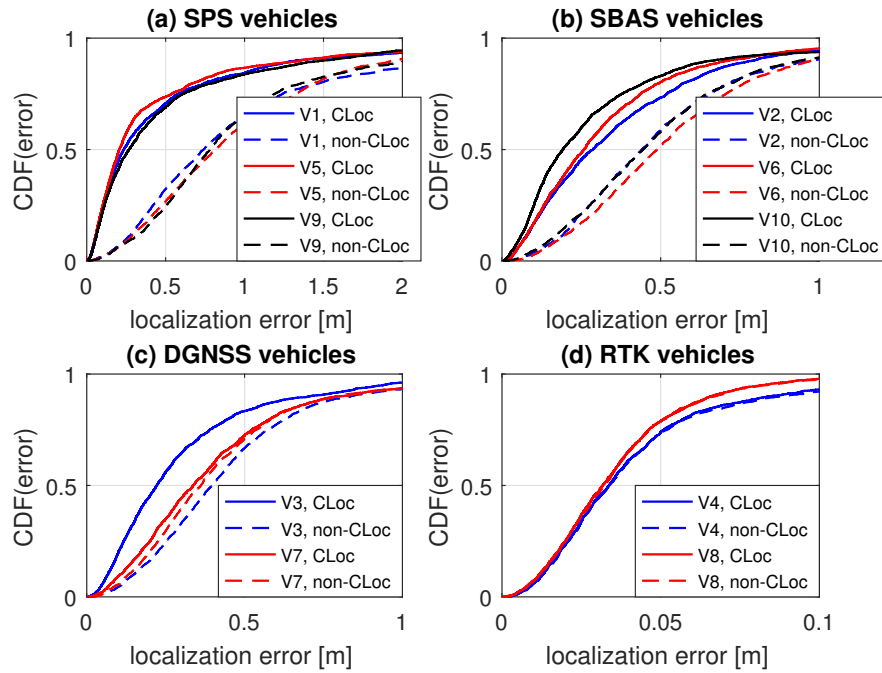
Figure 7.2: Empirical CDFs of localization errors of each vehicle in case of CLoc (GNSS+WSS+IMU+UWB) and non-CLoc (GNSS+WSS+IMU) for the Bologna scenario.
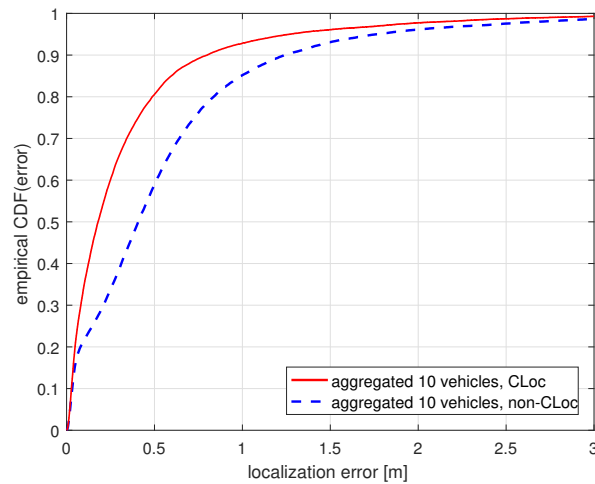
Figure 7.3: Empirical CDFs of aggregated localization errors over all 10 vehicles in case of CLoc (GNSS+WSS+IMU+UWB) and non-CLoc (GNSS+WSS+IMU) for the Bologna scenario.

with respect to other vehicles belonging to the same cooperating group (see Figure 7.4). Therefore, vehicle 2 has poorer accuracy in comparison with for example, vehicles 6 and 10 (see Figure 7.2(b)). In addition, regardless of their nominal GNSS capabilities, peripheral vehicles such as 2 and 7 are likely more penalized by poorer GDOP conditions in comparison with vehicles in the convex hull formed by the piconet's relative topology. In realistic operating conditions however, each vehicle would benefit from cooperation with
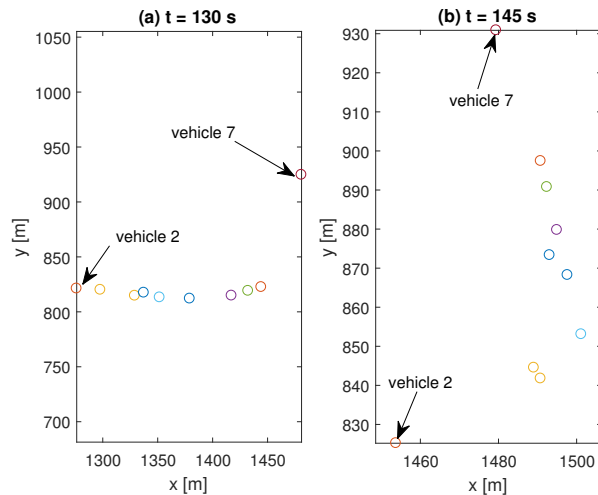
Figure 7.4: Relative geometry of the 10 simulated vehicles at t = 130 s and t = 145 s for the Bologna scenario.

respect to vehicles belonging to different so-called piconet (including vehicles driving in the opposite directions, even for a short period of time), unlike in our restrictive scenario.

Figure 7.3 shows the overall performance (i.e., over the 10 vehicles and over their respective trajectories). It can be seen that CLoc yields rather good performance with a median error of 0.18 m and a sub-meter worst-case accuracy at 95% of the empirical CDF.

Thus far, simulations show that CLoc could reach the required 25 cm accuracy. Note that within the worst-case setup, we still achieve 18 cm accuracy with a probability of 50%. Because we only exploit 10 mobility traces from SUMO, we are forced into cooperating with the provided set of neighbors. However, in practice, each vehicle would select in a dynamic -and thus, more optimal- way more optimal sets of neighbors as "virtual anchors" over time, considering the relative problem geometry, as already discussed in Chapter 3.

7.3 Offline Validation Based on Experimental Data

7.3.1 Experimental Settings

To validate the proposed algorithms based on experimental data, one large-scale test event took place on May 15th, 2017 at the TASS test facilities in Helmond, Netherlands. These tests were relying on an early version of the integrated physical proof of concept demonstrator developed in the HIGHTS project and involved a platoon consisting of 3 equipped cars driving in a row: TASS' Prius car (as lead vehicle), Objective's BMW (as 2nd vehicle)

Figure 7.5: Test vehicles involved in the first HIGHTS field trials carried out in Helmond: Objective's BMW, Tass's Prius and Ibeo's Passat (left to right).
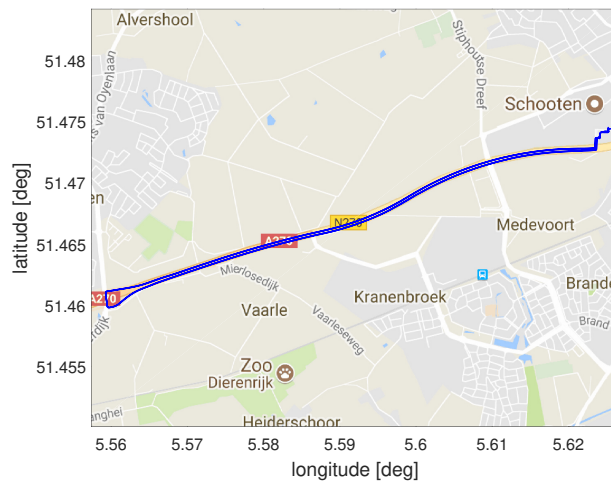
Figure 7.6: Test site and vehicles' trajectory in Helmond, Netherlands (original photo from Google Map).

and Ibeo's Passat (as 3rd and last vehicle)(see Fig. 7.5). During these experiments, each vehicle was equipped with a singe-band GPS receiver, a RTK GPS receiver, an ITS-G5 platform (i.e., Cohda MK5) and a central Blackhole data logging PC, making two full rounds along the A270/N270 highway section. The followed route deliberately included a combination of straight and curvy sections for better representativity and for realistic assessment. The true positions of the vehicles were logged using a RTK GPS for reference purposes (ground truth). Figure 7.6 shows the test site and the followed trajectories.

Due to some problems in the GPS measurements collected at Objective's vehicle during the trials, Ibeo's vehicle has been selected as the "ego" vehicle under test (i.e., in charge of performing cooperative data fusion). The latter receives CAMs encapsulating RTK GPS data from both Objective and Tass' vehicles, measures the corresponding RSSIs out of the received messages (IR-UWB devices were not yet integrated for V2V ranging in the demonstration platform by the time these first trials were conducted), and finally performs fusion with its own on-board GPS position to improve its position accuracy. Furthermore,
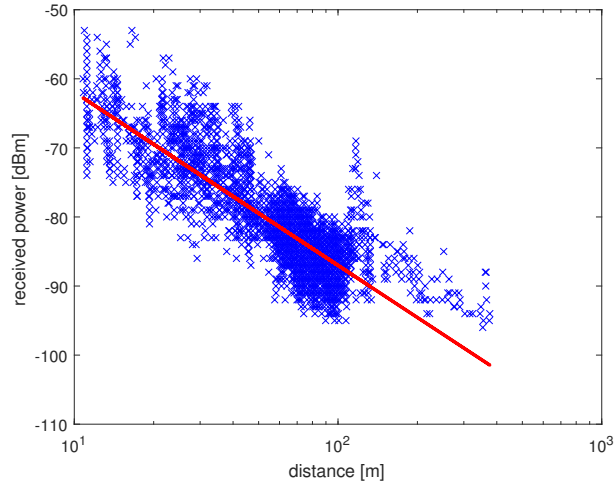
Figure 7.7: Pathloss measurements and approximate large-scale models. In the linear regression, $n_p = 2.5$ (path loss exponent) and $\sigma_{\mathrm{Sh}} = 3.7$ dB (standard deviation of shadowing).

it also tracks (i.e., updates) the neighboring RTK GPS information received in CAMs using mobility prediction since this information may be out-dated at the fusion time otherwise. From a LDM perspective, this can also be viewed as an improvement in comparison with basic position awareness (in the sense the "ego" perception about its neighbors does not only rely on the CAMs but has been updated).

To calibrate the required large-scale path loss model, we have considered both the RSSI using Cohda MK5 and the distance between the two involved vehicles using their GPS RTK receivers. The result of the linear regression analysis is shown in Figure 7.7. This path loss model will be used as the measurement model in the EKF-based fusion engine for CLoc. We use the EKF but not PF herein for some reasons. For this first field test followed by a real-time test later, we plan to implement the algorithm in a limited processing unit inside the Cohda MK5 but not in a connected PC in the vehicle as a starting point for the sake of simplicity. The Cohda MK5 has an integrated GPS inside so the fusion-based CLoc algorithm can access directly the GPS data as well as the RSSIs measured out of the received CAMs and the associated CAM data. On the other hand, the PF version will be implemented in the connected PC as soon as integrated process is optimized which is expected after this first test. Note that the fusion results based on EKF herein is generalized and comparable with PF.

7.3.2   Results

Figure 7.8(a) compares the performance of the CLoc method (i.e., fusing GPS and ITS-G5 RSSI) with that of both filtered and raw GPS positions. As it can be seen, the proposed CLoc approach outperforms the filtered GPS even though the localization accuracy gain is quite marginal and modest, as expected. This is likely due 1) to the very low number cooperative neighbors available in the test case (only 2, at most), 2) to very poor GDOP conditions, as the three vehicles were forming a "longitudinal" platoon most of the time and the "ego" vehicle considered for fusion was the leading one, and 3) to the relatively low CAM rate while providing RSSIs and neighboring positions, at approximately 3 Hz (in average) whereas a maximum 10 Hz could be used (i.e., nominal rate considered in most simulation-based evaluations of CLoc so far).

On the other hand, Figure 7.8(b) shows the performance associated with the LDM maintained at the IBEO's "ego" vehicle (i.e., the quality and validity of the presumed neighbors' positions). As expected, the prediction-based scheme achieves much higher localization accuracy than that without prediction. Specifically, the former performs prediction of neighboring vehicles based on their latest broadcast states (i.e., position and velocity) and a mobility model, whereas the latter simply relies on their raw positional information (i.e., communicated in the CAM). A closer look at this figure reveals that the accuracy gain is huge. Without prediction, the error accumulates quickly, especially when not receiving new CAMs due to too low CAM rate or simply packet loss. Moreover, higher position estimation rate (i.e., 8 Hz, as the GPS rate) would require an equivalent CAM rate to draw maximum benefits, which could not be met in these first experiments. Figure 7.9 illustrates this observation, showing the RMSE of the position awareness regarding the 2 neighbors (Objective and Tass) over time. Note that the value on the right vertical axis CAM update takes either 0 if not receiving any CAM or 1 if receiving a CAM at any iteration. Overall, prediction globally improves position awareness about neighbors in the LDM by a factor of 10.

As aforementioned, the CAM rate of about 3 Hz is relative low when compared to the fusion rate of 8 Hz. Therefore, most of the iterations just correspond to filtered GPS but not to a true CLoc fusion event, leading to modest accuracy gains. To avoid this, we have performed other offline test, reducing the fusion rate down to 4 Hz, as shown in Figure 7.10. The benefit of fusion-based CLoc over standalone GPS is thus more remarkable.

(a) Ibeo's "ego" vehicle

(b) LDM at the Ibeo's "ego" vehicle.
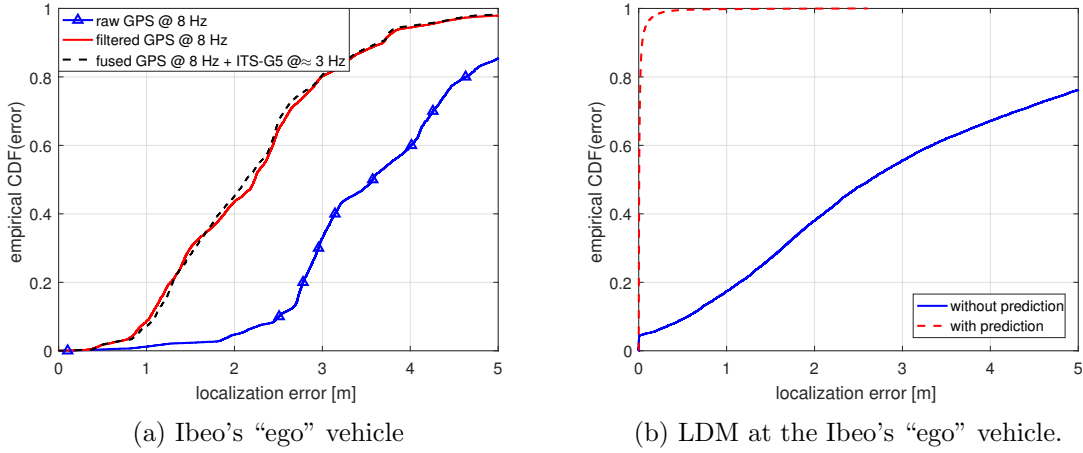
Figure 7.8: Empirical CDFs of localization errors for the first trip of field trials in Helmond.
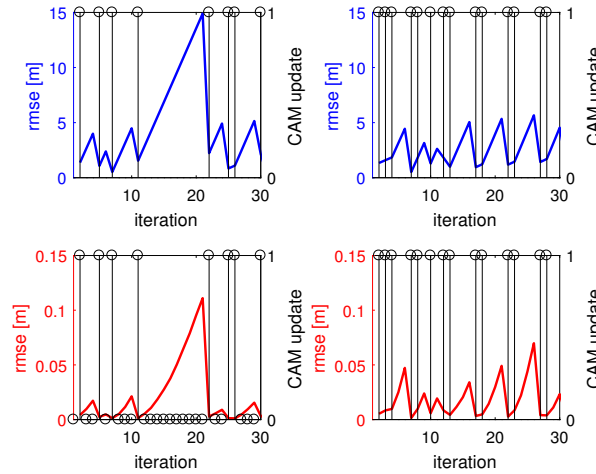
Figure 7.9: Localization RMSEs of the LDM at IBEO's "ego" vehicle as a function of time for the first trip of field trials in Helmond. Cooperative awareness of Objective's and Tass' vehicles positions without prediction (top left and top right, respectively) versus with prediction (bottom left and bottom right, respectively).

The impact of GDOP on the CLoc accuracy has also been investigated. For this sake, the localization error vector has been projected onto the cross-track and along-track axes. Considering the GDOP conditions in this test case (i.e., a platoon in line), the along-track errors are mostly improved by CLoc, as confirmed by Figure 7.11. The figure also shows that the cross-track errors are marginally improved. This is due to the fact that a "longitudinal" platoon was maintained during most of the test.

During the tests in Helmond, the 3 vehicles drove for a second time on the same route (2nd trip). The results are summarized in Figure 7.12 and Figure 7.13. Interestingly, the CLoc method now improves quite significantly accuracy, especially in the lower error regime, as shown in Figure 7.12(a) and Figure 7.13. As the distances between the 3 vehicles
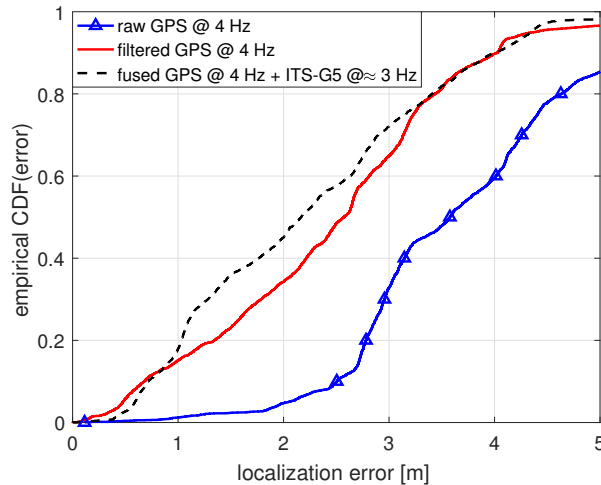
Figure 7.10: Empirical CDFs of localization errors of the Ibeo's "ego" vehicle for the first trip of field trials in Helmond with reduced position estimation rates.
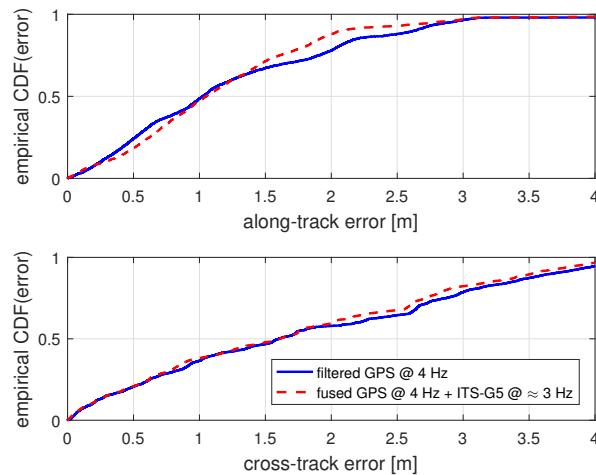
Figure 7.11: Empirical CDFs of along-track and cross-track errors of the Ibeo's "ego" vehicle for the first trip of field trials in Helmond, with reduced position estimation rates.

were shorter during this second trip, RSSI measurements could contribute as more reliable and meaningful distance-dependent information to the final position estimates[1].

7.4 Summary

This chapter contributes to the validation of algorithms from our CLoc framework. On the one hand, relying on simulated mobility traces and assuming V2V IR-UWB range measurements, several observations can be made at the system level in view of the context-aware localization strategy.

---

[1]Theoretically, RSSI-based range measurements have standard deviation proportional to the true distance.

(a) Ibeo's "ego" vehicle   (b) LDM at the Ibeo's "ego" vehicle.
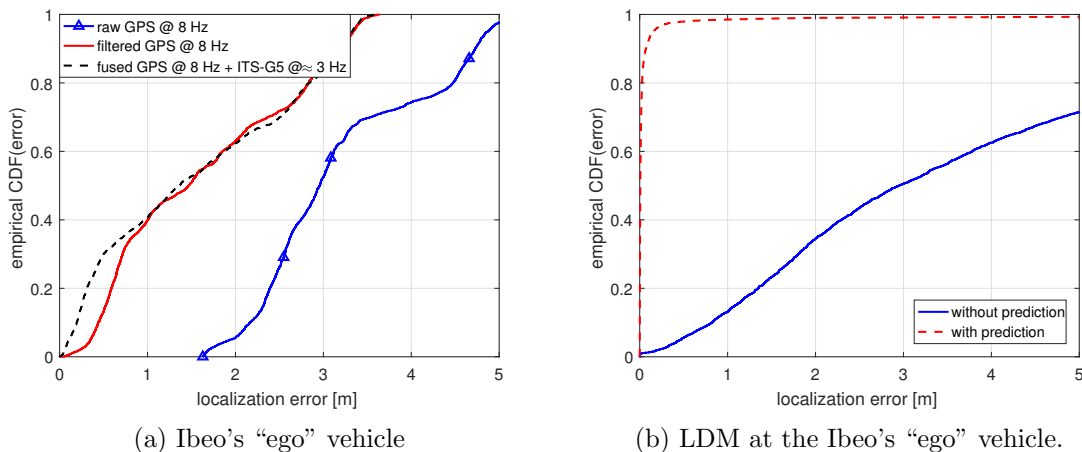
Figure 7.12: Empirical CDF of localization errors for the second trip of field trials in Helmond.
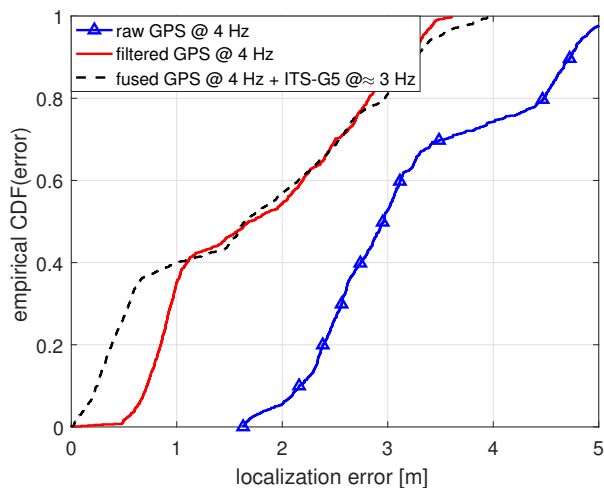
Figure 7.13: Empirical CDF of localization errors of the Ibeo's "ego" vehicle for the second trip of field trials in Helmond with reduced position estimation rates.

- Fusion with other on-board sensors (i.e., WSS and IMU) is always beneficial, contributing mostly to control and stabilize the errors in the dimension along and orthogonal to the road direction, regardless of environmental conditions;

- V2V cooperation is systematically beneficial, leading to sub-meter accuracy in WC error regimes and even 0.2 m accuracy in median error regimes, thus fulfilling the claimed applicative target;

- V2V cooperation is not necessarily useful if vehicle is equipped with a high-class GNSS by default (e.g., RTK and PPP), while operating in favorable conditions (i.e., open or intermediary urban environments);

- V2V cooperation rather strongly depends on the relative geometric configuration and connectivity conditions for isolated vehicles, for instance due to static NLOS situations (thus, leading to loose cooperative links) and/or due to "accordion" mobility pattern (e.g., when a peripheral node with respect to the rest of the VANET is stuck alone at an intersection red traffic light, whereas other vehicles ahead belonging to the same steady-state group have all turned already, thus leading to sparser connectivity and even poorer GDOP conditions). However, this shall be also mitigated in real operating conditions. Especially, in dense urban environments (i.e., where the expected gain should be by the way larger in comparison with nominal GNSS), each vehicle possibly relies on a plurality of vehicles around itself (not even specifically belonging to a unique group moving in the same direction);

- Mobility-based prediction in CLoc, even when relying on simplistic model such as the bicycle model, looks fairly robust enough with respect to possible model mismatch in case of realistic urban mobility (e.g., with more erratic behavior than steady-state mobility regimes for instance on highways).

On the other hand, offline experimental validations in a highway scenario, while relying uniquely on GPS data and notoriously dispersed ITS-G5 V2V RSSI measurements as input observations, show already interesting gains through V2V cooperation beyond nominal GNSS/GPS performance. This is the case not only in terms of "ego" longitudinal localization, but also (and even more significantly) in terms of position awareness regarding neighboring vehicles through mobility-based predictions (i.e., enabling accurate LDM updates). It has been shown that the observed performance gains mostly depends on the rate of ITS-G5 messages broadcast (in average 3 Hz in the conducted tests, to be compared with 10 Hz for the "ego" onboard GPS rate), as well as on a relatively unfavorable GDOP (i.e., the three vehicles involved in the experiments being strictly aligned for the whole experiments). Furthermore, the V2I RSSI information available in the collected data set could not be fully exploitable, due to uncertain RSUs placement. Accordingly, higher V2X ITS-G5 transmission rates (up to 10 Hz), a better geo-referencing of static RSUs serving as anchors, a more realistic varying platoon topology over time, and finally the use of more accurate ranging-enabled technologies such as IR-UWB should be recommended in future field validations.

Chapter 8

Conclusions and Perspectives

8.1 Conclusions

In this thesis, we have presented a Cooperative Localization (CLoc) framework for connected vehicles or vehicular ad hoc networks (VANETs), in which vehicles exploit the positioning capabilities of their neighbors and accordingly, enhance their own location estimates. Due to its maturity (but also to its foreseen massive deployment in the short term), we have primarily chosen ITS-G5/IEEE 802.11p as main supporting vehicular communication technology [1]. The general concept of CLoc, which has been covered rather extensively in the literature in a variety of applications, may look promising in this vehicular context too at very first sight. However, as traditional CLoc techniques are adapted neither to the VANET connectivity conditions nor to the experienced mobility patterns, their direct application is still non trivial and requires attention. Keeping these unprecedented challenges in mind, the main goal of this research work was to reach resilient sub-meter localization accuracy so as to meet the needs of Day-2 C-ITS applications. Our proposed solution has been tested through various sophisticated simulations and partly validated (offline) through experimental data from field tests. These validations have shown that the required level of accuracy could indeed be conditionally achieved (even in particularly pathological cases and in compliance with imposed standardization constraints), thanks to selective V2X cooperation and to multi-sensor fusion. The main contributions of this thesis can be summarized as follows.

---

[1] Note that our research methodology claims enough generality (e.g., aiming at the joint optimization of fusion algorithms and V2X transmission policy). Accordingly, it could get easily adapted to other relevant standards in turn (C-V2X such as LTE-V2X, 5G, etc.).

In Chapter 3, we have established a generic cooperative fusion framework based on a particle filter (PF) and adapted to the ITS-G5 communication technology. First, we have proposed prediction-based data resynchronization mechanisms to properly incorporate cooperative information incoming from asynchronous neighboring vehicles. This allows to mitigate possible biases in the neighboring position awareness, which must be injected into the fusion engine. We have also developed link selection mechanisms based on theoretical performance bounds so as to reduce complexity and minimize traffic (e.g., whenever coupled with a Tx censoring policy), without affecting significantly accuracy/latency. Results show for instance that the amount of required packets can be reduced by 70%, while loosing 14–18% of accuracy through selective fusion (in comparison with exhaustive fusion).

Chapter 4 adopts the same nominal framework as in Chapter 3 but it focuses more on the inherent specificities of V2V wireless connectivity (in terms of both propagation channel and communication channel congestion), evaluating and mitigating their impact-band (IR-UWB) ranging capabilities. On this occasion, we have shown that very poor initial GNSS prior information and/or unwanted error propagation induced by V2V cooperation among vehicles could prevent from drawing maximum benefits from very accurate ranging, or could even lead to filter overconfidence in biased results and thus, to global divergence. Applying fusion scheduling and/or adaptive observation noise dithering to our CLoc algorithms, we have observed that when the biases are correctly mitigated (i.e., avoiding error propagation between vehicles and avoiding filter overconfidence in too poor estimates), the GNSS+IR-UWB fusion scheme then outperforms any other CLoc algorithm and naturally, also the standalone GNSS receiver option. On the one hand, under heterogeneous GNSS conditions/classes at the cooperating vehicles, fusion scheduling has been shown to provide an accuracy of 0.4 cm with 95% probability (compared to 25% for conventional GNSS+IR-UWB fusion schemes). On the other hand, adaptive dithering achieves 0.2 m accuracy with 90% probability (compared to 48% for conventional GNSS+IR-UWB fusion schemes) in homogeneous GNSS capabilities.

In Chapter 6, we have proposed a hybrid V2X multisensor CLoc scheme, which requires additional on-board sensors (e.g., inertial or odometry sensors), camera-based lane detector, etc. and even possibly, fixed elements of infrastructure (e.g., road side units (RSUs)). The fusion with other on-board sensors (typically, WSS and IMU) has been shown always beneficial, contributing mostly to control and stabilize the error in the dimension orthog-

onal to the road direction. In tunnel scenarios, facing even more critical problems of fast divergence, we have proposed guidelines to apply hybrid CLoc with generalized V2X measurements. Considering more particularly V2X IR-UWB measurements (i.e., with respect to both mobile vehicles and RSUs), our CLoc solution can thus achieve median errors of 0.2 m approximately. The latter is also more attractive than CLoc assisted by GNSS repeaters in terms of both accuracy and cost of deployment. Finally, whenever ITS-G5 RSUs are used instead of IR-UWB enabled RSUs, we have shown they must be massively deployed (say, with less than 100 m as inter-side RSU interval) and thus, become costly.

In Chapter 7, results are first presented using a large-scale urban scenario that offers mixed environmental characteristics in view of GNSS performance (i.e., spanning from open environments to urban canyon), considering realistic mobility traces generated by a devoted traffic simulator (SUMO). We have also shown that, even in challenging setups (e.g., occasionally poor connectivity conditions and poor relative geometry), it is still possible to achieve 0.2 m accuracy with probability of 50%. One step ahead, we have performed offline validations using experimental data from a small-scale field test (3 vehicles only), relying uniquely on GPS data and notoriously dispersed IST-G5 V2V RSSI measurements as input observations. On this occasion, despite a quite restrictive scenario, we have already shown interesting gains through V2V cooperation, at least significantly beyond nominal GPS performance. This is the case not only in terms of "ego" longitudinal localization, but also (and even more significantly, by about 10x) in terms of position awareness regarding neighboring vehicles through mobility-based predictions (i.e., enabling accurate LDM updates).

To summarize, this comparative study has shown that a sub-meter accuracy is overall possible through CLoc. We have also given practical guidelines for the design of future CLoc systems, thus contributing to the development of reliable and accurate location-based services for C-ITS.

8.2 Perspectives

Given the achieved results and the current limitations of the proposed fusion-based CLoc solution, new axes of improvement and new research challenges have been identified, as follows.

Further validations with experimental data

- Investigating more complete scenarios in terms of deployment, scenario and mobility patterns (e.g., additional cars involved -say more than 3-, variable fleet constellation as a function of time so as to benefit from diverse GDOP conditions, challenging environments such as round-abouts or urban intersections, addition RSUs providing also support to CLoc, etc.);

- Using standard GNSS capabilities at side cooperating vehicles too (i.e., instead of RTKs so far);

- Considering more accurate accurate V2X range-dependent measurements (typically, IR-UWB TOF or ZigBee PDOA), while still possibly combining with RSSI measurements over ITS-G5 data links in a globally heterogeneous context (i.e., over the same links or over side links, thus providing further observation redundancy and diversity, and providing additional means to solve out ambiguities or remove outliers, etc.);

- Implementing and testing an online version of the proposed CLoc algorithm, running in real-time at the "ego" vehicle.

All the previous points are currently assessed (in progress) in the frame of the HIGHTS project and shall be reported in [137]. On the one hand, the GNSS and V2V RSSI measurements integrated as observations in the fusion filter are assumed to be affected by correlated noises. Accordingly, their direct incorporation into conventional fusion filters (i.e., assuming non-correlated measurement processes) would lead to inconsistent estimates with large fluctuations. The two proposed approaches, at both signal processing and protocol levels, can be combined to almost completely mitigate these deleterious correlation effects. The proposed solutions include the empirical estimation of crosslink correlations (hence, compensating for information loss), the use of differential measurements (i.e., subtracting the correlated part of the process), and decreased fusion rates (i.e., collecting uncorrelated -or at least less correlated- measurements). On the other hand, we have shown that combined cooperative message approximations and transmission power/rate control strategies could reduce both V2V channel congestion and overhead for particle-based cooperative fusion approaches, at almost no localization performance degradation in comparison with the nominal (unoptimized) scheme.

In Chapter 5, we have upgraded further the previous framework so as to perform hybrid V2V CLoc and integrate accurate impulse radio ultra-wide band (IR-UWB) ranging capabilities. On this occasion, we have shown that very poor initial GNSS prior information and/or unwanted error propagation induced by V2V cooperation among vehicles could prevent from drawing maximum benefits from very accurate ranging, or could even lead to filter overconfidence in biased results and thus, to global divergence. Applying fusion scheduling and/or adaptive observation noise dithering to our CLoc algorithms, we have observed that when the biases are correctly mitigated (i.e., avoiding error propagation between vehicles and avoiding filter overconfidence in too poor estimates), the GNSS+IR-UWB fusion scheme then outperforms any other CLoc algorithm and naturally, also the standalone GNSS receiver option. On the one hand, under heterogeneous GNSS conditions/classes at the cooperating vehicles, fusion scheduling has been shown to provide an accuracy of 0.4 cm with 95% probability (compared to 25% for conventional GNSS+IR-UWB fusion schemes). On the other hand, adaptive dithering achieves 0.2 m accuracy with 90% probability (compared to 48% for conventional GNSS+IR-UWB fusion schemes) in homogeneous GNSS capabilities.

In Chapter 6, we have proposed a hybrid V2X multisensor CLoc scheme, which requires additional on-board sensors (e.g., inertial or odometry sensors), camera-based lane detector, etc. and even possibly, fixed elements of infrastructure (e.g., roadside units (RSUs)). The fusion with other on-board sensors (typically, wheel speed sensor (WSS) and inertial measurement unit (IMU)

Large-scale/long-term context-aware CLoc strategies

- Coupling the identified optimal fusion strategies and settings (as a function of speed, road congestion, environment, etc.) to automatic context recognition to guarantee seamless CLoc continuity and robustness along real long-term trajectories;

Better synergies with underlying V2V communication means

- Investigating alternative V2V messages broadcast strategies (in terms of transmission rate, formats, power, etc.) not only in view of the ongoing ETSI standardization process (e.g., with the definition of so-called PoTi messages) but also with foreseen C-V2X standards (e.g., 4G LTE V2X, 5G, etc.) so as to ensure even lower footprint

and better reactivity of the CLoc, while still providing optimal position awareness;

- Finding dynamic and theoretically optimal trade-offs between cooperation potential (e.g., playing on the transmission power, and thus, on both the transmission range and the number of reachable neighbors) and V2X communication channel congestion (leading to higher collision rates and thus, to a lower rate for exploitable incoming messages feeding the fusion engine).

Related works have already been initiated and reported in conference paper [138].

Security and privacy of involved V2X cooperative links Even if it does not fall directly into the scope of the Ph.D. investigations reported herein, one critical aspect for future vehicular CLoc systems regards their robustness and immunity against service denial (e.g., through jamming, injection of malicious messages, etc.) and/or eaves-dropping, a fortiori whenever safety applications are in stake. Thus, adequate faults detection, as well as end-to-end authentication and data encryption strategies should be defined (as overlays complementing existing methods, or even as brand-new methods) in synergy with both V2X communication and localization functionalities.

New location-enabled automotive applications and functionalities The great potential of CLoc in terms of accurate and resilient positioning could be advantageously exploited and extended into various emerging automotive domains (i.e., beyond navigation, autonomous driving and advanced safety), thus opening virgin -or yet hardly covered- research fields, such as

- Investigating cooperative LDMs fusion schemes (thus, not only restricting cooperative exchanges to position awareness, but also to sensor-based perceptional information, such as car-centric occupancy grids based on lidars, etc.);

- Enabling on-board sensor data geo-referencing for future automotive Internet of Things (IoT) and related participative applications through crowd sensing;

- Considering cooperative and hybrid simultaneous localization and mapping (SLAM) beyond radio channel-SLAM approaches, thus contributing to context awareness and automated physical environment reconstruction/monitoring, which is essential to highly autonomous driving (HAD) too;

Chapter 9

Résumé Etendu des Travaux de Thèse

9.1 Introduction

La géolocalisation constitue une fonction critique, pour de pas dire un pré-reqquis en-sentiel, des futurs systèmes coopératifs de transport intelligent (C-ITS). L'ensemble des applications C-ITS de base (BSA) défini en [79] suppose par exemple la disponibilité de systèmes de navigation par satellites (GNSS), qui fournissent une précision de posi-tionnement de l'ordre de 3–10 mètres dans des conditions favorables d'utilisation [116]. Mais ce niveau de précision semble aujourd'hui très loin d'être suffisant pour des applica-tions telles que le véhicule autonome (HAD), le contrôle coordonné de flotte de véhicules (CCC), l'aide à la conduite (ADAS), ou encore, pour la prévention des risques d'accident pour les usagers vulnérables de la route (VRUs) (ex. piétons, cyclistes...). Ces dernières requièrent en effet une précision plutôt sub-métrique (typiquement, inférieure à 0.5 m) et qui plus est, constante quelles que soient les conditions d'utilisation. Une telle qualité de positionnement (c.-à-d., un tel niveau de précision et de résilience) n'est malheureuse-ment pas autorisée par les technologies actuellement disponibles sur le marché de masse (y compris le futur système Galileo) [9, 79], mais seulement par des technologies beau-coup plus coûteuses (ex., GPS RTK, association de LIDARs et de cartes haute-définition de l'environnement...), et/ou dont la mâturité n'a pas encore été réellement éprouvée (ex., GPS Bi-bande intégré bas-coût), et/ou dont la rapidité de convergence ne peut être garantie en toutes circonstances (ex. GPS PPP).

Des standards de communication à courte portée dédiés (DSRC) (c.-à-d., IEEE 802.11p ou ITS-G5), qui peuvent être perçus comme des extensions du standard WiFi spécifiquement adaptées au contexte véhiculaire, se sont rapidement développés ces dernières années, autorisant la transmission de données sans fil entre véhicules (V2V), vis-à-vis de l'infrastructure (V2I), voire vis-à-vis de dispositifs connectés appartenant au monde de l'Internet des objets (V2IoT). Selon ces standards, chaque véhicule diffuse périodiquement, par le biais de messages coopératifs (CAMs, selon le standard européen [139] ou BSMs aux Etats-Unis [98][1], sa propre position estimée (obtenue sur la base du GNSS), destinés à informer ses voisins de la situation et donc, d'un éventuel danger. Ces communications entre véhicules fournissent un cadre propice à l'amélioration de l'information de localisation, grâce à l'application de techniques de localisation coopératives (CLoc) [9, 59, 61, 65, 79, 92]. Chaque véhicule peut alors assister ses voisins, en particulier en cas de couverture GNSS dégradée.

Toutefois, les spécificités du canal de communication véhiculaire sont telles que les observations utiles à la localisation coopérative dans ce contexte (ex. la puissance reçue sur les liens radio V2V ITS-G5 et les relevés GPS...) peuvent être affectées par des erreurs importantes et potentiellement très dispersées (c.-à-d., en termes de biais et/ou d'écart type). Par ailleurs, si les techniques CLoc se sont déjà avérées probantes dans un certain nombre de contextes statiques ou faiblement mobiles (ex. réseaux de capteurs sans fil, MANETs...), elles donnent également lieu à des questions plus spécifiques dans le domaine véhiculaire. A titre d'exemple, on pourra citer l'asynchronisme des transmissions entre les différents véhicules impliqués, ainsi que l'asynchronisme des données encapsulées au sein des messages transmis (imposant de mettre en oeuvre des mécanismes de prédiction, préalablement à la fusion des données reçues), la complexité calculatoire et le trafic important en cas de coopération exhaustive/systématique vis-à-vis d'un grand nombre de voisins (imposant de mettre en oeuvre des mécanismes de sélection de voisins/liens en fonction du contexte), la congestion du canal de communication V2V et la limitation de la taille des paquets à transmettre (imposant une simplification du contenu des messages, ainsi qu'un contrôle des émissions en termes de puissance, de rafraichissement et/ou de trafic mixte de données), la corrélation dans l'espace -et donc, dans le temps- des observations réalisées en situation de mobilité sous la contrainte de taux de rafraichissement spécifiés

---

[1]En raison du rôle équivalent joué par les messages CAMs et BSMs dans ce travail de thèse, on se réfère uniquement aux messages CAMs par simplicité, sans perte de généralité.

par le standard (imposant la mise en oeuvre de traitements spécifiques au niveau signal, comme au niveau du protocole de fusion), la confiance parfois excessive des filtres de fusion et la propagation des erreurs sur le réseau, y compris en présence de mesures de distance V2V très précises (imposant là-aussi des méthodes avancées de traitement du signal et/ou un ordonnancement des étapes de fusion en fonction du voisinnage de chaque véhicule), une dilution géométrique de la précision défavorable dans la dimension perpendiculaire à la route ou encore, les environnements pathologiques dépourvus de couverture GNSS (imposant d'avoir recours à des modalités de mesure complémentaires)...

Ce rapport résume les travaux de recherche menés dans le cadre de cette thèse, ainsi que les diverses contributions apportées à la problématique de la localisation véhiculaire coopérative. Dans la Section 9.2, on pose tout d'abord le problème générique de la localisation coopérative CLoc, ainsi que les principaux challenges associés, avant d'introduire brièvement les principales contributions de l'état de l'art dans la Section 9.3. Ensuite, la Section 9.4 décrit une première proposition de schéma CLoc reposant uniquement sur des liens de communication V2V ITS-G5 et sur le GNSS (V2V CLoc), ainsi que les algorithmes correspondants (fusion, sélection de liens, réduction du niveau de corrélation des bruits d'observation...). En Section 9.5, on introduit la technologie radio impulsionnelle ultra large bande IR-UWB, qui permet de disposer de mesures de distances V2V plus précises. A cette occasion, on traite également de problèmes de confiance excessive du filtre de fusion, ainsi que de propagation de l'erreur entre véhicules. La Section 9.6, quant à elle, aborde la question de la dilution géométrique de la précision dans la dimension orthogonale à la route, en ayant recours à d'autres types de capteurs embarqués. Enfin, la Section 9.7 apporte quelques validations supplémantaires, sur la base d'expérimentations menées sur le terrain, ainsi que de simulations reposant sur des modèles de trafic plus réallistes.

9.2 Problématique et Enjeux

En matière de localisation sans fil, le terme de *coopération* revêt une signification particulière. Les méthodes dites *non-coopératives* visent en général à localiser des noeuds mobiles uniquement vis-à-vis d'une jeu d'ancres fixes dont les positions sont connues a priori. A contrario, les solutions dites *coopératives* (CLoc) exploitent la présence de noeuds voisins
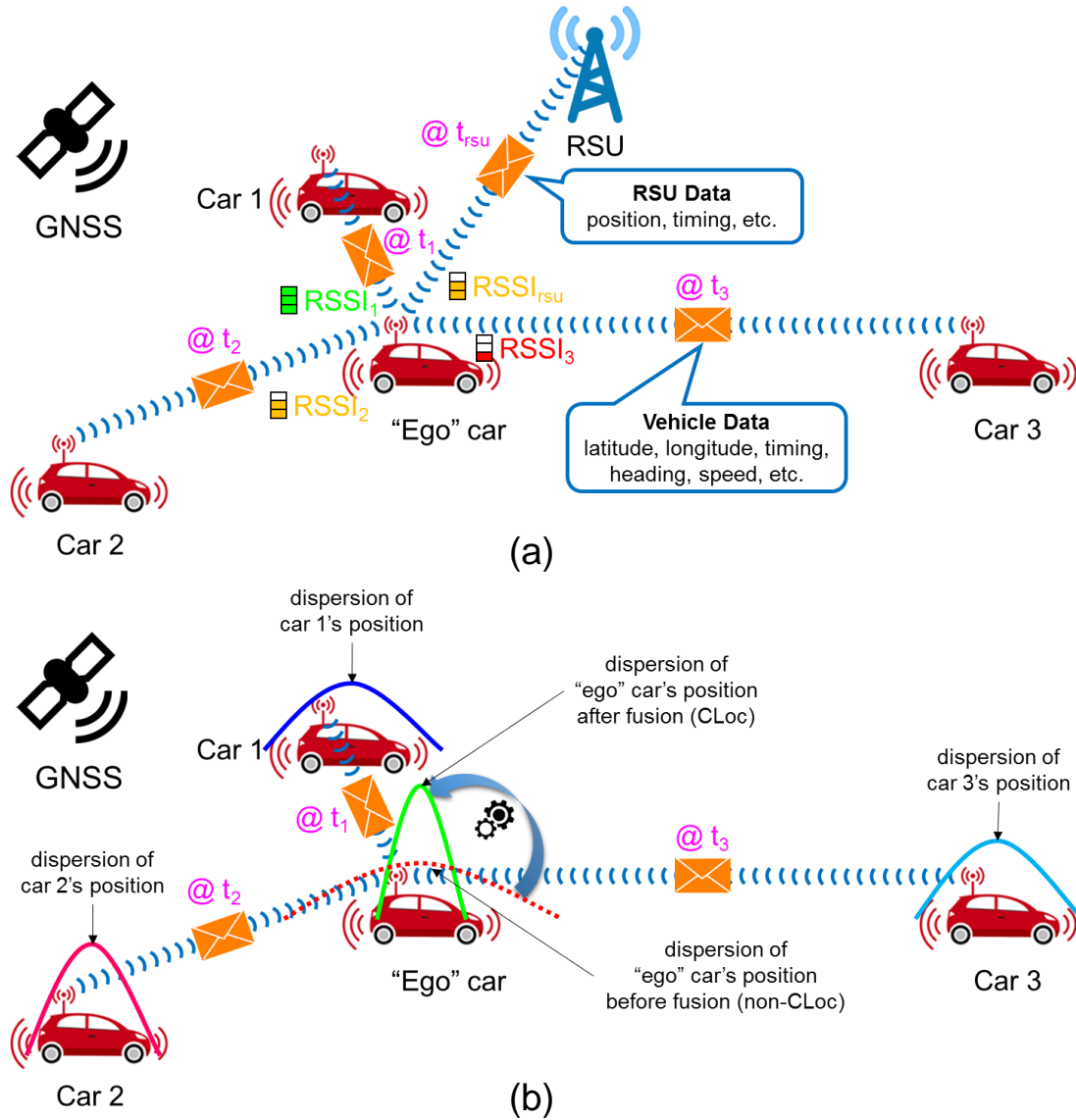
Figure 9.1: (a) Véhicules échangeant périodiquement des messages CAMs permettant d'assurer de nouvelles fonctions de localisation coopératives CLoc. Les instants de transmission $@t_i$ et le niveau de puissance transmise $RSSI_i$ dépendent du véhicule émetteur i (et donc, du lien V2V). (b) Véhicule local "Ego" recevant des messages CAMs asynchrones de la part d'"ancres virtuelles" et fusionnant l'ensemble des informations disponibles. On s'attend à ce que la dispersion associée au résultat de cette fusion coopérative soit plus fabvorable que celle résultant d'approches de localisation non-coopératives (c.-à-d., s'appuyant sur le GNSS seul).

(mobiles ou statiques) jouant le rôle d'"ancres virtuelles"[2] [94], en s'appuyant typiquement sur des méthodes distribuées de type *passage de messages* [84]. Ces schémas CLoc ont jusque-là été principalement appliqués aux réseaux de capteurs sans fil (WSNs) statiques ou encore à des réseaux ad hoc mobiles (MANET) présentant une faible dynamique.

De la même façon, dans le contexte des réseaux véhiculaires ad hoc (VANETs) (Cf.

---

[2]Le terme *virtuelles* est ici entendu dans le sens *mobiles* et *dont les positions peuvent être, elles-mêmes, entâchées d'erreurs.*

Figure 9.1), au lieu de considérer uniquement des ancres statiques telles que des unités de bord de route (RSU) géo-référencées, les approches CLoc renvoient aux stratégies exploitant les véhicules voisins comme des "ancres virtuelles". Plus précisément, les messages coopératifs CAMs périodiquement diffusés entre véhicules peuvent être utilisés au premier chef pour fusionner des données GNSS encapsulées (ou toute autre donnée renvoyant à une estimation de la localisation du véhicule à l'origine du message), mais aussi, de façon optionnelle[3] et opportuniste, afin de mesurer des métriques radio dépendant de la distance entre émetteur et récepteur, comme la puissance reçue (RSSI). Par rapport aux approches non-cooperatives, aucune connaissance a priori des positions des ancres fixes n'est alors requise[4] (ex. carte a priori de RSUs géo-référencées). On espère également bénéficier ainsi d'une forme de redondance et de diversité d'information, notamment grâce aux données transmises par les véhicules voisins.

Toutefois, en raison de la spécificité des motifs de mobilité et des contraintes géométriques de la route d'une part, ou encore de la fréquente fragmentation et de la très haute dynamicité de la topologie du réseau d'autre part (typiquement, donnant lieu à les liens radio dont la durée de vie n'excède pas une seconde pour des véhiculers évoluant en directions opposées), l'application des techniques CLoc au contexte VANETs présente de nombreux challenges.

Tout d'abord, les intervalles temporels entre CAMs consécutifs sont contraints par la charge du canal de communication V2X et par conséquents, les transmissions correspondantes sont non-periodiques. La réception de données vis-à-vis des "ancres virtuelles" environnantes s'effectue donc de manière totalement asynchrone[5] (Cf. Figure 9.1). Si ces phénomènes ne sont pas correctement pris en compte au niveau de la conception du filtre de fusion, des erreurs très significatives peuvent être commises in fine sur les résultats de localisation.

Un autre défi réside dans l'optimalité du filtre de fusion lorsque les observations disponibles en entrée (typiquement, les mesures GNSS et ITS-G5 RSSI) sont supposément affectées par des processus de bruit blancs et indépendants, alors même qu'elles peuvent être en pratique fortement corrélées dans le temps et/ou l'espace. Ces problèmes

---

[3]Par *optionnelle*, on entend aussi que d'autres technologies dédiées pourraient être expoitées spécifiquement pour la mesure de distance (ex. IR-UWB) en parallèle de communications V2X ITS-G5, comme on le verra par la suite.

[4]Au besoin, une telle connaissance doit toutefois être facilement intégrable au problème, en conservant le même cadre général de fusion.

[5]Qui plus est, les données encapsulées portent elles-mêmes sur des instants d'estimation asynchrones.

de corrélation résultent de la continuité locale des phénomènes physiques de propagation, de la spécificité des motifs de mobilité véhiculiare, ainsi que de taux de rafraichissement contraints par les standards. Ils sont perçus comme une limitation importante vis-à-vis des approches CLos de l'état de l'art.

L'optimalité de certaines implémentations du filtre de fusion peut aussi être mise à mal dans des espaces d'estimation à grande dimension, en fonction de la nature des données présentées en entrée. Typiquement, le filtrage Bayésien particulaire (PF) utilisé habituellement pour hybrider des données hétérogènes peut être confronté à des problèmes d'effondrement du nuage de particules (*depletion*) en cas de mesures de distances très précises (typiquement, via la technologie radio impulsionnelle ultra large bande IR-UWB) et de positions a priori très imprécises (typiquement, en cas de mauvaise initialisation GNSS). Ce phénomène peut donner lieu à des biais d'estimation, ainsi qu'à une confiance excessive dans les résultats de fusion, qui peuvent alors se propager sur le réseau du fait de la coopération.

Il existe enfin un compromis à trouver entre la précision de localisation atteignable et la complexité induite par la fusion (dans un contexte potentiellement contraint en termes de capacités de calcul embarquées, de latence, et/ou de consommation...), en fonction des éventuelles limitations ou déficiences du medium de communication V2X (e.g., trafic accru au niveau du réseau, congestion du canal, pertes de paquets...). A titre d'exemple, la coopération exhaustive, qui vise à prendre en compte l'ensemble des voisins disponibles (c.-à-d., indépendamment de la qualité de leurs liens radio respectifs et/ou de la qualité des informations qu'ils transmettent) peut générer une complexité calculatoire importante (au niveau de l'étape de fusion) ainsi qu'une surcharge du canal de communication (en raison de l'absence de mécanismes d'autocensure à l'émission). D'autre part, le filtre coopératif PF peut lui-même induire une forte compexité calculatoire et un surcoût en termes de tafic de données afin de garantir un niveau de performances optimal (ex. en rendant compte du nuage de particules représentant la densité a posteriori de l'état estimé au niveau du message à transmettre).

9.3 Analyse de l'Etat de l'Art et Méthodologie Suivie

En matière de localisation véhiculaire non-coopérative, des unités de bord de route RSUs peuvent être exploitées comme ancres. Chaque véhicle peut alors estimer de manière indépendante sa position à partir de techniques classiques de multi-latération (c.-à-d., utilisant des mesures de distances réalisées vis-à-vis de ces ancres), de simples informations de connectivité/proximité (potentiellement, alliées à des techniques de navigation inertielles de type *dead reckoning* [53]), voire des méthodes de reconnaissance de signatures radio ou *fingerprinting* (ex. assistées par du filtrage particulaire [54]). Cependant ces solutions dépendent fortement de la densité, de la disponibilité et de la géométrie relative de l'infrastructure déployée le long de la route. Par exemple, comme illustré sur la Figure 9.1, un simple lien V2I vis-à-vis d'une RSU serait insuffisant pour positionner sans ambiguïté géométrique le véhicle "Ego" à partir de techniques classiques de multi-latération.

Au contraire, l'approche CLoc permet d'exploiter des liens vis-à-vis des véhicules voisins mobiles et la connaissance de leurs propres positions estimées (*awareness*), ainsi que d'autres mesures V2V opportunistes [9, 61, 84, 104], comme illustré sur la Figure 9.1. Par exemple, les auteurs en [65] proposent un algorithme de poursuite distribué reposant sur un filtre de Kalman standard (KF). Ce dernier fusionne les positions GNSS avec les positions des voisins et des mesures de distances V2V (supposées parfaites) en cas de dégradation avérée des conditions GNSS. Dans un autre exemple, la solution coopérative proposée en [59] s'appuie sur une matrice de dissimilarités composées de mesures RSSI V2V. Ces mesures sont injectées en tant qu'observations dans un filtre KF étendu (EKF), alors que les données GNSS sont utilisées uniquement pour l'initialisation. En [61], la matrice des mesures V2V et les positions GNSS sont conjointement incorporées en tant qu'observation dans le filtre. Les auteurs de [73, 75] proposent d'échanger seulement des données GNSS brutes (ou des facteurs correctifs DGPS) de proche en proche via des liens de communication V2V, renforçant d'autant le positionnement relatif des véhicules. En [76, 77], une méthode coopérative d'accord/reconnaissance de cartes (*map matching*) vise à conformer la topologie relative obtenue par le biais des liens V2V avec la topologie de la route. Enfin, la méthode distribuée proposée en [78] s'affranchit de mesures explicites de distances entre véhicules, en se contentant d'un échange d'informations portant sur des obstacles passifs (poteaux, piétons, etc.) détectés simultanément au niveau de capteurs

LIDAR embarqués sur différents véhicules.

Alors même que le contexte véhiculaire impose des contraintes drastiques, la plupart des solutions coopératives ci-dessus reposent sur des hypothèses de travail simplistes ou trop optimistes, que ce soit en termes de propagation radio (Ex. paramètres constants pour les évanouissements lents affectant les mesures RSSI V2V, absence de corrélations...), de connectivité (Ex. portée de communication constante, nombre important et stable de voisins disponibles...), et/ou de protocole (Ex. transmissions parfaitement sychrones et périodiques, absence de contrôle à l'émission or rate...). De plus, le niveau de précision atteint sur la base de technologies à bas coût (dans le meilleur des cas, équivalent à celui du GNSS nominal en situations favorables d'utilisation) est encore largement insuffisant pour les applications véhiculaires de deuxième génération déjà mentionnées plus haut.

Les standards de communication V2X se trouvent bien évidemment au coeur de ces nouvelles fonctions CLoc. La Figure 9.2 revient donc sur les principales technologies pressenties pour équiper les futurs véhicules connectés, avec notamment le standard ITS-G5/IEEE 802.11p déjà en grande partie spécifié, le standard LTE V2X (aussi appelé C-V2X) en cours d'élaboration, et la future technologie 5G mmWave V2X. Dans le cadre de nos recherches, nous avons choisi de retenir la technologie ITS-G5 dans la mesure où cette dernière présente de loin le plus grand niveau de maturité, tout en remplissant d'ores et déjà la plupart des besoins exprimés en termes de portée (et donc, offrant un potentiel de coopération intéressant), de débit (au moins suffisant pour assurer la diffusion d'informations élémentaires de position) et de latence (ex. a minima, compatible avec les taux de rafraichissement des GNSS actuels). De plus, cette technologie, actuellement disponible sur le marché, a déjà été testée en conditions réelles d'utilisation, ce qui nous paraissait intéressant dans la perspective d'une implémentation et d'une validation à court-terme des méthodes de localisation coopératives. Au contraire, la technologie LTE V2X, qui se trouve encore en cours de spécification, nécessitera probablement plusieurs années avant d'être pleinement opérationnelle, tandis que la technologie 5G V2X (notamment en bandes millimétriques mmWave) demeure encore à un stade très prospectif[6].

La Figure 9.3 résume les technologies de radiolocalisation permettant d'assurer des mesures explicites (à courte portée) de paramètres radio dépendant de la distance en-

---

[6]La méthode d'optimisation conjointe proposée entre communications V2X et fonctions de localisation se veut toutefois agnostique et suffisamment générique pour être facilement adaptée à d'autres technologies sous-jacentes à terme.

Maturity	Technology	Delay	Range
Today	**ITS-G5 / 802.11p**	**~ 10 ms**	**300 – 1000 m**
Prospective	4G LTE V2X	~ 50 ms (V2I) ~ 10 ms (V2V)	300 – 900 m
Prospective	5G mmWave V2X	1 ms	< 200 m

Figure 9.2: Technologies de communication envisageables dans un contexte véhiculaire de fusion coopérative (en rouge, technologies retenues dans le cadre de la thèse).

Maturity	Technology	Frequency	Metric
Today	**ITS-G5 / 802.11p**	**5.9 GHz**	**RSSI**
Today	ZigBee / 802.15.4	2.4 GHz	RSSI / PDOA
Today	**IR-UWB / 802.15.4a**	**4 GHz**	**TOA (TOF) / TDOA**
Prospective	4G LTE V2X	2 GHz	Not defined
Prospective	5G mmWave V2X	30 – 100 GHz	AOA / AOD / TOA
Prospective	WiFi extension	2 GHz	Not defined

Figure 9.3: Analyse des différentes technologies de radiolocalisation envisageables dans un contexte véhiculaire de fusion coopérative (en rouge, technologies retenues dans le cadre de la thèse).

tre émetteur et récepteur, au sens de différentes métriques (ex. temps de vol aller-retour ou RT-ToF, (différence de) temps d'arrivée ou T(D)oA, puissance reçue ou RSSI, mesure différentielle de phase ou PDoA, angle d'arrivée ou AoA...). Alors que certaines technologies sont principalement pensées pour assurer un transfert de données (ex. mesures RSSI opportunistes sur la base de communications ITS-G5), d'autres technologies, véritablement dédiées à la radiolocalisation, s'avèrent beaucoup plus précises (ex. mesures RT-ToF en IR-UWB, avec une précision sur la distance de l'ordre de quelques cm à quelques dizaines de cm).

Sur la Figure 9.4, on représente l'architecture globale de fusion considérée dans le cadre du travail de thèse, ainsi que les différentes technologies mises en jeu à cette occasion (y compris des capteurs embarqués tels que GNSS, centrale inertielle, odomètre et caméra bas-coût pour la détection de voie). La Figure 9.5, quant à elle, illustre les différentes étapes de recherche suivies. Pour chaque étape, on s'intéressera à une difficulté particulière, inhérente au contexte véhiculaire coopératif, ainsi qu'aux moyens de la lever (notamment, avec l'ajout de nouvelles modalités).
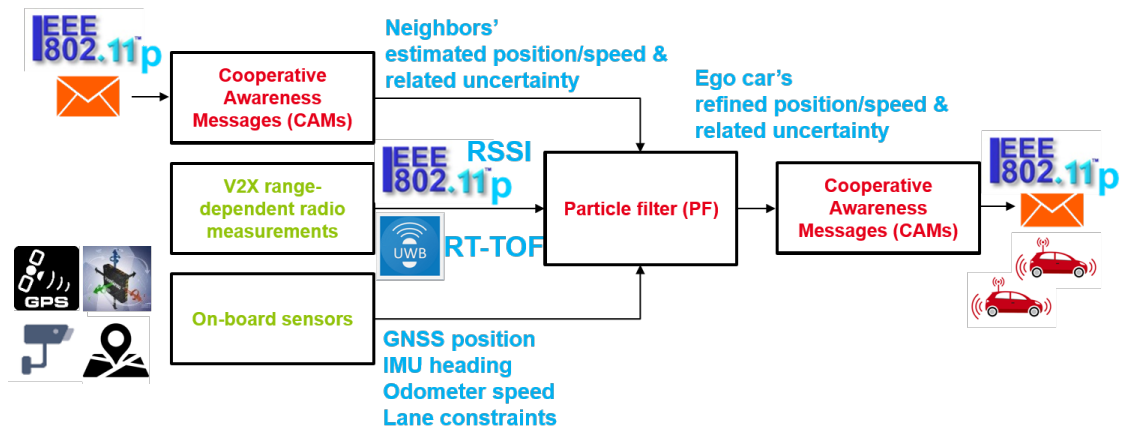
Figure 9.4: Architecture globale de fusion adoptée pour la localisation véhiculaire coopérative et technologies associées.
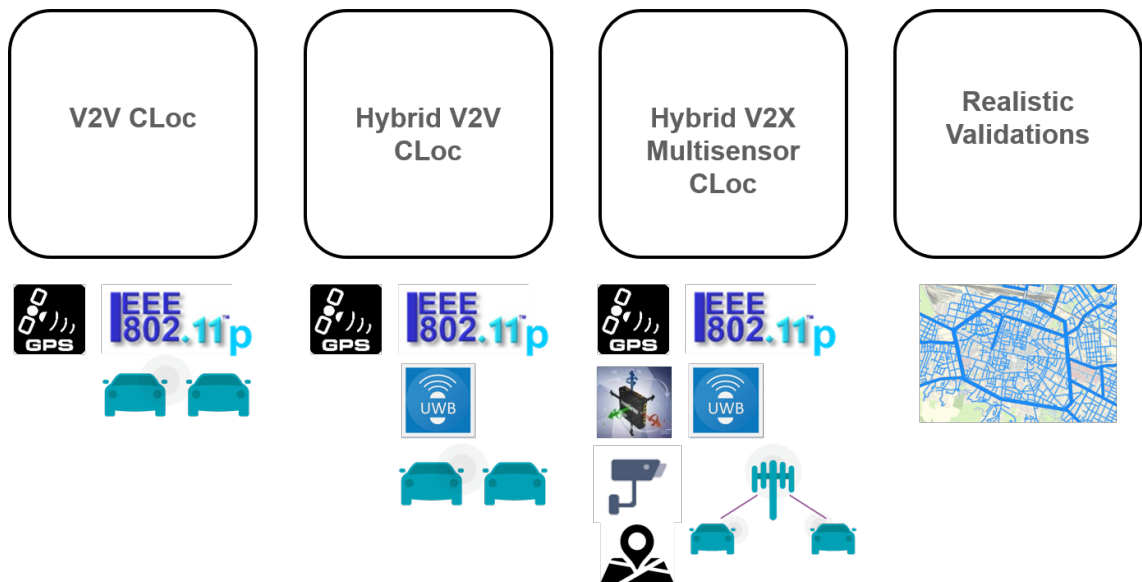
Figure 9.5: Approche graduelle suivie dans le cadre du travail de thèse, avec ajout progessif de nouvelles modalités.

9.4 Localisation coopérative à partir de communications V2V

9.4.1 Architecture Générique de Fusion de Données CLoc

Une première architecture de fusion à base de communications V2V et de GNSS a tout d'abord été proposée, incluant les étapes suivantes (Cf. Algorithme 6): i) mécanismes de prédiction permettant d'incorporer de manière cohérente les données asynchrones reçues de la part des voisins, reposant sur un modèle de mobilité *a priori*, comme décrit en [92] et illustré sur la Figure 9.6; ii) mécanismes de sélection des liens, s'appuyant sur les bornes théoriques de performance de positionnement, permettant de réduire la complexité du pro-
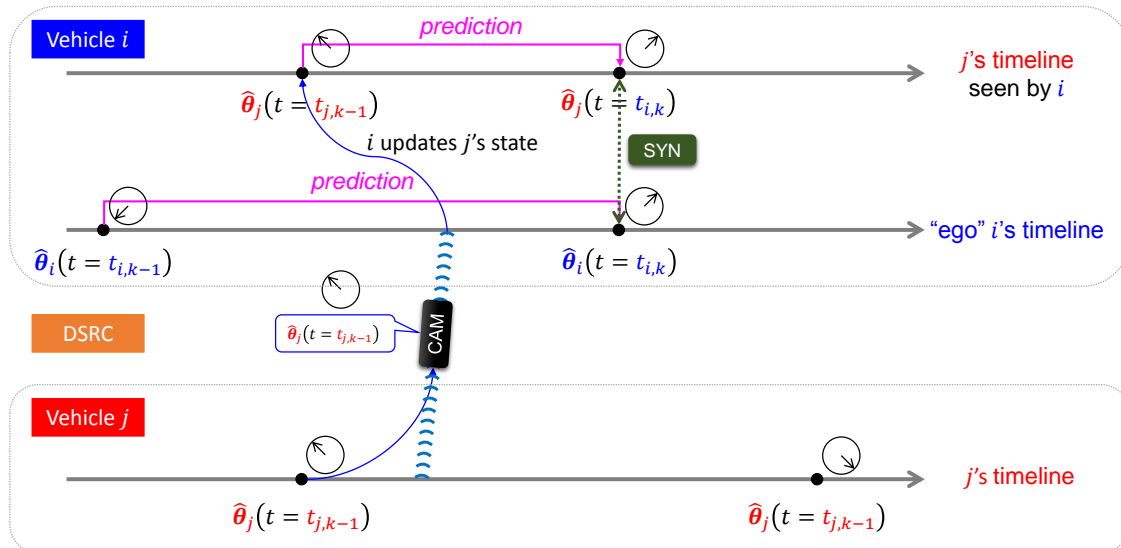
Figure 9.6: Exemple de gestion temporelle des données CLoc au niveau du véhicule "Ego" i (en charge de la fusion) vis-à-vis du véhicule voisin j. En raison de l'asynchronisme des quantités estimées $\hat{\boldsymbol{\theta}}_i(\cdot)$ et $\hat{\boldsymbol{\theta}}_j(\cdot)$, le véhicule i doit réaliser une prédiction afin de "resynchroniser" à l'instant de fusion $t_{i,k}$ l'ensemble des données (y compris les informations reçues de la part du voisin).

cessus de fusion (et potentiellement de réduire le trafic de données[7]) sans dégradation des performances de localisation en termes de précision/latence; iii) mécanismes de décorrélation, capables de forcer le caractère indépendant des observations présentées en entrée du filtre de poursuite; iv) stratégies d'émission révisitées, permettant d'adpater la puissance et/ou le taux de paquets transmis (voire également leur corrélation en réception); et finalement v) une approximation du contenu des messages à diffuser de manière à respecter un format standardisé, en termes de structure et de taille.

Algorithm 6 Architecture générique de fusion de données CLoc ITS-G5/GNSS

1: **Collecte des CAMs:** Réception de CAMs asynchrones de la part des voisins, mesures RSSI, et extraction du contenu des messages reçus (c.-à-d., variables estimées -typiquement, positions et vitesses- et éventuellement, incertitudes associées).

2: **Re-synchronisation des données:** Prédiction des états des véhicules "ego" et voisins au même point temporel de fusion en appliquant un modèle de mobilité et mise à jour de la carte locale dyanmique (LDM) des positions des voisins.

3: **Sélection de liens et dé-correlation des observations en temps/espace:** Parmi les voisins détectés et recensés au sein de la LDM, sélection du meilleur sous-ensemble d'"ancres virtuelles" à intégrer au processus de fusion, dé-corrélation optionnelle des mesures correspondantes retenues.

4: **Correction sur la base des observations:** Correction des états prédits sur la base des observations sélectionnées, produisant l'estimation finale de la position (et de la vistesse) du véhicule "Ego".

5: **Contrôle à l'émission:** Adaptation de la puissance et/ou du taux et/ou de la charge utile du paquet contenant les résultats de la fusion.

6: **Approximation et diffusion du message:** Si le message CAM contient une distribution (c.-à-d., rendant compte de l'incertitude sur les variables estimées), application d'une représentation paramétrique puis encapsulation des paramètres correspondants dans la charge utile du message CAM puis diffusion aux voisins.

---

[7]Pour peu qu'ils soient couplés à des mécanismes de contrôle à l'émission.
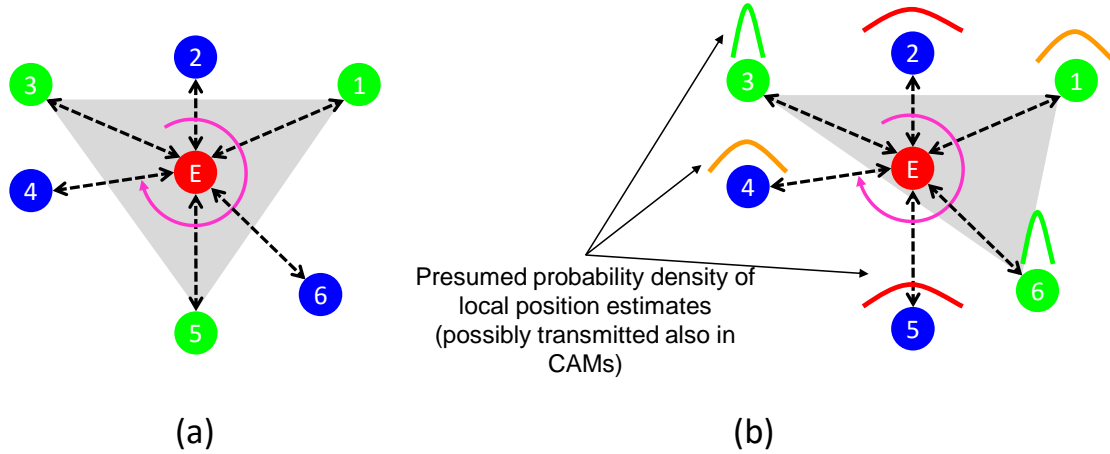
Figure 9.7: Sous-ensemble de voisins sélectionnés (vert) par le véhicule "ego" en charge de la fusion (rouge), selon des critères CRLB (a) non-Bayésien et (b) Bayésien. Dans cet exemple, le véhicule 5, pourtant mal positionné, serait sélectionné avec un critère non-Bayésien (et donc, inclus dans le processus de fusion), alors qu'il serait rejeté après application du critère Bayésien.

9.4.2 Sélection de Liens à Faible Complexité

Dans une seconde contribution [10], nous avons proposé de nouveaux algorithmes de sélection des liens visant à améliorer la coopération pour des conditions GNSS variables, tout en limitant la complexité du processus de fusion. Plus spécifiquement, nous avons proposé un couple de critères basés sur des versions non-Bayésienne et Bayésienne de bornes théoriques de type Cramér-Rao Lower Bound (CRLB), caractérisant les performances de positionnement coopératif pour un sous-ensemble donné de voisins, combinés à une procédure rapide de recherche (sous-optimale), alternative à la recherche exhaustive (i.e., en restreignant de manière heuristique les comparaisons CRLBS à des sous-ensembles pris uniquement parmi les plus proches voisins). La performance CLoc dépend de la qualité des liens radio (ex. via l'atténuation moyenne en puissance et la profondeur des évanouissements lents), de la topologie relative (c.-à-d., des positions relatives entre les "ancres virtuelles" et le véhicule "ego" en charge de la fusion) et/ou de la dilution géométrique de la précision (GDOP), et enfin, des incertitudes portant sur les positions estimées par le véhicule "ego" et ses voisins. Le critère CRLB non-Bayésien proposé initialement en [92] rend compte des deux premiers aspects, sans toutefois capturer l'effet du dernier facteur. Il traite l'ensemble des positions du problème comme des quantités déterministes et exactes[8]. Cette approche peut être suffisante dans un contexte non-

---

[8]On est donc amené à injecter dans le calcul de la CRLB, en lieu et place des positions exactes des véhicules voisins, leurs positions estimées (reçues avec les messages CAMs), donnant lieu à une approxi-

coopératif, lorsqu'on est amené à sélectionner uniquement un jeu d'ancres statiques (ex., RSUs), ou encore, lorsque l'ensemble des voisins présentent un même niveau de connaissance a priori et/ou un même niveau d'erreur sur leurs positions estimées (ex. dans un canyon urbain et/ou du fait de l'utilisation d'une même classe de récepteurs GNSS). Cependant, dans la mesure où l'approche coopérative CLoc repose sur des "ancres virtuelles" qui sont localisées de manière imprécise ou, tout du moins, très variable d'une ancre à l'autre, nous avons donc proposé également un critère CRLB Bayésien intégrant l'incertitude a priori sur les positions des voisins, de manière à ne sélectionner que les liens les plus informatifs en vue de la fusion.

En [**?**], on présente en particulier une étude comparative des deux critères de sélection dans deux scénarios complémentaires. Dans le premier scénario, on considère le même type de dégradation du signal GNSS pour une même flotte d'une quinziaine de véhicules pénétrant dans un canyon urbain (c.-à-d., avec un grand nombre de véchiles expérimentant le même niveau d'erreur GNSS), tandis que dans le second scénario, on considère des disparités "à moindre échelle" en termes de qualité GNSS (c.-à-d., avec des véhicules équipés de classes GNSS différentes). A cette occasion, en comparaison d'approches de coopération exhaustives, on montre que les approches sélectives réduisent de manière drastique la complexité en réduisant le nombre de paquets nécessaires au processus de fusion (par un facteur de plus de 70%), en souffrant d'une détérioration raisonable de l'erreur, d'environ 10% seulement dans des conditions normales GNSS et d'environ 14 à 18% pour la portion la plus défavorable où le GNSS est perdu (Cf. Figure 9.8). Les résultats confirment par ailleurs la supériorité du critère CRLB Bayésien sur le critère non-Bayésien dans un contexte GNSS hétérogène, avec cette fois un niveau tout proche de la fusion exhaustive, ouvrant ainsi la voie à des approches de sélection et/ou de fusion de l'information dépendantes du contexte détecté (Cf. Figure 9.9).

En résumé, on a pu démontrer l'intérêt des mécanismes de fusion sélective, ainsi que de l'incertitude a priori sur les positions estimées par les véhicules voisins.

9.4.3 Limitation de la Corrélation des Bruits d'Observation

Une seconde contribution concerne les phénomènes de corrélation affectant des observations injectées dans le problème de fusion. En pratique, la corrélation des processus de

---

mation de la CRLB exacte.
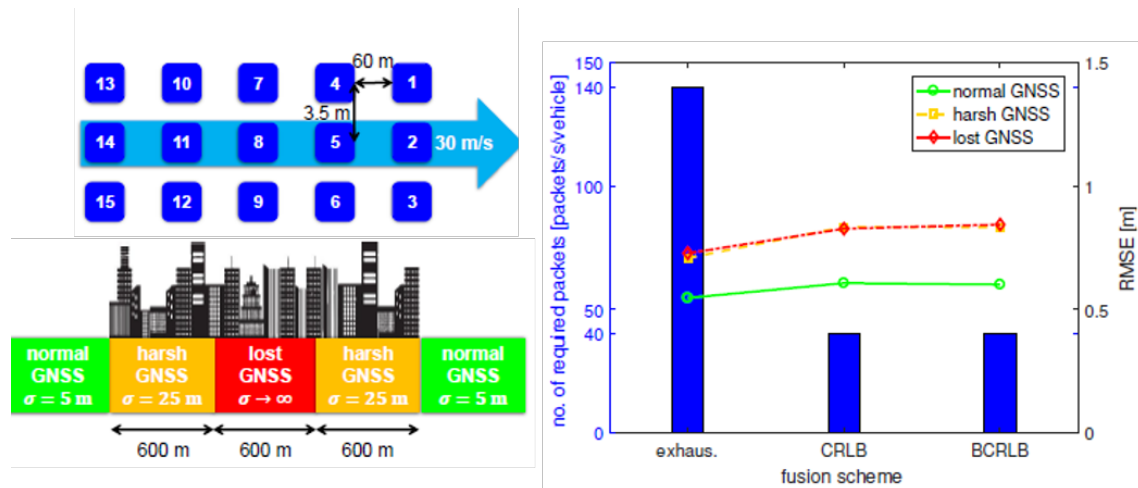
Figure 9.8: Flotte de 15 véhicules (gauche-haut); pénétrant dans un canyon urbain offrant des conditions GNSS homogènes pour l'ensemble de la flotte (gauche-bas); Erreur RMSE et nombre de messages CAMs reçus effectivement injectés dans la processus de fusion ITS-G5 V2V RSSI/GNSS pour des critères de sélection basés sur des bornes théoriques non-Bayésiennes (CRLB) et Bayésiennes (BCRLB)(droite).
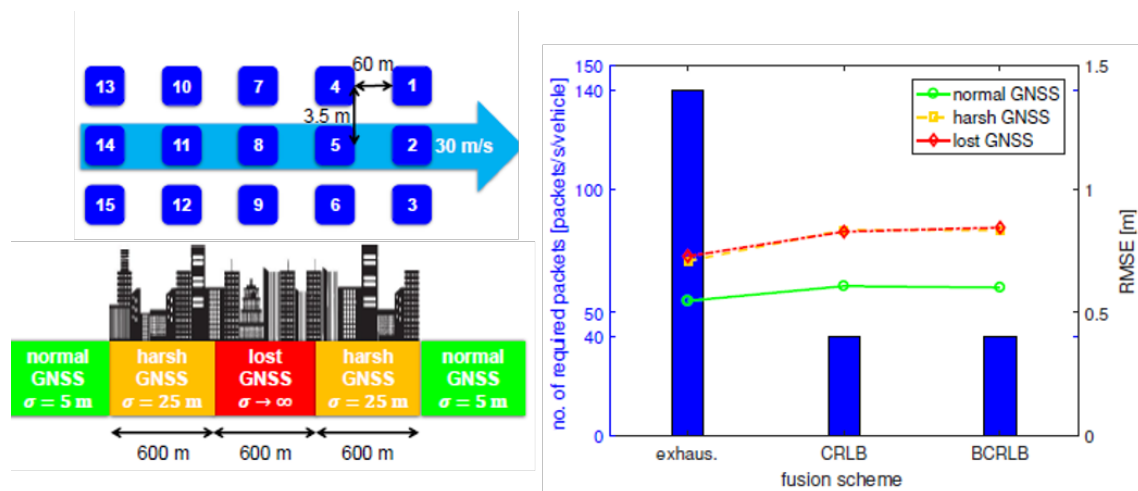
Figure 9.9: Flotte de 15 véhicules présentant des conditions GNSS hétérogènes (gauche); CDF empirique de l'erreur de positionnement issu de la fusion ITS-G5 V2V RSSI/GNSS, pour des stratégies de sélection basées sur des bornes théoriques non-Bayésiennes (CRLB) et Bayésiennes (BCRLB)(droite).

bruit d'observation (et donc, leur corrélation dans le temps en situation de mobilité) résulte de la conjonction de différents facteurs en lien avec les containtes pesant sur la mobilité véhiculaire.

Tout d'abord, les conditions GNSS (bonnes ou mauvaises) peuvent rester inchangées pendant plusieurs échantillons consécutifs et ce, au niveau de plusieurs véhicules voisins. De la même façon, les variations lentes (résultant d'obstructions ou non) affectant les mesures de puissance reçu RSSI peuvent demeurer relativement identiques et stables entre

deux CAMs consécutives (ex. 100 ms) sur un lien V2V ITS-G5 vis-à-vis d'un même voisin (autocorrélation dans le temps), de même que deux liens V2V quasi-simultanés et issus de deux véhicules émetteurs proches l'un de l'autre subiront des évanouissements corrélés (inter-corrélation dans l'espace).

L'incorporation de telles mesures au niveau des filtres de fusion constitue alors un enjeu majeur si ces derniers supposent les processus parfaitement indépendants, venant ainsi violer une hypothèses nécessaires à leur optimalité [86,87,89,104]. On illustre intuitivement
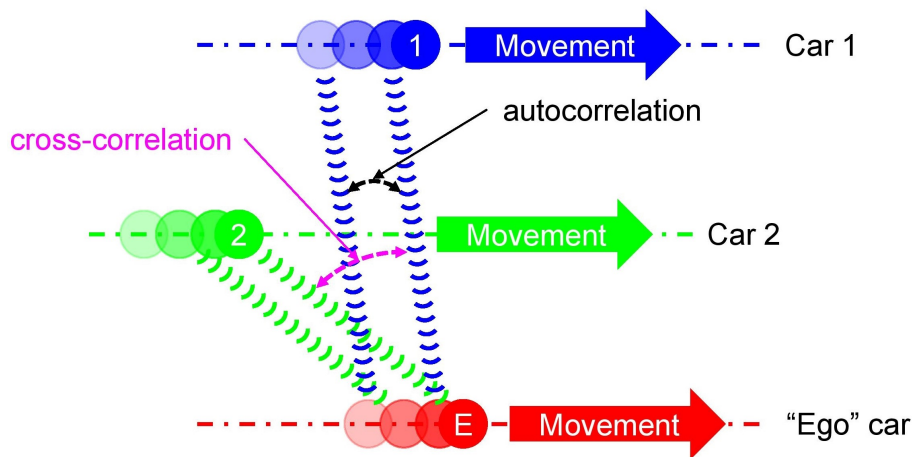
Figure 9.10: Auto-corrélation/Inter-corrélation des évanouissements lents affectant les mesures de puissances reçues RSSI sur la base de liens V2V ITS-G5 dans un contexte VANET (avec mobilité de l'émetteur et du récepteur).

ces phénomènes de corrélation sur la Figure 9.10. Ces phénomènes de corrélation affectent aussi indirectement l'usage des données GNSS elles-mêmes au niveau du véhicule "ego" en charge de la fusion. Des messages CAMs successifs issus de véhicules proches intègreront ainsi potentiellement une information GNSS corrélée si l'intervalle de temps entre les instants d'émission est plus petit que le temps nécessaire à ces véhicules pour parcourir une distance équivalente à la distance de décorrélation GNSS. Dès lors, en [11], nous avons proposé plusieurs méthodes de décorrélation au niveaux signal et protocole, pouvant être combinées ou non selon le contexte, afin de restaurer toute la capacité du filtre de fusion.

La première technique s'appliquant aux mesures V2V RSSI repose sur l'intuition selon laquelle la connaissance du niveau d'inter-corrélation entre les différentes composantes du vecteur d'observation fournit une information constructive au filtre [103]. Plus spécifiquement, cette information est utile pour filtrer le bruit d'observations au niveau de l'étape de correction (Cf. Algorithme 6), dans la mesure où la distribution des évanouissements lents est mieux prise en compte. Dans notre cas, cette inter-corrélation peut être estimée de

manière empirique sur la base des dernières positions estimées, ainsi que sur le modèle point-à-point proposé par Wang *et al.* [111]. La seconde technique appliquée au niveau

(a)   (b)
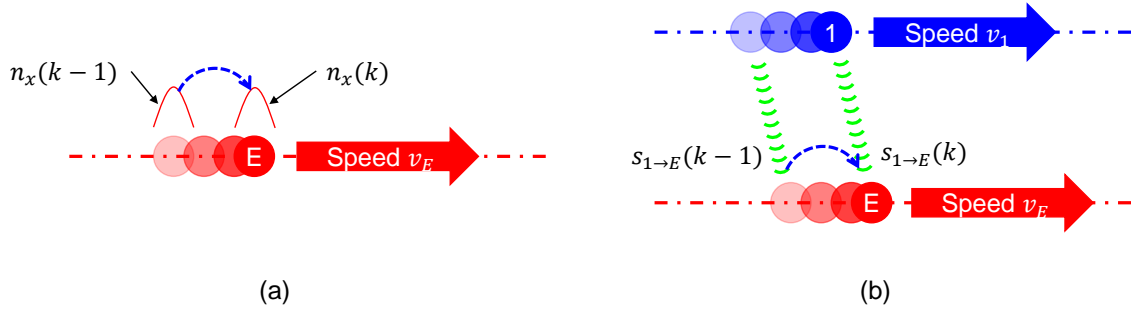
Figure 9.11: Illustration de la technique différentielle DM appliquée (a) à la coordonnée GNSS x et (b) aux mesures V2V RSSI. Les termes de bruit GNSS $n_x(k)$ et $n_x(k-1)$ sont corrélés, avec des propriétés de corrélation connues. Dès lors, la partie corrélée comprise dans $n_x(k)$ peut être prédite à partir de $n_x(k-1)$ et ensuite soustraite de $n_x(k)$. Le bruit résiduel résultant de l'opération est idéalement i.i.d et de moindre variance. L'application de la même méthode aux évanouissements lents $s_{1 \rightarrow E}(k)$ et $s_{1 \rightarrow E}(k-1)$ affectant les mesures V2V RSSI est triviale.

signal, également appelée méthode des Mesures Différentielles (DM), peut être appliquée aux erreurs GNSS comme au mesures V2V RSSI. Comme son nom l'indique, l'idée principale consiste à blanchir les termes de bruits en soustrayant leur partie corrélée commune, en gardant inchangée leurs composantes indépendantes. Ce problème peut être résolu à partir d'un modèle de prédiction du bruit, basé sur la connaissance a priori de ses propriétés de corrélation spatiale (fonction de corrélation en fonction des positions relatives, pour un type d'envionnement donné). En particulier, en considérant une certaine classe de fonction de covariance (typiquement, de forme exponenielle décroissante avec la distance), les erreurs GNSS et les évanouissements lents affectant les mesures RSSI peuvent faire l'objet d'une prédiction au sens de modèles Gauss-Markov (au premier ordre).

La technique DM vise donc à soustraire une version prédite de l'observation courante au lieu de l'injecter directement dans le filtre de fusion, comme illlustré sur la Figure 9.11.

Contrairement aux deux approches précédentes, la dernière proposition consiste simplement à réduire délibérément le taux de fusion, sans manipuler les observations. Pour chaque type d'observation (GNSS et RSSI), comme les mesures sont spatialement corrélées sur une distance de décorrélation d_{cor} (supposée connue pour un type d'environnement donné), un véhicule se déplaçant en ligne droite sur une distance D peut collecter dans le temps jusqu'à $1 + \lfloor D/(\gamma d_{\text{cor}}) \rfloor$ mesures non-corrélées où $\gamma \geq 1$ est une indication de l'indépendance des échantillons (e.g., $\gamma_1 = 1$ et $\gamma_2 = 2$ correspondant à 50% et 75% de

réduction du niveau de corrélation, respectivement) , comme illustré sur la Figure 9.12. Cette simple technique peut s'avérer toutefois peu appropriée au GNSS, dans la mesure où la distance de décorrélation peut atteindre plusieurs centaines de mètres [79]. Elle est cependant beaucoup plus efficace pour les mesures RSSIs, du fait d'une distance de décorrélation beacoup plus réduite, typiquement en environnement urbain (ex. 10–20 m [101, 102, 111]).
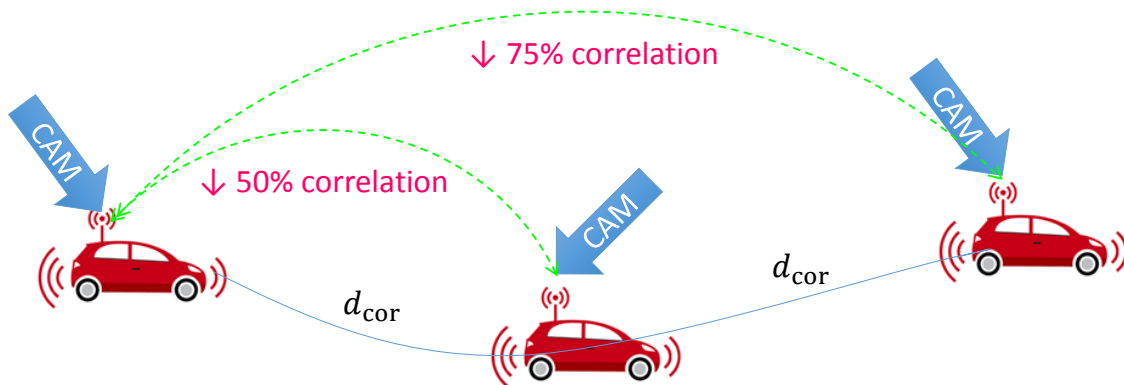
Figure 9.12: Illustration de la réduction délibérée du taux de fusion permettant de collecter des échantillons V2V RSSI non-corrélées.

Ces diférentes approches ont été évaluées par le biais de simulations Monte Carlo dans trois scénarios et environnements représentatifs (c.-à-d., autoroute, canyon urbain et tunnel). Les résultats obtenus montrent que notre proposition est susceptible de fournir des gains en précision de l'ordre de 60% dans des environnements très corrélés, tout en enregistrant une dégrédation limitée d'environ 15% par rapport à une situation idéalisée où les processus d'observation seraient non-corrélés (Cf. Figure 9.13).

A partir de ces résultats, on note que les caractéristiques de l'environnement, c.-à-d. la distance de décorrélation, le type de mobilité, la disponibilité GNSS..., influencent grandement la façon dont le moteur de fusion doit traiter les observations présentées en entrée afin de limiter les problèmes liés à la corrélation. En particulier, une certaine technique de décorrélation peut s'avérer très efficace dans un environnement donné, mais peu probante, voire contre-productive (Cf. autres résultats sur les taux de rafraichissement par ailleurs) dans d'autres circonstances. Dès lors, on a suggéré une stratégie dépendante du contexte d'utilisation, qui assiste le moteur de fusion CLoc afin d'obtenir la meilleure précision possible au regard de la corrélation. Le Tableau 9.1 résume les techniques recommandées (ou la combinaison de techniques) selon chaque modalité et chaque type d'environnement. Ainsi, lorsqu'un véhicule pénètre dans un environnement spécifique (ex. sur la base d'une

Figure 9.13: CDF empirique d'erreur de positionnement issu de la fusion ITS-G5 V2V RSSI/GNSS pour différentes stratégies de dé-corrélation des bruits d'observation pour un scénario de type autoroute.

Table 9.1: Techniques recommandées en fonction du contexte pour une dé-corrélation optimale des bruits d'observation (Fusion ITS-G5 V2V RSSI/GNSS).

Modality	Highway	Urban Canyon	Tunnel
V2V RSSI	adaptive sampling	optional	differential measurement
GNSS position	differential measurement	differential measurement	N/A

carte *a priori*), le système peut déterminer la technique la plus appropriée, ainsi que les paramèters associés, pour réaliser la décorrélation des processus d'observation avant fusion.

9.4.4   Approximation des Messages et Contrôle des Emissions

Dans notre contexte de fusion cooopérative, dans la mesure où certaines des observations injectées (typiquement, les mesures V2V RSSIs ici) sont non-linéaires en fonction des variables d'état estimées (ex., position, vitesse, cap...), le choix d'un filtre particulaire semble assez naturel. Ce dernier permet également d'assurer l'évolutivité du système à moindre effort, dans le cas où d'autres capteurs/modalités sont intégrées au problème (Cf. sections suivantes). Cependant, pour atteindre des performances optimales, il est admis que ce type de filtre génère une complexité calculatoire importante pour des espaces
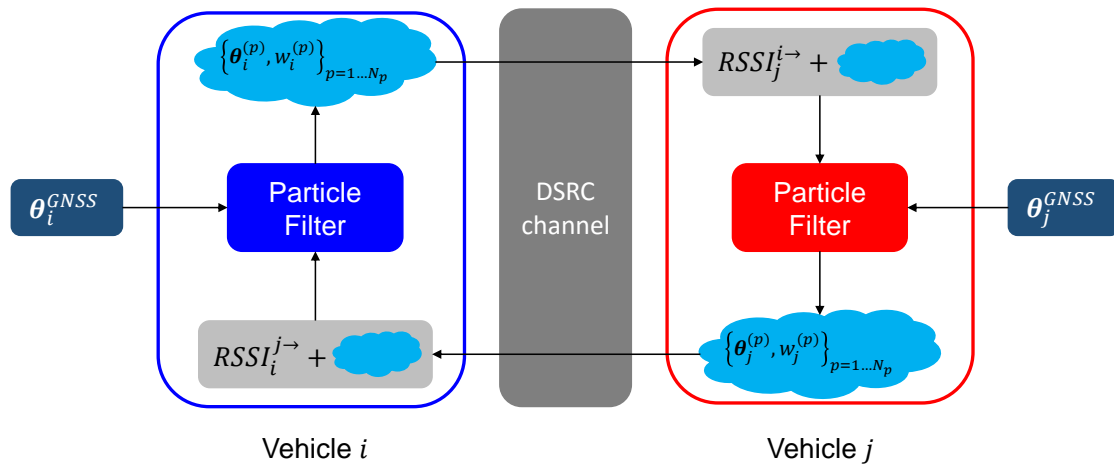
Figure 9.14: Flot de données dans un contexte de fusion coopérative à base de filtre particulaire entre deux véhicules où, pour le véhicule i, θ_i^{GNSS}, $RSSI_i^{j\rightarrow}$ et $\{\theta_i^{(p)}, w_i^{(p)}\}_{p=1\ldots N_p}$ représentent respectivement l'estimation GNSS, la mesure RSSI réalisée à partir du message CAM reçu de la part de j, et le nuage de N_p particules ets représenté par $\theta_i^{(p)}$ et $w_i^{(p)}$, respectivement les états et poids associés. Le canal de communication ITS-G5 (DSRC) est sujet à des limitations imposées par le standard (ex. taille maximmale des messages: $300-800$ octets, capacité maximale: 6Mbps, contrôle décentralisé de congestion imposant une réduction à 2Hz du taux d'émission des messages en cas de de surcharge avérée du réseau...).

d'estimation à grandes dimensions (typiquement en lien avec la simulation d'un grand nombre de particules), ainsi qu'un surcoût en termes de communications, dans sa forme coopérative (ex. pour rendre compte du nuage de particules par passage de message). Par exemple, des milliers de particules (ex. de l'ordre de 1000) sont communément considérées dans les systèmes de navigation embarqués [80]. Dès lors, un positionnement 2-D à base de particules demanderait 16000 octets[9], qui surchagerait les messages CAMs (100–800 octets) [140] et excéderait de loin les limites en termes de *Maximum Transfer Unit* (MTU) des canaux ITS-G5 (2312 octets) [139]. La Figure 9.14 fournit une illustration simplifiée des échanges d'information CLoc entre dexu véhicules i et j. Comme déjà mentionné, il est impossible de diffuser explicitement le nuage de particules complet via des transmissions ITS-G5 standardisées. Dès lors, sa représentation doit être simplifiée et réduite à quelques scalaires qui peuvent être en pratique supportés par les messages CAMs. Les véhicules voisins recevant ces messages doivent alors être en mesure de reconstruire fidèlement le nuage de particules initial, à partir de ces seuls scalaires. Une solution consiste à réaliser une approximation paramétrique continue du nuage de particules. En partciulier, après iden-

---

[9]Une particule 1-D est en général représentée sur un format du type *binary64* occupant 8 octets (64 bits).
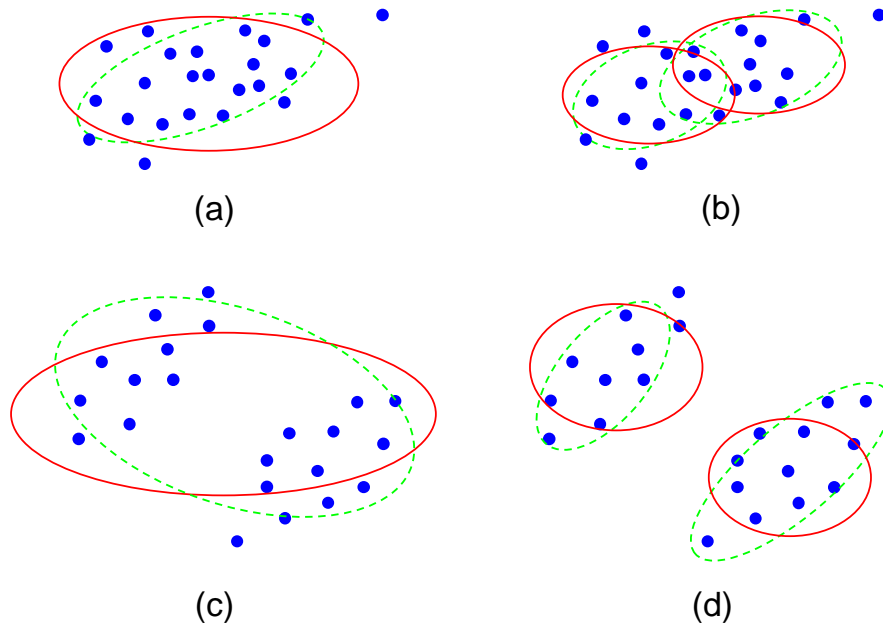
Figure 9.15: Simplified 2-D position representations including nonparametric (i.e., particles as blue dots) and parametric (i.e., diagonal Gaussian modes as red ellipses and full Gaussian modes as green dash ellipses) approaches. Each explicit particle representation costs two scalars, each diagonal Gaussian mode occupies 4 scalars, and each full Gaussian mode requires 5 scalars. One more scalar is needed for the weight in case of bimodal distribution.

tificaton des modes dominants, chaque nuage est approximé par une distribution connue, communément sous forme de mixture de Gaussiennes. La Figure 9.15 illustre comment une position 2-D représentée par un nuage de particules peut être approximée par le biais de densités uni- ou bi-modales, pour deux configurations différentes présentant -ou non- un risque d'ambiguïté (Cf. Figure 9.15(c)-(d) et 9.15(a)-(b), respectivement).

En [12], différents modèles de mixtures Guassiennes (GMMs) ont ainsi été comparés dans notre contexte de localisation véhiculaire CLoc à base de filtres PF. Il a alors été relevé que l'utilisation d'approximations multi-modales ne s'avérait pas toujours bénéfique pour des scénarios concrets de déploiement (y compris lorsque la topologie de réseau présente des symétries en miroir) mais donnait lieu, a contrario, à une complexité calculatoire nettement accrue, en lien avec l'identification et la paramétrisation préalable des modes composant les mixtures.

Par ailleurs, en matière de contrôle décentralisé de la congestion du canal (DCC), les règles stipulées par l'ETSI recommandent de réduire le taux d'amission des messages CAMs de 10 Hz à 2 Hz (correspondant à une charge du réseau de 60%), menant potentiellement à une dégradation des performances de positionnement. Pour compenser
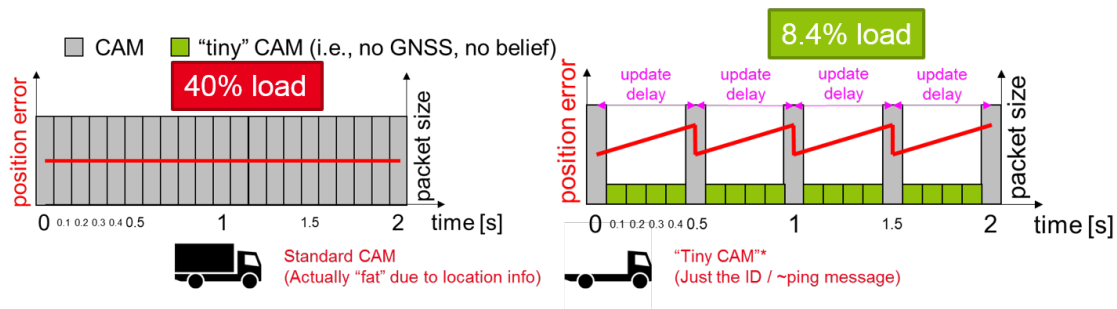
Figure 9.16: Proposition de trafic mixte de données à l'émission, incluant des messages CAMs standards et des messages limités (Tiny), afin de réduire la charge induite sur le réseau par les nouvelles fonctions de localisation coopératives.

cette perte d'information, en combinaison avec les approximations de messages déjà mentionnées, nous avons aussi proposé de revoir les stratégies de contrôle à l'émission afin de supporter des taux et des charges utiles de paquets variables (trafic mixte), en mélangeant des messages "légers" ("Tiny" CAMs), sans *payload* aux taux critique de 10 Hz et des CAMs conventionelles au taux de 2 Hz (limite du DCC de l'ETSI). Les messages "légers" permettent alors de continuer à réaliser des observations V2V RSSI au taux de 10-Hz RSSI, et donc de corriger au même taux les prédictions réalisées sur la base des données comprises dans les CAMs conventionnelles. De plus, grâce à des mécanismes de contrôle en puissance, ces messages "légers" CAMs peuvent être diffusés sur des distances plus courtes (portée réduite par rapport aux messages CAMs conventionnels). En lien avec les travaux sur la sélection de lien présentés en section 9.4.2, la coopération peut en effet se restreindre au premier cerlce des plus proches voisins sans dégradation significative de la performance [10, 92]. En [12], les performances de cette politique de contrôle à l'émission ont aussi été évaluées, montrant qu'il était possible d'approcher le niveau de performance idéal d'une fusion de données au taux maximal de 10Hz (qui donnerait pour autant lieu une charge inacceptable sur le réseau, y compris en appliquant des techniques d'approximation de message citées plus haut), tout en générant une charge effective du canal minimale, proche de celle engendrée par le plus bas taux d'émission de 2Hz imposé par le DCC de l'ETSI (Cf. Figure 9.17).

D'autres études complémentaires [138] se sont intéressées à la proposition de nouveaux types de messages, plus courts et plus fréquents (typiquement jusqu'à 100Hz) que les messages CAMs conventionnels, et donc, encore mieux adaptés à la diffusion coopérative de l'informaton de localisation (notamment vis-à-vis des problèmes de caducité).
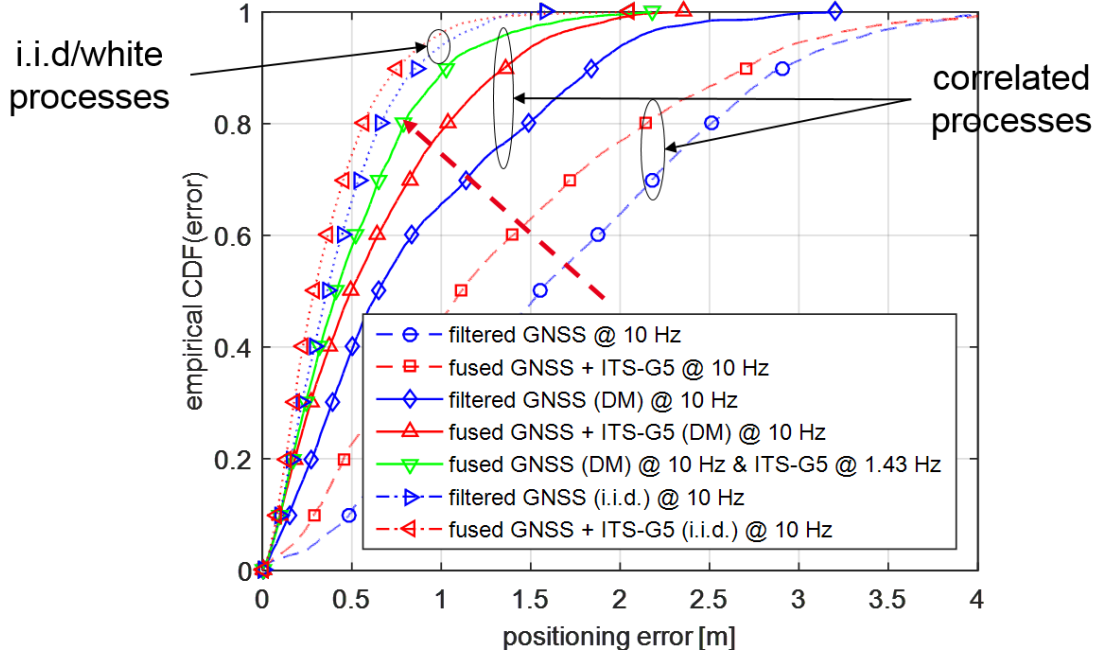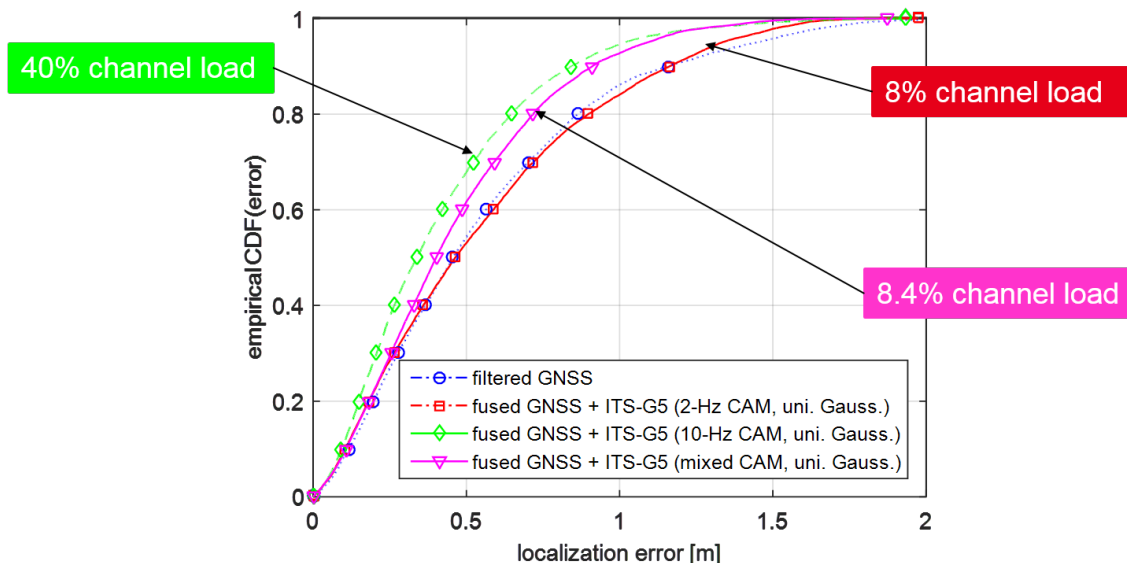
Figure 9.17: CDF de l'erreur de positionnement issu de la fusion ITS-G5 V2V RSSI/GNSS pour différentes stratégies de contrôle à l'émission (et pour une approximation Gaussienne unimodale du nuage de particules caractérisant la densité a posteriori de l'état estimé).

9.5 Localisation coopérative hybride à partir de communications V2V et de mesures de distances précises

Un espace destimation à grande dimension et/ou, de manière plus paradoxale, une fonction de vraisemblance très "étroite" (dans le cas d'observations très précises), peuvent s'avérer pénalisants pour le filtre PF en charge de réaliser la fusion de données. L'optimalité de ce dernier dépend en effet du nombre total de particules utilisées, du défaut "d'accord" entre le support de la densité a priori de l'état estimé et le support de la fonction de vraisemblance exploitée pour pondérer les particules. Ces problèmes peuvent donner lieu à un phénomène d'effondrement du nuage de particules (*depletion*), et in fine, dans un excès de confiance du filtre dans ses résultats. Des quanités estimées biaisées (typiquement positions) peuvent alors se propagation sur le réseau, du fait de la coopération et de l'échange de messages. Dans le contexte VA-CLoc, cette situation se présente par exemple lorsque la position est initialisée via un GNSS de mauvaise qualité (donc avec une densité a priori très évasée), lorsqu'on doit réaliser une estimation (i.e., correction) de l'état des voisins (donc présentant un espace d'estimation à grande dimension), et/ou lorsque l'on incorpore des mesures de distances V2V très précises, typiquement sur la base de la technologie IR-UWB [13].

Au niveau protocole, une première technique (en deux étapes) a alors été proposée,
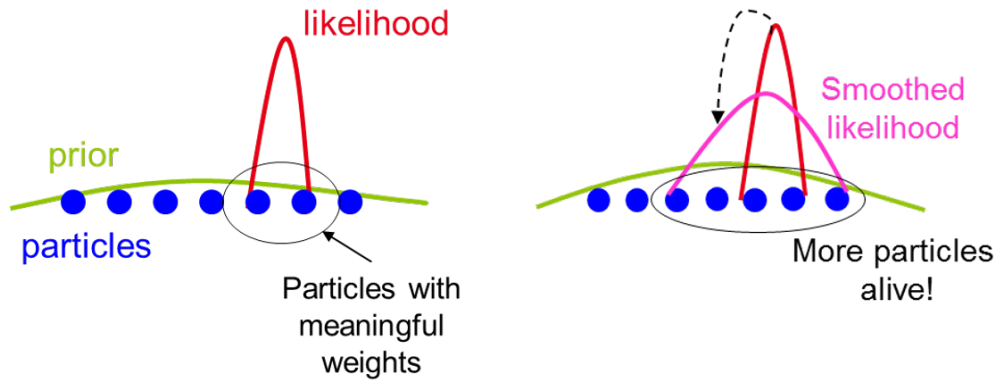
Figure 9.18: Illustration de l'effet de l'augmentation artificielle du niveau de bruit d'observation associé aux mesures de distance (modèle de perception), donnant lieu à un support plus large de la fonction de vraisemblance servant à conférer leurs poids à un plus grand nombre de particules du filtre.

basée sur l'ordonnancement des mises à jour de fusion en fonction du voisinage. Cette dernière vise à éviter une contamination du reste du réseau, causée par les noeuds les plus mal positionnés. Mais cette technique suppose aussi la présence de noeuds bien positionnés. Une autre alternative introduite en [14] (Cf. Figure 9.18) permet d'ajuster de manière itérative le niveau de bruit d'observation admis au niveau du filtre, en fonction des performances théoriques attendues de localisation (au passage, en s'appuyant sur les mêmes calculs de bornes Bayésiennes Cramer Rao Lower Bounds que pour la phase de sélection de liens/voisins), améliorant sensiblement la consistance du filtre (et donc en réduisant les priblèmes de confiance excessive et les risques de propagation d'erreurs), en faisant passer la prbabilité de trouver une erreur de 20 cm typiquement de 50% à 90% (Cf. Figure 9.19).

9.6 Localisation coopérative hybride multi-capteurs

Dans la mesure où la mobilité véhiculaire est fortement contrainte par la topologie des voies/routes et les règles de conduite en vigueur (typiquement, les distances de sécurité à respecter), la topologie relative du réseau peut donner lieu à un mauvais conditionnement géométrique du problème de positionnement coopératif. Plus précisément, la topologie est "distordu" dans la direction colinéraire à la route (ex. 20–150 m de distance de sécurité contre 2.25–3.5 m de largeur de voie). En conséquence, la dilution géométrique de la précision GDOP est souvent défavorable dans la dimension orthogonale à la route. Dès lors, l'erreur de poisitionnement dans cette même dimension (emphcross-track) demeure
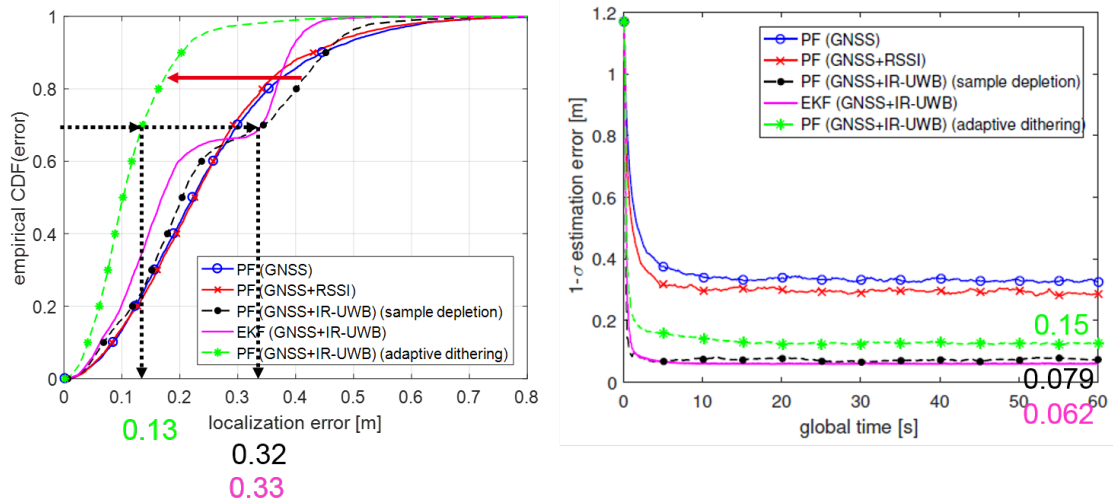
Figure 9.19:   CDF empirique de l'erreur de positionnement issu de la fusion ITS-G5/GNSS/IR-UWB et erreurs caractéristiques effectives à 1-σ (c.-à-d. à CDF=68%), pour différentes stratégies de filtrage (gauche) et évolution de l'erreur à 1-σ perçue au niveau des filtres, en fonction du temps (droite).

importante et domine l'erreur globale.

De manière à atténuer ces effets, on exploite en [15] une centrale inertielle comprenant un gyroscope (IMU) et un compte tour (WSS) afin de rendre compte du cap et de la vitesse du véhicule et/ou une méthode de détection de voie basée sur une caméra bas-coût (LC), permettant de tronquer la densité a posteriori de l'état estimé utilisée dans le filtre PF de fusion (c.-à-d., tronquant le nuage de particules avec des contraintes géométriques). La combinaison de ces techniques a alors permis d'améliorer la probablité de trouver une erreur inférieure à 0.5 m de 60% à 90% dans la dimension orthogonale à la route (Cf. Figure 9.20).

D'autres contributions en [16] (non détaillées dans ce résumé) portaient sur le traitement des environnements spécifiquement dépourvus de couverture GNSS (typiquement, dans les tunnels) en ayant recours à des mesures V2I complémentaires (IR-UWB RT-ToF ou ITS-G5 RSSI) vis-à-vis d'éléments fixes d'infrastructure (RSUs), combinées aux capteurs IMU et WSS. A cette occasion, on a chergché à identifier le meilleur compromis opérationnel entre performances de localisation et sur-coût de déploiement, notamment vis-à-vis d'une solution conventionnelle à base de répéteurs GSNSS.
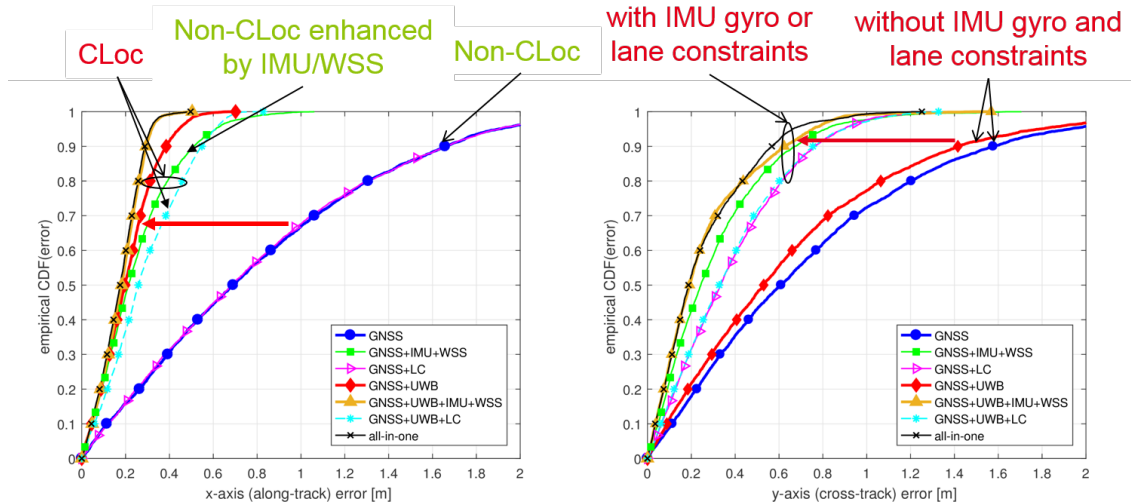
Figure 9.20: CDF empirique de l'erreur de positionnement issue de la fusion ITS-G5/GNSS/IR-UWB/IMU/WSS/LC, respectivement dans la dimension co-linéaire à la route (gauche) et dans la dimension orthogonale à la route (droite).

9.7 Validations

9.7.1 Simulations en présence d'un trafic réaliste

En s'appuyant sur le simulateur de trafic SUMO, 10 trajectoires de véhicules ont été extraites d'une simulation à large-échelle en milieu urbain, calibrée pour la ville de Bologne en Italie (Cf. Figure 9.21). En particulier, on a considéré une zone gérographique restreinte incluant une portion de canyon urbain et corespondant à une durée simulée d'environ 200 sec. Ce scénario permet notamment d'éprouver la sensibilité de nos algorithmes vis-à-vis (i) des variations enregistrées par la qualité GNSS en fonction des conditions environnementales (largeur de route et hauteur des bâtiments), (ii) de conditions non-régulières/erratiques de mobilité (ex. arrêts aux intersections), et (iii) de la topologie relative instantanée et du nombre de véhicules coopératifs. Au sein de la flotte testée alternativement, chaque véhicule joue le rôle de véhicule "ego" en charge de la fusion, assisté par les autres véhicules ("ancres virtuelles"). La fusion repose dsur un filtre PF avec 1000 particules. La phase de prédiction exploite les données issues d'un compte-tour (vitesse) et d'une centrale inertielle (cap). Pour la synchronisation des données, "ego" prediction and neighboring prediction are slightly different. Pour l'étape de correction au niveau du filtre le filtre, les observations sont constituées de positions GNSS et de mesures de distances IR-UWB (vis-à-vis des voisins dont un message CAM a été reçu). La précision des GNSS embarqués dépend de la portion de trajectoire considérée, ainsi que de sa classe (allouée

Figure 9.21: Environnement urbain mixte simulé avec trafic réaliste via SUMO.

arbitrairement, comme suit: 3 véhicules équipés de SBAS, 3 de SPS, 2 de DGNSS, 2 de RTK). L'écart type des mesures de distances V2V IR-UWB a été fixé à 0.122 m.

Les résultats obtenus (Cf. par exemple Figure 9.22) ont confirmé l'apport de la coopération V2V, donnant typiquement lieu pour l'ensemble de la flotte à une précision de positionnement 2D sub-métrique dans le régime pire-cas d'erreur (pour CDF = 95%) et même de l'ordre de 0.2-0.25m pour ce qui est de l'erreur médiane (pour CDF = 50%). Comme on pouvait s'y attendre, cette coopération ne s'avère plus utile dans le cas où un véhicule équipé d'un GNSS haut de gamme dispose de bonnes conditions de visiblité vis-à-vis des satellites, mais elle présente surtout un intérêt pour améliorer les techniques dites de *dead reckoning* en cas de perte ou de dégradation du signal GNSS. Par ailleurs, d'autres études complémentaires (non présentées dans ce résumé étendu) ont aussi montré que le pouvoir de la coopération dépendait largement de la configuration géométrique, ainsi que des conditions de connectivité, en particulier pour les véhicules les plus isolés (situés en périphérie du groupe). Enfin, l'étape de prédiction, bien que s'appuyant sur des hypothèses de mobilité assez rudimentaires, semble raisonablement robuste vis-à-vis des éventuels problèmes de désaccord entre modèles a priori et trafic réel.
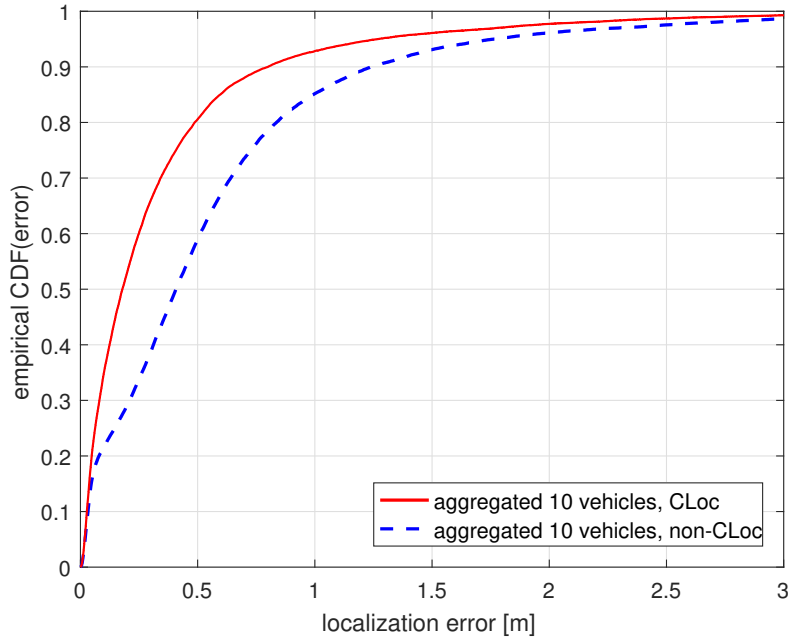
Figure 9.22: CDF empirique d'erreur de positionnement (aggrégée sur l'ensemble des 10 vehicles) pour une fusion VA-CLoc {GNSS+WSS+IMU/UWB} (rouge) et un position-nement *standalone* {GNSS+WSS+IMU} (bleu) dans le scénario SUMO simulé dans la ville de Bologne de la Figure 9.21.

9.7.2   Premières expérimentations

Un première campagne d'expérimentations à large échelle a été menée à Helmond, aux pays-Bas, en mai 2017. Le groupe testé comprenait trois véhicules (Cf. 9.23) conduisant en ligne. Chacun de ces véhicules étaient équipés d'un GPS standard, d'un GPS RTK (permettant notamment de déterminer la vérité terrain au niveau du véhicule "Ego" pour l'évaluation des performances) et enfin, de modules ITS-G5 (Cohda MK5) pour l'échange de données V2V. Ces véhicules ont effectués deux trajets complets le long d'une section de l'autoroute A270/N270 de plusieurs kilomètres. Ces trajets comprenaient délibérément des lignes droites et des virages, pour assurer une certain représentativité de l'étude[10]. Le troisième véhicule de la file était considéré comme le véhicule "Ego", ce dernier recevant des messages CAM (encapsulant des données GPS RTK) de la part des premier et second véhicules, mesurant la puissance reçue RSSI associée à ces messages (en tant que métriques explicites V2V dépendant de la distance), et finalement, fusionnant l'ensemble de ces infomations avec ses propres données GPS locales. Le taux d'émission des messages CAMs était d'approximativement 3 Hz, alors que le taux de fusion était plutôt d'environ 4 Hz.

---

[10]Une carte interactive de l'environnement de test est égalmeent disponible sur http://u.osmfr.org/m/151124
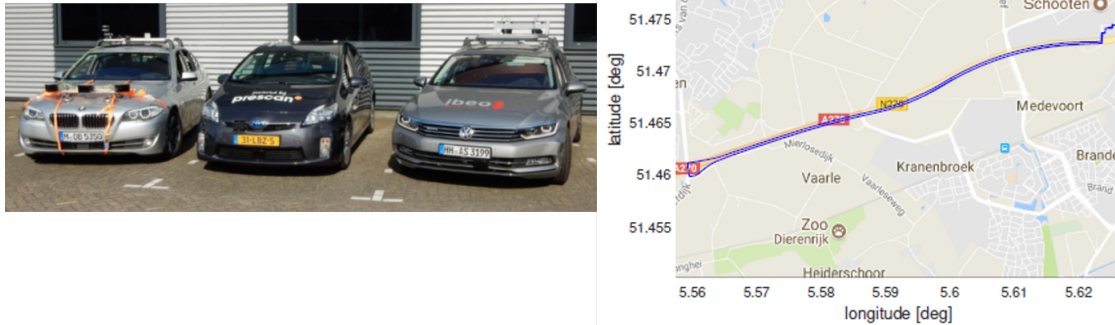
Figure 9.23: Trois véhicules coopératifs impliqués (gauche) dans le cadre d'une première campagne d'expérimentations menée sur une portion d'autoroute de plusieurs km (droite) à Helmond, aux Pays-Bas, en mai 2017.

Malgré ce taux relativement bas de 4 Hz, il a été montré que l'algorithme VA-CLoc surpassait assez nettement le GPS standard pour les deux trajets réalisés et ce, dans tous les régimes d'erreur (9.24), même si le gain était moins important qu'escompté initialement. Ce résultat est en partie lié à la forte dispersion observée sur la mesures V2V RSSI, mais aussi et surtout, au faible nombre de véchiules impliqués dans le processus de coopération (2, au plus), au faible taux d'émission des CAMs (3 Hz en moyenne, au lieu du taux critique attendu de 10 Hz) et finalement, à la topologie relative défavorable (les 3 véchiles circulant en ligne et le véhicule en charge de la fusion étant situé à l'arrière, donc en périphérie du groupe). D'autres analyses ont d'ailleurs permis de confirmer que l'erreur de localisation était de loin dominée par l'erreur commise dans la dimension orthogonale à la route, alors que le meilleur gain observé du fait de la coopération survient surtout dans la dimension co-linéaire à la route.

Dans le cadre du projet européen HIGHTS (H2020-636537), une seconde campagne d'expérimentations, plus complète et propice au test des algorithmes VA-CLoc, a eu lieu à Helmond en fin d'année 2018 (ex. mesures V2V IR-UWB disponibles, topologie VANET variable, fréquence d'émission des CAMs accrue...). Au moment de la rédaction de ce résumé étendu, les données étaient toujours en cours d'exploitation.

Critical ECDF		10%	50%	90%
Non-CLoc	1st trip	2.5 m	3.6 m	> 5 m
	2nd trip	2.1 m ↓ 76%	3.0 m ↓ 42%	4.7 m ↓ >20%
CLoc	1st trip	0.6 m	2.1 m	4.0 m
	2nd trip	0.2 m	1.6 m	3.2 m

Figure 9.24: Valeurs critiques d'erreur de positionnement (c.-à-d., pour CDF=10%, 50% et 90%) issue de la fusion ITS-G5/GNSS/IMU ou d'un positionnement *standalone* dans le cadre de la première campagne d'expérimentations menée sur une portion d'autoroute de plusieurs km.

Appendix A

Personal List of Publications and Contributions

A.1 Journal Publications

1. G.M. Hoang, B. Denis, J. Härri, D. T.M. Slock, "A unified GNSS/ITS-G5/IR-UWB fusion framework for resilient vehicular localization," to be submitted to the *IEEE Trans. Mobile Comp.*

2. G.M. Hoang, B. Denis, J. Härri, D. T.M. Slock, "Breaking the gridlock of spatial correlation in GPS-aided IEEE 802.11p-based cooperative positioning," *IEEE Trans. Veh. Technol.*, *Special Issue on Connected Vehicles*, vol. 65, no. 12, pp. 9554–9569, Dec. 2016.

A.2 Conference Publications

3. I. Khan, G.M. Hoang, and J. Härri, "Rethinking cooperative awareness for future V2X safety-critical applications," presented at the *Proc. IEEE Veh. Netw. Conf.*, Nov. 2017.

4. G.M. Hoang, B. Denis, J. Härri, and D. T.M. Slock, "Robust data fusion for cooperative vehicular localization in tunnels," in *Proc. IEEE Intell. Veh. Symp.*, Jun. 2017, pp. 1372–1377.

5. G.M. Hoang, B. Denis, J. Härri, and D. T.M. Slock, "Mitigating unbalanced GDoP

effects in range-based vehicular cooperative localization," in *Proc. IEEE Int. Conf. Commun. Workshops*, May 2017, pp. 659–664.

6. G.M. Hoang, B. Denis, J. Härri, and D. T.M. Slock, "Robust and low complexity Bayesian data fusion for hybrid cooperative vehicular localization," in *Proc. IEEE Int. Conf. Commun.*, May 2017, pp. 1–6.

7. G.M. Hoang, B. Denis, J. Härri, and D. T.M. Slock, "Cooperative localization in GNSS-aided VANETs with accurate IR-UWB range measurements," in *Proc. IEEE Workshop Positioning, Navigat. Commun.*, Oct. 2016, pp. 1–6. **Best Student Paper Award**.

8. G.M. Hoang, B. Denis, J. Härri, and D. Slock, "On communication aspects of particle-based cooperative localization in GPS-aided VANETs," in *Proc. IEEE Intell. Veh. Symp.*, Jun. 2016, pp. 20–25.

9. G.M. Hoang, B. Denis, J. Härri, and D. T.M. Slock, "Select thy neighbors: Low complexity link selection for high precision cooperative vehicular localization," in *Proc. IEEE Veh. Netw. Conf.*, Dec. 2015, pp. 36–43.

10. G.M. Hoang, B. Denis, J. Härri, and D. T.M. Slock, "Distributed links selection and data fusion for cooperative positioning in GPS-aided IEEE 802.11p VANETs," in *Proc. IEEE Workshop Positioning, Navigat. Commun.*, Mar. 2015, pp. 1–6.

A.3   Deliverables

11. HIGHTS D6.2: Integration, security and privacy, Nov. 2017.

12. HIGHTS D5.4: Specifications of implemented cooperative and fusion algorithms [Final], Nov. 2017.

13. HIGHTS D3.2: Protocols & Facilities (Cooperative Communications) [Consolidated], May 2017.

14. HIGHTS D5.3: Cooperative localization algorithms and hybrid data fusion schemes [Intermediary], May 2017.

15. HIGHTS D6.1: Description of the implementation, Oct. 2016.

16. HIGHTS D5.2: Specifications of implemented cooperative and fusion algorithms [Intermediary], Oct. 2016.

17. HIGHTS D3.1: Protocols & Facilities (Cooperative Communications) [Early], Jun. 2016.

18. HIGHTS D5.1: Cooperative localization algorithms and hybrid data fusion schemes [Early], May 2016.

A.4   Technical Report

19. G.M. Hoang, "Robust cooperative and communication-friendly localization in vehicular networks," Technical Report 4916, EURECOM, Apr. 2016.

Appendix B

General Taxonomy of Localization Algorithms

Localization algorithms can be classified in many ways and according to various criteria [30, 84, 96, 141, 142]. A possible taxonomy in the more specific context of VANETs or connected vehicles is briefly described in the following. Throughout this chapter (and also hereafter in the remainder of this thesis), we define anchor nodes as known-location nodes (or vehicles, devices, sensors, etc.). Similarly, target nodes refer to unknown-location nodes, for which locations must be determined.

B.1   Direct versus Two-Step

The localization technique can be performed directly from sensor signals (i.e., waveforms), which is also called direct localization, or by a two-step process consisting of i) an intermediary parameter measurement, during which certain parameters are extracted from the signals and ii) a position estimation step, during which the position is inferred based on those signal parameters. Various types of parameter measurements are surveyed in Section C.

When compared to the direct approach, the two-step approach is typically adopted due to its low complexity and modularity at a price of suboptimal solutions [29, 96, 143] due to estimation problem (e.g., range estimation) in the intermediate step and measurement model approximations [144].

B.2   Centralized versus Distributed

From both architecture and computation points of view, centralized algorithms adopt a data fusion center which maintains an aggregate state vector for all target nodes whereas in distributed algorithms, multiple fusion engines on the nodes compute their own positions based only on locally gathered information [84, 96, 104, 141]. Specifically, centralized algorithms aim at computing the locations of multiple nodes simultaneously after collecting all required input information to a central point in the network (at as self-elected or assigned vehicle leader, as an element of the road infrastructure/edge server, or even in the cloud). On the contrary, in distributed strategies, each single node carries out its own data collection and calculations, based on the information received from its neighbors. Accordingly, these approaches tend to alleviate the usual scalability, overhead, latency, and high computation issues of centralized approaches [104]. However they provide usually suboptimal solutions in terms of accuracy and may face convergence issues in comparison with centralized schemes.

B.3   Absolute versus Relative

Absolute localization produces position estimates in a global coordinate system while different local coordinate systems are used by different nodes in relative localization.

Though several ITS applications are only interested in solving relative localization such as ACC or even some autonomous driving systems[1], absolute localization is a critical requirement for the deployment of C-ITS to operate effectively. This is because each vehicle needs to exchange its position and velocity data in order to predict other vehicles' positions and build its own LDM. If two vehicles determine their positions in different coordinate systems, these positions cannot be used to infer the necessary information (e.g., the distance between them).

B.4   Range-Based versus Range-Free

Range-based techniques (aka fine-grained technique) rely on the point-to-point (P2P) distance or angle estimation between nodes (e.g., signal-strength-based, time-based, direction-

---

[1]In [145], the Stanford team demonstrates an autonomous car relying on a lidar-based relative localization approach in a stored map without any absolute GNSS.

based, or hybrid techniques). Accordingly, the position of a target node is estimated using trilateration or triangulation. On the other hand, range-free techniques (aka coarse-grained techniques) exploit connectivity information to achieve the position estimation. They could be based on either hop counts (e.g., DV-hop [146]) as a distance estimate to anchor nodes, or centroid algorithms where the position estimate is the average of the positions of detected anchor nodes [147], or area-based techniques such as point-in-triangulation (PIT) and approximate PIT (APIT) tests [148]. Range-free systems are cost-effective at the expense of less accurate position estimates compared to range-based ones [141, 149], for instance due to strong inter-node range approximations and/or anisotropic network properties.

B.5 Noncooperative versus Cooperative

Depending on the use of device-to-device (D2D) communications between the mobile target nodes, one can also classify localization techniques as noncooperative localization (non-CLoc) or cooperative localization (CLoc). In non-CLoc, target nodes only exchange information and make measurements with multiple anchor nodes. This may be not sufficient depending on the infrastructure density and the nominal one-hop transmission range. On the contrary, in CLoc, the target nodes additionally communicate (and make measurements) with other mobile target nodes in range, especially when they are isolated from the anchor nodes. Accordingly, the information gain from extra pairwise measurements contributes to improve the accuracy, robustness, and coverage of the localization system, through redundancy and spatial diversity [84, 97].

B.6 Deterministic versus Probabilistic

Probabilistic algorithms compute the probability distribution (of the position estimate) conditioned on the observation (i.e., posterior distribution) from the statistical models of the measurements (i.e., likelihood) and estimated positions (i.e., prior distribution). The deterministic option, however, does not exploit probability distributions (e.g., noise distribution, prior distribution) but estimation is for instance based on least squares (LS) or weighted least squares (WLS)[2]. Generally speaking, if the statistical models are known,

---

[2]However, under simplified additive centered Gaussian measurement noise assumptions, maximum likelihood (ML) (requiring likelihood only but no prior) is equivalent to WLS.

probabilistic algorithms outperform deterministic ones [30, 88, 141].

B.7   Stand-alone Sensor versus Multisensor Fusion

Based on single or multiple information sources, localization techniques can be classified into stand-alone sensor and multisensor fusion localizations, respectively. In principle, multisensor fusion improves accuracies that cannot be achieved by the use of a stand-alone sensor [3]. Other advantages include robustness, reliability, extended spatial, temporal coverage, and increased confidence, etc. Yet, one main challenge lies in the design of optimal fusion algorithms and architectures, which may lead to performance gains or losses. Various types of data fusion methods applied to localization and tracking are recalled with more details in Section D.

Appendix C

Location-dependent Radio Metrics and Related Technologies

As the focus of this thesis is CLoc enabled by wireless communications, this section presents various radio measurement categories that can be obtained from these links. We also discuss position estimation techniques as well as preferred technologies for each type of measurement.

C.1 Received Signal Strength Indicator

Received power (based on received signal strength indicator (RSSI) available in most wireless devices) is classically impacted by distance-dependent average path loss, large-scale (slow) fading/shadowing due local radio obstructions (or other local physical propagation phenomena) and small-scale (fast) fading due to multipath under mobility (i.e., self-mobility and/or scatterers mobility). From a localization perspective, RSSI readings are usually averaged values (in either time or frequency) to mitigate the latter small-scale fading and capture uniquely the most meaningful range-dependent effects (i.e., path loss and correlated shadowing) [96, 150, 151]. Admittedly, a widely used representation of the power path loss relies on the following log-normal model:

$$P_r(d) = P_0(d_0) - 10n_p \log_{10}\left(\frac{d}{d_0}\right) + s, \qquad (C.1)$$

where $P_r(d)$ [dBm] is the average received power at a distance d from the emitter, $P_0(d_0)$ [dBm] the reference received power at a test distance d_0, n_p the path loss exponent, and s [dB]
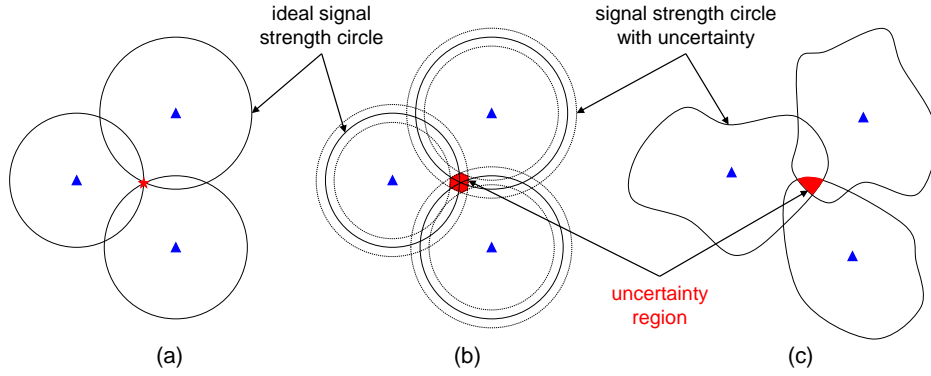
Figure C.1: Trilateration via RSSI measurements (a) in the absence of errors, (b) with some uncertainty due to inaccuracies in both measurements and model quantification, and (c) with more complicated error statistics.

a Gaussian random variable with zero mean and standard deviation σ_{Sh} accounting for shadowing. This model is accepted in both LOS and NLOS scenarios though it is hard to estimate channel parameter for the latter [141].

Under ideal circumstances, each RSSI measurement accounts for the position of a target node on a circle, which is the distance between the transmitter and the receiver. In 2-D localization, the intersection of at least three circles gives the position of the target node, which is called trilateration (circular positioning problem), as shown in Figure C.1(a). In practice, it is rare that all circles (or more complicated shapes than a circle depending on error statistics) coincide exactly, as illustrated on Figures C.1(b) and (c).

Although position estimation can be performed directly from RSSI measurements without estimating the distances, the accuracy of distance estimation indicates how much informative and useful a particular RSSI measurements can be with respect to positioning. Thus, the CRLB for an unbiased distance estimate $\widehat{d}_{\mathrm{RSSI}}$ of d from the RSSI measurement under the received power model in (C.1) is expressed as [29]:

$$\sqrt{\mathrm{var}(\widehat{d}_{\mathrm{RSSI}})} \geq \frac{\log 10}{10} \frac{\sigma_{\mathrm{Sh}}}{n_p} d. \tag{C.2}$$

This bound shows that RSSI-based range estimates have a standard deviation proportional to the true distance. For $n_p = 2.5$ and $\sigma_{\mathrm{Sh}} = 3.7$ dB[1], at the actual range of 50 m, the measured distance would be 67 m. This inaccuracy is one of the main drawbacks of RSSI ranging and positioning. In addition, RSSI is a highly parametric that requires model

---

[1]These values are based on a small-scale field measurement campaigns carried out on a highway in Helmond, Netherlands in May 2017 (see Chapter 7 for more details).

calibration. It offers limited reliability, especially in non-static multipath environments, where channel parameters (i.e., path loss, shadowing, etc.) may vary/change between the moment they have been characterized and the moment they are exploited for localization to interpret RSSI as meaningful range-dependent metrics. Yet, the main advantages of this metric are its simplicity and its relaxed synchronization requirements. Due to the issues mentioned above, it is mostly valuable in densely connected networks (and thus, following cooperative approaches), where measurement redundancy and spatial diversity over multiple links somehow compensate for single-link inaccuracy.

C.2   Time of Arrival

Time of arrival (TOA) is the measured time at which a wireless signal first arrives at a receiver and equals to the time of transmission plus a propagation delay. Range measurement $d_{j \to i}$ is then deduced from this delay between transmitter j and receiver i as $d_{j \to i} = c(t_i - t_j)$ where t_j is the time of transmission, t_i the TOA at the receiver, and c the speed of light ($c \approx 3 \times 10^8$ m/s). Importantly, t_j is known by the receiver (e.g., encapsulated in the transmitted data packet) only if both involved devices are tightly synchronized. This technique is called one-way TOA, as illustrated in Figure C.2(a). As it is challenging to maintain highly accurate time synchronization between mobile devices, multiple-way TOA schemes are usually employed.

On the one hand, in two-way ranging (or round-trip time of flight (TOF)), node i transmits a packet to node j at time $t_{i,0}$ according to its local clock. Node j receives this packet at time $t_{j,0}$ according to its local clock and responses with an acknowledgment packet at time $t_{j,1} = t_{j,0} + \Delta t_j$ after a processing delay Δt_j. Node i eventually receives the response packet encapsulating the Δt_j at time $t_{i,1}$ and computes the distance $d_{j \to i}$ through the relation $2d_{j \to i} = c(t_{i,1} - t_{i,0} - \Delta t_j)$, as shown in Figure C.2(b). Though two-way protocol can resolve clock offsets, a relative clock drift still induces a ranging errors (due to delay Δt_j measured by neighboring device's clock). On the other hand, three-way ranging consists in a two-way ranging transaction coupled with the transmission of an extra packet used to correct the relative clock drift, as shown in Figure C.2(c). This simple scheme does not require any clock tracking mechanism at the expense of an increased number of exchanged ranging packets. Details on how three-way ranging procedures can estimate
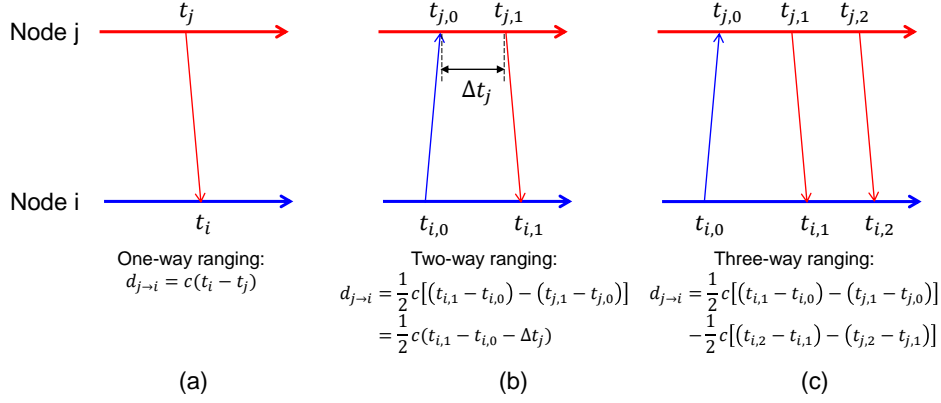
Figure C.2: (a) One-way, (b) two-way, and (c) three-way ranging protocols.

these clock-related biases are provided in [152]. Ranging protocol aspects will be described with more details in Section 5.2.1. Besides the above timing errors that can be partially solved by ranging protocols, other main sources of errors include additive noise, multipath, and mainly NLOS conditions.

First, the CRLB on TOA-based ranging for a single-path additive white Gaussian noise (AWGN) channel is given by [97]:

$$\sqrt{\text{var}(\widehat{d}_{\text{TOA}})} \geq \frac{c}{2\sqrt{2}\pi\beta\sqrt{\text{SNR}}}, \tag{C.3}$$

where $\beta = \sqrt{\int_{-\infty}^{\infty} f^2 |S(f)|^2 df / \int_{-\infty}^{\infty} S(f)^2 df}$ is the effective bandwidth of the transmitted signal $s(t)$ with spectrum $S(f)$ and SNR denotes the signal-to-noise ratio.

Second, multipath propagation induces additional errors on TOA-based range estimates. Specifically, several replicas of the transmitted signal arriving at the receiver via different propagation paths decrease the SNR of the desired direct path [97]. This direct path, carrying the correct distance information, might be weaker than the strongest path and/or interfered by close secondary multipath components. Thus, multipath challenges the receiver to detect the first arriving path [96, 97]. Instead of finding the highest peak of the cross-correlation, the time when the cross-correlation exceeds a threshold (e.g., false alarm based on noisy parts of the signal, probability of missed direct path based on *a priori* statistics) is discussed in [153].

Third, if the direct path is completely or partially obstructed, estimated distances are larger than the actual distance, leading to measurement outliers (i.e., while assuming LOS channel conditions) [141, 154]. This problem can be countered by many NLOS mitigation

techniques (e.g., WLS, constrained LS, identify and discard algorithms, robust estimators, etc.) surveyed in [154].

The bound in (C.3) indicates that increasing the effective bandwidth provides more accurate estimation of the TOA. Accordingly, IR-UWB and mmWave signals, whose bandwidths are larger than 500 MHz and possible hundreds of MHz respectively, have considered as ones of the best candidates for high localization accuracy. A significantly large bandwidth also offers fine multipath resolution on the order of a nanosecond, thereby leading theoretically to highly accurate ToA estimation.

Last but not least, by performing ranging via at least three anchor devices for 2-D localization similarly to the RSSI metrics, one can compute a mobile position through trilateration.

C.3   Time Difference of Arrival

Time difference of arrival (TDOA) performs the time difference of TOA measurements in order not to depend on the timing offset of the target node. In other words, this measurement only requires tight synchronization between the anchor nodes but no synchronization between anchor and target nodes. TDOA can operate according to one of the following schemes. For network-centric localization, the target node broadcasts a signal to the anchor nodes and these anchors shares their estimated TOA to compute the TDOA values. For self-localization, multiple signals from synchronous anchor nodes arrives at the target node to compute the TDOA measurements. This mobile-centric option is also called O-TDOA (for observed TDOA) and is in use in certain cellular systems where base stations are synchronized through GPS time. In this case, TDOA can also be computed by maximizing the cross-correlation value between the signals coming from a pair of anchor nodes [96, 155, 156].

In 2-D localization, each TDOA measurement gives a hyperbola (with foci at the two anchor nodes) on which the target node lies. Conceptually, the ideal position of the target node is then the intersection of all hyperbolas, which is called hyperbolic localization. The TDOA-based localization is depicted in Figure C.3. Finally, the preferred underlying technologies as obviously similar to that considered for TOA-based localization.
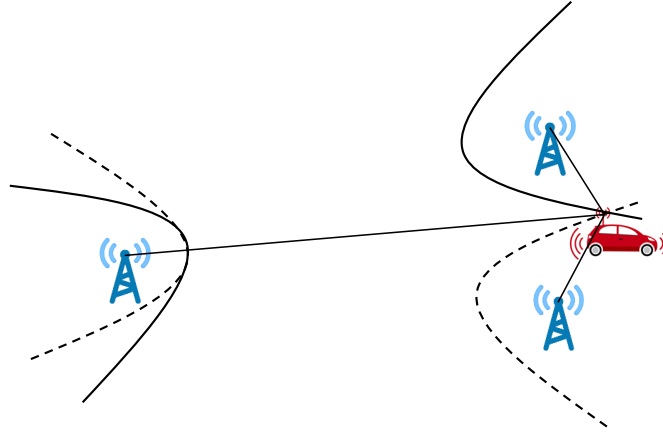
Figure C.3: 2-D localization based on TDOA measurements.

C.4   Angle of Arrival

Angle of arrival (AOA) estimation provides relative direction information to neighboring devices. Nodes equipped with antenna array or directional antennas can measure this AOA [97, 142]. By measuring the difference in arrival times for a transmitted signal at different antenna elements, the direction of an incoming signal is obtained, as illustrated in Figure C.4(a) for a simple case of uniform linear array (ULA) [96]. Note that narrowband AOA-enabled devices often rely on phase delay ϕ rather than time delay τ through the relation $\phi = 2\pi f_c \tau$, where f_c is the center frequency [97].

The location of the target node is then determined by the intersection of two angle direction lines, each formed by the target node to anchor nodes, which is called triangulation, as shown in Figure C.4(b). However, some configurations do not allow to identify the unique position of the target node i.e., $\theta_1 = \theta_2 = 90°$ in the simplified example of Figure C.4(c). Accordingly, one would need more anchor nodes to resolve this ambiguity. Obviously, small angular error translates to a large error in lateral distance especially when the target node is far from the anchor nodes.

The adoption of multiple antenna elements implies higher costs and lager device sizes. In addition, this technique is vulnerable to multipath propagation, NLOS scenarios, and array precision [154, 157]. Yet, AOA is a key measurement for future 5G localization since mmWave frequency allows to package more antenna elements in a small area [97, 158] and angular estimation is somehow an intrinsic feature and a communication-oriented requirement in 5G mmWave (e.g., to be able to track the mobile users). Interestingly, the combination of high attenuation at these mmWave frequencies as well as the use of
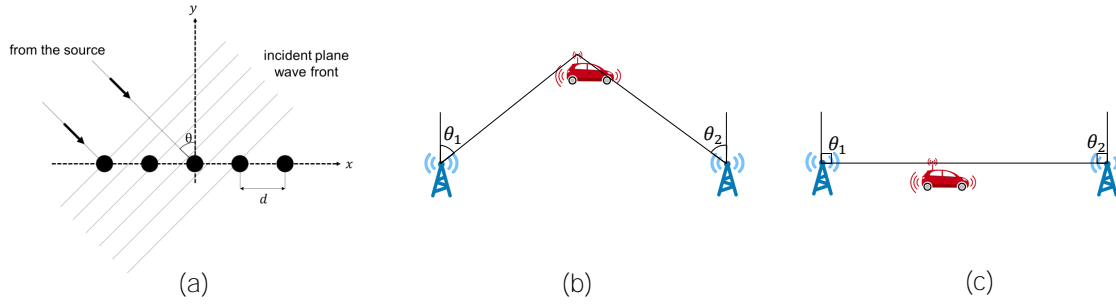
Figure C.4: (a) Signal arrival at a ULA, (b) 2-D triangulation, and (c) ambiguous triangulation.

directive antenna systems mitigate usual multipath issues, thus contributing to improve the accuracy of AOA measurements.

C.5   Phase Difference of Arrival

Phase difference of arrival (PDOA) basically consists in sending signals on several frequencies and measuring the phase offsets at the receiver. As a signal propagates in time, how fast its phase accumulates depends on its frequency. Considering transmitted signals at frequencies f_1 and f_2, the TOA (and thus the distance) is proportional to the phase difference and inversely to the frequency difference $f_2 - f_1$. Yet 2π phase periodicity and multipath cause unavoidable ambiguities in estimating the distance [157]. A good example is the "Chronos" WiFi-based system recently demonstrated by MIT that performs PDOA over multiple sub-bands of the WiFi spectrum spanning from 2.4 GHz to 5.8 GHz (thus emulating synthetic ultra large bandwidth), while claiming decimeter-level accuracy [159]. On the other hand, IEEE 802.15.4/ZigBee-compliant devices can also issue ranging solutions based on PDOA measurements [18].

C.6   Hybrid Measurements

Hybrid measurement merges more than one type of measurement among the RSSI, TOA, TDOA, AOA, and PDOA metrics previously discussed. This could either be based on multiple measurements issued over each given link, or based on multiple radio technologies, following a heterogeneous deployment scenarios (i.e., one per metrics). Such hybrid method helps to improve accuracy and robustness/resilience (for instance, when a certain kind of metrics/technology fails, other independent kinds/technologies may still operate

properly, etc.), and to avoid ambiguity in case of limited available infrastructure (e.g., number of anchor nodes) [29, 141, 160].

If both the AOA and TOA are jointly measured, one anchor node is sufficient. This scheme can solve out the near-far effect in cellular networks, when a mobile station is much closer to its serving base station than others. Accordingly, the SNR of the farther base stations is much lower causing a degradation in the quality of the measurements with respect to them, and thus localization accuracy if using trileration or hyperbolic approaches [30]. Hybrid AOA/TDOA approaches can thus eliminate the ambiguity when the target node and the two anchor nodes are linear in Figure C.4(c). Various combinations are feasible depending on applications, infrastructure, as well as environment. They are summarized in [141].

C.7   Fingerprinting

Fingerprinting or pattern matching is based on the fact that the mapping between the signal characteristics and the position of a target node is bijective or one-to-one. Any fingerprinting localization technique is conducted in two phases, namely:

- Training (offline) stage: A database is built in a site survey by dividing it into small grids. The database then maps the small grid positions onto the characteristics of the measurements called fingerprints. Besides the mostly experimented RSSI in WLAN and cellular networks, fingerprints could also include TOA, AOA, multipath power delay profile (PDP), channel impulse response (CIR), etc. [18, 29, 96]. Note that more recent approaches -yet not fully mature- tend to build and refine the database on the wing, following a participatory approach, jointly with the following online stage.

- Real-time (online) stage: The online signal measurement is correlated with the stored fingerprints based on a "matching criterion". The position of the target node is derived from the location(s) whose fingerprint(s) best match(es) the measurement. The algorithm can be deterministic based on similarity metric (e.g., k-nearest neighbors (k-NN), support vector machine (SVM), linear discriminant analysis (LDA), etc.) or probabilistic based on statistical inference (e.g., Bayesian network, expectation-maximization (EM), Kullback-Leibler divergence (KLD), etc.) [161].

One major challenge of the fingerprinting is the construction of a database which may easily grow very large depending on the complexity of the fingerprints and the granularity of the grid positions. In addition, the database must be updated as often as there are significant changes in the environment, meaning a lot of efforts. Yet prominent advantages of fingerprinting-based positioning are its accuracy and its robustness in challenging multipath and NLOS [29,141]. Moreover, the technique does not require any measurement model.

Appendix D

Multisensor Fusion Methods

In the previous section, we have mostly revised general radio-based localization metrics, pointing out their pros/cons, as well as representative standards and technologies relying on these metrics. One step ahead, introducing heterogeneous measurement data, and even including possibly other modalities (i.e., non-radio metrics such as inertial units, maps, etc.) in the problem leads to the definition of fusion architectures and algorithms.

D.1   Architectures for Multisensor Fusion

Depending on where the data fusion task is performed in the global data flow, there exists three types of fusion paradigms as follows [3]:

- Fusion of raw observational data (aka data level fusion) is illustrated in Figure D.1(a). Data from each sensor are aligned in time for central processing. Theoretically, this centralized fusion architecture is the most accurate way to fuse data [3]. Sequential estimation techniques such as Kalman filters are for instance used herein and will be presented also in this chapter.

- Fusion of states is described in Figure D.1(b). Each sensor provides an estimate of the state (i.e., position and velocity) using its individual measurements. These states from multiple sensors are aligned and then fed into a fusion engine to obtain a fused state. In general, state level fusion is not as accurate as the data level fusion because of information loss between the sensors and the fusion process [3].

- Hybrid fusion that allows fusion of either raw data or states is depicted in Figure D.1(c). The hybrid architecture provides more flexibility to combine states and
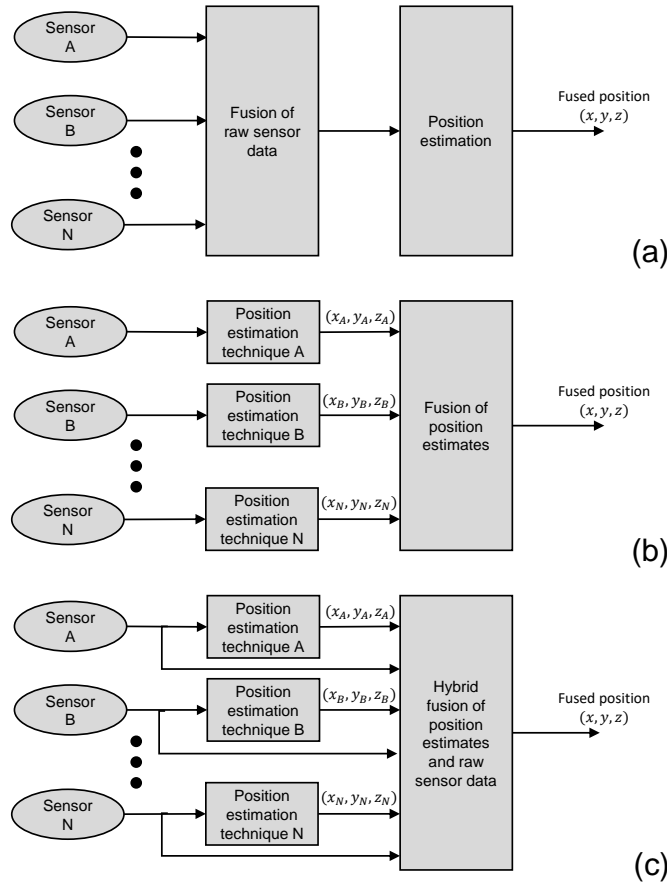
Figure D.1: Generic fusion architectures: (a) centralized (low-level), (b) autonomous (high-level), (c) hybrid (partial reproduction and simplification of [3]).

data depending on available sensor information.

D.2   Statistical Estimators

In this section, we provide a brief overview of important estimation techniques, which are at the center of the fusion architectures discussed above. Mathematically, an unknown parameter $\mathbf{x}$ (e.g., position or state) is estimated from an observation $\mathbf{z}$ (e.g., sensor measurements). The problem can be formulated by the following observation model (aka measurement model):

$$\mathbf{z} = \mathbf{h}(\mathbf{x}) + \mathbf{n}, \tag{D.1}$$

where $\mathbf{h}$ is the observation (measurement) model function and $\mathbf{n}$ is the observation (measurement) noise. Depending on the availability of prior information about $\mathbf{x}$, non-Bayesian or Bayesian estimation techniques can be applied. Within the context of the Bayesian techniques, we then consider sequential estimation (i.e., filtering) which is central for tracking

problems.

D.2.1   Non-Bayesian Estimators

Two popular non-Bayesian estimators in which the state of interest $\mathbf{x}$ is assumed to be an unknown deterministic parameter are least squares (LS) and maximum likelihood (ML) estimators.

The LS estimator does not require any information about the statistics of $\mathbf{n}$ and minimize the squared error as follows:

$$\widehat{\mathbf{x}}_{\text{LS}} = \arg\min_{\mathbf{x}} \|\mathbf{z} - \mathbf{h}(\mathbf{x})\|^2. \tag{D.2}$$

If the measurements are characterized by different accuracies, the weighted LS (WLS) can be performed as

$$\widehat{\mathbf{x}}_{\text{WLS}} = \arg\min_{\mathbf{x}} (\mathbf{z} - \mathbf{h}(\mathbf{x}))^{\dagger} \mathbf{W}(\mathbf{z} - \mathbf{h}(\mathbf{x})), \tag{D.3}$$

where $\mathbf{W}$ is the positive definite (and by definition symmetric) weighting matrix, whose entries reflect the confidence in the different measurements.

The ML estimator exploits the statistics of $\mathbf{n}$ and maximizes the likelihood function $p(\mathbf{z}|\mathbf{x})$ as follows:

$$\widehat{\mathbf{x}}_{\text{ML}} = \arg\max_{\mathbf{x}} p(\mathbf{z}|\mathbf{x}). \tag{D.4}$$

D.2.2   Bayesian Estimators

Two popular Bayesian estimators which assume $\mathbf{x}$ as a random variable with *a priori* distribution $p(\mathbf{x})$ are the minimum mean squared error (MMSE) and the maximum *a posteriori* (MAP) estimators.

The MMSE estimator is the mean of the posterior distribution $p(\mathbf{x}|\mathbf{z}) \propto p(\mathbf{x})p(\mathbf{z}|\mathbf{x})$ as

$$\widehat{\mathbf{x}}_{\text{MMSE}} = \int \mathbf{x} p(\mathbf{x}|\mathbf{z}) d\mathbf{x}. \tag{D.5}$$

The MAP estimator is the mode of the distribution as

$$\widehat{\mathbf{x}}_{\text{MAP}} = \arg\max_{\mathbf{x}} p(\mathbf{x}|\mathbf{z}). \tag{D.6}$$

Algorithm 7 Bayesian filter algorithm $(bel(\mathbf{x}_{k-1}), \mathbf{z}_k)$

1: **Prediction:**
$$bel^-(\mathbf{x}_k) = \int p(\mathbf{x}_k|\mathbf{x}_{k-1})bel(\mathbf{x}_{k-1})d\mathbf{x}_{k-1}.$$

2: **Correction:**
$$bel(\mathbf{x}_k) = \alpha_k p(\mathbf{z}_k|\mathbf{x}_k)bel^-(\mathbf{x}_k),$$
where α_k is a normalization factor.

D.3 Bayesian Filters

In the previous section, the position of a target node is estimated using a single observation at a time of interest. However, in practice, multiple observations are performed over time, thus more accurate position estimates can be achieved by incorporating all of them. It turns out that the task is simple for static node but not straightforward for mobile node. To do this, a dynamic model (aka mobility model) of the target node is needed. Accordingly, the tracking problem can be formulated using a state-space approach:

$$\mathbf{x}_k = \mathbf{f}_k(\mathbf{x}_{k-1}) + \mathbf{w}_k, \tag{D.7a}$$

$$\mathbf{z}_k = \mathbf{h}_k(\mathbf{x}_k) + \mathbf{n}_k, \tag{D.7b}$$

where $\mathbf{x}_k$ is the state vector at time k, $\mathbf{f}_k(\cdot)$ the dynamic model function, $\{\mathbf{w}_k\}_{k=1}^{\infty}$ an independent and identically distributed (i.i.d.) process noise sequence, $\mathbf{z}_k$ the measurement vector, $\mathbf{h}_k(\cdot)$ the observation model function and $\{\mathbf{n}_k\}_{k=1}^{\infty}$ an i.i.d. measurement noise sequence. For simplicity, it is assumed that the process as well as the observation noises are additive, and there is no control factor in the dynamic model. The state vector can include more elements of interest (e.g., velocity, heading, etc.) in addition to the position coordinates.

A Bayesian filter represents its belief about a system at time k as a conditional probability over the state $\mathbf{x}_k$ given all available measurements $\mathbf{z}_{1:k} = \{\mathbf{z}_1, \mathbf{z}_2, \ldots, \mathbf{z}_k\}$ i.e.,

$$bel(\mathbf{x}_k) = p(\mathbf{x}_k|\mathbf{z}_{1:k}). \tag{D.8}$$

It is assumed that the prior belief $bel(\mathbf{x}_0) = p(\mathbf{x}_0)$ is known. Under the Markov assumption, the belief $bel(\mathbf{x}_k)$ can be recursively calculated from the $bel(\mathbf{x}_{k-1})$ to track the state of a dynamic system following Algorithm 7. In the following sections, we will describe various optimal and suboptimal approaches to implement the Bayesian filter algorithm.

Algorithm 8 Kalman filter algorithm ($\mathbf{x}_{k-1}$, $\boldsymbol{\Sigma}_{k-1}$, $\mathbf{z}_k$)

1: **Prediction:**

$$\widehat{\mathbf{x}}_{k|k-1} = \mathbf{F}_k \widehat{\mathbf{x}}_{k-1},$$
$$\boldsymbol{\Sigma}_{k|k-1} = \mathbf{F}_k \boldsymbol{\Sigma}_{k-1} \mathbf{F}_k^\dagger + \mathbf{Q}_k.$$

2: **Correction:**

$$\mathbf{S}_k = \mathbf{H}_k \boldsymbol{\Sigma}_{k|k-1} \mathbf{H}_k^\dagger + \mathbf{R}_k,$$
$$\mathbf{K}_k = \boldsymbol{\Sigma}_{k|k-1} \mathbf{H}_k \mathbf{S}_k^{-1},$$
$$\widehat{\mathbf{x}}_k = \widehat{\mathbf{x}}_{k|k-1} + \mathbf{K}_k(\mathbf{z}_k - \mathbf{H}_k \widehat{\mathbf{x}}_{k|k-1}),$$
$$\boldsymbol{\Sigma}_k = (\mathbf{I} - \mathbf{K}_k \mathbf{H}_k) \boldsymbol{\Sigma}_{k|k-1}.$$

D.4   Kalman Filter

Kalman filter (KF), named after its inventor R. E. Kalman in 1960 [162], is the most famous and fundamental technique for implementing Bayes filters. The KF parameterizes beliefs by the moments representation. Specifically, the belief $bel(\mathbf{x}_k)$ is represented by the mean $\widehat{\mathbf{x}}_k$ and the covariance $\boldsymbol{\Sigma}_k$. Posterior beliefs are always Gaussian in linear Gaussian systems due to the property of Gaussian distribution that multiplying or adding two Gaussians results in another Gaussian. This conjugate distribution makes the KF optimal when recursively computing the posterior distribution for a linear Gaussian system. Accordingly, the linear Gaussian form of the state-space model (D.7) can be expressed as follows:

$$\mathbf{x}_k = \mathbf{F}_k \mathbf{x}_{k-1} + \mathbf{w}_k, \tag{D.9a}$$

$$\mathbf{z}_k = \mathbf{H}_k \mathbf{x}_k + \mathbf{n}_k, \tag{D.9b}$$

where $\mathbf{F}_k$ and $\mathbf{H}_k$ are known matrices defining the linear functions. The noises $\mathbf{w}_k \sim \mathcal{N}(\mathbf{0}, \mathbf{Q}_k)$ and $\mathbf{n}_k \sim \mathcal{N}(\mathbf{0}, \mathbf{R}_k)$ are herein statistically independent. The Kalman filter algorithm is thus presented in Algorithm 8 without mathematical derivation. The details can be found in many papers and textbooks [27, 86, 88, 162, 163].

The complexity of the KF is $\mathcal{O}(n_x^2 + n_z^{2.4})$ for each iteration, where n_x and n_z are the dimensions of the state vector $\mathbf{x}_k$ and the measurement vector $\mathbf{z}_k$, respectively [88]. In particular, the $\mathcal{O}(n_x^2)$ and $\mathcal{O}(n_z^{2.4})$ are due to the matrix multiplication when updating the covariance matrix $\boldsymbol{\Sigma}_k$ and the matrix inversion when computing the Kalman gain $\mathbf{K}_k$, respectively.

Algorithm 9 Extended Kalman filter algorithm $(\widehat{\mathbf{x}}_{k-1}, \boldsymbol{\Sigma}_{k-1}, \mathbf{z}_k)$

1: **Prediction:**

$$\widehat{\mathbf{x}}_{k|k-1} = \mathbf{f}_k(\widehat{\mathbf{x}}_{k-1}),$$
$$\boldsymbol{\Sigma}_{k|k-1} = \widehat{\mathbf{F}}_k \boldsymbol{\Sigma}_{k-1} \widehat{\mathbf{F}}_k^\dagger + \mathbf{Q}_k.$$

2: **Correction:**

$$\mathbf{S}_k = \widehat{\mathbf{H}}_k \boldsymbol{\Sigma}_{k|k-1} \widehat{\mathbf{H}}_k^\dagger + \mathbf{R}_k,$$
$$\mathbf{K}_k = \boldsymbol{\Sigma}_{k|k-1} \widehat{\mathbf{H}}_k \mathbf{S}_k^{-1},$$
$$\widehat{\mathbf{x}}_k = \widehat{\mathbf{x}}_{k|k-1} + \mathbf{K}_k(\mathbf{z}_k - \mathbf{h}_k(\widehat{\mathbf{x}}_{k|k-1})),$$
$$\boldsymbol{\Sigma}_k = (\mathbf{I} - \mathbf{K}_k \widehat{\mathbf{H}}_k) \boldsymbol{\Sigma}_{k|k-1}.$$

D.5 Extended Kalman Filter

In practice, the assumptions of linear dynamic and observation models with added Gaussian noises are difficult to satisfy in order to apply the KF. The extended Kalman filter (EKF) eases one of these assumptions i.e., the linearity assumption. The key idea underlying the EKF is a linearization via Taylor expansion. Considering the state-space model in (D.7) where $\mathbf{w}_{i,k}$ and $\mathbf{v}_{i,k}$ are additive white Gaussian noises, it is expanded in Taylor series with terms up to the first order as follows:

$$\mathbf{x}_k \approx \mathbf{f}_k(\widehat{\mathbf{x}}_{k-1}) + \widehat{\mathbf{F}}_k(\mathbf{x}_{k-1} - \widehat{\mathbf{x}}_{k-1}) + \mathbf{w}_{i,k}, \tag{D.10a}$$

$$\mathbf{z}_k \approx \mathbf{h}_k(\widehat{\mathbf{x}}_{k|k-1}) + \widehat{\mathbf{H}}_k(\mathbf{x}_k - \widehat{\mathbf{x}}_{k|k-1}) + \mathbf{v}_{i,k}, \tag{D.10b}$$

where $\widehat{\mathbf{F}}_k$ and $\widehat{\mathbf{H}}_k$ are the Jacobian matrices evaluated at $\widehat{\mathbf{x}}_{k-1}$ and $\widehat{\mathbf{x}}_{k|k-1}$, respectively. Accordingly, the EKF in Algorithm 9 has almost the same equations as the KF in Algorithm 8. Higher order EKFs that retain further terms in the Taylor expansion are possible, but rarely employed due to additional complexity [87,89]. Note that the Jacobian matrices must exist to apply the EKF.

As the goodness of the linearization depends on the degree of nonlinearity of the state-space model and the degree of uncertainty of the state estimate, special care has to be taken when initializing and running the EKF in order to keep the uncertainty small [88]. Besides, the complexity of the EKF is on the same order as that of KF i.e., $\mathcal{O}(n_x^2 + n_z^{2.4})$. The difference is that the EKF has to compute the Jacobian matrices at each iteration of the algorithm.

D.6   Unscented Kalman Filter

Besides Taylor expansion in the EKF, one alternative is stochastic linearizion through the use of a set of weighted so-called sigma points, and the resulting filter is known as unscented Kalman filter (UKF). Specifically, these sigma points are deterministically extracted from the Gaussian approximation of the belief $bel(\mathbf{x}_k)$ and are propagated through the true nonlinear functions $\mathbf{f}(\cdot)$ and $\mathbf{h}(\cdot)$. When compared with the EKF, the UKF computes the posterior beliefs better than that of the EKF i.e., matching the third order of Taylor expansion [164].

Central for the UKF is unscented transformation (UT) that propagates mean and covariance information through nonlinear transformations [164]. For an n-dimensional random variable $\mathbf{x}$ with mean $\bar{\mathbf{x}}$ and covariance $\boldsymbol{\Sigma}_x$, the resulting $2n+1$ sigma points $\mathcal{X}^{(i)}$ with associated weights $w_m^{(i)}$ and $w_c^{(i)}$ used for reconstructing the mean and the covariance, are respectively generated using [165], as follows:

$$
\begin{aligned}
\mathcal{X}^{(0)} &= \bar{\mathbf{x}} \\
\mathcal{X}^{(i)} &= \bar{\mathbf{x}} + \left(\sqrt{(n+\lambda)\boldsymbol{\Sigma}_x} \right)_i, \qquad i = 1, \ldots, n, \\
\mathcal{X}^{(i)} &= \bar{\mathbf{x}} - \left(\sqrt{(n+\lambda)\boldsymbol{\Sigma}_x} \right)_{i-n}, \quad i = n+1, \ldots, 2n, \\
w_m^{(0)} &= \lambda/(n+\lambda), \\
w_c^{(0)} &= \lambda/(n+\lambda) + (1 - \alpha^2 + \beta), \\
w_m^{(i)} &= w_c^{(i)} = 1/(2(n+\lambda)), \qquad i = 1, \ldots, 2n,
\end{aligned}
\tag{D.11}
$$

where $\lambda = \alpha^2(n+\kappa) - n$, α and κ are scaling parameters that influence how far the sigma points are away from the mean $\bar{\mathbf{x}}$, β applies prior knowledge about the distribution of $\mathbf{x}$ ($\beta = 2$ is the optimal for Gaussian distribution), and $(\sqrt{(n+\lambda)\boldsymbol{\Sigma}_x})_i$ indicates the ith row of the Cholesky factorization of $(n+\lambda)\boldsymbol{\Sigma}_x$. These sigma points are then propagated through $\mathbf{f}(\cdot)$ and $\mathbf{h}(\cdot)$ depending on the step, thus capturing how these functions changes the shape of the input distribution. The UKF algorithm employing the UT is described in Algorithm 10.

The complexity of the UKF is as that of EKF with a constant factor [88]. In many practical applications, the difference between EKF and UKF is modest [88], however the UKF is free from computing the error-prone Jacobian matrices. Last but not least, the

---

Algorithm 10 Unscented Kalman filter algorithm $(\widehat{\mathbf{x}}_{k-1}, \boldsymbol{\Sigma}_{k-1}, \mathbf{z}_k)$

1: **Prediction:**

$$\mathcal{X}_{k-1} = (\widehat{\mathbf{x}}_{k-1}, \widehat{\mathbf{x}}_{k-1} + \sqrt{(n+\lambda)\boldsymbol{\Sigma}_{k-1}}, \widehat{\mathbf{x}}_{k-1} - \sqrt{(n+\lambda)\boldsymbol{\Sigma}_{k-1}}),$$

$$\mathcal{X}_{k|k-1}^{*} = \mathbf{f}(\mathcal{X}_{k-1}),$$

$$\widehat{\mathbf{x}}_{k|k-1} = \sum_{i=0}^{i=2n} w_m^{(i)} \mathcal{X}_{k|k-1}^{*(i)}$$

$$\boldsymbol{\Sigma}_{k|k-1} = \sum_{i=0}^{i=2n} w_c^{(i)} (\mathcal{X}_{k|k-1}^{*(i)} - \widehat{\mathbf{x}}_{k|k-1})(\mathcal{X}_{k|k-1}^{*(i)} - \widehat{\mathbf{x}}_{k|k-1})^{\dagger} + \mathbf{Q}_k.$$

2: **Correction:**

$$\mathcal{X}_{k|k-1} = (\widehat{\mathbf{x}}_{k-1}, \widehat{\mathbf{x}}_{k-1} + \sqrt{(n+\lambda)\boldsymbol{\Sigma}_{k|k-1}}, \widehat{\mathbf{x}}_{k-1} - \sqrt{(n+\lambda)\boldsymbol{\Sigma}_{k|k-1}}),$$

$$\mathcal{Z}_{k|k-1} = \mathbf{h}(\mathcal{X}_{k|k-1}),$$

$$\widehat{\mathbf{z}}_k = \sum_{i=0}^{i=2n} w_m^{(i)} \mathcal{Z}_{k|k-1}^{(i)}$$

$$\mathbf{S}_k = \sum_{i=0}^{i=2n} w_c^{(i)} (\mathcal{Z}_{k|k-1}^{(i)} - \widehat{\mathbf{z}}_k)(\mathcal{Z}_{k|k-1}^{(i)} - \widehat{\mathbf{z}}_k)^{\dagger} + \mathbf{R}_k,$$

$$\boldsymbol{\Sigma}_{k|k-1}^{x,z} = \sum_{i=0}^{i=2n} w_c^{(i)} (\mathcal{X}_{k|k-1}^{(i)} - \widehat{\mathbf{x}}_{k|k-1})(\mathcal{Z}_{k|k-1}^{(i)} - \widehat{\mathbf{z}}_k)^{\dagger},$$

$$\mathbf{K}_k = \boldsymbol{\Sigma}_{k|k-1}^{x,z} \mathbf{S}_k^{-1},$$

$$\widehat{\mathbf{x}}_k = \widehat{\mathbf{x}}_{k|k-1} + \mathbf{K}_k(\mathbf{z}_k - \widehat{\mathbf{z}}_k),$$

$$\boldsymbol{\Sigma}_k = \boldsymbol{\Sigma}_{k|k-1} - \mathbf{K}_k \mathbf{S}_k \mathbf{K}_k^{\dagger}.$$

UKF still requires (approximately) Gaussian distributions.

D.7 Particle Filter

Particle filter (PF), aka the sequential Monte Carlo (SMC) method, is a nonparametric solution to nonlinear and non-Gaussian problems in which the KF-based methods above may diverge. In PF, the belief $bel(\mathbf{x}_k)$, which can be arbitrarily complex and multimodal, is approximated by a particle cloud $\{\mathbf{x}_k^{(p)}, w_k^{(p)}\}_{p=1}^{P}$ of random samples or particles $\mathbf{x}_k^{(p)}$ and associated weights $w_k^{(p)}$ such that $\sum_p w_k^{(p)} = 1$ as follows [87, 88, 166]:

$$bel(\mathbf{x}_k) = p(\mathbf{x}_k | \mathbf{z}_{1:k}) \approx \sum_{p=1}^{P} w_{i,k}^{(p)} \delta(\mathbf{x}_k - \mathbf{x}_k^{(p)}), \tag{D.12}$$

where $\delta(\cdot)$ denotes the Dirac delta function. This is obtained by marginalizing the approximation of the full posterior distribution i.e., $p(\mathbf{x}_{0:k} | \mathbf{z}_{1:k}) \approx \sum_{p=1}^{P} w_{i,k}^{(p)} \delta(\mathbf{x}_{0:k} - \mathbf{x}_{0:k}^{(p)})$. However, it is challenging and expensive from the computation point of view to draw samples directly from $p(\mathbf{x}_{0:k} | \mathbf{z}_{1:k})$ due to its complex functional form [87, 89]. Thus, an

---

Algorithm 11 Particle filter algorithm $(\{\mathbf{x}_{k-1}^{(p)}, w_{k-1}^{(p)}\}_{p=1}^{P}, \mathbf{z}_k)$

1: Draw samples $\mathbf{x}_k^{(p)}$ from the importance distribution:

$$\mathbf{x}_k^{(p)} \sim q(\mathbf{x}_k|\mathbf{x}_{k-1}^{(p)}, \mathbf{z}_k), \quad p = 1, \ldots, P.$$

2: Calculate new weights

$$w_k^{(p)} \propto w_{k-1}^{(p)} \frac{p(\mathbf{z}_k|\mathbf{x}_k^{(p)})p(\mathbf{x}_k^{(p)}|\mathbf{x}_{k-1}^{(p)})}{q(\mathbf{x}_k^{(p)}|\mathbf{x}_{k-1}^{(p)}, \mathbf{z}_k)}, \quad p = 1, \ldots, P,$$

and normalize them to sum to unity.
3: Preform resampling:

- Sequential importance resampling (SIR): Generate new P samples with replacement from the cloud $\{\mathbf{x}_k^{(p)}\}_{p=1}^{P}$ so that the probability to take sample p is $w_k^{(p)}$ and reset $w_k^{(p)} = 1/P$.
- Adaptive sampling: Only resample as above when the effective number of samples is less than a predefined threshold N_{th} (e.g., $N_{\text{th}} = 2P/3$ [80] or $P/10$ [89])

$$\widehat{N}_{\text{eff}} = \frac{1}{\sum_p (w_k^{(p)})^2} < N_{\text{th}}.$$

---

approximate distribution called the importance distribution $q(\mathbf{x}_{0:k}|\mathbf{z}_{1:k})$ is used instead, from which one can easily draw samples. The weights are determined according to the importance sampling principle [166]. In addition, the importance distribution is chosen to factorize such that $q(\mathbf{x}_{0:k}|\mathbf{z}_{1:k}) = q(\mathbf{x}_k|\mathbf{x}_{0:k-1}, \mathbf{z}_{1:k})q(\mathbf{x}_{0:k-1}|\mathbf{z}_{1:k-1})$ in order to avoid redrawing the samples and recomputing the weights for the entire time sequence when new measurements are integrated. Put differently, one only draws new state from the importance distribution $q(\mathbf{x}_k|\mathbf{x}_{0:k-1}, \mathbf{z}_{1:k})$, or even simpler $q(\mathbf{x}_k|\mathbf{x}_{k-1}, \mathbf{z}_k)$ due to the Markov assumption. This solution is known as sequential importance sampling (SIS). The PF algorithm is then described in Algorithm 11.

Note that the algorithm includes a resampling step to avoid particle depletion, which corresponds to a situation when all the particles have zero or negligible weights [87,89,166]. The idea underlying this step is to remove particles with very small weights and duplicate particles with significant weights. Yet it also ruins the diversity of samples after a while. One schemes to counteract this effect is to do the resampling when it is actually needed, which is called adaptive sampling. Other approaches include resample-move algorithm, regularization, or Markov chain Monte Carlo (MCMC) steps, etc. [167].

Also note that Algorithm 11 is a generic framework to develop many variants of the PF depending on the choice of the importance distribution. The most basic and well-known embodiment consists in using the state transition distribution as the importance distribution i.e., $p(\mathbf{x}_k|\mathbf{x}_{k-1}^{(p)})$ [87–89]. The resulting filter is called bootstrap PF as stated in

---

Algorithm 12 Bootstrap particle filter algorithm $(\{\mathbf{x}_{k-1}^{(p)}, w_{k-1}^{(p)}\}, \mathbf{z}_k)$

1: Draw samples $\mathbf{x}_k^{(p)}$ from the state transition distribution:

$$\mathbf{x}_k^{(p)} \sim p(\mathbf{x}_k | \mathbf{x}_{k-1}^{(p)}), \quad p = 1, \ldots, P.$$

2: Calculate new weights

$$w_k^{(p)} \propto p(\mathbf{z}_k | \mathbf{x}_k^{(p)}), \quad p = 1, \ldots, P,$$

and normalize them to sum to unity.

3: Preform resampling.

Algorithm 12. This eases the implementation, but due to the inefficiency of the importance distribution it may require a very large number of particles [89]. Other popular variants are discussed in [87, 168].

PF is approximately a factor P/n_x more complex than the EKF, where P is the number of particles and n_x denotes the state dimension [80]. As the number of particles should be large enough to cover the space of all states [88], it increases exponentially with the increase in the state dimension. Accordingly, PF are inappropriate for high dimensional problems. The effects of dimensionality can be diminished by marginalizing out states that can be modeled without sampling, known as Rao–Blackwellized particle filter (RBPF) [80, 166] or mixture Kalman filter (MKF) [169].

Appendix E

Performance Metrics

To evaluate the positioning/tracking performance, we first define the localization error E_i of the "ego" vehicle i. E_i is a random variable which takes sampled value $e_{i,k}$ at time $t_{i,k}$ as follows:

$$e_{i,k} = \|\widehat{\mathbf{x}}_{i,k} - \mathbf{x}_{i,k}\|, \tag{E.1}$$

where $\widehat{\mathbf{x}}_{i,k}$ and $\mathbf{x}_{i,k}$ represent respectively the 2-D estimated and true positions of the "ego" car i at time $t_{i,k}$. We are then interested in the empirical Cumulative Distribution Function (CDF) of the positioning error E_i. Said differently, the probability that the positioning error does not exceed a certain threshold can be specified for all threshold values, that is

$$F(x) = \mathbb{E}_i \{p\,(e_i \leq x)\}, \tag{E.2}$$

where the expectation $\mathbb{E}_i\{\cdot\}$ is taken over all the vehicles in the VANET. We then extract characteristic values of the error statistics, such as the median error (CDF of 50%) or the so-called worst-case (WC) error (arbitrarily defined for a CDF of 90% herein).

The second metric that we consider is the root mean square error (RMSE) of the whole VANET's position estimates as a function of time, which we defined as

$$\text{RMSE}_{\text{VANET}}(k) = \sqrt{\mathbb{E}_i\{e_{i,k}^2\}}, \tag{E.3}$$

where the expectation $\mathbb{E}_i\{\cdot\}$ is taken over all the vehicles in the cluster during the global time window k[1].

---

[1] Recalling that vehicles asynchronously estimate their own positions grouped by the global time windows (Figure **??**), we do not extrapolate these positions at specific instants to avoid introducing extra errors.

Appendix F

Generation of Correlated Observations

As the spatial/temporal correlation properties and models have been investigated in Section 4.2.1, we herein recall the SOS-based approach to generate the corresponding processes in our simulations. Given the true 2-D GNSS receiver's position $\mathbf{x} = (x, y)^\dagger$, the 2-D correlated GNSS x- and y-error maps $\hat{n}^x(\mathbf{x})$, $\hat{n}^y(\mathbf{x})$ are drawn as follows:

$$\hat{n}^{(\cdot)}(\mathbf{x}) = \sigma_{\text{GNSS}}^{(\cdot)} \sqrt{\frac{2}{N}} \sum_{n=1}^{N} \cos\left(2\pi \mathbf{f}_n^{(\cdot)\dagger} \mathbf{x} + \psi_n^{(\cdot)}\right), \tag{F.1}$$

where $(\cdot)$ can be either x- or y-coordinate, $\{\psi_n^{(\cdot)} t\}_{n=1}^{N}$ represents a set of random phase terms uniformly distributed over $[0, 2\pi)$, $\{\mathbf{f}_n^{(\cdot)}\}_{n=1}^{N} = \{f_{x,n}^{(\cdot)}, f_{y,n}^{(\cdot)}\}_{n=1}^{N}$ the 2-D random discrete spatial frequencies that can be generated according to a given joint pdf $p(\mathbf{f}^{(\cdot)})$ related to the 2-D power spectral density (PSD) of the shadowing process (i.e., performing 2-D Fourier transformation on (4.1)), by using a frequency sampling Monte Carlo method (MCM), as detailed in [114].

Regarding the V2V RSSI measurements, with knowledge of both Tx's 2-D position $\mathbf{x}_t = (x_t, y_t)^\dagger$ and Rx's position $\mathbf{x}_r = (x_r, y_r)^\dagger$, the 4-D spatially correlated shadowing map $\hat{s}(\mathbf{x}_t, \mathbf{x}_r)$ is then generated using [111], as follows:

$$\hat{s}(\mathbf{x}_t, \mathbf{x}_r) = \sigma_{\text{Sh}} \sqrt{\frac{2}{N}} \sum_{n=1}^{N} \cos\left(2\pi \mathbf{f}_n^\dagger \left(\mathbf{x}_t^\dagger, \mathbf{x}_r^\dagger\right)^\dagger + \phi_n\right), \tag{F.2}$$

where $\{\phi_n\}_{n=1}^{N}$ are random phase terms uniformly distributed over $[0, 2\pi)$, $\{\mathbf{f}_n\}_{n=1}^{N} =$

$\{\mathbf{f}_n^t, \mathbf{f}_n^r\}_{n=1}^N = \{f_{x,n}^t, f_{y,n}^t, f_{x,n}^r, f_{y,n}^r\}_{n=1}^N$ 4-D random spatial frequencies generated according to a given joint pdf related to the 4-D PSD of the shadowing process (i.e., performing 4-D Fourier transformation on (4.3)) through MCM, again like in [111, 114].

Moreover, following [111], we consider the shadowing symmetric property in V2V networks, leading to identical fluctuations on both sides of the link i.e., $s(\mathbf{x}_t, \mathbf{x}_r) = s(\mathbf{x}_r, \mathbf{x}_t)$ due to a common channel propagation path. Accordingly, we "symmetrically" manipulate the aforementioned 4-D spacial frequencies and phases through symmetric MCM.

$\{\mathbf{f}_n^t, \mathbf{f}_n^r\}_{n=1}^N = \{f_{x,n}^t, f_{y,n}^t, f_{x,n}^r, f_{y,n}^r\}_{n=1}^N$

Bibliography

[1] K. Sjoberg, P. Andres, T. Buburuzan, and A. Brakemeier, "Cooperative intelligent transport systems in Europe: Current deployment status and outlook," *IEEE Vehicular Technology Magazine*, vol. 12, no. 2, pp. 89–97, June 2017.

[2] A. Festag, "Cooperative intelligent transport systems standards in Europe," *IEEE Communications Magazine*, vol. 52, no. 12, pp. 166–172, December 2014.

[3] D. L. Hall and J. Llinas, "An introduction to multisensor data fusion," *Proceedings of the IEEE*, vol. 85, no. 1, pp. 6–23, January 1997.

[4] *An introduction to GNSS: GPS, GLONASS, BeiDou, Galileo and other Global Navigation Satellite Systems*, 2nd ed.   Calgary, Alberta, Canada: NovAtel, 2015.

[5] F. de Ponte Müller, "Survey on ranging sensors and cooperative techniques for relative positioning of vehicles," *Sensors*, vol. 17, no. 2, January 2017.

[6] A. Amditis, P. Lytrivis, and E. Portouli, *Sensing and Actuation in Intelligent Vehicles*.   London, UK: Springer, 2012, ch. 3, pp. 31–60.

[7] J. Härri *et al.*, "Protocols & facilities (cooperative communications) [early]," HIGHTS Project Deliverable 3.1, May 2015.

[8] B. Denis *et al.*, "Cooperative localization algorithms and hybrid data fusion schemes [early]," HIGHTS Project Deliverable 5.1, May 2016.

[9] D. Caveney, "Cooperative vehicular safety applications," *IEEE Control Systems*, vol. 30, no. 4, pp. 38–53, 2010.

[10] G. M. Hoang, B. Denis, J. Härri, and D. T. M. Slock, "Select thy neighbors: Low complexity link selection for high precision cooperative vehicular localization," in *Proc. IEEE Vehicular Networking Conference*, 2015, pp. 36–43.

[11] ——, "Breaking the gridlock of spatial correlations in GPS-aided IEEE 802.11p-based cooperative positioning," *IEEE Trans. on Veh. Technol.*, vol. PP, Jun. 2016.

[12] ——, "On communication aspects of particle-based cooperative positioning in GPS-aided VANETs," in *Proc. CCP IV'16*, Jun. 2016, pp. 20–25.

[13] G. M. Hoang, B. Denis, J. Härri, and D. T. M. Slock, "Cooperative localization in GNSS-aided VANETs with accurate IR-UWB range measurements," in *2016 13th Workshop on Positioning, Navigation and Communications (WPNC)*, October 2016, pp. 1–6.

[14] ——, "Robust and low complexity bayesian data fusion for hybrid cooperative vehicular localization," in *2017 IEEE International Conference on Communications (ICC)*, May 2017, pp. 1–6.

[15] ——, "Mitigating unbalanced gdop effects in range-based vehicular cooperative localization," in *2017 IEEE International Conference on Communications Workshops (ICC Workshops)*, May 2017, pp. 659–664.

[16] ——, "Robust data fusion for cooperative vehicular localization in tunnels," in *2017 IEEE Intelligent Vehicles Symposium (IV)*, June 2017, pp. 1372–1377.

[17] H. Hartenstein and L. P. Laberteaux, "A tutorial survey on vehicular ad hoc networks," *IEEE Communications Magazine*, vol. 46, no. 6, pp. 164–171, June 2008.

[18] "D4.1 – Use-Case related evaluated distance estimation technologies," *HIGHTS* Deliverable, May. 2015.

[19] *Intelligent Transport Systems (ITS); Vehicular Communications; Basic Set of Applications; Part 2: Specification of Cooperative Awareness Basic Service*, ETSI Std. EN 302 637-2 V1.3.2, Oct. 2014.

[20] J. B. Kenney, "Dedicated Short-Range Communications (DSRC) Standards in the United States," *Proc. IEEE*, vol. 99, no. 7, pp. 1162–1182, Jul. 2011.

[21] F. Qu, F. Y. Wang, and L. Yang, "Intelligent transportation spaces: vehicles, traffic, communications, and beyond," *IEEE Communications Magazine*, vol. 48, no. 11, pp. 136–142, November 2010.

[22] "5G automotive vision," White Paper, 5G-PPP, Oct. 2015.

[23] "IEEE802.11p ahead of LTE-V2V for safety applications," White Paper, NXP Semiconductors & Autotalks, Sep. 2017.

[24] T. Rappaport, R. Heath, R. Daniels, and J. Murdock, *Millimeter wave wireless communications*, 1st ed. Prentice Hall, 2014.

[25] J. Choi, V. Va, N. Gonzalez-Prelcic, R. Daniels, C. R. Bhat, and R. W. Heath, "Millimeter-wave vehicular communication to support massive automotive sensing," *IEEE Communications Magazine*, vol. 54, no. 12, pp. 160–167, December 2016.

[26] E. D. Kaplan and C. Hegarty, *Understanding GPS: Principles and Applications*. Boston, MA, USA: Artech House, 2005.

[27] P. Groves, *Principles of GNSS, Inertial, and Multisensor Integrated Navigation Systems*, 2nd ed. Boston-London, UK: Artech House, 2013.

[28] S. Gleason and D. Gebre-Egziabher, *GNSS Applications and Methods*, 1st ed. Norwood, MA: Artech House, 2009.

[29] G. Sun, J. Chen, W. Guo, and K. J. R. Liu, "Signal processing techniques in network-aided positioning: a survey of state-of-the-art positioning designs," *IEEE Signal Processing Magazine*, vol. 22, no. 4, pp. 12–23, July 2005.

[30] H. Noureddine Al Moussawi, "Some signal processing techniques for wireless cooperative localization and tracking," Ph.D. dissertation, Télécom Bretagne, Univ. Bretagne Occidentale, Brest, France, Nov. 2012.

[31] D. Titterton and J. Weston, *Strapdown Inertial Navigation Technology*, 2nd ed., ser. IEE Radar, Sonar, Navigation and Avionics Series. Institution of Engineering and Technology, 2004.

[32] E. Abbott and D. Powell, "Land-vehicle navigation using gps," *Proceedings of the IEEE*, vol. 87, no. 1, pp. 145–162, Jan 1999.

[33] O. J. Woodman, "An introduction to inertial navigation," Univ. Cambridge, Comp. Lab., Tech. Rep. UCAM-CL-TR-696, Aug. 2007. [Online]. Available: http://www.cl.cam.ac.uk/techreports/UCAM-CL-TR-696.pdf

[34] M. Grewal and A. Andrews, "How good is your gyro [ask the experts]," *IEEE Cont. Syst. Mag.*, vol. 30, no. 1, pp. 12–86, Feb. 2010.

[35] R. Neul *et al.*, "Micromachined angular rate sensors for automotive applications," *IEEE Sens. J.*, vol. 7, no. 2, pp. 302–309, Feb. 2007.

[36] I. Skog and P. Handel, "In-car positioning and navigation technologies: A survey," *IEEE Transactions on Intelligent Transportation Systems*, vol. 10, no. 1, pp. 4–21, March 2009.

[37] M. G. Petovello, "Real-time integration of a tactical-grade IMU and GPS for high-accuracy positioning and navigation," Ph.D. dissertation, Univ. Calgary, Calgary, Alberta, Canada, Apr. 2003.

[38] S. Godha, "Performance evaluation of low cost MEMS-based IMU integrated with GPS for land vehicle navigation application," Ph.D. dissertation, Univ. Calgary, Calgary, Alberta, Canada, Feb. 2006.

[39] S. M. Patole, M. Torlak, D. Wang, and M. Ali, "Automotive radars: A review of signal processing techniques," *IEEE Signal Processing Magazine*, vol. 34, no. 2, pp. 22–35, March 2017.

[40] M. Hammarsten and V. Runemalm, "3d localization and mapping using automotive radar," Master's thesis, 2016.

[41] E. Ward and J. Folkesson, "Vehicle localization with low cost radar sensors," in *2016 IEEE Intelligent Vehicles Symposium (IV)*, June 2016, pp. 864–870.

[42] M. Cornick, J. Koechling, B. Stanley, and B. Zhang, "Localizing ground penetrating radar: A step toward robust autonomous ground vehicle localization," *J. Field Robot.*, vol. 33, no. 1, pp. 82–102, Jan. 2016.

[43] J. Levinson and S. Thrun, "Map-based precision vehicle localization in urban environments," in *Robotics: Science and Systems*, 2007.

[44] ——, "Robust vehicle localization in urban environments using probabilistic maps," in *2010 IEEE International Conference on Robotics and Automation*, May 2010.

[45] X. Guo, "Feature-based localization methods for autonomous vehicles," Ph.D. dissertation, Free Univ. of Berlin, Berlin, Germany, Feb. 2017.

[46] G. P. Stein, Y. Gdalyahu, and A. Shashua, "Stereo-assist: Top-down stereo for driver assistance systems," in *Proc. IEEE Intell. Veh. Symp.*, Jun. 2010, pp. 723–730.

[47] S. Leßmann, M. Meuter, D. Müller, and J. Pauli, "Probabilistic distance estimation for vehicle tracking application in monocular vision," in *Proc. IEEE Intell. Veh. Symp.*, Jun. 2016, pp. 1199–1204.

[48] S. Nedevschi *et al.*, "High accuracy stereo vision approach for obstacle detection on non-planar roads," in *Proc. IEEE Intell. Eng. Syst.*, Sep. 2014, p. 211–216.

[49] D. Nister, O. Naroditsky, and J. Bergen, "Visual odometry," in *Proceedings of the 2004 IEEE Computer Society Conference on Computer Vision and Pattern Recognition, 2004. CVPR 2004.*, vol. 1, June 2004, pp. I–652–I–659 Vol.1.

[50] D. Scaramuzza and F. Fraundorfer, "Visual odometry [tutorial]," *IEEE Robotics Automation Magazine*, vol. 18, no. 4, pp. 80–92, Dec 2011.

[51] A. J. Davison, I. D. Reid, N. D. Molton, and O. Stasse, "Monoslam: Real-time single camera slam," *IEEE Transactions on Pattern Analysis and Machine Intelligence*, vol. 29, no. 6, pp. 1052–1067, June 2007.

[52] T. Taketomi, H. Uchiyama, and S. Ikeda, "Visual slam algorithms: a survey from 2010 to 2016," *IPSJ Transactions on Computer Vision and Applications*, vol. 9, no. 1, p. 16, Jun 2017.

[53] H. Lu, S. Zhang, X. Liu, and X. Lin, "Vehicle tracking using particle filter in Wi-Fi network," in *Proc. VTC'10-Fall*, Sept. 2010.

[54] L. Sun, Y. Wu, J. Xu, and Y. Xu, "An RSU-assisted localization method in non-GPS highway traffic with dead reckoning and V2R communications," in *Proc. CECNet'12*, Apr. 2012, pp. 149–152.

[55] C. Goetze *et al.*, "Geolocation referencing sub-system," HIGHTS Project Deliverable 2.2, May 2015.

[56] A. Fascista, G. Ciccarese, A. Coluccia, and G. Ricci, "A localization algorithm based on v2i communications and aoa estimation," *IEEE Signal Processing Letters*, vol. 24, no. 1, pp. 126–130, Jan 2017.

[57] M. Koivisto, A. Hakkarainen, M. Costa, J. Talvitie, K. Heiska, K. Leppänen, and M. Valkama, "Continuous high-accuracy radio positioning of cars in ultra-dense 5g networks," in *2017 13th International Wireless Communications and Mobile Computing Conference (IWCMC)*, June 2017, pp. 115–120.

[58] R. Parker and S. Valaee, "Vehicle localization in vehicular networks," in *IEEE Vehicular Technology Conference*, Sept 2006, pp. 1–5.

[59] ——, "Vehicular node localization using received-signal-strength indicator," *IEEE Trans. Veh. Technol.*, vol. 56, no. 6, pp. 3371–3380, Nov. 2007.

[60] N. Alam and A. G. Dempster, "Cooperative positioning for vehicular networks: Facts and future," *IEEE Transactions on Intelligent Transportation Systems*, vol. 14, no. 4, pp. 1708–1717, Dec 2013.

[61] J. Yao, A. Balaei, M. Hassan, N. Alam, and A. Dempster, "Improving cooperative positioning for vehicular networks," *IEEE Trans. Veh. Technol.*, vol. 60, no. 6, pp. 2810–2823, Jul. 2011.

[62] M. Efatmaneshnik, N. Alam, A. Kealy, and A. G. Dempster, "A fast multidimensional scaling filter for vehicular cooperative positioning," *Journal of Navigation*, vol. 65, no. 2, p. 223–243, 2012.

[63] M. Efatmaneshnik, A. T. Balaei, N. Alam, and A. G. Dempster, "A modified multidimensional scaling with embedded particle filter algorithm for cooperative positioning of vehicular networks," in *2009 IEEE International Conference on Vehicular Electronics and Safety (ICVES)*, Nov 2009, pp. 7–12.

[64] M. Rohani, D. Gingras, V. Vigneron, and D. Gruyer, "A new decentralized bayesian approach for cooperative vehicle localization based on fusion of gps and vanet based inter-vehicle distance measurement," *IEEE Intelligent Transportation Systems Magazine*, vol. 7, no. 2, pp. 85–95, Summer 2015.

[65] N. Drawil and O. Basir, "Intervehicle-communication-assisted localization," *IEEE Trans. Intel. Transp. Syst.*, vol. 11, no. 3, pp. 678–691, Sep. 2010.

[66] N. Alam, A. T. Balaei, and A. G. Dempster, "A dsrc doppler-based cooperative positioning enhancement for vehicular networks with gps availability," *IEEE Transactions on Vehicular Technology*, vol. 60, no. 9, pp. 4462–4470, Nov 2011.

[67] J. Liu, B. g. Cai, and J. Wang, "Cooperative localization of connected vehicles: Integrating gnss with dsrc using a robust cubature kalman filter," *IEEE Transactions on Intelligent Transportation Systems*, vol. 18, no. 8, pp. 2111–2125, Aug 2017.

[68] A. H. Sakr and G. Bansal, "Cooperative localization via dsrc and multi-sensor multi-target track association," in *2016 IEEE 19th International Conference on Intelligent Transportation Systems (ITSC)*, Nov 2016, pp. 66–71.

[69] A. Amini, R. M. Vaghefi, J. M. de la Garza, and R. M. Buehrer, "Improving gps-based vehicle positioning for intelligent transportation systems," in *2014 IEEE Intelligent Vehicles Symposium Proceedings*, June 2014, pp. 1023–1029.

[70] S. B. Cruz, T. E. Abrudan, Z. Xiao, N. Trigoni, and J. Barros, "Neighbor-aided localization in vehicular networks," *IEEE Transactions on Intelligent Transportation Systems*, vol. 18, no. 10, pp. 2693–2702, Oct 2017.

[71] E. Richter, M. Obst, R. Schubert, and G. Wanielik, "Cooperative relative localization using vehicle-to-vehicle communications," in *2009 12th International Conference on Information Fusion*, July 2009, pp. 126–131.

[72] N. Alam, A. T. Balaei, and A. G. Dempster, "Relative positioning enhancement in vanets: A tight integration approach," *IEEE Transactions on Intelligent Transportation Systems*, vol. 14, no. 1, pp. 47–55, March 2013.

[73] K. Liu, H. B. Lim, E. Frazzoli, H. Ji, and V. C. S. Lee, "Improving positioning accuracy using gps pseudorange measurements for cooperative vehicular localization," *IEEE Transactions on Vehicular Technology*, vol. 63, no. 6, pp. 2544–2556, July 2014.

[74] M. Rohani, D. Gingras, and D. Gruyer, "Dynamic base station dgps for cooperative vehicle localization," in *2014 International Conference on Connected Vehicles and Expo (ICCVE)*, Nov 2014.

[75] K. Lassoued, P. Bonnifait, and I. Fantoni, "Cooperative localization with reliable confidence domains between vehicles sharing gnss pseudoranges errors with no base station," *IEEE Intelligent Transportation Systems Magazine*, vol. 9, no. 1, pp. 22–34, Spring 2017.

[76] N. Mattern, M. Obst, R. Schubert, and G. Wanielik, "Co-operative vehicle localization algorithm - Evaluation of the CoVeL approach," in *Proc. SSD*, Mar. 2012, pp. 1–5.

[77] M. Rohani, D. Gingras, and D. Gruyer, "A novel approach for improved vehicular positioning using cooperative map matching and dynamic base station dgps concept," *IEEE Transactions on Intelligent Transportation Systems*, vol. 17, no. 1, pp. 230–239, Jan 2016.

[78] G. Soatti, M. Nicoli, N. Garcia, B. Denis, R. Raulefs, and H. Wymeersch, "Enhanced vehicle positioning in cooperative its by joint sensing of passive features," in *IEEE International Conference on Intelligent Transportation Systems*, 2017.

[79] A. Boukerche, H. A. B. F. Oliveira, E. F. Nakamura, and A. A. Loureiro, "Vehicular ad hoc networks: A new challenge for localization-based systems," *Comput. Commun.*, vol. 31, no. 12, pp. 2838–2849, 2008.

[80] F. Gustafsson, F. Gunnarsson, N. Bergman, U. Forssell, J. Jansson, R. Karlsson, and P.-J. Nordlund, "Particle filters for positioning, navigation, and tracking," *IEEE Trans. Signal Process.*, vol. 50, no. 2, pp. 425–437, Feb. 2002.

[81] J. Härri, C. Bonnet, and F. Filali, "The challenges of predicting mobility," EURE-COM, Sophia Antipolis, France, Tech. Rep. 2240, Aug. 2006.

[82] F. Bai and A. Helmy, *A survey of mobility models in wireless ad hoc networks*, University of Southern California, 2006.

[83] B. Liang and Z. J. Haas, "Predictive distance-based mobility management for pcs networks," in *INFOCOM '99. Eighteenth Annual Joint Conference of the IEEE*

Computer and Communications Societies. Proceedings. IEEE, vol. 3, Mar 1999, pp. 1377–1384 vol.3.

[84] H. Wymeersch, J. Lien, and M. Win, "Cooperative localization in wireless networks," *Proc. IEEE*, vol. 97, no. 2, pp. 427–450, Feb. 2009.

[85] M. A. Caceres, F. Penna, H. Wymeersch, and R. Garello, "Hybrid cooperative positioning based on distributed belief propagation," *IEEE Journal on Selected Areas in Communications*, vol. 29, no. 10, pp. 1948–1958, December 2011.

[86] D. Simon, *Optimal State Estimation: Kalman, H Infinity, and Nonlinear Approaches.* Newark, NJ, USA: Wiley, 2006.

[87] M. Arulampalam, S. Maskell, N. Gordon, and T. Clapp, "A tutorial on particle filters for online nonlinear/non-Gaussian Bayesian tracking," *IEEE Trans. Signal Process.*, vol. 50, no. 2, pp. 174–188, Feb. 2002.

[88] S. Thrun, W. Burgard, and D. Fox, *Probabilistic Robotics (Intelligent Robotics and Autonomous Agents).* The MIT Press, 2005.

[89] S. Särkkä, *Bayesian filtering and smoothing.* New York, NY, USA: Cambridge Univ. Press, 2013.

[90] K. Das and H. Wymeersch, "Censoring for bayesian cooperative positioning in dense wireless networks," *IEEE J. Sel. Areas Commun.*, vol. 30, no. 9, pp. 1835–1842, Oct. 2012.

[91] S. Zirari and B. Denis, "Velocity-based CRLB predictions for enhanced cooperative links selection in location-enabled mobile heterogeneous networks," in *Proc. IEEE Workshop Positioning, Navigat. Commun.*, Mar. 2013, pp. 1–6.

[92] G. M. Hoang, B. Denis, J. Härri, and D. T. M. Slock, "Distributed link selection and data fusion for cooperative positioning in GPS-aided IEEE 802.11p VANETs," in *Proc. IEEE Workshop Positioning, Navigat. Commun.*, Mar. 2015, pp. 1–6.

[93] S. V. de Velde, G. T. F. de Abreu, and H. Steendam, "Improved censoring and nlos avoidance for wireless localization in dense networks," *IEEE Journal on Selected Areas in Communications*, vol. 33, no. 11, pp. 2302–2312, Nov. 2015.

[94] N. Patwari, A. Hero, M. Perkins, N. Correal, and R. O'Dea, "Relative location estimation in wireless sensor networks," *IEEE Trans. Signal Process.*, vol. 51, no. 8, pp. 2137–2148, Aug. 2003.

[95] H. L. V. Trees and K. L. Bell, *Bayesian Bounds for Parameter Estimation and Nonlinear Filtering/Tracking.* Piscataway, NJ, USA: Wiley and IEEE Press, 2007.

[96] Z. Sahinoglu, S. Gezici, and I. Gvenc, *Ultra-wideband Positioning Systems: Theoretical Limits, Ranging Algorithms, and Protocols.* New York, NY, USA: Cambridge Univ. Press, 2011.

[97] N. Patwari, J. Ash, S. Kyperountas, A. Hero, R. Moses, and N. Correal, "Locating the nodes: Cooperative localization in wireless sensor networks," *IEEE Signal Process. Mag.*, vol. 22, no. 4, pp. 54–69, Jul. 2005.

[98] "Vehicle Safety Communications-Applications (VSC-A), Final Report," U.S. Dept. Transp., Nat. Highway Traffic Safety Admin., Tech. Rep. DOT HS 811 492A, Sept. 2011.

[99] B. Kloiber, J. Härri, T. Strang, S. Sand, and C. R. García, "Random transmit power control for DSRC and its application to cooperative safety," *IEEE Trans. Dependable Secure Comput.*, vol. 13, no. 1, pp. 18–31, Jan. 2016.

[100] L. Cheng, B. E. Henty, F. Bai, and D. D. Stancil, "Highway and rural propagation channel modeling for vehicle-to-vehicle communications at 5.9 GHz," in *Proc. IEEE Antennas Propag. Soc. Int. Symp.*, Jul. 2008, pp. 1–4.

[101] L. Mihaylova, D. Angelova, D. Bull, and N. Canagarajah, "Localization of mobile nodes in wireless networks with correlated in time measurement noise," *IEEE Trans. Mobile Comp.*, vol. 10, no. 1, pp. 44–53, Jan. 2011.

[102] M. Gudmundson, "Correlation model for shadow fading in mobile radio systems," *Electron. Lett.*, vol. 27, no. 23, pp. 2145–2146, Nov. 1991.

[103] N. Patwari and P. Agrawal, "Effects of correlated shadowing: Connectivity, localization, and RF tomography," in *Proc. ACM/IEEE IPSN'08*, Apr. 2008, pp. 82–93.

[104] H. Li and F. Nashashibi, "Cooperative multi-vehicle localization using split covariance intersection filter," *IEEE Intell. Transp. Syst. Mag.*, vol. 5, no. 2, pp. 33–44, Apr. 2013.

[105] F. Meyer, O. Hlinka, H. Wymeersch, E. Riegler, and F. Hlawatsch, "Distributed localization and tracking of mobile networks including noncooperative objects," *IEEE Trans. on Sig. and Info. Proc. over Net.*, vol. 2, no. 1, pp. 57–71, Mar. 2016.

[106] J. Lien, U. J. Ferner, W. Srichavengsup, H. Wymeersch, and M. Z. Win, "A comparison of parametric and sample-based message representation in cooperative localization," *Int. J. of Nav. and Obs.*, vol. 2012, 2012.

[107] V. Savic and S. Zazo, "Cooperative localization in mobile networks using nonparametric variants of belief propagation," *Ad Hoc Netw.*, vol. 11, no. 1, pp. 138–150, 2013.

[108] C. Pedersen, T. Pedersen, and B. H. Fleury, "A variational message passing algorithm for sensor self-localization in wireless networks," in *Proc. ISIT'11*, Jul. 2011, pp. 2158–2162.

[109] W. Yuan, N. Wu, B. Etzlinger, H. Wang, and J. Kuang, "Cooperative joint localization and clock synchronization based on gaussian message passing in asynchronous wireless networks," *IEEE Transactions on Vehicular Technology*, vol. 65, no. 9, pp. 7258–7273, Sept. 2016.

[110] "Minimum operational performance standards for Global Positioning System/Wide area augmentation system airborne equipment," RTCA, Inc., Tech. Rep. DO-229D, 2006.

[111] Z. Wang, E. Tameh, and A. Nix, "Joint shadowing process in urban peer-to-peer radio channels," *IEEE Trans. Veh. Technol.*, vol. 57, no. 1, pp. 52–64, Jan. 2008.

[112] T. Abbas, K. Sjöberg, J. Karedal, and F. Tufvesson, "A measurement based shadow fading model for vehicle-to-vehicle network simulations," *Int. J. of Ant. and Prop.*, vol. 2015, 2015.

[113] C. M. Bishop, *Pattern Recognition and Machine Learning (Information Science and Statistics).* Secaucus, NJ, USA: Springer-Verlag New York, Inc., 2006.

[114] X. Cai and G. Giannakis, "A two-dimensional channel simulation model for shadowing processes," *IEEE Trans. Veh. Technol.*, vol. 52, no. 6, pp. 1558–1567, Nov. 2003.

[115] J. Kunisch and J. Pamp, "Wideband car-to-car radio channel measurements and model at 5.9 GHz," in *Proc. VTC'08-Fall*, Sept. 2008.

[116] C. R. Drane and C. Rizos, *Positioning Systems in Intelligent Transportation Systems*, 1st ed.   Norwood, MA, USA: Artech House, 1998.

[117] O. Hlinka, F. Hlawatsch, and P. M. Djuric, "Distributed particle filtering in agent networks: A survey, classification, and comparison," *IEEE Sig. Proc. Mag.*, vol. 30, no. 1, pp. 61–81, Jan. 2013.

[118] C. L. Huang, Y. P. Fallah, R. Sengupta, and H. Krishnan, "Adaptive intervehicle communication control for cooperative safety systems," *IEEE Network*, vol. 24, no. 1, pp. 6–13, Jan. 2010.

[119] G. M. Hoang, M. Gautier, and A. Courtay, "Cooperative-cum-constrained maximum likelihood algorithm for uwb-based localization in wireless bans," in *2015 IEEE International Conference on Communications (ICC)*, June 2015, pp. 2704–2709.

[120] J. Hamie, B. Denis, and C. Richard, "Constrained decentralized algorithm for the relative localization of wearable wireless sensor nodes," in *2012 IEEE Sensors*, Oct 2012, pp. 1–4.

[121] H. Ko, B. Kim, and S. H. Kong, "Gnss multipath-resistant cooperative navigation in urban vehicular networks," *IEEE Transactions on Vehicular Technology*, vol. 64, no. 12, pp. 5450–5463, Dec. 2015.

[122] M. G. Petovello, K. O. Keefe, B. Chan, S. Spiller, C. Pedrosa, and P. Xie, "Demonstration of inter-vehicle uwb ranging to augment dgps for improved relative positioning," *Journal of Global Positioning Systems*, vol. 11, no. 1, pp. 11–21, 2012.

[123] M. Pelka, D. Amann, M. Cimdins, and H. Hellbrück, "Evaluation of time-based ranging methods: Does the choice matter?" in *Proc. IEEE WPNC*, Oct. 2017.

[124] L. D. Nardis and M. G. D. Benedetto, "Overview of the ieee 802.15.4/4a standards for low data rate wireless personal data networks," in *2007 4th Workshop on Positioning, Navigation and Communication*, March 2007, pp. 285–289.

[125] J. X. Lee, Z. Lin, and C. P. S. Francois, "Symmetric double side two way ranging with unequal reply time," in *2007 IEEE 66th Vehicular Technology Conference*, Sept 2007, pp. 1980–1983.

[126] Y. Jiang and V. C. M. Leung, "An asymmetric double sided two-way ranging for crystal offset," in *2007 International Symposium on Signals, Systems and Electronics*, July 2007, pp. 525–528.

[127] M. Kwak and J. Chong, "A new double two-way ranging algorithm for ranging system," in *2010 2nd IEEE InternationalConference on Network Infrastructure and Digital Content*, Sept 2010, pp. 470–473.

[128] A. I. Baba and M. M. Atia, "Burst mode symmetric double sided two way ranging," in *2011 IFIP Wireless Days (WD)*, Oct 2011, pp. 1–3.

[129] M. Maman, B. Denis, M. Pezzin, B. Piaget, and L. Ouvry, "Synergetic MAC and higher layers functionalities for UWB LDR-LT wireless networks," in *Proc. ICUWB'08*, vol. 3, Sept. 2008, pp. 101–104.

[130] D. Macagnano, G. Destino, F. Esposito, and G. Abreu, "Mac performances for localization and tracking in wireless sensor networks," in *2007 4th Workshop on Positioning, Navigation and Communication*, March 2007, pp. 297–302.

[131] A. Guizar, A. Ouni, C. Goursaud, N. Amiot, and J.-M. Gorce, "Impact of mac scheduling on positioning accuracy for motion capture with ultra wideband body area networks," in *Proceedings of the 9th International Conference on Body Area Networks*, ser. BodyNets '14.   ICST, Brussels, Belgium, Belgium: ICST (Institute for Computer Sciences, Social-Informatics and Telecommunications Engineering), 2014, pp. 365–371.

[132] M. Maman, B. Denis, and L. Ouvry, "An intuitive prioritised medium access scheme for tracking applications in uwb ldr-lt networks," in *2008 IEEE 19th International*

Symposium on Personal, Indoor and Mobile Radio Communications, Sept 2008, pp. 1–6.

[133] "D5.2 - Specifications of implemented cooperative and fusion algorithms," *HIGHTS* Deliverable, Aug. 2016.

[134] DoD, "GPS Standard Positioning Service (SPS) performance standard," Sep. 2008.

[135] D. Krajzewicz, J. Erdmann, M. Behrisch, and L. Bieker, "Recent development and applications of SUMO - Simulation of Urban MObility," *International Journal On Advances in Systems and Measurements*, vol. 5, no. 3&4, pp. 128–138, December 2012.

[136] P. Richardson and D. Shan, "Experimental data collection and performance analysis of outdoor uwb positioning system under static and mobile conditions," *EURASIP Journal on Wireless Communications and Networking*, vol. 2009, no. 1, p. 618036, Feb 2010.

[137] "Final platform description," HIGHTS Project Deliverable 6.3, May 2018.

[138] M. I. Khan, G.-M. Hoang, and J. Härri, "Rethinking cooperative awareness for future V2X safety-critical applications," in *VNC 2017, IEEE Vehicular Networking Conference, November 27-29, 2017, Torino, Italy*, 11 2017.

[139] "Intelligent Transport Systems (ITS); Access layer specification for Intelligent Transport Systems operating in the 5 GHz frequency band," *ETSI Std. EN 302 663 V1.2.0*, Nov. 2012.

[140] K. S. Bilstrup, E. Uhlemann, and E. G. Strom, "Scalability issues of the mac methods stdma and csma of ieee 802.11p when used in vanets," in *Proc. ICC'10*, May 2010, pp. 1–5.

[141] A. Tahat, G. Kaddoum, S. Yousefi, S. Valaee, and F. Gagnon, "A look at the recent wireless positioning techniques with a focus on algorithms for moving receivers," *IEEE Access*, vol. 4, pp. 6652–6680, 2016.

[142] "Wireless sensor network localization techniques," *Computer Networks*, vol. 51, no. 10, pp. 2529 – 2553, 2007.

[143] P. Closasy, C. Fernández-Pradesz, and J. A. Fernández-Rubioy, "Direct position estimation approach outperforms conventional two-steps positioning," in *2009 17th European Signal Processing Conference*, Aug 2009, pp. 1958–1962.

[144] S. Zhang, E. Staudinger, W. Wang, C. Gentner, A. Dammann, and E. Sandgren, "Diploc: Direct signal domain particle filtering for network localization," in *Proceedings of the 28th International Technical Meeting of The Satellite Division of the Institute of Navigation (ION GNSS+ 2015)*, Sep. 2015, pp. 2267 – 2274.

[145] J. Levinson, M. Montemerlo, and S. Thrun, "Map-based precision vehicle localization in urban environments," in *Proceedings of Robotics: Science and Systems*, Atlanta, GA, USA, June 2007.

[146] D. Niculescu and B. Nath, "Dv based positioning in ad hoc networks," *Telecommun. Syst.*, vol. 22, no. 1-4, pp. 267–280, Jan. 2003. [Online]. Available: http://dx.doi.org/10.1023/A:1023403323460

[147] N. Bulusu, J. Heidemann, and D. Estrin, "Gps-less low-cost outdoor localization for very small devices," *IEEE Personal Communications*, vol. 7, no. 5, pp. 28–34, Oct 2000.

[148] T. He, C. Huang, B. M. Blum, J. A. Stankovic, and T. Abdelzaher, "Range-free localization schemes for large scale sensor networks," in *Proceedings of the 9th Annual International Conference on Mobile Computing and Networking*, ser. MobiCom '03. New York, NY, USA: ACM, 2003, pp. 81–95. [Online]. Available: http://doi.acm.org/10.1145/938985.938995

[149] Y. Zhang, W. Wu, and Y. Chen, "A range-based localization algorithm for wireless sensor networks," *Journal of Communications and Networks*, vol. 7, no. 4, pp. 429–437, Dec 2005.

[150] R. D. Taranto, S. Muppirisetty, R. Raulefs, D. Slock, T. Svensson, and H. Wymeersch, "Location-aware communications for 5G networks: How location information can improve scalability, latency, and robustness of 5G," *IEEE Sig. Proc. Mag.*, vol. 31, no. 6, pp. 102–112, Nov. 2014.

[151] F. Gustafsson and F. Gunnarsson, "Mobile positioning using wireless networks: possibilities and fundamental limitations based on available wireless network measurements," *IEEE Signal Processing Magazine*, vol. 22, no. 4, pp. 41–53, July 2005.

[152] "LT system-PHY, MAC and Network layers," PULSERS Deliverable D3a2.1, Jan. 2007.

[153] D. Dardari, A. Conti, U. Ferner, A. Giorgetti, and M. Z. Win, "Ranging with ultrawide bandwidth signals in multipath environments," *Proceedings of the IEEE*, vol. 97, no. 2, pp. 404–426, Feb 2009.

[154] I. Guvenc and C. C. Chong, "A survey on toa based wireless localization and nlos mitigation techniques," *IEEE Communications Surveys Tutorials*, vol. 11, no. 3, pp. 107–124, rd 2009.

[155] H. Soganci, S. Gezici, and H. V. Poor, "Accurate positioning in ultra-wideband systems," *IEEE Wireless Communications*, vol. 18, no. 2, pp. 19–27, April 2011.

[156] H. Liu, H. Darabi, P. Banerjee, and J. Liu, "Survey of wireless indoor positioning techniques and systems," *IEEE Transactions on Systems, Man, and Cybernetics, Part C (Applications and Reviews)*, vol. 37, no. 6, pp. 1067–1080, Nov. 2007.

[157] D. Dardari, P. Closas, and P. M. Djurić, "Indoor tracking: Theory, methods, and technologies," *IEEE Transactions on Vehicular Technology*, vol. 64, no. 4, pp. 1263–1278, April 2015.

[158] H. Wymeersch, G. Seco-Granados, G. Destino, D. Dardari, and F. Tufvesson, "5g mm-wave positioning for vehicular networks," *IEEE Wireless Communications Magazine*, 2017.

[159] D. Vasisht, S. Kumar, and D. Katabi, "Decimeter-level localization with a single wifi access point," in *Proceedings of the 13th Usenix Conference on Networked Systems Design and Implementation*, ser. NSDI'16. Berkeley, CA, USA: USENIX Association, 2016, pp. 165–178. [Online]. Available: http://dl.acm.org/citation.cfm?id=2930611.2930623

[160] M. Laaraiedh, L. Yu, S. Avrillon, and B. Uguen, "Comparison of hybrid localization schemes using rssi, toa, and tdoa," in *17th European Wireless 2011 - Sustainable Wireless Technologies*, April 2011, pp. 1–5.

[161] S. He and S. H. G. Chan, "Wi-Fi fingerprint-based indoor positioning: Recent advances and comparisons," *IEEE Commun. Surveys Tuts.*, vol. 18, no. 1, pp. 466–490, 2016.

[162] R. E. Kalman, "A new approach to linear filtering and prediction problems," *ASME Journal of Basic Engineering*, 1960.

[163] Y. Bar-Shalom, *Tracking and Data Association*. San Diego, CA, USA: Academic Press Professional, Inc., 1987.

[164] S. J. Julier and J. K. Uhlmann, "Unscented filtering and nonlinear estimation," *Proceedings of the IEEE*, vol. 92, no. 3, pp. 401–422, Mar 2004.

[165] E. A. Wan and R. V. D. Merwe, "The unscented kalman filter for nonlinear estimation," in *Proceedings of the IEEE 2000 Adaptive Systems for Signal Processing, Communications, and Control Symposium (Cat. No.00EX373)*, 2000, pp. 153–158.

[166] A. Doucet, S. Godsill, and C. Andrieu, "On sequential monte carlo sampling methods for bayesian filtering," *Statistics and Computing*, vol. 10, no. 3, pp. 197–208, Jul. 2000.

[167] B. Ristic, S. Arulampalm, and N. Gordon, *Beyond the Kalman filter : particle filters for tracking applications / Branko Ristic, Sanjeev Arulampalm, Neil Gordon.* Artech House Boston, Ma. ; London, 2004.

[168] F. Gustafsson, "Particle filter theory and practice with positioning applications," *IEEE Aerosp. Electron. Syst. Mag.*, vol. 25, no. 7, pp. 53–82, Jul. 2010.

[169] R. Chen and J. S. Liu, "Mixture kalman filters," *Journal of the Royal Statistical Society: Series B (Statistical Methodology)*, vol. 62, no. 3, pp. 493–508, 2000.